Technical Summary

Drafting Authors:
Bhupesh Adhikary (Nepal), Richard Allan (UK), Paola A. Arias (Colombia), Kyle Armour (USA), Govindasamy Bala (India, USA), Nicolas Bellouin (UK, France), Pep Canadell (Australia), Christophe Cassou (France), Annalisa Cherchi (Italy), Bill Collins (USA), Erika Coppola (Italy), Sarah Connors (France, UK), Faye Cruz (Philippines), Frank Dentener (Italy, Netherlands), Aida Diongue Niang (Senegal), Paco Doblas-Reyes (Spain), Alessandro Dosio (Italy), Hervé Douville (France), François Engelbrecht (South Africa), Veronika Eyring (Germany), Erich Fischer (Switzerland), Piers Forster (UK), Baylor Fox-Kemper (USA), Jan Fuglestvedt (Norway), John Fyfe (Canada), Nathan Gillett (Canada), Leah Goldfarb (France, USA), Sergey Gulev (Russian Federation), Jose Manuel Gutierrez (Spain), Rafiq Hamdi (Belgium), Mathias Hauser (Switzerland), Edward Hawkins (UK), Helen Hewitt (UK), Richard Jones (UK), Darrell Kaufman (USA), Svitlana Krakovska (Ukraine), Gerhard Krinner (France), June-Yi Lee (Republic of Korea), Jochem Marotzke (Germany), Valérie Masson-Delmotte (France), Seung-Ki Min (Republic of Korea), Vaishali Naik (USA), Gemma Teresa Narisma (Philippines), Friederike Otto (UK, Germany), Matthew Palmer (UK), Izidine Pinto (Mozambique), Anna Pirani (Italy), Gian-Kasper Plattner (Switzerland), Krishnan Raghavan (India), Roshanka Ranasinghe (Netherlands, Sri Lanka, Australia), Joeri Rogelj (Austria, Belgium), Maisa Rojas (Chile), Alexander Ruane (USA), Lucas Ruiz (Brazil), Jean-Baptiste Sallée (France), Bjorn H. Samset (Norway), Pedro Scheel Monteiro (South Africa), Sonia Seneviratne (Switzerland), Jana Sillmann (Norway, Germany), Anna Amelia Sörensson (Argentina), Trude Storelvmo (Norway), Sophie Szopa (France), Claudia Tebaldi (USA), Peter Thorne (Ireland, UK), Bart van den Hurk (Netherlands), Robert Vautard (France), Carolina Vera (Argentina), Cunde Xiao (China), Sönke Zaehle (Germany), Panmao Zhai (China), Xuebin Zhang (Canada), Kirsten Zickfeld (Canada, Germany)

Contributing Authors:
Guðfinna Aðalgeirsdóttir (Iceland), Lincoln Alves (Brazil), Irina Gorodetskaya (Portugal, Belgium/Russia), James Kossin (USA), Flavio Lehner (Switzerland), Chao Li (China), Thorsten Mauritsen (Sweden, Denmark), Thomas Maycock (USA), Malte Meinshausen (Australia/Germany), Sophie Nowicki (Canada), Adam Phillips (USA), Lucas Ruiz (Argentina), Stéphane Sénési (France), Sabin Thazhe Purayil (India), Blair Trewin (Australia), Andrew Turner (UK)

Date of Draft:
01/03/2020

Note:
TSU compiled version

Table of Content

TS.1 Framing ... **6**

TS.1.1 Context of AR6 WGI ... **7**

TS.1.1.1 A changing climate ... 7

TS.1.1.2 International climate policy ... 8

TS.1.2 Developments in climate science ... **9**

TS.1.2.1 Developments in observational capabilities ... 9

TS.1.2.2 Developments in modelling capabilities ... 10

TS.1.2.3 Risk framing in the AR6 ... 12

TS.1.2.4 Regional information ... 14

TS.1.2.5 Event Attribution ... 15

TS.1.3 Dimensions of Integration: Scenarios, Warming Levels, and Cumulative Emissions **16**

TS.1.3.1 Scenarios ... 16

TS.1.3.2 Warming levels ... 22

TS.1.3.3 Cumulative carbon emissions ... 22

TS.1.4 Baselines ... **22**

Box TS.1: Global temperature definitions ... **23**

TS.2 Large scale climate change ... **26**

TS.2.1 Changes in drivers of global change ... **26**

TS.2.2 Atmospheric temperature and circulation ... **27**

TS.2.2.1 Surface and upper air temperatures ... 28

TS.2.2.2 Tropospheric circulation ... 31

TS.2.2.3 Summary of atmospheric temperature and circulation changes ... 32

Box TS.2: Low-probability, high-warming storylines ... **32**

TS.2.3 The Ocean ... **34**

TS.2.3.1 Temperature, heat content and energy budget ... 34

TS.2.3.2 Salinity ... 35

TS.2.3.3 Circulation ... 35

TS.2.3.4 Ocean changes by depth ... 36

TS.2.3.5 Ocean pH (acidification), de-oxygenation, and ocean carbon sink ... 36

TS.2.3.6 Summary of ocean changes ... 36

TS.2.4 Cryosphere ... **37**

TS.2.4.1 Sea ice extent/area and thickness ... 37

TS.2.4.2 Snow cover, permafrost and glaciers ... 38

TS.2.4.3 Ice sheet mass and extent ... 39

TS.2.4.4 Summary of cryospheric changes ... 39

Box TS.3: Sea Level **39**

TS.2.5 Water cycle **42**
TS.2.5.1 Observed changes 42
TS.2.5.2 Attribution 42
TS.2.5.3 Projected changes 43
TS.2.5.4 Summary of water cycle changes 45
TS.2.6 The Carbon Cycle **46**
TS.2.6.1 Emissions and reservoir changes 46
TS.2.6.2 Changing Mechanisms that Influence Carbon Feedbacks on Land and in the Ocean 47
TS.2.6.3 Future changes to the ocean and terrestrial carbon cycles 47
TS.2.6.4 Summary of observed, present and projected carbon cycle changes 48
TS.2.7 Extremes **48**
TS.2.7.1 Temperature extremes 49
TS.2.7.2 Heavy precipitation and floods 49
TS.2.7.3 Droughts 50
TS.2.7.4 Tropical cyclones 50
TS.2.7.5 Marine extremes 51
TS.2.7.6 Compound events 51

Box TS.4: Irreversibility, Abrupt Change and Tipping Points **55**

TS.2.7.7 Summary of observed and projected changes in extremes 58
TS.2.8 Changes across the global climate system **59**

Cross-Section Box 1: Scenario-based future climate system changes across timescales **62**

Cross-Section Box 2: Global warming levels **68**

TS.3 Forcing, Feedbacks and Responses **73**
TS.3.1 Radiative forcing and energy budget **73**
TS.3.2 Feedbacks and metrics of climate response **75**
TS.3.3 Drivers of Water Cycle Change **80**
TS.3.4 Climate Stabilization, Net-Zero Emissions and Carbon Budgets **82**
TS.3.4.1 Carbon budgets and climate stabilization 82
TS.3.4.2 Carbon Dioxide Removal 85
TS.3.5 Climate and Air Quality Response to SLCFs in SSP Scenarios **86**
TS.3.6 Solar Radiation Modification **87**
TS.4 Regional change **88**
TS.4.1 Construction of regional climate information and messages **89**
TS.4.1.1 Sources and methodologies to generate regional climate change information 89
TS.4.1.2 Methodologies and approaches for generating regional climate change messages 91
TS.4.1.3 Climate Services 92

TS.4.1.3.1 Summary ... 93

Box TS.5: The Interactive Atlas and multiple lines of evidence for constructing regional climate change message. ... 94

TS.4.2 Multiple drivers of regional climate variability ... 95

TS.4.2.1 Regional fingerprint of external forcing ... 95

TS.4.2.1.1 Anthropogenic forcing ... 96

TS.4.2.1.2 Natural forcing (solar, volcanic aerosols) ... 96

TS.4.2.2 Internal modes of variability and regional teleconnections ... 96

TS.4.2.3 Interplay between drivers of climate variability at regional scales ... 101

TS.4.2.3.1 Regional feedbacks ... 101

TS.4.2.3.2 Relative importance of the drivers and implication in terms of uncertainties ... 102

TS.4.2.4 Summary ... 103

Box TS.6: Monsoons ... 104

TS.4.3 Regional climate change and its implications for climate extremes and climatic impact drivers ... 106

TS.4.3.1 Construction of regional climate change information ... 107

TS.4.3.2 Generic changes in climatic impact drivers ... 107

TS.4.3.3 Summary of regional changes in climatic impact drivers (CIDs) ... 110

Box TS.7: Box on Case Studies ... 111

TS.4.3.4 Africa ... 113

TS.4.3.5 Asia ... 115

TS.4.3.5.1 Middle East Asia ... 116

TS.4.3.5.2 North Asia ... 117

TS.4.3.5.3 East Asia ... 118

TS.4.3.5.4 South East Asia ... 118

TS.4.3.5.5 South Asia ... 119

TS.4.3.6 Australasia ... 120

TS.4.3.7 Central and South America ... 122

TS.4.3.7.1 Central America ... 122

TS.4.3.7.2 South America ... 123

TS.4.3.8 Europe ... 125

TS.4.3.9 North America ... 127

TS.4.3.10 Small Islands ... 130

TS.4.3.11 Polar regions ... 132

TS.4.3.11.1 Antarctica ... 132

TS.4.3.11.2 Arctic ... 133

TS.4.3.12 Open and deep ocean ... 135

TS.4.3.13 Typological domains 136
TS.4.3.13.1 Mountain regions 136
TS.4.3.13.2 Monsoons 137
TS.4.3.13.3 Other typological domains 138

Box TS.8: Urban box 139

TS.4.3.14 Summary 140

Appendices TS 147
Appendix TS.A TS.4 Traceback Tables 147
Appendix TS.B Acronyms and Abbreviations for the AR6 WGI Technical Summary 168

Figures 172

This Technical Summary is a bridge between the comprehensive assessment of the Working Group I and the high-level summary for policymakers (SPM). It supports the SPM, providing traceability between the SPM and the relevant findings from the underlying chapters. The Technical Summary is built from the Executive Summaries of the individual chapters and also brings together different lines of evidence from different chapters to allow a synthesis of key assessments.

Throughout this Technical Summary, key assessment findings are reported using the IPCC calibrated uncertainty language (Chapter 1, Box 1.1). All three IPCC WGs use two metrics to communicate the degree of certainty in key findings, which is based on author teams' evaluations of underlying scientific understanding:

(1) Confidence[1] is a qualitative measure of the validity of a finding, based on the type, amount, quality and consistency of evidence (e.g. data, mechanistic understanding, theory, models, expert judgment) and the degree of agreement; and
(2) Likelihood[2] provides a quantified measure of uncertainty in a finding expressed probabilistically (e.g. based on statistical analysis of observations or model results, or both, and expert judgement by the author team or from a formal quantitative survey of expert views, or both). Where appropriate, findings can also be formulated as statements of fact without uncertainty qualifiers. Throughout IPCC reports, the calibrated language is clearly identified by being typeset in italics. {Box 1.1}

The Technical Summary is structured into four sections. TS1 presents the overall framing and context of the whole report. TS2 synthesises information about the large-scale changes in all components of the climate system (atmosphere, ocean, cryosphere and carbon cycle). TS3 summarises knowledge and understanding of forcing, feedbacks and responses. Finally, TS4 summarises regional change. Two Appendices accompany this Technical Summary: TS.A comprises the Traceback Tables for TS Section 4 and TS.B supplies a list of acronyms and abbreviations that are used in the Technical Summary.

TS.1 Framing

This first section discusses the context of the Intergovernmental Panel on Climate Change (IPCC) Sixth Assessment Report (AR6), presents some key developments in climate science and highlights the frameworks adopted for presenting the findings of the Working Group I contribution to AR6, including the choice of future scenarios and methods for producing regional information.

IPCC Working Group I (WGI) assesses the most current physical science of climate change, evaluating multiple lines of evidence and knowledge gained from examining direct observations of Earth's climate, reanalysis datasets that combine observations with weather forecast models, information from paleoclimate archives that reveal how Earth's climate has evolved over hundreds to millions of years, simulations from climate models, along with studies of physical and biogeochemical climate processes. This section sets the scene for the WGI contribution to AR6, and places the assessment in the context of ongoing global changes and international policy responses.

The AR6 WGI is structured to enhance the visibility of key knowledge developments since the AR5 potentially relevant for policymakers. The main content of the full report, which forms the basis of this

[1] In this Technical Summary, the following summary terms are used to describe the available evidence: limited, medium, or robust; and for the degree of agreement: low, medium, or high. A level of confidence is expressed using five qualifiers: very low, low, medium, high, and very high, and typeset in italics, e.g., *medium confidence*. For a given evidence and agreement statement, different confidence levels can be assigned, but increasing levels of evidence and degrees of agreement are correlated with increasing confidence (see Chapter 1, Box 1.1 for more details).

[2] In this Technical Summary, the following terms have been used to indicate the assessed likelihood of an outcome or a result: *virtually certain* 99–100% probability, *very likely* 90–100%, likely 66–100%, *about as likely as not* 33–66%, *unlikely* 0–33%, *very unlikely* 0–10%, *exceptionally unlikely* 0–1%. Additional terms (extremely *likely*: 95–100%, *more likely than not* >50–100%, and *extremely unlikely* 0–5%) may also be used when appropriate. This Report also uses the term '*likely* range' or '*very likely* range' to indicate that the assessed likelihood of an outcome lies within the 17–83% or 5–95% probability range respectively. Assessed likelihood is typeset in italics, e.g., *very likely* (see Chapter 1, Box 1.1 for more details). Throughout the WGI report and unless stated otherwise, uncertainty is quantified using 90% uncertainty intervals. The 90% uncertainty interval, reported in square brackets [x to y], is expected to have a 90% likelihood of covering the value that is being estimated. The range encompasses the median value and there is an estimated 5% likelihood of the value being below the lower end of the range (x) or above its upper end (y). Uncertainty intervals are not necessarily symmetric about the corresponding best estimate. A best estimate of that value is also given where available.

Technical Summary, is based on three pillars: information on large-scale climate change (Chapters 2-4), understanding of the physical and biogeochemical processes of the climate system (Chapters 5-9), and regional information (Chapters 10-12 and Atlas). Integration across the WGI report and with Working Groups II and III occurs through a general introduction to dimensions of integration (Chapter 1; see TS.1.3), regional climate information and changes in climate impact drivers relevant for risk assessments (Chapters 8-12, Atlas), and integrating quantities such as equilibrium climate sensitivity (ECS), remaining cumulative carbon emission budgets for given temperature levels, and radiative forcing due to CO_2 and non-CO_2 components (Chapters 4-7). A key development since the AR5 is a common definition of risk adopted across the three Working Groups (see TS.1.2.3).

TS.1.1 Context of AR6 WGI

TS.1.1.1 A changing climate

The WGI contribution to AR6 assesses scientific information on climate change relevant for a world whose climate system is changing. The series of five IPCC Assessment Reports since 1990 have comprehensively and consistently laid out the vast evidence of a changing climate system, with the Fourth and Fifth Assessment Reports (AR4, 2007; AR5, 2013) both concluding that warming of the climate system is unequivocal.

Ongoing observed changes to the climate system include increasing global surface air and sea temperatures, loss of ice and glacier mass, sea level rise, increasing ocean heat content, declining ocean pH, changing ocean salinity patterns and stratification, changes to precipitation patterns and extreme weather and rising atmospheric greenhouse gas concentrations as well as changes in the abundances of Short-lived Climate Forcers (SLCFs) which are highly variable temporally and spatially (Figure TS.1). Multiple independent lines of evidence indicate the unusual nature of the present rate and scale of global changes, as well as already committed future changes, even when seen in the context of a multi-millennial period (Figure TS.9).

[START FIGURE TS.1 HERE]

Figure TS.1: Changes are observed throughout the climate system. Left: The main domains of the climate system: Atmosphere, land and biosphere, cryosphere and ocean. Right: The evolution of a range of indicators of ongoing changes, since 1850 or the start of the observational record, covering all four climate system domains. Each stripe indicates the global, annual mean anomaly for a single year (except for precipitation which shows a latitude band mean, and the biosphere which shows local observations), relative to a multi-year baseline (except for CO2 concentration, which is absolute, and glacier mass loss, which shows integrated values). Grey indicates missing data. Datasets and baselines used are: CO2: Antarctic ice cores (Lüthi et al., 2008; Bereiter et al., 2015) and direct air measurements (Tans and Keeling, 2019) (see Figure 1.3 for details). Precipitation: Global Precipitation Climatology Centre (GPCC) V8 (updated from Becker et al., 2013), baseline 1961-1990 using land areas only. Latitude bands are 33°N-66°N and 15°S-30°S. Glacier mass loss: TO BE UPDATED. Biosphere: Cherry blooming dates from Aono and Saito, 2010, grape harvest dates from Labbe et al., 2019. Surface air temperature: HadCRUT5.0 (Morice et al., submitted), baseline 1961-1990. Sea level: (Dangendorf et al., 2019), baseline 1900-1929. Ocean heat content: (Zanna et al., 2019), baseline 1961-1990. {Figure 1.2}

[END FIGURE TS.1 HERE]

[START FIGURE TS.2 HERE]

Figure TS.2: Long-term context of anthropogenic climate change based on selected paleoclimatic reconstructions over the past 800,000 years, observed changes and future projections using CMIP6 SSPs (2081-2100) and CMIP5 RCP-extensions (2300) for three key indicators: atmospheric CO_2 concentrations, global mean surface temperature (GMST), and global mean sea level (GMSL). Details available from Figure 1.3. Dots/whiskers on the right-hand side panels of the figure (grey background) indicate the projected median and ranges derived from SSP-based (2081-2100; Chapters 4 and 9) and RCP-extension simulations (2300; IPCC SROCC, 2019). Best estimates (dots) and uncertainties (whiskers) as assessed by Chapter 2 (Figure 2.33 and Annex II) for each of the three indicators and selected paleo-reference periods used in this report (Cross-Chapter Box 2.1) are included in the "paleoclimate" (left) and "observed" (middle) panels. The scenarios used here are introduced in Section TS1.3. [PLACEHOLDER: year 2300 RCP extensions (ECP) based projections to be updated to SSP-based projections from Ch4/9 for the FGD if available]

[END FIGURE TS.2 HERE]

Understanding of key features of the climate system is robust and well established. 19th-century scientists first hypothesized the possibility of anthropogenic climate change and identified the major heat-absorbing greenhouse gases. Other major anthropogenic drivers such as radiation-scattering aerosols and land use change were identified by the mid-1970s. The principal natural drivers of climate change (changes in solar irradiance, volcanoes, orbital factors, and changes in global biogeochemical cycles) have been studied since the early 20th century. Since systematic scientific assessments began in the 1970s, the influence of human activity on the climate system has evolved from a hypothesis to a fact. {1.3, Figure TS.3}

[START FIGURE TS.3 HERE]

Figure TS.3: Timeline of key events and climate knowledge developments. {1.3}

[END FIGURE TS.3 HERE]

TS.1.1.2 International climate policy

International efforts to address the risks posed by the observed and projected changes in Earth's climate began with the United Nations Framework Convention on Climate Change (UNFCCC, 1992), whose objective is to prevent 'dangerous anthropogenic interference with the climate system'. In response to this objective, the Paris Agreement (2015) set the goals of 'holding the increase in global average temperature to well below 2°C above pre-industrial levels and pursuing efforts to limit the temperature increase to 1.5°C above pre-industrial levels'. As part of these efforts, each country submitted a Nationally Determined Contribution (NDC) indicating its planned emission reductions. The NDCs submitted so far are insufficient to achieve the Paris goals (*high confidence*). IPCC SR1.5 concluded that "Pathways reflecting current nationally stated mitigation ambition until 2030 are broadly consistent with cost-effective pathways that result in a global warming of about 3°C by 2100, with warming continuing afterwards (*medium confidence*)". {1.2.2}

AR6 provides information of relevance to the 2023 global stocktake, a five-yearly evaluation of alignment between overall global climate mitigation and adaptation efforts, the Paris Agreement's long-term goals, and its means of implementation and support. This WGI report assesses, among other topics, remaining cumulative carbon emission budgets for a range of temperature levels, effects of long-lived and short-lived climate forcers, projected changes in sea level rise and extreme events, and attribution to anthropogenic climate change. The information drawn from the WGI assessment is complementary to the information from IPCC Special Reports, the contributions from WGII and WGIII and the Synthesis Report. An overview of WGI assessment findings that could potentially help inform the global stocktake including pointers to the respective WGI chapters is provided in Cross-Chapter Box 1.2. {1.2.2, Cross-Chapter Box 1.2}

Climate change is not an isolated global challenge, and IPCC reports are relevant for other international development issues as well, such as the UN 2030 Agenda, which defines Sustainable Development Goals (SDGs), and the Sendai Framework for Disaster Risk Reduction. Also, efforts to constrain climate change take place in the context of other major environmental problems, such as biodiversity loss. Climate change is a "direct driver that is increasingly exacerbating the impact of other drivers on nature and human well-being", according to the Intergovernmental Science-Policy Platform on Biodiversity and Ecosystem Services (IPBES). {1.2.2}

In addition to the global climate change adaptation and mitigation policy relevance, AR6 assesses science that informs decisions on policies related to air quality, in particular, the role of short-lived climate forcers (SLCFs). SLCFs can produce a cooling or warming and are, in most cases, also air pollutants whose regulation is essential for attainment of some of the SDGs. SLCFs include aerosols (sulphate, nitrate, ammonium, carbonaceous aerosols, mineral dust, and sea salt) and chemically reactive gases (methane, ozone, halogenated species, nitrogen oxides, carbon monoxide, non-methane volatile organic compounds, sulphur dioxide, and ammonia). Their emissions are regulated from local to regional levels for species causing local air quality issues, and from continental to the global level for halogenated species or sulfates involved in global environmental issues such as stratospheric ozone depletion (through the Montreal protocol, revised by the Kigali amendment in 2016), or acidic rains. {1.2.2, 6.5, 6.6}

The Special Report on Global Warming of 1.5°C (SR1.5) report concluded that achieving Paris Agreement goals, including limiting warming to 1.5°C, would require simultaneous and ambitious reductions of SLCFs and long-lived GHGs within the next decades. However, except for methane and halogenated species, regulations of SLCF emissions have so far been decided independently from climate policies. A dedicated set of policies developed with a focus on co-benefit solutions would be required to maximize climate mitigation and air quality improvements. {TS3.6, 6.5, Box 6.2, FAQ 6.2}

In summary, the IPCC 6th Assessment cycle occurs in the context of increasingly visible climate changes and renewed efforts in international climate governance. {1.2}

TS.1.2 Developments in climate science

Climate science is continually evolving as a result of more and better observations of the Earth system, advances in our understanding of the climate system, ability to perform larger ensembles of simulations or simulations run at higher resolutions, and improved knowledge of climate-related risks. This section discusses major developments in observations, modelling, the provision of regional information, the framing of climate risks and the ability to identify human influences on changes in extreme events.

The complexity and comprehensiveness of climate projections has also increased since the FAR. Nevertheless, early climate change projections published since the 1980s are in close agreement with the rate and pattern of subsequent observed surface temperature change, especially when accounting for differences between the emission scenarios used in those early projections and the emissions that actually occurred. {1.3.6}

A synthesis of the evolution of key attribution findings throughout the current and previous ARs is shown in Figure TS.3. The IPCC Second Assessment Report (1995) identified a discernible human influence on the climate. Since this initial assessment and throughout subsequent assessments (TAR, 2001; AR4, 2007 and AR5, 2013), the evidence for human influence on the climate system has progressively strengthened. AR5 concluded that human influence on the climate system is clear, evident from increasing greenhouse gas concentrations in the atmosphere, positive radiative forcing, observed warming, and physical understanding of the climate system. This evidence is now even stronger. {3.3-3.8}

[START FIGURE TS.4 HERE]

Figure TS.4: Synthesis of evolution of key attribution findings throughput IPCC Assessment Reports, from the First Assessment Report (FAR) through AR6. Based on Table 1.A.1 from Chapter 1.

[END FIGURE TS.4 HERE]

TS.1.2.1 Developments in observational capabilities

Progress in climate science relies on the quality and quantity of observations from a range of platforms, including surface-based instruments, aircraft observations, satellite-based retrievals, *in situ* measurements and paleoclimate records. Overall, capabilities to observe the physical climate system have continued to improve and expand, but losses in existing observational capacity are also occurring. {1.5.1}

New syntheses of previously published paleoclimate data (Technical Annex II) have been facilitated by advances in community curated open-data systems. These data collections are suited to analyses by new statistical methods that have enabled increasingly larger-scale and more robust reconstructions of the spatial and temporal patterns of past climate changes over multiple time scales. However, some paleoclimate archives such as corals, tropical glaciers, and trees are rapidly disappearing owing to a range of issues, including high temperatures caused by anthropogenic climate change (*high confidence*). {1.5.1, 2.3.1, Cross-Chapter Box 2.4, 7.5.3}

Records arising from several recently instigated satellite measurement techniques are now of sufficient duration to be relevant for climate assessments. For example, globally distributed, high-vertical-resolution profiles of temperature and humidity in the upper troposphere and stratosphere can be obtained from the early 2000s using global navigation satellite systems. However, there is an emerging loss of observational data coverage or continuity due to reductions in certain satellite coverage, surface station networks, and radiosonde launches. {1.5.1, 2.3.2}

Reanalyses are frozen versions of data assimilation and numerical models run retrospectively using a range of available historical observations to constrain the model at each time step. Given generation upon generation improvements, they are now increasingly used as an additional line of evidence in assessments of the state and evolution of the climate system. Reanalysis datasets provide internal consistency with the assimilating model's physics across multiple physical quantities, and derived information about variables and locations that are not directly observed. This does not guarantee long-term homogeneity, but newer reanalyses generally show greater skill at capturing long-term change than prior versions. New reanalyses have been developed with various combinations of increased resolution, extended records, more consistent data assimilation, and an improved representation of the coupled atmosphere-ocean system. {1.5.2}

Substantial quantities of known instrumental observations of weather and other climate variables, which could fill gaps in existing datasets, remain undigitised. Observational records for mountainous regions, data sparse regions and cities cause difficulties that pose limits to the assessment of regional climate change. For instance, there is *high confidence* on elevation-dependant warming in most of the mountain ranges, but field measurements are extremely limited at high elevations. It is *virtually certain* that the scarcity and decline of observations (e.g., in southern Mediterranean, Africa, or India) increase the uncertainty of long-term temperature and precipitation estimates. {1.5.1, 10.2.2, 10.6, Cross-Chapter-Box 10.3}

TS.1.2.2 Developments in modelling capabilities

Developments in modelling capabilities since the AR5 include increases in the number of research groups participating in modelling intercomparison projects, the number of Earth system models, and the number of intercomparison experiments.

The latest generation of climate models has an improved representation of physical processes relative to previous generations. A wider range of Earth System Models now represent biogeochemical cycles. Higher-resolution models that capture smaller-scale processes and extremes are also available. More modelling centres are participating in multi-model intercomparisons for the present report than for any previous IPCC Assessment Report. {1.4.2, 1.5.3, 1.5.4}

Key model intercomparisons supporting this assessment include the Coupled Model Intercomparison Project Phase 6 (CMIP6) and the Coordinated Regional Climate Downscaling Experiment (CORDEX), for global and regional models respectively. A range of results from the previous CMIP Phase 5 (CMIP5) are also used, complementing the assessment.

Since the AR5, the increased use of 'large ensembles', or multiple simulations with the same climate model, is supporting improved understanding of the relative roles of internal variability and forced change in the climate system.

A broad set of simplified climate models are assessed and are being used to transfer climate information across research communities, such as for impacts or mitigation pathways consistent with certain levels of future warming. {1.4.2, 1.5.3 and 1.5.4}

For most large-scale indicators of climate change, the mean climate simulated by the latest generation climate models underpinning this assessment has improved compared to the models assessed in the AR5 (*high confidence*). High resolution models exhibit reduced biases in some but not all aspects of surface and ocean climate (*medium confidence*). While a broad range of warming rates across models and a lengthening observational record mean that significant differences between the climate response in individual models and observations can often be identified, the multi-model mean captures most aspects of observed climate change well (*high confidence*). {3.8.2}

In CMIP6, there are a variety of biases in SST and SSS reduced in comparison to CMIP5, though biases in equatorial regions remain essentially unchanged. Despite some persisting regional biases, CMIP6 coupled climate models generally reproduce observed SST trends over the past century, and there is *high confidence* in their ability to inform on future large-scale SST changes." {3.5.1.1, 9.2.1.1, Figure 9.3, Figure 9.4}

[START FIGURE TS.5 HERE]

Figure TS.5: (a) Evolution of inclusion of processes and resolution from CMIP3 to CMIP6 (based on Figure 1.17). (b) Centred pattern correlations between models and observations for the annual mean climatology over the period 1980–1999. Results are shown for individual CMIP3 (black), CMIP5 (blue) and CMIP6 (brown) models as short lines, along with the corresponding ensemble range (shading). The correlations are shown between the models and the reference observational data set listed in Table 3.5. In addition, the correlation between the reference and alternate observational data sets are shown (solid grey circles). To ensure a fair comparison across a range of model resolutions, the pattern correlations are computed after regridding all datasets to a resolution of 2.5º in longitude and 2.5º in latitude. Only one realization is used from each model from the CMIP3, CMIP5 and CMIP6 historical simulations.

[END FIGURE TS.5 HERE]

Simulations at kilometre-scale resolution add value to the representation of convection (*high confidence*) and many local-scale phenomena such as land-sea breezes and influences of soil-moisture (*medium confidence)*, which are, in turn, relevant for triggering convection. Convection permitting models can also improve the simulation of the life cycle of convective storms and related precipitation extremes. Since they still rely on model-dependent lateral boundary conditions provided by GCMs and/or RCMs with parameterized convection, there is however only *medium confidence* in their added value for projecting seasonal or annual mean water cycle changes. {8.5.1, 10.3.3}

Model deficiencies and unresolved small-scale processes still preclude a strong model consensus about future water cycle changes whatever the scenario, time horizon or global warming level is. The range of model responses is particularly large at the transition between wet and dry regions and seasons, and for soil moisture and freshwater reservoirs that are sensitive to small differences in precipitation or evapotranspiration changes, poor representation of land surface processes or lack of consideration of land use change and irrigation. {8.5.1}

There is *medium confidence* that increasing global climate model resolution helps reducing systematic errors, although there is *high confidence* that higher resolution alone does not solve all performance limitations. {10.3.3}

Other processes that are still insufficiently well represented and simulated by climate models include:

The magnitude and timing of future mass loss remains uncertain due to scenario uncertainty, low resolution

GCM forcing, model oversimplification, and limited observations for calibration (*medium confidence*). {9.5.1, 9.6.3}

Slight Antarctic regional increases or decreases in ice area result from regional wind forcing (*medium confidence*), and projections require accurate modelling of regional variations (*high confidence*). Limited model resolution and poorly understood regional processes infer *low confidence* in regional projections of Antarctic sea-ice area. {9.3.1, 9.3.2, 3.4.1}

In summary, developments in climate models including new and better representation of physical, chemical and biological processes, as well as higher resolution, have improved the simulation of many large-scale indicators of climate change in many aspects of the Earth system, providing confidence in their projections of future changes (Figure TS.4). There is still a low model consensus for future water cycle changes due to model deficiencies. Some aspects of the cryosphere such as sea-ice and ice sheets and permafrost are still poorly modelled.

TS.1.2.3 Risk framing in the AR6

As part of the AR6, a cross-Working Group process developed a common language for discussing risk, which is broadly defined as the potential for adverse consequences that derives from the interaction of three components: hazards, exposure and vulnerability. More specifically, risk is defined in the AR6 as the "potential for adverse consequences for human or ecological systems, recognising the diversity of values and objectives associated with such systems. In the context of climate change, risks can arise not only from impacts of climate change, but also from potential human responses to climate change. Relevant adverse consequences include those on lives, livelihoods, health and wellbeing, economic, social and cultural assets and investments, infrastructure, services (including ecosystem services), ecosystems and species". In the context of climate change responses, risks result from the possibility that such responses may not achieve the intended objective(s), or from potential trade-offs with, or negative side-effects on, other societal objectives, such as the United Nations Sustainable Development Goals (SDGs). Risks can arise for example from uncertainty in implementation, effectiveness, or outcomes of climate policy; climate-related investments; technology development or adoption; and system transitions. {1.2.2, 1.2.4, 1.4.4, Cross Chapter Box 1.3}

In this context, the aim of WG1 is to provide a characterization of the climate component in the risk assessment, its past and current characteristics, including attribution of observed changes, and its future evolution. Accordingly, the concept of risk does not apply to this physical system component, but only to human and ecological systems, after the additional dimensions of exposure and vulnerability are considered. Such systematic risk framing is intended to aid formulation of effective responses to the challenges posed by current climatic changes, and to better inform risk assessment and decision making. {1.2.2, 1.2.4, 1.4.4, Cross Chapter Box 1.3}

Recognizing however that the risk framework only addresses the detrimental part of the consequences of climate change, and that WG1 assesses only the physical part of climate change and not the consequences on or responses of human and ecological systems, in AR6 a choice was made to describe physical system changes in a value-neutral fashion, without pre-judging consequences, by using the term "climatic impact drivers" to describe natural or human-induced climate events or trends that may have detrimental or beneficial impacts on elements of society or ecosystems. In this context, the term hazard refers to climate-related physical events or trends having potential detrimental effects. {Cross Chapter Box 1.3}

Climatic impact drivers affect a wide range of sectors (*high confidence*). They can be measured by indices to represent thresholds that are critical for sectoral assets, including direct information about the climatic impact driver's profile (magnitude, frequency, duration, timing, spatial extent). They can utilize proxies for climatic impact drivers that are more difficult to directly observe or simulate. In many cases, the different assets within the same sector require different tailored indices to characterise weather or climate conditions affecting the sector. These indices can use thresholds which can vary by specific sectoral system, region and asset. {12.3, Table TS.1}

In the assessment of risks resulting from dynamic interactions of climatic impact drivers with the exposure and vulnerability of affected human or ecological systems, all three components may each be subject to uncertainty in terms of magnitude and likelihood of occurrence, and each may change over time and space due to climate variability and change, socio-economic changes and human decision-making (Figure TS.6). {Cross Chapter Box 1.3}

[START TABLE TS.1 HERE]

Table TS.1: Relevance of key climatic impact drivers (and their respective changes in intensity, frequency, duration, timing, and spatial extent) for major categories of sectoral assets, as assessed in 12.3 across many studies and applications. High relevance indicates climatic impact drivers that are most prominent and widely studied for their direct connection to assets, while lower relevance indicates weaker linkages and less commonly-studied driving behaviours. Specific levels of risk, and opportunity depend on the changing character of regional hazards, vulnerability, and exposure to be assessed in WGII. {12.3, Table 12.2}

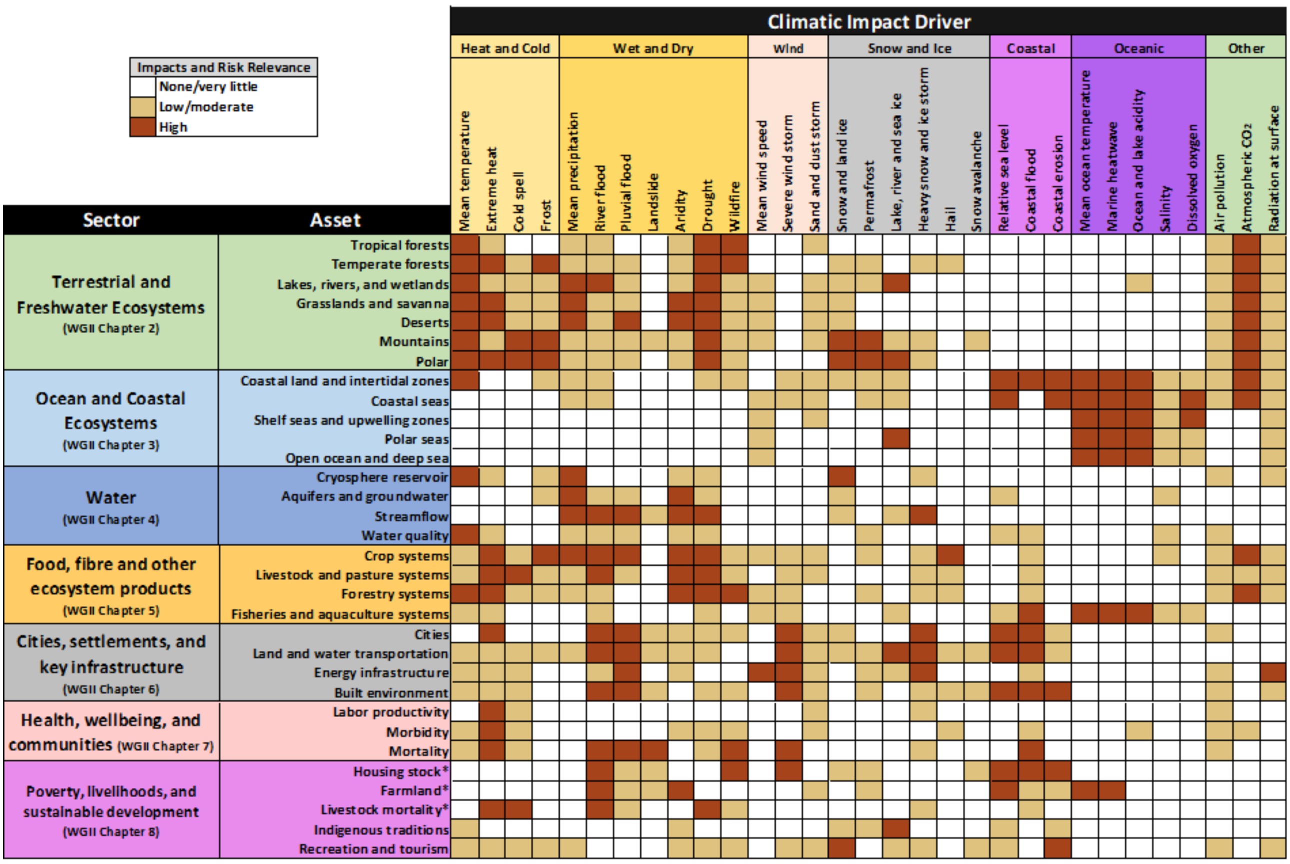

* This asset category is distinguished by the threat of a full loss of key investments and living environments rather than a recoverable damage or loss of productivity or profit

[END TABLE TS.1 HERE]

Besides assessing risk for specific regions and sectors, WGII has historically (since the TAR, 2001) conducted synthesis assessments of key risks and Reasons for Concern (RFCs). The AR6 cycle, starting with the Special Reports (SR1.5, SROCC and SRCCL), has used these aggregated concepts to characterise their connection to global mean temperature levels when possible. The WG1 contribution to these synthesis assessments is to relate the climatic impact drivers to increasing warming levels. {12.5.2}

Many climatic impact drivers that are relevant to regional and sectoral assessment and have also been identified as essential for contributing to Representative Key Risks (WGII Ch16), have a strong, direct relationship with global climate indices. For example, global surface air temperature (GSAT) is related to metrics describing heat and wet/dry hazards), CO_2 concentration in the atmosphere is related to ocean pH, and global mean sea level rise (GMSLR) is related to indices describing extreme sea levels. For a majority of these climate hazard indices a direct relationship with GSAT warming can be identified (*medium confidence*), while for other indices the time/scenario dimension remains a determinant (*medium confidence*), and in some cases threshold behaviours cannot be excluded (*medium confidence*). {12.5.2}

The risk framework used in the AR6 is supported by an increased use of storylines in WG1, which contribute to building a robust and more comprehensive picture of climate information, allowing a more flexible consideration of risk that can explicitly address low-likelihood, high-impact events (Box TS.2). In this context, WGI is mainly concerned with 'physical climate storylines', which are self-consistent and plausible unfoldings of a physical trajectory of the climate system, or a weather or climate event, on timescales from hours to multiple decades. These aspects are important as the greatest risk need not occur at the highest likelihood outcome and will often occur at low-likelihood outcomes because of the nature of the impact. {Box TS.2, Figure TS.5, 1.2.2, 1.2.4, 1.4.4, Cross Chapter Box 1.3, 1.4.4}

For example, the CMIP6 models with the highest ECS and TCRs values are assigned low probability but are nevertheless useful as they provide insights into high-risk, low-probability futures. Furthermore, high-warming storylines are *very likely* also associated with substantial changes in the hydrological cycle due to strong thermodynamic changes that are potentially amplified or offset by dynamical changes. {4.8, 7.5.6}

[START FIGURE TS.6 HERE]

Figure TS.6: Illustrating concepts of low-likelihood, high impact events. (top) Schematic likelihood distribution (pdf) consistent with the IPCC AR6 assessments that "Equilibrium climate sensitivity (ECS) is *likely* in the range 2.5°C to 4.0°C and *very likely* in the range 2.0°C to 5.0C" (see Figure 1.12 for details). The assessed '*likely'* and '*very likely*' ranges are highlighted. (bottom) The likelihood that ECS is larger than the indicated value (1-cdf). The colours indicate the additional risk due to climate change using the Reasons For Concern, specifically RFC1 (bottom left, the risks to unique and threatened systems) and RFC3 (bottom right, the risks due to the distribution of impacts) as assessed in IPCC AR5, assuming that GMST has stabilised after an increase in radiative forcing equivalent to a doubling of CO_2. The dashed black line highlights the 10% likelihood.

[END FIGURE TS.6 HERE]

TS.1.2.4 Regional information

Climate change is a global phenomenon, but it manifests in different ways in different regions. Its impacts are generally experienced at local, national and regional scales, and these are also the scales at which decisions are made. In an effort to provide policymakers and others with relevant and useful information and to facilitate integration across the three WGI contributions, AR6 features an expanded focus on regional information. That focus is also reflected in this Technical Summary.

Regional climate is determined by a complex interplay of global external forcings, large-scale internal modes of climate variability and teleconnections, as well as regional-scale climate processes, feedbacks and forcings. Depending on the specific context, regional climates may refer to large areas such as a monsoon region or to smaller areas such as a coastline, a mountain range or a human settlement like a city. Users (understood as anyone incorporating climate information into their activity) often request climate information from a provider from within this range of scales, since regional operating and adaptation decision scales range from the local to the sub-continental level. In this context, the term region is used in a general sense to indicate the range of scales of relevance for impact and adaptation without prescribing any formal regional boundaries. However, the report offers climate information for a number of predefined and unified set of reference land and ocean regions. These regions are sub-continental domains defined in terms of characteristic climate and environmental features. Higher-resolution, typological regions (such as monsoon areas, mountains, and megacities), are used to integrate across similar climatological, geological and human domains. {Cross-Chapter Box 1.1, 1.4.6, 1.8}

A variety of methodologies and approaches have been developed to construct climate change information for regions. The sources include global and regional climate models (GCMs and RCMs, respectively) and statistical methods, among many others (TS.4.1.1). Regional observations likewise play a key role in the process of formulating regional climate information. High-quality observations that allow monitoring the regional aspects of climate are used to adjust inherent model biases and are the basis for assessing model performance. Climate information also benefits from attributing observed changes to large- and regional-scale anthropogenic and natural drivers and forcings (TS.4.2).

To increase confidence in future projections of regional climate, there is *high confidence* that multiple sources of observations and tailored diagnostics are needed to evaluate climate model performance. There is *very high confidence* that the availability of multiple observational records at regional scale is fundamental for assessing climate model performance. {10.2.2}

All these sources are used to distil contextualised regional climate information from multiple lines of evidence (TS.4.1.1). Useful climate information for vulnerability, impacts, adaptation, and climate service applications (a novel element since AR5, TS 4.1.3) depends on the regional context and sectoral assets. Regional climate change information for impacts and for risk assessment requires an assessment of the changing profile of tailored climatic impact drivers that link climate conditions to sectors. These climatic impact drivers can take the form of hazards when they lead to negative impacts, or can lead to beneficial impacts, or both, depending on sector and/or region. {12.1, 12.2}

This climate information is then further distilled in a co-production process involving the user and the producer resulting in a regional climate message. The distillation process leading to the message considers the specific context of the question at stake, the values of both the user and the producer, and the challenge of communicating across different communities. {TS.4.1.2, Figure TS.6}

[START FIGURE TS.7 HERE]

Figure TS.7: Simplified view of the construction of a regional climate message including sources, context, values and storylines, with the processes that lead to the distillation of the message. The chapters and sections where the elements entering the message construction are assessed are indicated. {Figure 10.1}

[END FIGURE TS.7 HERE]

With the aim of aiding decision-making, that occurs at local or regional scales, a common risk framework across all three working groups has been implemented. Methodologies have been developed to construct more impact- and risk-relevant climate change information tailored to regions and to identify stakeholders. Storyline approaches are utilised in order to build climate information based on multiple lines of evidence, and which can explicitly address low-likelihood, high-impact events for consideration in risk assessments.

TS.1.2.5 Event Attribution

Attribution techniques are now offering new insights into the links between human influence on the climate system and climate and in particular weather events and providing improved understanding of current climatic impact drivers. Various attribution methods are applied across all three AR6 WGs and are fundamental to determining how climate change has contributed to observed changes, such as a long-term trend or an extreme event. If anthropogenic forcing is found to be a major driver of such an observed change, then it can be used to illustrate a narrative of the near future. Attribution methods are also applied to quantify the influence from a range of drivers on observed impacts or changes and can include the results of adaptation or mitigation actions. {1.5.2, Cross-Chapter Box 1.4, 1.4.4, Annex I}

Since the AR5, there have been major new developments and knowledge advances regarding changes in weather and climate extremes. Evidence of observed changes in extremes and for an attributable human influence on those changes have strengthened, particularly for extreme precipitation, droughts, tropical cyclones, and compound extremes. There is also evidence of an increase in the land area affected by concurrent extremes. {11.1, 11.3, 11.4, 11.5, 11.6, 11.7, 11.8, Box 11.3}.

Event attribution—the process of evaluating the human and natural contributions to an extreme event or a trend in extreme events—considers the drivers of a particular event or class of events. The events assessed are usually recent records that have been broken or major events with widespread impacts. Events can range in scale from a one-day record temperature in a city to several years of drought over a region. The basic principle of many approaches in event attribution is that the characteristics of the event are analysed under present-day climate conditions and in counterfactual conditions in a modelled 'world that might have been' without anthropogenic climate change. Many events have now been examined, using a wide range of methods. The framing of the question can have a major effect on the results of an extreme event attribution analysis. Different approaches can lead to different messaging, such as: 'This particular type of event is X% more *likely* to occur in the current climate' (frequency); 'This event is *likely* to have a greater intensity due to climate change' or 'The anomaly is half due to climate change' (magnitude). Another approach describes facets of the weather and thermodynamic status of the event. These sorts of statements can all be informative, depending on the context, and even seemingly conflicting findings can be reconcilable, when the original framing is understood. Another aspect of framing is the assumptions in the null hypothesis of no change. For climate event attribution, given the confidence of the assessment that anthropogenic climate forcing has indeed altered our climate (AR5), some studies start with this as an accepted fact and then describe how the forcing has altered the event, in its magnitude or other aspects. {Cross Chapter Box 1.4}

TS.1.3 Dimensions of Integration: Scenarios, Warming Levels, and Cumulative Emissions

This section introduces three ways to synthesize and integrate knowledge of climate change across topics and chapters. These 'dimensions of integration' include (i) emission and concentration scenarios underlying the climate change projections assessed in this report, (ii) levels of projected changes in global mean temperature, and (iii) using total amounts of cumulative carbon emissions for projections (see Figure TS.8). All three dimensions can, in principle, be used to synthesize knowledge not just across disciplines in the physical climate sciences, but also across climate change related impacts, adaptation, and mitigation research. Additional choices, combined with these 'dimensions of integrations, can act to facilitate integration across the WG1 report and across the whole AR6, for example, the choice of reference periods and time windows for which changes are assessed (Table TS1.3). {Table TS1.3, 1.6 - 1.6.4, Cross-Chapter Box 1.5, 11.1, 11.2, 12.5.2}

Scenarios have a long history in IPCC as a method for systematically examining possible futures (see section TS2). Global mean temperature levels are closely related to a number of regional climate impacts, regional changes in extremes and many indices of climatic impact drivers connected to 'Reasons for Concern' (see Cross-Section Box 2). Cumulative carbon emissions are related in a nearly linear fashion to increases in global mean surface air temperature, are important components of scenarios, and are also key for assessments of mitigation options. {Cross-Section Box 2, 1.6}

[START FIGURE TS.8 HERE]

Figure TS.8: The Dimensions of Integration (DI) across Chapters and Working Groups in the IPCC AR6 assessment report. This report adopts three explicit dimensions of integration to integrate knowledge across chapters and Working Groups. The first dimension (DI 1) are scenarios, the second dimension (DI 2) are global-mean temperature levels relative to pre-industrial levels and the third dimension (DI 3) are cumulative CO_2 emissions. {Figure 1.28}

[END FIGURE TS.8 HERE]

TS.1.3.1 Scenarios

Scenarios are plausible descriptions of how the future may develop based on a coherent and internally consistent set of assumptions about key socio-economic factors, including demographics, economic processes, technological innovation, governance, lifestyles, and the relationships among these driving forces. Rather than predicting the future, scenarios examine future developments in a "what-if" sense. The evolution of future anthropogenic emissions is a key characteristic of the different scenarios, emerging from their socio-economic assumptions. Once these emissions are represented as external forcings for climate model simulations, the resulting future climate outcomes are assessed by WGI as part of AR6. Except for seasonal and most decadal predictions, future climate projections are conditional on the respective scenario. Earth system models (ESMs) are run in coordinated model intercomparison projects, using standardized simulation protocols, most recently, for example, as part of the CMIP6 exercise. The outcomes from climate models run under the different scenarios can be translated into climatic impact drivers for the purpose of supporting impact research. Chapter 12 of WGI assesses future projections of these drivers at regional scales, to facilitate corresponding WGII assessments, one of the way by which AR6 has implemented explicit connections across WGs. {1.6.1, 1.5.4, Cross-Chapter Box 1.5, Glossary}

A new set of emission or concentration scenarios, derived from the socio-economic futures described by the Shared Socioeconomic Pathways (SSPs), is used to synthesize knowledge across the physical sciences (through the climate model simulations produced according to them), impact, and adaptation and mitigation research. The core set of illustrative SSP scenarios used in this report include pathways with lower emissions compared to previous assessment reports, including scenarios potentially consistent with a 1.5°C warming. Throughout this report, SSP scenarios are referred to as SSP2-4.5 or similar, where the first part of the label (SSP2 in this case) refers to the SSP used in deriving the emissions and concentrations, and the second part (4.5 in this case) refers to the approximate radiative forcing (in Wm^{-2}) in the year 2100, also providing a link to the Representative Concentration Pathways (RCPs) used in the AR5 (See Figure Box TS.1, Figure 1). It should be noted that as was the case for RCPs climate models compute their own radiative forcing as a consequence of the imposed forcing agents. Therefore these labels are only approximations to the actual, model dependent outcome at 2100. One of the underlying assumptions of the new scenario framework is that different SSPs may produce emission/concentration pathways consistent with the same radiative forcing levels, given appropriate assumptions on mitigation policies throughout the century. {1.6.1-1.6.4, Cross-Chapter Box 1.5, 4.4.2}

[START FIGURE TS.9 HERE]

Figure TS.9: SSP-RCP scenario matrix, with the SSP socioeconomic narratives shown as columns and the indicative radiative forcing levels by 2100 shown as rows. RCPs are shown for comparison. {1.6.1, Figure 1.24}

[END FIGURE TS.9 HERE]

Five illustrative SSP scenarios are used consistently across this report: SSP1-1.9, SSP1-2.6, SSP2-4.5, SSP3-7.0, and SSP5-8.5. The five scenarios bracket a wide range of plausible future emissions. The lowest, SSP1-1.9, represents a low greenhouse gas emission, high mitigation future which may limit warming to less than 1.5°C above pre-industrial levels. In contrast, the highest SSP5-8.5, represents a future with no climate policy, leading to continued and sustained growth in atmospheric greenhouse gas concentrations and related high warming (Figure TS.10). The quantification of the various forcing agents in the SSP scenarios offers unprecedented detail for climate model simulations. They encompass a broader range of future trajectories for some of the forcing agents than CMIP5 RCPs, for example regarding SO_2 emissions and future land use. {1.6, Box 1.3, 1.6, Figure 1.25, 4.2.2, Cross-Chapter Box 7.1}

As in the RCPs, the SSP SLCF emission trajectories assume a long-term coupling of economic growth and specific emission rates. However, SSP trajectories span a wider range of SLCF emissions than considered in the RCPs scenarios, reflecting the potential for large regional differences in ambition of air pollution legislation and discrepancies in effectiveness of its implementation. SSPs differ in their assumed pollution policies, with SSP1-1.9, SSP1-2.6 and SSP5-8.5 largely identified as strong pollution control scenarios wherein ozone precursor and aerosol and their precursor emissions decline strongly in the mid to long term (methane emissions follow climate mitigation narratives declining rapidly in SSP1-1.9 and SSP1-2.6 but declining only after 2070 in SSP5-8.5), SSP2-4.5 a medium pollution control scenario with SLCF emissions following current trends, and SSP3-7.0 a weak pollution control scenario with strong increases in SLCFs over the 21st century. {6.6.1, Figure 6.4}

Studies utilizing the RCPs complement the assessment based on SSP scenarios in order to fill gaps where no results from the latter are available, or where the AR6 results are compared to results from earlier IPCC reports. See Table TS1.3 for succinct descriptions of the illustrative SSP scenarios and their closest RCP and SRES scenarios. For many climate model outcomes, it is expected that the differences between corresponding trajectories from the two scenario sets (e.g., RCP8.5 and SSP5-8.5 run by the same model) will be smaller than the differences between the two generations of models (e.g., SSP5-8.5 run by the CMIP5 and the CMIP6 versions of the same model). {1.6, 4.2.2, Cross-Chapter Box 7.1}

[START FIGURE TS.10]

Figure TS.10: SSP-Stripes: Historical global-mean surface air temperatures illustrated as warming stripes from blue (cold) to red (warm) until 2015 and climate model projections for possible futures under five scenarios from "very low" SSP1-1.9 to "very high" SSP5-8.5 . The underlying future climate projection data is taken from MIROC6 - an Earth System Model (ESM) with a relatively low climate sensitivity. The majority of CMIP6 ESMs show higher future projections. The points in time when total CO_2 emissions peak, reach halved levels of the peak and reach net-zero emissions are indicated by crosses, diamonds and open circles, respectively. {1.6.1.3; Figure 1.22}

[END FIGURE TS.10 HERE]

In addition to transient emission and concentration scenarios derived from assumptions about socio-economic futures, idealized scenarios and time-slice experiments independent of scenarios are also used to force climate models and those results are assessed in this report. Examples of idealized scenarios are trajectories where CO_2 concentrations increase by 1% per year or are instantly quadrupled from a pre-industrial level. These idealized forcings are used for sensitivity experiments, and to diagnose patterns of climate feedbacks across the suite of models in this report. {1.6.1}

The use of different scenarios for climate change projections introduces a 'scenario-uncertainty' in the projections. Depending on the spatial and time scales of the projection, and on the variable of interest, the relative importance of scenario uncertainty compared to other sources of uncertainty like model structural choices and internal variability may vary substantially. {1.4.3, 1.6}

The choice of scenarios assessed in WGI follows several criteria:

- Availability: all the scenarios but for SSP1-1.9 are in Tier1 of ScenarioMIP, therefore prioritized by the modelling centres participating in the ScenarioMIP exercise;
- Comparability with RCPs and therefore with the AR5 assessment;
- Span of a large range of plausible future emissions, and therefore climate outcomes;
- Strong representation of component forcings of interest like SLCFs, land use change, allowing assessment of sensitivities. {1.5.4, 1.6}

The individual chapters in the underlying full WGI report present results from different sets of scenarios, according to the criteria specified above, as specifically relevant to their individual assessments. Table TS.1 describes this use in detail.

[START TABLE TS.2 HERE]

Table TS.2: Scenarios across WGI AR6. Some chapters do not use or discuss scenario-dependent results; those are marked with "N.A." (not applicable).

WGI AR6 Chapter	Scenarios	Description
Ch1: Framing, context, methods	SSP scenarios, RCPs, and older generations	Introduces the new SSP scenarios, describing their development in the context of the older scenarios, especially relating them to RCPs and SRES scenarios.
Ch2: Changing state of the climate system	N.A.	N.A. Chapter focus on observations and paleoclimate information.
Ch3: Human influence on the climate system	N.A.	Exception when using the first years of RCP4.5 or SSP2-4.5 grafted at the end of historical simulations, for comparison with up-to-date observational records
Ch4: Future global climate: scenario-based projections and near-term information	Core set of SSP scenarios. RCP2.6, RCP4.5 and RCP8.5.	Chapter focus on scenario-based projections.
Ch5: Global carbon and other biogeochemical cycles and feedbacks Ch6: Short-lived climate forcers Ch8: Water cycle changes Ch9: Ocean, cryosphere, and sea level change	Exhaustive use of both RCPs and SSP scenarios, in some cases extending to non-core elements, for example when assessing effects of overshoot.	Literature based on RCPs anchors the assessment, with updates for SSP scenarios when available.
Ch7: The Earth's energy budget, climate feedbacks, and climate sensitivity	Idealized scenarios	Focusing on metrics (TCR, ECS) and feedbacks uses idealized experiments
Ch10: Linking global to regional climate change	SSP scenarios, RCPs	Presents case studies, and therefore a diversity of scenario choices (e.g. RCPs if using CORDEX; SSPs if using CMIP6) to illustrate methodological approaches to the provision of regional climate information.
Ch11: Weather and climate extreme events in a changing climate	N.A.	Organized as projections by warming levels.
Ch12: Climate change information for regional impact and for risk assessment	SSP1-2.6, SSP5-8.5, RCP2.6, RCP8.5	Focus on the signal of mitigation emerging at regional levels starting from the mid-term, hence the necessity of choosing the bracketing range, consistently across CMIP5 and CMIP6

		results.
Atlas	SSP1-2.6, 2-4.5 and 5-8.5; RCP2.6, 4.5, and 8.5	Same rationale as Ch12; the interactive Atlas adds capabilities to explore the whole set of SSP scenarios and RCPs (in addition to warming levels)

[END TABLE TS.2 HERE]

[START TABLE TS.3 HERE]

Table TS.3: Overview of the set of illustrative SSP scenarios used in this report and approximately corresponding earlier climate scenarios RCPs and SRES (in terms of total anthropogenic radiative forcing trajectories). The core set of SSP scenarios used most commonly in this report are highlighted bold. {1.6.1.3, Box 1.3, Table 1}

SSPX-Y scenario	**Description**	**Corresponding RCP scenarios (Approx.)**	**Corresponding SRES scenario (Approx.)**
SSP1-1.9	Represents the very low end of the range of scenarios in the literature measured by their radiative forcing pathway. Relevant to the Paris agreement policy discussion as expected to achieve a 1.5°C warming level by 2100.	No equivalently low RCP scenario.	Not available. Lowest SRES scenario is higher than SSP1-1.9.
SSP1-2.6	Represents the low end of the range of future forcing pathways in the Integrated Assessment Modelling (IAM) literature.	RCP2.6, but given recent emission increases, the illustrative SSP scenarios are higher in 2020 than the RCP2.6 level.	Not available. Lowest SRES scenario is higher than SSP1-2.6.
SSP4-3.4	Fills a gap at the low end of the range of future forcing pathways. Analysis of avoided impacts compared to 2.6 and 4.5 would inform mitigation choices given the large mitigation cost differences between the latter two levels.	Not available. In between RCP 2.6 and RCP 4.5	Not available.
SSP2-4.5	Represents the medium part of the range of future forcing pathways.	RCP4.5 and until 2050 also RCP6.0 as the latter was similar to RCP4.5 in the early decades.	SRES B1 or A1T

SSP4-6.0	Fills in the range of medium forcing pathways.	RCP6.0 in the later part of the century, while the new scenario remains above it (and therefore above RCP4.5 as well) in the early decades.	Also SRES B1 or A1T
SSP3-7.0	Represents the medium to high end of the range of future forcing pathways	In between RCP6.0 and RCP8.5, although non-CO_2 emissions higher than in RCPs	SRES A2
SSP5-8.5	Represents the high end of the range of future pathways in the IAM literature. No climate policy.	RCP8.5, although CO_2 emissions under SSP5-8.5 are higher towards the end of the century. Methane emissions under SSP5-8.5 are lower than under RCP. When used with the same model settings, there is an indication that SSP5-8.5 results in slightly higher temperatures than RCP8.5 (see Cross-Chapter Box 7.1).	SRES A1FI, the fossil intensive SRES A1 scenario.
SSP3-7.0 Low NTCF	A variation of the baseline scenario SSP3-7.0, but with mitigation of non-CO_2 species black carbon and other SLCF. Depending on the application, methane is also reduced.	SSP3-7.0 low-NTCF is between RCP6.0 and RCP8.5. RCP scenarios generally showed a narrow and comparatively low level of SLCF emissions across the range of RCPs.	Not available.
SSP5-3.4 Overshoot	A mitigation variation of SSP5-8.5. Initially follows unconstrained emission growth in a fossil-intensive setting until 2040 and then implements the deepest net negative CO_2 emissions of all SSP scenarios in the second half of the 21st century. Reaches SSP1-2.6 forcing levels in the 22nd century.	Not available. Until 2040 similar to RCP8.5.	Not available. Initially, until 2040, similar to SRES A1FI.

[END TABLE TS.3 HERE]

TS.1.3.2 Warming levels

Using levels of warming (e.g., 1.5°C or 2°C above pre-industrial levels) as a way to assess and communicate information about changes and impacts makes it possible to perform a range of risk assessments independently of specific scenarios or time periods at which a warming threshold might be reached (e.g., through RFCs). But the timing of reaching each warming level can also be related to scenarios and the cumulative carbon emissions for each level can be estimated as needed. {1.6.2}

As a result, warming levels are a dimension of integration that is highly relevant across scientific disciplines and socio-economic actors. For example, global mean temperature levels relative to pre-industrial levels are the quantity in which the 1.5°C and 'well below 2°C' Paris Agreement targets are formulated. In addition, global mean temperature has been found to be nearly linearly related to a number of regional climate changes, for both mean and extreme indices. Finally, the evolution of aggregated impacts with temperature levels have been widely used and embedded in the WGII assessment. This includes the 'Reasons for Concern' (RFC) and other burning ember diagrams in IPCC WGII. The RFC framework has been further expanded in the SR1.5, the SROCC and SRCCL by explicitly looking at the differential impacts between half-degree warming levels and conditioning the evolution of risk to socio-economic assumptions. Working Group 1 contributes an evaluation of changes in climatic impact drivers found to be relevant to this type of synthetic risk assessment according to warming levels. {1.4.4, 1.6.2, 12.5.2}

As the IPCC SR1.5 concluded "Climate models project robust differences in regional climate characteristics between present-day and global warming of 1.5°C, and between 1.5°C and 2°C", this report adopts half-degree temperature bands as the smallest interval, starting from a pre-industrial reference point, across which climate projections, impacts, adaptation challenges and mitigation challenges can be integrated, within and across the three WGs. The categorisation uses 1.0°C (close to present day conditions), 1.5°C, 2.0°C, 3.0°C, and 4.0°C as a primary set of levels. More details on the assessment using warming levels are given in Cross-Section Box 2. {1.4, 1.6.2, Cross-Chapter Box 1.2, Table 1.5}

TS.1.3.3 Cumulative carbon emissions

The WGI AR5 and SR1.5 highlighted the near-linear relationship between cumulative carbon emissions and global mean surface air temperatures. This implies that continued CO_2 emissions will cause further warming and changes in all components of the climate system, independent of any specific scenario or pathway. This report thus uses cumulative carbon emissions to compare impacts across scenarios and topics, and to categorise emission scenarios. The advantage of using cumulative CO_2 emissions is that it is an inherent emission scenario characteristic rather than an outcome of the scenario-based projections, where uncertainties in the cause–effect chain from emissions to temperature change are important. {1.6.3}

TS.1.4 Baselines

Variations in observed and simulated climate variables are often presented as 'anomalies', that is, the differences relative to a 'baseline' or 'reference period', rather than using absolute values. Several baseline or reference periods are defined and used consistently throughout AR6. The term 'baseline' implies a period against which anomalies are calculated, whereas a 'reference period' could include a transient state. The choice of a baseline period has important consequences comparing observations with simulations, and for presenting climate projections. There is usually no perfect choice of baseline as many factors have to be considered and compromises may be required. {1.4.1}

Table TS.4 defines a range of periods used within WGI and across AR6: paleo reference periods, a pre-industrial baseline, a modern reference period and a range of future reference periods used to present projections in the near-, mid- and long-term (Table TS.4).

The choice of pre-industrial baseline is particularly important because of its relevance to the Paris Agreement. The term 'pre-industrial' is reserved for the period around 1750, normalizing anthropogenic forcing to zero at that time. Mean global temperature during the 1850-1900 period has often been used as a pragmatic approximation for pre-industrial global temperature, but it is *more likely than not* that this choice results in a slight underestimation of the total anthropogenic change in global mean surface temperature (GMST) (*medium confidence*). Box TS.1 discusses the differences between GMST and global surface air temperature (GSAT); the latter is adopted for projections of global temperature change in the SPM. {1.4.1, Cross Chapter Box 1.2, Cross Chapter Box 1.3}

Several anthropogenic factors influenced the climate between 1750 and 1900, primarily an increase in anthropogenic greenhouse gas and aerosol emissions, and changes in land use. Between 1750 and 1850 atmospheric CO_2 levels increased by around 7 ppm, which is equivalent to 15 GtC of increased carbon in the atmosphere. Estimates of emissions from fossil fuel burning (~1 GtC, Boden et al., 2017) cannot explain this increase, so CO_2 emissions from land use changes are implicated as being a significant source. The atmospheric concentration of other greenhouse gases also increased over the same period and there was a cooling influence from increased anthropogenic aerosol emissions. It is estimated that the net radiative forcing for the 1850-1900 period was around 0.15 Wm^{-2} relative to 1750, with a GHG forcing of around 0.3 Wm^{-2}, partially offset by other anthropogenic radiative forcings (aerosols and land use changes) of around -0.15 Wm^{-2}, but with a larger uncertainty than for GHGs. The net radiative forcing in 1850-1900 from changes in solar activity and volcanic activity is estimated to be smaller than ± 0.05 Wm^{-2}. {2.2.3, 2.2.6}

It is *very likely* that net increases in atmospheric greenhouse gas concentrations alone would have warmed the planet between 1750 and the 1850-1900 period. This warming influence was at least partially offset by a cooling influence from anthropogenic aerosol emissions. The net increase of GMST caused by anthropogenic factors between 1750 and 1850-1900 is *likely* -0.1 to 0.2°C (*medium confidence*), with potential implications for remaining cumulative carbon emission budgets for given temperature levels. {Cross Chapter Box 1.3, 1.4.1}

The long-term context of changes in GMST, relative to the 1850-1900 baseline, is shown in Figure TS.2.

[START BOX TS.1 HERE]

Box TS.1: Global temperature definitions

Observed global surface temperature has traditionally been defined as the blend of air temperature at screen height (nominally 2 metres) over land, and sea surface temperature (SST) over the ocean. This is referred to as global mean surface temperature (GMST). Analysis of ESM simulations usually considers global surface air temperature (GSAT), defined as air temperature computed at 2 m height over both land and ocean. The two measures, while closely linked, are not directly equivalent. The AR5 and earlier assessments had implicitly assumed equivalence which, with *high confidence,* can no longer be justified.

Translating global temperature estimates

Numerous observational datasets exist for GMST, but there is none for GSAT. Given that model analyses generally consider GSAT it is necessary to convert observed GMST to GSAT to facilitate direct comparisons. Recourse to model-based evidence is required to estimate the differences between GMST and GSAT. At the global scale, air temperature over the ocean is expected by all modern ESMs to warm slightly faster than SST. Several studies analysing ESMs point to warming at rates averaging between 3 and 7% faster in GSAT than GMST. Reanalyses provide an alternative means of estimating the effect and they yield an estimate of 2-4% for globally complete fields. Given these lines of evidence, an inflation of 4% (2-7%) is applied to the globally (quasi-)complete instrumental GMST records to provide an implied GSAT estimate (*limited evidence, high agreement*) to enable direct comparison to model-based estimates. The uncertainty in this conversion value propagates through to analyses that rely upon it.

Implications of GMST vs GSAT on important assessment aspects

Whether to use GMST or GSAT has a relatively minor effect on our estimates of total temperature changes since the 1850-1900 reference period (Box TS.2, Figure 1; Box TS.2, Table 1), and certainly less of an impact in the current assessment cycle than the 0.1°C combined effect of dataset innovations and new products since the AR5 (2.3.1.1.3). Analyses which join historical observed GMST changes with modelled GSAT fields currently experience a 'definition gap' of 0.04 (0.02-0.08)°C of missing warming at the switchover based upon the 4% (2-7%) adjustment factor assessed. This gap was 0.02°C at the time of the 3rd Assessment Report. As the switchover date between the observed past and the projected future is moved forward in successive reports this would generate an artificial suggestion of cooler temperature projections due to an increasing definition gap.

This definition gap has potentially important implications for aspects such as: the remaining carbon budget to reach the 1.5°C Paris Agreement target as assessed in SR1.5, especially given the increased proximity to that target arising from dataset innovations assessed within this report; observation-based estimates of the Transient Climate Response; and projections under various scenarios on centennial timescales. The impact on a number of key aspects of the assessment are highlighted in Box TS.2 Table 1.

[START BOX TS.1, FIGURE 1 HERE]

Box TS.1, Figure 1: Left panel: example of the growing impact with time of the use of surface air temperatures everywhere (GSAT) versus surface air temperatures over land and sea surface temperatures over the ocean (GMST), showing the ensemble mean of a single GCM using historical and RCP4.5 forcings out to 2100. Right panel: quantification of the growing impact of the hybrid choice to merge historical GMST and projected GSAT (the definition gap). Observed GMST and implied GSAT using the adjustment of 4% are shown up until 2018. Thereafter model-based projections are shown for GMST and GSAT.

[END BOX TS.1, FIGURE 1 HERE]

[START BOX TS.1, TABLE 1 HERE]

Box TS.1, Table 1: The impact of using GMST versus GSAT for selected key metrics. The observed warming estimates are based upon the 3 datasets that extend to 1850 assessed in Chapter 2. The multi-model estimates are based upon the subset of CMIP6 models assessed in Chapter 4 and are the unconstrained ranges. [Discussions remain on whether additional key metrics – e.g. ECS, TCR, carbon budgets for 1.5 and 2°C can be added.

Metric	Value using GMST	Value using GSAT
Observed warming 1850-1900 to 2009-2018	1.06C (0.95 − 1.17C)	1.10°C (0.97 – 1.25°C)
Observed warming 1850-1900 to 1995-2014	0.87°C (0.76 − 0.98°C)	0.91°C (0.78 – 1.05°C)
Multi-model mean warming from 1850-1900 to 2081-2100 under SSP-2-4.5	2.82°C (1.76 – 3.91°C)	2.94°C (1.89 – 3.99°C)
Multi-model mean warming from 1850-1900 to 2081-2100 under SSP-5-8.5	4.60°C (2.84 – 6.40°C)	4.79°C (3.05 – 6.53°C)

[END BOX TS.1, TABLE 1 HERE]

[END BOX TS.1 HERE]

[START TABLE TS.4 HERE]

Table TS.4: Reference periods and baselines used throughout WGI. Paleo periods are listed from oldest to youngest, followed by recent and future reference periods. See Figure TS.2, 2.33 and Cross-Chapter Boxes 1.3 and 2.1 for information on the climate state during these periods.

Period	**Age/year***	**Characteristic climate forcing**
Paleocene-Eocene thermal maximum (PETM)	55.9–55.7 Ma	Carbon cycle: Major transfer of C from lithosphere to atmosphere
Early Eocene climatic optimum (EECO)	53–49 Ma	Paleogeography: Different continental margins and ocean gateways
mid-Pliocene warm period (MPWP)	3.3–3.0 Ma	Carbon cycle and paleogeography: Minor difference relative to now
Last Interglacial (LIG)	129–116 ka	Orbital: Enhanced high-latitude summer insolation
Last Glacial Maximum (LGM)	21–19 ka	Orbital: Diminished high-latitude summer insolation
last deglacial transition (LDT)	18–11 ka	Orbital: Increasing high-latitude summer insolation
mid-Holocene (MH)	6.5–5.5 ka	Orbital: Enhanced high-latitude summer insolation
Medieval Warm Period (MWP)	950–1250 CE	Volcanic and solar
Little Ice Age (LIA)	1450–1850 CE	Volcanic and solar
Pre-industrial	1750 CE	None: year from which anthropogenic influence is measured
Approximate pre-industrial	1850-1900 CE	None: used as an approximate pre-industrial state for global temperature change, and as a historical baseline for other variables
Modern	1995-2014 CE	Anthropogenic: chosen as baseline to present projections
Most recent decade	2009-2018 CE	Anthropogenic
FUTURE PERIODS	**Years**	**Why chosen?**
Near-term future	2021-2040	To inform short term adaptation decisions
Mid-term future	2041-2060	To inform adaptation and mitigation decisions
Long-term future	2081-2100	To inform mitigation decisions
Post-2100	2100 onwards	To inform some risk management strategies

[END TABLE TS.4 HERE]

TS.2 Large scale climate change

This section summarizes knowledge about the drivers of observed and projected large-scale climate change and the attribution of observed changes to human activities. It also describes observed and projected large-scale changes associated with major components of the climate system: atmosphere, ocean, cryosphere, and carbon cycle. In each of the subsections, reconstructed past, observed recent, and projected near- and long-term changes are presented, where possible, in an integrated way. Observed and projected changes in extreme events are described in a separate subsection. The last section presents an integrated assessment of the findings across all climate system components. Two separate boxes outside of this section summarize projected global changes as functions of global warming level and forcing scenarios.

TS.2.1 Changes in drivers of global change

Drivers of the climate system, such as changes in the atmospheric concentrations of greenhouse gases or aerosols, act to modify the net incoming shortwave radiation and / or the longwave radiation emitted to space. The resulting imbalance in the energy flowing in and out of the climate system, which may be quantified using the effective radiative forcing (ERF) (introduced in the AR5 and further assessed in TS.3), leads to climatic changes. In this subsection, evidence for historical changes in key climate system drivers (long-lived GHGs, SLCFs, and natural forcings) is outlined using a combination of direct observations and proxy evidence, while section TS.2.5 assesses the carbon cycle processes and relation of observed changes in CO_2 to emissions and sinks. Section TS.3 assesses the resulting ERF and climate system responses.

Since 1750 concentrations of well-mixed greenhouse gases (CO_2, CH_4, N_2O) have increased at rates unseen in the past 800 ka and are higher than at any point in this period (Figure TS.11). As of 2018, the concentrations had increased since the preindustrial by 129 ± 2 ppm (46%) for CO_2, 1135 ± 7 ppb (157%) for CH_4, and 61 ± 4 ppb (23%) for N_2O (*very high confidence*). In 2018, the three gases reached levels of 407.4 ± 0.3 ppm, 1858.6 ± 3 ppb, and 331.2 ± 0.3 ppb, respectively. Changes from 1750 to present are larger than the multi-millennial change from the last glacial maximum to the Holocene interglacial for CO_2 and CH_4, and are of comparable magnitude for N_2O (*very high confidence*). Current CO_2 concentrations are also unprecedented in the last 2 million years (*high confidence*). There have been times in Earth's history when CO_2 concentrations were much higher than at present, but multiple lines of evidence show with *medium confidence* that the rate at which CO_2 increased in the atmosphere during the Industrial Era has been at least 10 times higher than at any other time during the last 66 million years. {2.2.3, 2.2.4, 5.1.1, Figure 5.1, Figure 5.2}

Atmospheric CH_4 resumed its long-term growth trend in 2007 at an average rate of 7.1 ± 2.7 ppb yr^{-1} for the last decade (2009–2018) (*high confidence).* The concentration of N_2O has increased by 0.80 ± 0.07 ppb yr^{-1} since the 1990s, predominantly driven by the global increase in emissions from the expansion and intensification of agriculture (*high confidence*). Agricultural N_2O emissions have increased by about 80% since the early 1900s, and by 30% since the 1980s. There is *high confidence* that increased use of nitrogen fertiliser and manure contributed to about 70% of the increase during the 1980–2016 period. {5.2.2, 5.2.3}

[START FIGURE TS.11 HERE]

Figure TS.11: Changes in well-mixed Greenhouse gas (WMGHG) concentrations. a) changes in CO_2 from proxy sources over the past 3.5Ma. b) changes in all three WMGHGs from ice core records over the past 800ka with inset changes since the Last Glacial Maximum and over the Common Era respectively. c) Directly observed changes since the mid-20th century. d) Changes in CO_2 over much longer periods and under various SSP scenarios considered in this report including the rate of change which is highly unusual. *[PURPOSE: Main driver of climate system changes over the industrial period, changes exceptional in long-term context. - Includes GHG growth rates: shows that although the paleo perturbations were as large or larger than the anthropogenic one, that the rates were at least an order of magnitude lower.]*

[END FIGURE TS.11 HERE]

Synthetic greenhouse gases consist of CFCs, HCFCs, HFCs and other gases and have only been produced since the industrial revolution. The ERF of synthetic GHGs had increased by 4% from 2011 to 2018, reflecting predominantly a decrease in use of CFCs, overcompensated by an increase in use of their replacements. The concentrations of HFCs are increasing at an accelerating rate (*high confidence*). {2.2.4, 6.2.2}

Radiative effects of atmospheric aerosols are discussed in depth in TS3.1. Atmospheric aerosol concentrations across the Northern Hemisphere mid-latitudes increased since 1700, but have declined in the past 20 years (*medium confidence*). Southern Hemisphere trends prior to the satellite era have *low confidence*. Aerosol Optical Depth (AOD) has decreased since 2000 over the mid-latitude continents of the Northern and Southern Hemispheres, but increased over South Asia and East Africa (*high confidence*). These trends are more pronounced yet in fine-mode AOD. Global carbonaceous aerosol budgets and trends remain poorly characterised due to limited observations but black carbon (BC) is declining in several regions of the world (*low confidence*). {2.2.4, 2.2.5, 2.2.6, 6.2.1, 6.2.2}

Stratospheric ozone has declined between 60˚S - 60˚N from 1980 to 2018 by 2.2% (*high confidence*). The strongest ozone loss in the stratosphere continues to occur in austral spring over Antarctica (ozone hole), with emergent signs of recovery after 2000. Due to discrepancies in satellite and *in situ* records, there is *low confidence* in stratospheric water vapour change. Over the last decade, strong shifting patterns in emissions have led to changes in atmospheric abundances of SLCFs which are highly variable temporally and spatially. Since the 1950s, surface ozone has increased by 30-70% across the Northern Hemisphere and Tropics (*medium confidence*); since the mid-1990s, the decadal increase of free tropospheric ozone has been 2-7 % in northern mid-latitudes, 2-12 % in the tropics (*high confidence*) and <5 % in southern mid-latitudes (*medium confidence*). The oxidising capacity of the troposphere (i.e., global mean abundance of hydroxyl (OH) radical) chemically regulates the lifetimes and therefore the radiative forcing of methane, ozone, secondary aerosols and halogenated species. The oxidising capacity has increased since 1980 primarily driven by increases in anthropogenic nitrogen oxides (NO_x) emissions and decreases in anthropogenic carbon monoxide (CO) emissions (*medium confidence*). There has been little net change in global mean OH since 1850 up to around 1980 (*low confidence*). Over the 1980 to 2015 period, interannual variations in OH have remained within 3% (*high confidence*), suggesting that OH is not the primary driver of recent observed growth in CH_4. {2.2.4, 2.2.5, 2.2.6, 2.2.7, 6.2, Cross-Chapter Box 5.1}

Changes in ERF due to solar and volcanic forcings over the period of instrumental observations are small in comparison to other drivers, and not unusual in the long-term context (*high confidence*). Solar activity since 1900 was high but not exceptional compared to the past 9000 years (*high confidence*). The average magnitude and variability of volcanic aerosol forcing since 1900 has not been unusual when compared to the past 2500 years (*medium confidence*). {2.2.1, 2.2.2}

Since 1750, changes in the drivers of the climate system are dominated by increases in greenhouse gas concentrations that act to warm the Earth system. The concentrations of the three major well-mixed greenhouse gases - CO_2, CH_4, and N_2O - have increased to levels unseen in at least 800 ka. For CO_2 there is *high confidence* that levels as high as today have not been experienced for at least 2 Myr. The concentrations of all three species have changed by almost as much (N_2O) or more (CO_2 and CH_4) in the last 250 years than they did over several thousand years from the last glacial maximum to the present Holocene interglacial. Forcing reductions from declining CFC concentrations have been surpassed by increases in their replacements. The concentrations of anthropogenic aerosols, which mainly act to cool the climate system, globally peaked around 2000 and have slowly declined since, although regionally they continue to increase in South Asia and East Africa (*high confidence*). The decline of stratospheric ozone has ceased in recent years (*high confidence*) while tropospheric ozone concentrations have increased (*medium confidence*). Observed changes in solar insolation and aerosol emissions from volcanic activity have been small in comparison to the anthropogenic drivers and are not unusual in a multi-millenial context (*high confidence*).

TS.2.2 Atmospheric temperature and circulation

This section presents and summarizes assessments of large-scale changes in climate, focusing primarily on temperature changes, including at all levels in the atmosphere and at the surface. These assessments consider observed changes and their attribution to human influences, future changes, and an evaluation of climate models. Precipitation and humidity changes in the atmosphere and at the surface are summarized in subsection TS2.5.

TS.2.2.1 Surface and upper air temperatures

Over the last 50 years, global mean surface temperature (GMST) has increased at an observed rate unprecedented in at least the last two thousand years (*medium confidence*), and it is *about as likely as not* that no multi-centennial period since the last interglacial period (125 ka) was warmer globally than the most recent decade (Figure TS.12). From 1850-1900 to 1995-2014, GMST increased by 0.87°C (0.76°C - 0.98°C), and to the most recent decade (2009–2018) by 1.06°C (0.95°C–1.17°C). The estimated change in global surface air temperature (GSAT) from 1850-1900 to 2009-2018 is 1.10°C (0.97°C - 1.25°C), 4% (2 - 7%) larger than the change in GMST (*high confidence*) (Box TS.1). Each of the last four decades has in turn been warmer than any decade that preceded it since 1850. Temperatures have increased faster over land than over the ocean since 1850-1900, with warming to 2009-2018 of 1.44°C (1.32°C–1.60°C) and 0.89°C (0.80°C–0.96°C), respectively. During the Mid-Pliocene Warm Period, around 3.3-3.0 Ma (million years ago), GMST was 3 ± 1°C warmer, and during the last interglacial period (125 ka), it was 1.5 ± 0.5°C warmer than 1850-1900 (*medium confidence*). {Cross-chapter Box 1.3, 2.3.1, Cross-chapter Box 2.1, Cross-Chapter Box 2.3, Cross-Chapter Box 2.4}

[START FIGURE TS.12 HERE]

Figure TS.12: Earth's surface temperature history with key findings annotated within each panel. (a) Global mean surface temperature over the Common Era (time series) and during three paleo reference periods. Median multi-method reconstruction (black line), with 2.5th and 97.5th percentiles of the ensemble members (grey bands), smoothed with a 31-year low-pass filter. Mean global ground surface temperature reconstruction from borehole temperature profiles (gold line). Mean temperature of three instrumental-based datasets as shown in panel (b) (red line). Large circles are best estimates (bars are ± 2SD) for mid-Holocene, last glacial maximum, and last interglacial period based on the assessment in section 2.3.1.1.1. All temperatures relative to the 1850-1900 reference period. (b) Annually (top panel) and decadally (bottom panel) resolved averages for the 5 GMST datasets assessed in Section 2.3.1.1.3 from 1850 to 2018. The grey shading in each panel shows the uncertainty associated with the HadCRUTv5 estimate. (c) Multi-product mean annual time series for the products assessed in Section 2.3.1.1.3 for SST over the ocean (blue trace) and LSAT over the land (red trace) and indicating the warming in the most recent 10 years compared to the 1850-1900 reference period. (d) Spatially resolved trends (°C per decade) for HadCRUTv5 over 1900-1980 and then 1981-2018. Trends have been calculated where data is present in both the first and last decade and for at least 70% of all years within the period using OLS. Significance is assessed with AR(1) correction and denoted by stippling. *[PURPOSE: The key multi-panel GSAT figure, showing 2000-yr and 170-yr time series, paleo estimates, geographical patterns of recent changes (Arctic & continental amplification).]*

[END FIGURE TS.12 HERE]

The *likely* range of human-induced warming in GSAT in 2010-2019 relative to 1850-1900 of 0.8-1.4°C (Figure TS.13) encompasses the observed warming of 0.97°C - 1.25°C[3], and it is *extremely likely* that human influence is the main driver[4] of the observed warming. The latter assessment is similar to that of the AR5, and balances evidence from studies using new attribution approaches that better account for observational, model and methodological uncertainties, and the strong warming observed since the publication of the AR5, with remaining uncertainty in the magnitude of internal climate variability and its representation in models.

[3] The *likely* range for human-induced warming expressed in terms of GMST is 0.8°C -1.3°C, again encompassing the best estimate and range of observed GMST warming of 1.0-1.2 °C.

[4] In this section and in the underlying chapters, 'main driver' means responsible for more than 50% of the change.

It is also consistent with an estimate of the human-induced GSAT rise based on assessed ranges of ERF, Equilibrium Climate Sensitivity and Transient Climate Response. Over the same period the *likely* range of GSAT warming due to well-mixed greenhouse gas increases from human activities is 0.9°C -2.0°C, and the *likely* range of GSAT change due to aerosols and other anthropogenic forcings is -0.7°C -0.2°C. {3.3.1, 7.3.5, Cross-Chapter Box 7.1}

[START FIGURE TS.13 HERE]

Figure TS.13: Attribution of GSAT evolution (left) and 2010-2019 change relative to 1850-1900 (right) based on assessed ERFs and an emulator (top), and CMIP6 models simulations and attribution studies (bottom). GSAT response to individual forcings simulated by an emulator (Cross-Chapter Box 7.1) with assessed climate system parameters and ERF time series (top left), and temperature change between 1850-1900 and 2010-2019 (top right). Stacked bars show the median temperature response to each individual forcing, and uncertainty ranges show the responses to anthropogenic (ANT), well-mixed greenhouse gas (GHG), other anthropogenic (OTH) and natural (NAT) forcings. Observed GMST and simulated GMST in response to greenhouse gases, other anthropogenic forcings, natural forcings and combined forcings (lower left, modified from FAQ 3.3, Figure 1), and assessed GSAT changes to 2010-2019 relative to 1850-1900, attributable to anthropogenic forcings, well-mixed GHGs, other anthropogenic forcings and natural forcings (lower right, Figure 3.7). Bars labelled 'Chapter 7' correspond to the uncertainty ranges shown in the top right, and are one line of evidence used to derive the assessed attributable GSAT changes shown. Observed GSAT changes are taken from Cross-Chapter Box 2.3. *[PURPOSE: Summary of natural and anthropogenic global climate forcings since 1750, and assessed GSAT responses - Clearly shows human influence on global climate system.]*

[END FIGURE TS.13 HERE]

CMIP6 paleoclimate simulations show comparable biases to those in the previous-generation CMIP5 models for the MH, whereas for the LGM, there is reduced inter-model spread and better agreement with new reconstructions for some diagnostics (*medium confidence*).{3.3.1, 3.8.2, Figure 3.1}

The observed slower GMST increase in the 1998-2012 period was temporary and with *high confidence* induced by variations in solar and volcanic forcing and internal variability, particularly Pacific Decadal Variability that partly offset the anthropogenic warming tendency over this period. Global upper to mid (0 to 2000 m) ocean heat content, which represents more than 90% of the Earth's energy imbalance continued to increase throughout this period (*very high confidence*). Using updated observational data sets and like-for-like comparison of simulated and observed GMST, all observed estimates of the 1998-2012 trend lie within the 5-95% range of CMIP6 trends. Therefore, the observed 1998-2012 trend is consistent with the CMIP6 multi-model ensemble of trends over the same period (*high confidence*). Since 2012, GMST has warmed strongly, with the past five years (2014-2018) being the hottest five-year period between 1850 and 2018 (*high confidence*). {3.3.1, 3.5.1, Cross-Chapter Box 3.1}

Near-term (2021-2040) projections of the evolution of the climate system depend only weakly on the forcing scenario (see Table TS.5). More detail, assuming that there will be no large volcanic eruption in the near term, is provided in Cross-section Box 1. As assessed in Cross-section Box 2, the best estimate for reaching a global warming level of 1.5°C – neglecting the influence of natural internal variability – is around 2030, across all scenarios.

The assessment of future GSAT changes (see Table TS.5, Figure TS.14 and Cross-Section Box 2) is based on multiple lines of evidence, combining new projections for the SSP scenarios with observational constraints based on past simulated warming as well as the AR6-updated assessment of equilibrium climate sensitivity and transient climate response. Including lines of evidence in addition to the projection simulations has been possible through substantial research progress since previous IPCC assessments and has both reduced the assessed uncertainty ranges and increased the confidence in them. There is *very high confidence* that the uncertainties in equilibrium climate sensitivity and transient climate response dominate the uncertainty ranges at this time scale for a given scenario. {2.3.1, 3.3.1, 4.5.1}

[START FIGURE TS.14 HERE]

Figure TS.14: Lines of evidence for assessed GSAT. (a) CMIP6 annual-mean GSAT simulations and various contributions to uncertainty in the projections ensemble. The figure shows anomalies relative to the period 1995–2014 (left y-axis), converted to anomalies relative to 1850–1900 (right y-axis); the difference between the y-axes is 0.91°C. Shown are historical simulations with 29 CMIP6 models (grey) and projections simulations following scenario SSP2-4.5 (dark yellow). The cyan curve shows the observations (HadCRUT5, (Morice et al., 2020)). The black curve and dark shading show, respectively, the central estimate and *very likely* range of assessed 20-year averaged future GSAT change. Light blue shading shows the contribution of internal variability to annual-mean GSAT change; the shading is based on the 50-member ensemble CanESM5 such that the deviations from the CanESM5 ensemble mean have been added to the central estimate of assessed GSAT change. The inset shows a cut-out from the main plot and additionally for the period 2019–2028 in purple, green, and blue the initialised prediction ensembles from three models contributing to DCPP (Boer et al., 2016); solid curves show the ensemble means and shading the range of each prediction system. (b) Raw CMIP6, historically constrained CMIP6, emulator, and assessed GSAT changes for the long-term period, 2081–2100, relative to the average over 1995–2014 (left y-axis) and 1850–1900 (right y-axis); the y-axes differ by 0.91°C. The emulator ranges are defined through choices for climate feedback parameter and ocean heat uptake coefficient such that the best estimate, lower bound of the *very likely* range, and upper bound of the *very likely* range of the emulator ECS and TCR take the corresponding values of AR6-assessed ECS and TCR. The assessed ranges (horizontal black lines and grey boxes) are constructed by taking the average of the constrained CMIP6 estimates (blue bars) and the emulator estimates (green bars). (c) Multi-model mean change in annual-mean near-surface air temperature (°C) in 2041–2060 and 2081–2100 in (top) SSP1-2.6 and (bottom) SSP5-8.5 relative to 1995–2014. Stippling indicates regions where the multi-model mean change exceeds two standard deviations of pre-industrial internal variability and where at least 90% of the models agree on the sign of change, as a measure of robustness. Hatching indicates regions where the multi-model mean signal is less than one standard deviation of internal variability. {1.3, 2.3, 4.3, Box 4.1, 7.5} *[PURPOSE: This figure shows time series, period differences, and maps of GSAT following multiple lines of evidence. The multiple lines of evidence are raw CMIP6 projections, historically constrained CMIP6 projections, initialized predictions, and emulator results (Cross-Chapter Box 7.1). This figure combines Box 4.1 Figure 1, Figure 4.9, and Figure 4.21.]*

[END FIGURE TS.14 HERE]

[BEGIN TABLE TS.5 HERE]

Table TS.5: Assessment results for GSAT change, based on multiple lines of evidence. The change is displayed in °C relative to the 1995–2014 reference period for selected time periods (near term 2021–2040, mid-term 2041–2060, and long-term 2081–2100), and as the time when certain temperature thresholds are crossed, relative to the period 1850–1900. The observed warming in 1995–2014 relative to 1850–1900 is 0.91°C (0.78–1.05°C) (Box TS.1, Table 1). The timing of crossing a threshold does not include the uncertainty arising from natural internal variability. The entries give both the best estimate and, in parentheses, the *very likely* (5–95%) range. There is *high confidence* in the changes over the twenty-year periods relative to 1995–2014, which combine constrained CMIP6 projections and emulator results (Cross-Chapter Box 7.1). There is *medium confidence* in the timings when certain global warming levels are reached, which are based on a combination of emulator results and one set of constrained CMIP6 projections for SSP1-2.6, SSP2-4.5, and SSP5-8.5 but solely on emulator results for SSP1-1.9 and SSP3-7.0. An entry n.a. means that the global warming level is not attained during the period 2021–2100. [Note: This table is identical to Table 4.6 in Section 4.3.4, where the timing entries for when certain global warming levels are reached use the GMST instead of GSAT change, from 1850–1900 to 1995–2014. The table thus assumes an offset of 0.86°C, rather than 0.91°C, between these two time periods. The table will be updated with the proper GSAT offset in the FGD.] *[PURPOSE: Assessed GSAT changes. Complements Figure TS.14. Central look-up table for assessed warming.]*

	SSP1-1.9	SSP1-2.6	SSP2-4.5	SSP3-7.0	SSP5-8.5

Near term, 2021–2040, relative to 1995–2014	0.7 (0.4, 0.9)	0.6 (0.4, 0.8)	0.7 (0.4, 0.9)	0.7 (0.4, 0.9)	0.7 (0.5, 1.0)
Mid-term, 2041–2060, relative to 1995–2014	0.8 (0.5, 1.1)	0.9 (0.6, 1.2)	1.1 (0.8, 1.5)	1.3 (0.9, 1.8)	1.6 (1.1, 2.0)
Long-term, 2081–2100, relative to 1995–2014	0.6 (0.3, 0.9)	1.0 (0.6, 1.4)	1.9 (1.3, 2.5)	2.9 (2.0, 3.8)	3.6 (2.6, 4.7)
1.5°C, relative to 1850–1900	2028 (2022, n. a.)	2033 (2024, 2053)	2031 (2024, 2042)	2029 (2023, 2038)	2028 (2022, 2036)
2°C, relative to 1850–1900	n.a. (n.a., n.a.)	n.a. (2047, n.a.)	2050 (2040, 2073)	2046 (2036, 2060)	2042 (2035, 2051)
3°C, relative to 1850–1900	n.a. (n.a., n.a.)	n.a. (n.a., n.a.)	n.a. (2074, n.a.)	2074 (2058, 2098)	2064 (2054, 2078)
4°C, relative to 1850–1900	n.a. (n.a., n.a.)	n.a. (n.a., n.a.)	n.a. (n.a., n.a.)	2100 (2079, n.a.)	2082 (2069, 2100)

[END TABLE TS.5 HERE]

The CMIP6 multi-model ensemble range of projected GSAT increase by the end of the 21st century, relative to the period 1995-2014, is approximately 20% larger than the CMIP5 range. The range increases mainly because the upper end of the projected warming range increases, due to models with higher equilibrium climate sensitivity in CMIP6, compared to CMIP5 (*high confidence*). {4.3.1, 4.3.4, 7.6}

It is *virtually certain* that the average warming over land will be higher than over the ocean in the period 2081-2100. It is *very likely* that the warming in the Arctic will be more pronounced than in the global average over the 21st century. The warming pattern *likely* varies across seasons with northern high latitudes warming more during boreal winter than summer (*medium confidence*). Models project regions with increasing and decreasing year-to-year variability of seasonal mean temperatures. {4.5.1}

The troposphere has warmed since at least the 1950s and it is *virtually certain* that the stratosphere has cooled. It is *very likely* that human influence, dominated by greenhouse gases, was the main driver of warming of the troposphere since the start of comprehensive satellite observations in 1979, and *extremely likely* that human influence, dominated by stratospheric ozone depletion, was the main driver of the cooling of the lower stratosphere since 1979. It is *very likely* that projected long-term tropospheric warming will be larger than the global mean in the Arctic lower troposphere and near surface. It is *very likely* that global mean stratospheric cooling will be larger for scenarios with higher atmospheric CO_2 concentrations. In the tropics the upper troposphere has warmed faster than the near-surface since at least 2001 when new techniques permit more robust quantification (*medium confidence*). There is *medium confidence* that most CMIP5 and CMIP6 models overestimate observed warming in the upper tropical troposphere during the satellite era. Based on the latest updates to satellite observations of stratospheric temperature, simulated and observed changes of global mean temperature through the depth of the stratosphere are more consistent than based on previous datasets, but some differences remain (*medium confidence*). It is *likely* that tropical upper tropospheric warming will be larger than at the tropical surface. It is *virtually certain* that the tropopause height has risen over 1980-2018, but there is *low confidence* in the magnitude. {2.3.1, 3.3.1, 4.5.1}

TS.2.2.2 Tropospheric circulation

The Hadley Circulation has *very likely* widened and intensified since at least the 1980s, mostly in the Northern Hemisphere. Since the 1980s, global monsoon intensity has *likely* increased, being dominated by

Northern Hemisphere summer trends (*medium confidence*). There is *medium confidence* that greenhouse gas increases and stratospheric ozone depletion have contributed to the expansion of the zonal mean Hadley cell in the Southern Hemisphere since around 1980. However, the expansion of the zonal mean Hadley cell in the Northern Hemisphere and changes in the Pacific Walker circulation strength have not exceeded the range of internal variability (*medium confidence*). {2.3.1, 3.3.3}

Since the 1970s near-surface winds have *likely* weakened over land. Over the ocean, near-surface winds *likely* strengthened over 1980-2000, but divergent estimates lead to *low confidence* thereafter. Extratropical storm tracks have *likely* shifted poleward since the 1980s, and the present Northern Hemisphere storm track positions are similar to those in both the mid-Holocene (*low confidence*) and the Medieval Warm Period (*medium confidence*). There is only *low confidence* about how the Northern Hemisphere storm tracks have been influenced by anthropogenic forcings given the multiple drivers and complex interplay between climate change and internal climate variability over the North Atlantic and North Pacific. There is only *low confidence* for the poleward shift of Northern Hemisphere mid-latitude jet and storm tracks in the long-term relative to the recent past under SSP5-8.5 due to large natural variability and structural differences amongst models. {2.3.1, 3.3.3, 4.3.3, 4.4.3, 4.5.1, 4.5.3, 8.2.2, 8.3.2}

There is *high confidence* that Southern Hemisphere storm tracks and associated precipitation have migrated polewards over recent decades, especially in the austral summer and autumn. There is *high confidence* that human influence has contributed to this observed poleward shift in austral summer. While ozone depletion was the main driver of the trend in the closely related SAM index in summer over 1980-2000 (*high confidence*), its influence was reduced after ~2000 because stratospheric ozone no longer declined, resulting in comparable contributions from long-lived GHG and ozone changes to trends over the 1979-2014 period. In the near term (2021-2040), natural internal variability will *likely* obscure forced trends in the Southern Hemisphere summertime mid-latitude circulation because of the opposing influences from stratospheric ozone recovery and increases in other greenhouse gases. In the long-term (2081-2100), models project a poleward shift and strengthening of the Southern Hemisphere mid-latitude jet under SSP5-8.5 relative to the recent past (1995-2014, *medium confidence*). It is *likely* that wind speeds associated with extratropical cyclones will intensify in the Southern Hemisphere storm track for high-emission scenarios. {2.3.1, 3.3.3, 3.7.2, 4.3.3, 4.4.3, 4.5.1, 4.5.3, 8.2.2, 8.3.2}

Models capture the general characteristics of the tropospheric circulation, including monsoons. Systematic errors are, however, still present, for example in the frequency of blocking events in the North Atlantic, and rainfall associated with monsoons. {3.3.3, 3.7.2}

TS.2.2.3 Summary of atmospheric temperature and circulation changes

The effects of human-induced climate change have been clearly identified in observations of atmospheric temperature and circulation, and these effects are projected to intensify in the future. Global mean surface air temperature has increased by 1.10°C (*very likely* range of 0.97°C - 1.25°C in 2009-2018 relative to 1850-1900), driven by greenhouse-gas induced warming *(likely* range 0.9°C - 2.0°C) and partly offset by the response to aerosols and other anthropogenic forcings (*likely* range -0.7°C - 0.2°C). Future emissions choices will impact changes in climate over the remainder of the 21st century. While additional future warming is projected to be less than the observed warming since 1850 under a low emissions scenario (*very likely* 0.3°C–0.9°C under SSP1-1.9 in 2081-2100 relative to 1995-2014), it is projected to be two to four times the observed warming under a high emissions scenario (2.6°C–4.7°C under SSP5-8.5). It is *virtually certain* that this warming will be stronger over land than ocean and *very likely* that it will be stronger over the Arctic than the rest of the globe. Several aspects of the atmospheric circulation have *likely* changed since the mid-20th century, including broadening of the Hadley Circulation and a poleward shift of extratropical storm tracks. In the Southern Hemisphere, there is *medium confidence* that human influence has contributed to the observed circulation changes.

[START BOX TS.2 HERE]

Box TS.2: Low-probability, high-warming storylines

Previous IPCC reports have focused their assessment on the projected *likely* range of changes. However, an integrated risk assessment requires considering also high potential levels of warming whose probability is low, but potential impacts on society and ecosystems are high (Box TS.2 Figure 1). A too narrow focus on the *likely* range potentially ignores the largest changes in the physical climate system that are *unlikely* yet plausible, and potentially associated with the highest risks. {4.8}

[START BOX TS.2, FIGURE 1 HERE]

Box TS.2, Figure 1: Illustrating concepts of low-likelihood, high impact events. The colours indicate the additional risk due to climate change using the Reasons For Concern (see IPCC AR5 WGII SPM), specifically RFC1 describing the risks to unique and threatened systems. The likelihood of additional risks assuming radiative forcing follows the assessed GSAT change under the SSP2-4.5 scenario. *[PURPOSE: To illustrate the concepts of low-likelihood, high-impact events.]*

[END BOX TS.2, FIGURE 1 HERE]

The upper end of the projected warming range increases, due to models with higher equilibrium climate sensitivity in CMIP6, compared to CMIP5 (*high confidence*). {4.3.1, 4.3.4, 7.6}. Here we use the assessed range of GSAT rather than the raw output of unconstrained projections. Low-probability high-warming storylines are here assessed for a level of warming consistent with the upper bound of the assessed *very likely* range. The warming consistent with the upper bound of the assessed *very likely* range corresponds to a warming of 4.6°C in 2081–2100 relative 1995–2014 for SSP5-8.5 and 1.4°C for SSP1-2.6 (drawn from {4.8}). CMIP6 models with warming levels consistent with the upper bound and beyond are *very unlikely* but cannot be excluded. Note that by definition the lower bound of the *likely* model range is equally probable but is not highlighted here given the focus on storylines associated with highest risks.

Low-probability high-warming storylines consistent with *very unlikely* high warming rates show patterns of large wide-spread temperature and precipitation changes that strongly exceed the multi-model mean in all scenarios. Even for SSP1-2.6, a high-warming storyline shows 2-3°C warming over much of Eurasia and North America and more than 4°C warming relative to present-day over the Arctic (Box TS.2, Figure2). For SSP5-8.5 a high-warming storyline is associated with wide-spread warming of more than 6°C over most extra-tropical land regions and even over parts of the Amazon. Over large parts of the Arctic annual mean temperatures increase by more than 10°C relative to present-day in such a high-warming storyline.

Furthermore, high-warming storylines are *very likely* also associated with changes in the hydrological cycle that substantially exceed the multi-model mean. Quantifying precipitation changes associated with high-warming storylines is challenging as models with the most pronounced GSAT warming are not necessarily associated with the strongest precipitation response in all regions. The multi-model mean response pattern shows a smoother pattern than in individual simulations since model differences in the location of the largest changes tend to cancel each other. Models with GSAT warming consistent with or exceeding the upper bound of the assessed *very likely* warming range show a much larger area fraction of drying and tend to project a larger fraction of strong precipitation increases than the multi-model mean {4.8}.

[START BOX TS.2, FIGURE 2 HERE]

Box TS.2, Figure 2: (a,c) CMIP6 multi-model mean and (b,d) low-probability high-warming storyline for annual mean temperature change in 2081–2100 relative to 1995–2014 in (a,b) SSP1-2.6 and (c,d) SSP5-8.5. The low-probability high-warming for 2081–2100 corresponds to multi-model average across the five models with GSAT warming nearest to the upper bound of the assessed *very likely* range. (e,f) Area fraction of changes in (e,g) annual mean precipitation and (f,h) precipitation minus evapotranspiration (P-E) in 2081–2100 relative to 1995–2014 in (e,f) SSP1-2.6 and (g,h) SSP5-8.5 for individual model simulations (thin black lines) and high-warming storylines with GSAT warming near the upper bound (thin red lines) and exceeding the upper bound (thin brown lines). The grey range illustrates the 5–95% range across CMIP6 models and the thick black line the area fraction of the multi-model mean pattern. *[PURPOSE: To illustrate high warming storylines compared to the CMIP6 multi-model-mean.]*

[END BOX TS.2, FIGURE 2 HERE]

[END BOX TS.2 HERE]

TS.2.3 The Ocean

Observations, models and evidence from the paleo-record indicate that the recent changes in the ocean are exceptional; many highlight the role of the ocean in stabilizing the Earth's climate through the carbon, water and energy cycles. The sea surface temperature and ocean heat content consistently increase over the period where sufficient observations are available, and model projections indicate that these trends will continue even under strong mitigation of greenhouse gas emissions, leading to substantial committed ocean climate change. While the surface ocean respond quickly through direct interactions with the changing atmosphere and cryosphere, the deep and abyssal ocean are linked to the surface by circulations that take centuries or millennia to spread change, resulting in a much slower response to climatic forcing. The rate of thermosteric sea level rise due to expanding deep waters is slow and persistent for the same reason (Box TS.3), and a breakthrough in this report is closing the observed budget for sea level and energy contributions consistently, indicating that the present monitoring system is able to quantify the important processes. Major changes to circulations have not yet been observed, but may be anticipated for some currents, such as the Atlantic Meridional Overturning Circulation, in coming centuries under strong forcing scenarios (Box TS.3). The acidification and de-oxygenization of the ocean is ongoing and these changes, combined with increasing temperatures, are having important impacts on ocean biology and ecosystems (see SROCC).

In the open and deep ocean, changes are projected for sea surface temperature, heat extremes, waves, sea ice extent, oxygen and acidity. {12.4.8}

[START FIGURE TS.15 HERE]

Figure TS.15: Key recognizable indicators of oceanic climate change. *[Purpose: Immediately meaningful indicators of ocean changes from a global perspective: observed trends and projections of marine heat waves, Arctic sea ice, pH. Could include O_2 change as well (From Figure 5.21; Cross-Chapter Box 9.1, Figure 1; 9.15). Placeholder for more simplified statistics.]*

[END FIGURE TS.15 HERE]

TS.2.3.1 Temperature, heat content and energy budget

The global ocean has warmed since at least 1971 when globally representative measures are available. It is warming faster now than implied by centennially resolved proxy records at any point since at least the last deglacial transition (*medium confidence*). Updated observations and model simulations both show warming that extends throughout the entire water column (*high confidence*), and warming is largest in the Southern Ocean and the North Atlantic. It is *extremely likely* that anthropogenic forcing has made a substantial contribution to the ocean heat content (OHC) increase over the historical period that extends into the deeper ocean (*high confidence*), resulting in a *likely* global mean thermosteric sea-level rise of 0.04 ± 0.01 m over the period 1971-2015. At the sea surface, it is certain that global sea-surface temperature has increased since the beginning of the 20th century at a *very likely* rate of 0.053 ± 0.002°C, which increased to 0.087±0.007°C since 1979. This surface warming has been associated with an increased frequency (*high confidence*) and persistence (*medium confidence*) of marine heatwaves since 1982, which are discussed in TS2.6. {Figure TS.15, 2.3.3, 2.3.4, Cross-Chapter Box 2.4, 3.5.1, 9.2.1, 9.2.2, 9.2.4, 9.6.1, 9.6.3, 9.6.4, Cross-Chapter Box 9.1}

The ocean will continue to warm over the 21st century (very high confidence), and it is *likely* that this warming will continue at least to 2300 even for low emission scenarios because of ocean inertia, but with a rate dependent on the scenario (Figure TS.16). The current ocean state is unprecedented for centuries to millennia for some indicators (*high confidence*). It is warming faster now than implied by centennially resolved proxy records at any point since at least the last deglacial transition (*medium confidence*). Over years to a decade, regional heat patterns are dominated by internal and circulation variability that does not affect global heat content while at longer time-scales the pattern is dominated by additional heat gained at the surface changing water-masses. These longer time-scale processes commit the ocean to *virtually certain* warming until 2040 regardless of emissions. After 2040, similar spatial patterns of present warming will continue to warm at a rate dependent on present and future emissions (*high confidence*). Between 1996-2014 and 2100, the global mean thermosteric sea-level rise associated with ocean heat uptake is *likely* to be 0.15 (0.13-0.17) m for SSP1-2.6, 0.19 (0.17-0.22) m for SSP2-4.5, 0.24 (0.23-0.26) m for SSP3-7.0, and 0.29 (0.28-0.31) m for SSP5-8.5. At the sea surface, it is *virtually certain* that global mean SST will continue to increase throughout the 21st century, resulting in the exceedance of many hazard thresholds relevant to marine ecosystems (*medium confidence*). {2.3.3, 2.3.4, Cross-Chapter Box 2.4, 9.2.2, 9.2.4, 9.6.1, 9.6.3, 9.6.4, Cross-Chapter Box 9.1, 12.4.8}.

TS.2.3.2 Salinity

It is *virtually certain* that near-surface ocean salinity spatial patterns are more pronounced (fresh waters get fresher, saltier waters get saltier) since at least 1950, consistent with an enhanced hydrological cycle (*medium confidence*). It is *extremely likely* that human influence has contributed to this surface ocean change as well as change in the subsurface ocean. Across basins, the Atlantic has become saltier and the Pacific and Southern ocean have freshened (*very likely*). Changes to the coincident atmospheric water cycle and ocean-atmosphere fluxes (evaporation and precipitation) are the primary drivers of the basin-scale observed surface salinity changes (*high confidence*) with changes to water masses in the subsurface ocean reflecting the changed conditions at the surface locations where they were previously. The observed depth-integrated basin-scale salinity changes have been attributed to anthropogenic forcing, with CMIP5 models able to reproduce these patterns only in simulations that include greenhouse gases (*medium confidence*). Future projections reproduce the “fresh waters get fresher, salty waters get saltier” paradigm on large scales (*high confidence*), including complex regional changes resulting in stronger freshening of the Pacific, Indian and Southern Ocean, with a saltier subtropical Atlantic (*medium confidence*) {2.3.3, 2.3.4, Cross-Chapter Box 2.4, 3.5.2, Cross-Chapter Box 2.4, 9.2.1, 9.2.2, 12.4.8}.

TS.2.3.3 Circulation

Direct observations show the Atlantic Meridional Overturning Circulation (AMOC) has weakened since at least the mid 2000s (*high confidence*). There are indicators of AMOC weakening during the 20th century, but *confidence is low* due to large method uncertainties and superposed multidecadal variations. While, the observational record is not long enough to determine if these changes are due to internal variability solar and volcanic forcing or a response due to anthropogenic forcing, the AMOC will *likely* decline in response to human-induced climate change for all future scenarios. Projected AMOC decline by 2100 is only weakly dependent on emission scenario ranging from 40% in SSP1-1.9 to 50% in SSP5-8.5 (*medium confidence*). An abrupt collapse of the AMOC before 2100 is *unlikely* with deep uncertainty beyond 2100 associated with meltwater fluxes from Greenland and Antarctica. {2.3.3, 2.3.4, Cross-Chapter Box 2.4, 3.5.4, 9.2.3}

Detecting long-term changes in other large-scale circulation systems remains challenging due to observation limitations, but the Southern Ocean overturning circulation, eastern boundary upwelling systems and Indonesian Throughflow are predicted to respond to changes in the atmospheric circulation (*high confidence*). Southern Ocean upper ocean will enhance as a result of intensifying winds (*medium confidence*). Upwelling favourable winds in eastern boundary upwelling systems will change with a dipole spatial pattern within each system, shortening and reducing upwelling on poleward-side, and enhancing and lengthening upwelling on equatorward-side (*high confidence*). The Indonesian Throughflow is projected to decline on the centennial time scale by most models as a response of wind change {9.2.3}.

TS.2.3.4 Ocean changes by depth

There is *high confidence* that the observed ocean heat content increase from 1970s to 2018 is distributed with 60% in the 0–700m layer, 30% in the 700–2000m layer and 10% in the 2000–6000m layer, consistent with models partitioning industrial-era (1865 to 2017) heat uptake. The vertical structure of ocean warming and salinity change reflects water mass formation processes and ocean circulation, explaining the largest changes at depth are observed in the Southern Ocean and North Atlantic Ocean. Surface-intensified temperature and salinity changes have increased the stability of the upper ocean stratification. New analysis shows that surface ocean stratification has increased from 1970 to 2018 at the rate of 5–20% per decade, more than ten times higher than reported by SROCC (*medium confidence*). Observed near-surface ocean changes and associated regional patterns are predicted to persist at a rate dependent on emissions (*high confidence*), and in consequence, upper ocean stratification will continue to increase in the 21st century {3.5.1, 9.2.1, 9.2.2, 9.2.4, 9.6.1, 9.6.3, 12.4.8}.

TS.2.3.5 Ocean pH (acidification), de-oxygenation, and ocean carbon sink

It is *virtually certain* that the uptake of anthropogenic CO_2 has substantially contributed to the acidification of the global ocean (Figure TS.15). This uptake is driving changes in seawater chemistry that results in the decrease of pH and associated reductions in the level of calcium carbonate minerals that form skeletons or shells of a variety of marine organisms. These trends of ocean acidification are becoming clearer globally with a *very likely* range of 0.017 to 0.027 decrease in pH units per decade since the late 1980s in the ocean surface layer (*high confidence*). There is *very high confidence* that surface pH values as low as today have not been experienced in the last two million years. Ocean acidification is spreading downward into the ocean interior over time, having already reached depths surpassing 2000 meters. The observed increase in CO_2 concentration in the subtropical and equatorial North Atlantic since mid-2000 is *likely* in part associated with an increase in ocean temperature, a response that corresponds to the expected weakening of the ocean carbon sink with warming. {2.3.3, 2.3.4, Cross-Chapter Box 2.4, 3.6.2, 5.3.2, 5.3.3, Figure 5.20, Figure 5.21}

Deoxygenation has occurred in the upper kilometre of open ocean since 1970, alongside an expansion of the volume of oxygen minimum zones (*medium confidence*). Consistent with the AR5 there is *medium confidence* that deoxygenation in the surface ocean is due in part to anthropogenic forcing. Future ocean warming will assist the development of hypoxic or minimal oxygen zones {Figure TS.16, 2.3.3, 2.3.4, Cross-Chapter Box 2.4, 3.6.2, 12.4.8}.

During the 21st century, there is a *high confidence* that de-oxygenation will continue, and that the ocean will further acidify as CO_2 levels continue to rise (Figure TS.16). Earth system models project significant and irreversible changes that start to occur in polar regions within the next 15 years, as surface waters begin to become seasonally undersaturated with respect to aragonite. This is *very likely* to occur in Southern Ocean surface waters by 2030 under all concentration pathways except very low RCP2.6. For de-oxygenation, model estimates predict a further loss of ocean oxygen content of 2–4% until year 2100, with a peak de-oxygenation a thousand years after the stabilization of radiative forcing. {5.3.3, 5.4.8}

[START FIGURE TS.16 HERE]

Figure TS.16: [Preliminary – – From SROCC Figure 1.5 to be expanded in the FGD to include ocean heat content (2 y-axis to include pot'l temperature change), SST, and pH in same format as sea level (paleo, obs, historical, projections] *[PURPOSE: Ocean summary figure (excl. sea level, which appears in Box TS.3). Observed, simulated present, projected changes of globally relevant non-sea-level ocean variables.]*

[END FIGURE TS.16 HERE]

TS.2.3.6 Summary of ocean changes

The observed changes in the ocean are unprecedented over recent millennia. The changing state of ocean heat content and pH indicate the important role of the ocean in the energy and carbon budgets. The more rapid changes observed near the ocean surface illustrate the slow transmission of the planetary warming signal into the deeper ocean through ocean circulations. Sea surface temperature has changed more rapidly than depth-averaged temperature, but with greater variability. Sea surface salinity changes provide independent evidence for substantial changes in the water cycle. The increasing near-surface warming, ocean acidification, salinity changes, and increasing stratification are all manifest in the ocean photic zone, indicating the potential for important biological impacts associated with these changes, as discussed in the SROCC. As deeper waters become increasingly affected by changes circulating downward from the surface, slow changes to ocean circulation and sea level (Box TS.3) will continue for centuries after surface anthropogenic forcing ceases. There is substantial paleo-evidence of abrupt collapse of ocean circulations and the coupled ocean–cryosphere systems, leading to significant sea level rise (Box TS.4). Higher emissions scenarios increase the probability of substantial systematic changes in ocean circulation over the 21st century and the likelihood of abrupt changes in the coming centuries, with important consequences for large-scale climate change.

TS.2.4 Cryosphere

Cryospheric components of the climate system (sea ice, ice sheets, glaciers, seasonal snow, frozen ground, and lake and river ice) are sensitive indicators of climate change and active elements of the system associated with important positive feedbacks. Ice sheets and glaciers are large freshwater reservoirs and key contributors to both observed and projected global sea level change. This section summarizes current knowledge about observed changes, including proxy evidence, their causes and projected changes for sea ice, ice sheets, glaciers, permafrost and seasonal snow. Findings related to the cryosphere in this report build on the 2019 Special Report on the Ocean and Cryosphere in a Changing Climate (SROCC) and take into account results of recent model intercomparison exercises, among other results published since SROCC.

TS.2.4.1 Sea ice extent/area and thickness

SROCC stated with *medium confidence* that pan-Arctic sea ice loss is unique during the past 1000 years Arctic sea ice has retreated and seasonal area has declined consistently since 1979 (Figure TS.15, Figure TS.17a). No significant trend in overall Antarctic sea ice is detected from 1979 to 2018 (Figure TS.17b). Arctic summer sea ice area averaged over the last decade was the lowest since at least 1850. {2.3.2, 3.4.1, 9.3.1, 9.3.2}

Human activities have *very likely* induced at least half of Arctic summer sea ice loss since 1979. Arctic sea-ice area in all months is linearly related to global mean atmospheric temperature and cumulative anthropogenic CO_2 emissions, which implies no tipping point for the loss of Arctic summer sea ice. In the Arctic, despite large differences in the mean sea ice state, loss of sea ice extent and thickness during recent decades is captured by all CMIP5 and CMIP6 models. By contrast, global climate models generally capture neither the observed increase in Antarctic sea ice extent during 1979-2015 nor the reduced sea ice extent observed since 2016, and there is *low confidence* in the possible causes of these changes. Slight Antarctic regional increases or decreases in ice area result from regional wind forcing (*medium confidence*), and projections require accurate modelling of regional variations (*high confidence*). Limited model resolution and poorly understood regional processes infer *low confidence* in regional projections of Antarctic sea-ice area (Figure TS.17b). {3.4.1, 9.3.1, 9.3.2}

Following the SSP2-4.5, SSP3-7.0, and SSP5-8.5 scenarios, it is *likely* that the Arctic Ocean will become effectively ice-free (coverage below 1 million km^2) in September averaged over 2081–2100 (*high confidence*), as shown in Cross-section Box 2, Figure 1c. The vast majority of CMIP6 simulations show an ice-free Arctic in September before cumulative anthropogenic CO_2 emissions reach 1000 $GtCO_2$ (*high confidence*). {3.4.1, 4.3.2, 9.3.1, 9.3.2, 12.4.8}

[START FIGURE TS.17 HERE]

Figure TS.17: Observed, simulated and projected relative changes of cryospheric components of the climate system. a) March (late winter, close to annual maximum) Arctic sea ice anomaly (reference period: 1979-2018); b) September (late winter, close to annual maximum) Antarctic sea ice anomaly (reference period: 1979-2018); c) Northern hemisphere spring (April to June average) seasonal snow extent (reference period: 1995-2014); d) global volume of permafrost in the top 3 m below the surface (reference period: 1995-2014). Observations shown where available. *[PURPOSE: Shows that observed losses occur across all major cryosphere components (except Antarctic sea ice), and that models reproduce this loss where it occurs. Shows that projected cryospheric loss is consistent across cryosphere elements & highly scenario-dependent. Complement for glaciers and ice sheets in sea level box. Antarctica (not shown here, but in sea level box) is the only cryospheric component that isn't highly scenario-dependent on a 100-yr time scale (at least in current models)].*

[END FIGURE TS.17 HERE]

TS.2.4.2 Snow cover, permafrost and glaciers

Northern hemisphere spring snow cover has been decreasing since at least 1978 (*very high confidence*), and the snow onset season has been delayed (*medium confidence*). Further decrease of Northern Hemisphere seasonal snow cover is *virtually certain* (Figure TS.17c). There is *medium confidence* that Northern hemispheric spring snow-cover loss trend extends back to the 1920s. Reductions in spring snow cover extent have occurred across the Northern Hemisphere since at least 1978 (*very high confidence*) and mountain snow cover has decreased since 1950 globally. Northern hemisphere spring snow area changes are proportional to northern hemisphere extratropical land surface air temperature changes at $(-1.9 \pm 0.9) \times 10^6$ km^2 per °C. {2.3.2, 9.5.3}

It is *very likely* that anthropogenic influence contributed to the observed reductions in Northern Hemisphere springtime snow cover since 1950. The seasonal cycle in Northern Hemisphere snow cover is better reproduced by CMIP6 than CMIP5 models. Projected snow cover sensitivity to GSAT on multi-decadal time scales is about -2×10^6 km^2 per °C from November to May (*high confidence*) {Cross-section Box TS.2 Figure 2, 3.4.2, 9.5.3}

Arctic and mountain permafrost has been lost over recent decades and globally permafrost has warmed by 0.3°C in the last decade (*medium confidence*). Although permafrost currently still persists in areas of the Northern hemisphere where it was absent prior to 3000 years ago, increases in temperatures in the upper 30m over the past three to four decades have been widespread (*high confidence*). Permafrost warming is thus *very likely* a pan-Arctic phenomenon. {9.5.2, 2.3.2, Cross-Chapter Box 2.1, Cross-Chapter Box 2.4}

There is *high confidence* that further global warming will lead to permafrost volume loss (Figure TS.17d). For each °C of warming (up to 4°C above preindustrial level), global permafrost volume in the top 3 m will decrease by about 25% ± 5% (*medium confidence*) (see Cross-Section Box 2, Figure 2). Because current-generation climate models tend to neglect several abrupt physical disturbances impacting frozen ground, it is possible that permafrost decay rates simulated in these models in response to climate change are currently underestimated (*low confidence*). {9.5.2}

Current glacier retreat is global and unprecedented since 1850 (*very high confidence*). The number of glaciers that retreat is highly anomalous in the context of the last 2000 years (*high confidence*). Glaciers *likely* contributed 0.025±0.018 m to sea level rise between 1971 and. Global glacier mass loss since the last decades of the 20th century cannot be explained without human induced warming (*high confidence*). {2.3.2, Cross-Chapter Box 2.1, Cross-Chapter Box 2.4, 3.4.2, 3.4.3, 9.5.1, 9.6.3}

Globally, glaciers are not in equilibrium with current climate and will diminish even if climate stabilizes (*very high confidence*). The magnitude and timing of future global glacier mass loss remains uncertain due to scenario uncertainty, low-resolution GCM forcing, model oversimplification, and limited observations for calibration. Under continued warming, glaciers will be lost globally (see Box TS.3, Figure 1) and regions with small glaciers, such as the European Alps and low latitude mountains, will lose most or all glaciers by

2100 (*high confidence*). It is *likely* that glaciers will contribute 0.07-0.11 m and 0.11-0.18 m to GMSL by 2100 under SSP1-2.6 and SSP5-8.5, respectively. {9.5.1, 9.6.3}

TS.2.4.3 Ice sheet mass and extent

The Greenland ice sheet was smaller than at present during the last interglacial period (*high confidence*) and the mid-Holocene (*medium confidence*). After reaching a recent maximum during the Little Ice Age (between 1450 and 1850), the ice sheet retreated overall, with some decades *likely* close to equilibrium. It is *virtually certain* that the Greenland ice sheet has lost mass since the 1990s and will continue to lose mass. There is *high confidence* that annual mass losses have been consistently negative since the early 2000s. Over the period 1992-2018, Greenland *likely* contributed 0.0106 ± 0.0009 m to sea level rise with surface melt slightly exceeding losses through ice discharge and/or submarine melt. Greenland ice mass loss (Box TS.3, Figure 1) will be mostly due to increased surface melt under all emission scenarios (*high confidence*). For future warming levels between 2°C and 3°C, there is *medium confidence* that the Greenland Ice Sheet will pass a threshold where long-term mass loss becomes irreversible over centennial timescales. It is *likely* that the Greenland ice sheet will contribute 0.07 (0.03 to 0.12) m and 0.13 (0.09-0.19) m to GMSL by 2100 under SSP1-2.6 and SSP5-8.5 respectively. {2.3.2, Cross-Chapter Box 2.1, Cross-Chapter Box 2.4, 9.4.1, 9.4.2, 9.6.3}

It is *very likely* that the Antarctic Ice Sheet has lost mass since at least the early 1990s and *likely* that it will continue to lose mass until the end of the century under all emissions scenarios. The grounded Antarctic Ice Sheet has *likely* contributed 0.0069 ± 0.0014 m to sea level rise over 1992-2018 and loss has accelerated over the last decades (*medium confidence*) dominated by ice discharge over the West Antarctic Ice Sheet and the Antarctic Peninsula. Mass balance has not changed significantly across eastern Antarctica since the onset of modern measurements in the early 1990s, but has decreased rapidly in western Antarctica, accelerating 3-fold since the 1990s (*medium confidence*). Ice shelf basal melting dominates current dynamical losses and will remain the dominant driver of West Antarctic mass losses (*high confidence*). Antarctic snowfall will *likely* increase by about 4-8% per °C of regional temperature change, partially compensating for dynamic losses. There is *high confidence* that Antarctic ice shelf basal melting will increase, but *low confidence* in the projected melt rates. It is *likely* that the Antarctic ice sheet will contribute 0.12 (0.00-0.26) m to GMSL by 2100 with little scenario dependence (Box TS.3, Figure 1), but there is deep uncertainty regarding the Antarctic contribution beyond 2100 linked to potential destabilization of the West Antarctic Ice Sheet. {Box TS.3, 2.3.2, Cross-Chapter Box 2.1, Cross-Chapter Box 2.2, Cross-Chapter Box 2.4, 9.4.1, 9.4.2, 9.6.3, Box 9.3}

TS.2.4.4 Summary of cryospheric changes

In summary, observed loss of cryosphere over recent decades is widespread and consistent with global warming, and several components are now in states unseen in centuries (*high confidence*), as reported in the SROCC. Anthropogenic influence has been identified as the *very likely* dominant cause for the observed reductions of Northern Hemisphere spring snow cover, global glacier mass, and Arctic sea ice. Except for the Antarctic ice sheet, for which a slight mass gain in a warming climate cannot be excluded under strong mitigation scenarios, there is *high confidence* that future warming will lead to reduced extents and/or volumes of all other cryospheric elements of the climate system (sea ice, Greenland Ice Sheet, glaciers, permafrost and seasonal snow cover). Deep uncertainty persists with respect to the evolution of the Antarctic Ice Sheet, in particular due to potential instability of the West Antarctic Ice Sheet. Projected cryospheric changes for different scenarios and warming levels are put into global contexts in Cross-section Box 1 and Cross-section Box 2.

[START BOX TS.3 HERE]

Box TS.3: Sea Level

Global sea-level change is driven by changes in ocean density through temperature change and changes in the ocean mass as a result of changes in the cryosphere or the terrestrial water storage. Regional sea-level change is associated with the circulation and density-driven changes in the ocean, redistribution of mass between terrestrial ice and water reservoirs and the ocean and vertical land motion. Extreme sea levels arise from a combination of surges, tides, and waves, superimposed on the local sea-surface height.

Sea-level projections in the AR6 are updated from those provided in SROCC with contributions to sea level change estimated from the latest model projections described in the ocean and cryosphere sections (TS2.3 and TS2.4). Sea-level has a longer timescale response to greenhouse gas emissions than surface temperature, leading to a weaker scenario-dependence over the 21st century than GSAT and long-term committed sea-level rise associated with ongoing ocean heat uptake and the slow adjustment of the ice sheets. On multi-decadal-to-centennial timescales there is deep uncertainty in sea-level projections associated with the response of the ice sheets. To summarize the results reported in this box, recent decades have seen an acceleration of global sea-level rise (*high confidence*) and it is *virtually certain* that GMSL will continue to rise over the 21st century in response to continuing accumulation of heat in the climate system.

Global Mean Sea Level (GMSL) has been both much higher and much lower than present within the past 55 million years. Between 1900 and 2018 global mean sea level (GMSL) has risen by 0.19 m (*likely* 0.15-0.22 m), mostly from ocean thermal expansion and glacier melt. For 1971-2018, all major contributions to energy and sea level change are known and consistent (*high confidence*) giving increased confidence in the planetary heating rate since AR5 from a consistent closure of the sea-level budget for the period 1971-2018. Since 1993, the *very likely* observed GMSL change of 3.16 (2.79-3.53) mm/yr is consistent with the sum of the independently determined contributions to sea-level change. {2.3.3, 2.3.4, Cross-Chapter Box 2.4, 3.5.3, 7.2.2, Table 7.1 Box 7.2, 9.6.1; Cross-Chapter Box 9.2}

The rate of GMSL rise is accelerating (*high confidence*). GMSL increased faster since 1900 than any century over the last three millennia, and GMSL change has accelerated since the late 1960s, at an average rate of 0.084 (0.059-0.090) mm yr^{-2} over 1993-2015. This acceleration is primarily due to the acceleration of polar ice sheet mass loss and other processes forced by global warming. {2.3.3, Cross-Chapter Box 2.4, 3.5.3, Box 7.2, 9.6.1; Cross-Chapter Box 9.2}

Since the AR5, studies have highlighted that simulations that exclude anthropogenic greenhouse gases are unable to capture the thermosteric sea level rise of the historical period and that model simulations that include all forcings (anthropogenic and natural) most closely match observed estimates. Combining the attributable contributions from glaciers, ice sheet surface mass balance and thermal expansion, it is *very likely* that anthropogenic forcings are the main driver of the observed global mean sea level rise since 1970. {3.5.1, 3.4.3, 3.5.3, Box 7.2, 9.6.1, Cross-Chapter Box 9.2

It is *virtually certain* that GMSL will continue to rise with heat continuing to accumulate in the Earth system over the 21st century. GMSL rise due to thermal expansion, glacier melt, and Greenland ice sheet melt is highly dependent on emissions scenario after 2050. There is little scenario dependence in the contribution of the Antarctic ice sheet to projections of GMSL in 2100. Under SSP5-3.4-OS, global sea level continues to rise in all models up to 2100 despite a reduction in CO_2 to 2040 levels (*high confidence*). {Box TS.6, Table 1; Box TS.3, Figure 1}

[START BOX TS.3, TABLE 1 HERE]

Box TS.3, Table 1: Projections of the *likely* range of GMSL (m) between 1995-2014 and 2100 based on CMIP6 and ISMIP6 projections.

	Total	Thermosteric	Glaciers	Greenland ice sheet	Antarctic ice sheet
SSP1-2.6	0.33-0.64	0.13-0.17	0.07-0.11	0.03-0.12	0.00-0.26
SSP2-4.5	0.40-0.71	0.17-0.22			

SSP3-7.0	0.51-0.81	0.23-0.26			
SSP5-8.5	0.60-0.90	0.28-0.31	0.11-0.18	0.09-0.19	0.00-0.26

[END BOX TS.3, TABLE 1 HERE]

GMSL is *extremely unlikely* to increase by less than 0.2 m by 2100 under SSP1-2.6 and SSP 2-4.5. To keep GMSL change by 2100 below 0.3 m, as well as a mitigation scenario being followed, feedbacks which lead to ice sheets gaining mass, or stabilizing feedbacks, would need to take place. Feedbacks such as increased snowfall as global temperatures increase, refreezing of surface melt water within the snowpack, meltwater inducing local cooling of the ocean and in turn air temperature over ice sheets, rapid bedrock rebound or lowering of local sea level associated with ice-sheet retreat are beginning to be captured in models. {4.6.3, 4.7.1, 4.7.2, 9.6.3, Box 9.3}

Probabilistic projections incorporating expert judgment on future ice sheet trajectories suggest that GMSL rise of 2.0 ± 0.1 m by 2100 is likely only if the Greenland contribution is in excess of 46 cm and the Antarctic contribution is in excess of 42 cm. Substantial contributions to GMSL from both ice sheets would require a high-emissions trajectory leading to substantial atmospheric and ocean warming which could precipitate a cascade of feedbacks, such as the elevation mass-balance feedback for Greenland, or trigger instabilities to produce contributions exceeding those simulated by the ISMIP6 ensemble. In Antarctica, ice shelf basal melting could increase due to positive ice-ocean feedback, a retreat of the ice sheet into deeper bedrock could trigger a marine ice sheet instability, the disintegration of ice shelves due to increased surface melt could result in vertical cliff of grounded ice which could then collapse in a self-sustaining manner. These processes are being captured in some models, but deep uncertainty persists in the projected Antarctic ice sheet evolution and potential collapse of the West Antarctic Ice Sheet. {Box 9.3}

There is medium confidence that heat will continue to accumulate in the Earth's system beyond 2100 for another century or more, even under strong mitigation of greenhouse gas emissions, driving future sea-level rise. However, on the timescale of 2300, there is deep uncertainty associated with uncertainty in the ice sheet response. By 2300, GMSL rise under SSP1-2.6 (based on RCP2.6) will likely be 0.3-2.9 m and extremely likely be below 4.7 m. By 2300, GMSL rise under SSP5-8.5 (based on RCP8.5) is extremely likely to be less than 15.5 m (medium confidence). {Box TS.3 Figure 1, 9.6.3, Box 9.3}

[START BOX TS.3, FIGURE 1 HERE]

Box TS.3, Figure 1: The idea is to combine Figure 2.27 (observations / paleo) with Figure 9.30 (projections), along with Figure 9.19 (GrIS), Figure 9.20 (AIS), Figure 9.22 (glaciers), and Figure. CCB92.1 (Thermosteric). This shows thermosteric, glaciers, AIS, GrIS and total sea level for historical where possible (including paleo ranges) and projections (to 2300 when available). Not clear if all panels should have aligned x axis years & y-axis scale for SL. *[PURPOSE: To summarise the different components of GMSL change, both in terms of historical observations and future projections. One of the issues is avoiding redundancy with sections 2.3 and 2.4. An alternative, simplified approach might focus on the total GMSL time series and tabulate the different contributions for past observed periods and for future projections by scenario]*

[END BOX TS.3, FIGURE 1 HERE]

Regional sea-level rise rate increased fastest in the Indo-Pacific, Northwest Pacific and subtropical North Atlantic over 1993-2015 and the projected change is largest in [PLACEHOLDER FOR REGIONAL PROJECTIONS]. Large uncertainties remain in closing the sea-level budget on regional and local scales and attribution of regional sea-level change to anthropogenic forcing also remains difficult. The anthropogenic signal in regional sea-level change will have emerged over 50% of the ocean area by 2040 (*medium confidence*). {Box TS.3 Figure 2, 9.6.1, 9.6.3}

Changes in extreme still water levels over the 20th century were primarily driven by regional relative sea level change increasing median high-tide flooding frequency by 165%. By 2050, 1% average annual probability extreme water levels are projected to occur 11 and 14 times more frequently under SSP1-2.6 and SSP5-8.5 respectively, becoming an annual event at about 20% of the tide gauge stations (*high confidence*). {Box TS.6 Figure 2, 9.6.4, Cross-Chapter Box 9.1}

[START BOX TS.3, FIGURE 2 HERE]

Box TS.3, Figure 2: [Placeholder] Example local sea-level projections compared to local tide gauge observations to illustrate the range of future behaviours and observed interannual variability. Combined with flooding frequency elements of Figure 9.34 to make the link to projected changes in coastal sea-level extremes (see Section TS4). *[PURPOSE: To illustrate the large geographic variations in regional sea-level change/projections (we cannot rely on GMSL for this information) and the differing regional variability as shown by tide gauge records. Then to make the link to changes in local sea-level extremes, which are dominated by the time-mean sea-level change (rather than changes in drivers of extremes).]*

[END BOX TS.3, FIGURE 2 HERE]

[END BOX TS.3 HERE]

TS.2.5 Water cycle

The water cycle describes the circulation of water in its different phases (vapour, liquid and solid) within and across the various components of the climate system. This subsection assesses recent and future water cycle changes across all components of the climate system.

TS.2.5.1 Observed changes

Global total column water vapour content has *likely* increased since satellite observations commenced in the 1980s. Near surface specific humidity has *likely* increased over the ocean and *very likely* increased over land since at least the 1970s. Yet, relative humidity has *very likely* decreased over land areas since 2000, particularly over mid-latitude regions of the Northern Hemisphere. {2.3.1, 8.3.1}

Globally averaged, land precipitation has *likely* increased since 1950, with a faster increase since the 1990s (*medium confidence*), while there is *low confidence* in ocean precipitation changes due to large observational uncertainties. There is also *low confidence* in the paleo context given limitations in proxy-based reconstructions at continental and global scales. Yet, there is *medium confidence* that the global water cycle has strengthened since at least 1980, meaning that global precipitation has increased but at a lesser rate than the atmospheric water content (*medium confidence)*. {2.3.1}

TS.2.5.2 Attribution

There is growing evidence and *high confidence* that human activities have affected the global water cycle since pre-industrial times. It is *likely* that human influence has contributed to tropical moistening in the upper troposphere since 1979 (*medium confidence*). It is *likely* that human influence has contributed to observed changes in large-scale precipitation patterns since 1950. New attribution studies find a detectable increase in high latitude precipitation over the Northern Hemisphere. There is *medium confidence* that ozone depletion has increased precipitation over the Southern Ocean and decreased it over southern midlatitudes during austral summer, in agreement with the observed strengthening of the Southern Annular Mode. There is *medium confidence* that rainfall over the wet regions of the tropics has increased due to enhanced greenhouse gas forcing, although such a long-term trend has been partly obscured by both natural decadal variability and anthropogenic aerosols (*high confidence*). Based on historical simulations with individual versus all radiative forcings, there is also *medium confidence* that anthropogenic aerosols have suppressed the effects of GHG forcing on the precipitation (P) and net water availability (P-E) over the land regions of the tropics and the Northern Hemispheric extratropics since the early 20th century, and more prominently during the last 6-7 decades. Due to large natural decadal variability, signatures of human-induced changes in P and P-E are not clearly detectable over the land regions of the Southern Hemispheric extra-tropics. {2.3.1, 3.3.2, 3.3.3, 8.3.1, 8.3.2, Box 8.1}

It is *extremely likely* that human influence has contributed to observed near-surface and subsurface oceanic salinity changes since the mid-20th century, with a clear "fresh-get-fresher, salty-get-saltier" pattern. Over land, observational uncertainty leads to *low confidence* in global trends in precipitation minus evaporation. Anthropogenic emissions of greenhouse gases have contributed to regional changes in runoff and river discharge (*medium confidence*). There is *high confidence* that earlier retreat of springtime snow cover and enhanced glacier melt has already contributed to changes in streamflow seasonality in high-latitude and mountain catchments. There is *high confidence* that anthropogenic emissions of GHGs have enhanced summer mid-latitude land surface drying and contributed to severe aridity in the Mediterranean, and *medium confidence* that an anthropogenic GHG signal is contributing to increased aridity in other Mediterranean-like regions. {2.3.1, 3.3.2, 3.5.2, 8.3.1}

[START FIGURE TS.18 HERE]

Figure TS.18: Time series of past relative changes (1850-2014) of precipitation (P, left column) and precipitation minus evaporation (P-E, right column) over land areas for all historical forcings (black), aerosol forcing only (blue), and GHG forcing only (red). Top row: NH extratropics (30N-60N); middle row: Tropics (30S-30N); bottom row: SH extratropics (30S-60S). *[PURPOSE: Illustrate key message that anthropogenic aerosol forcing has obscured the effects of GHG forcing on the precipitation (P) and net flux of water from the atmosphere to the Earth's surface (precipitation minus evaporation i.e., P-E) over the land regions of the tropics and the Northern Hemispheric extratropics since the early 20th century, with more prominent changes during the last 6-7 decades. Signatures of human induced changes in P and P-E are not clearly detectable over the land regions of the Southern Hemispheric extra-tropics which are dominated by large internal variability.]*

[END FIGURE TS.18 HERE]

TS.2.5.3 Projected changes

Global-mean land and global-mean ocean precipitation are *very likely* to increase as global surface air temperature increases over the 21st century under all five SSPs (cf. Table TS.6, Figure TS.19). Based on multiple lines of evidence, global-mean land precipitation is *very likely* to increase approximately 1–3% per 1°C warming in globally averaged surface air temperature. Compared to the projected increase in global land precipitation, the projected increase in moisture availability (precipitation minus evapotranspiration) is much weaker for SSP1-2.6, due to enhanced global land surface evapotranspiration (*high confidence*), but is larger for SSP5-8.5, thereby indicating a soil moisture limitation to the global increase of land surface evapotranspiration in low-mitigation scenarios (*medium confidence*). Global continental runoff is projected to increase in all SSPs, in line with the enhanced precipitation intensities, glacier melting and permafrost thawing (medium confidence) {Figure TS.17, Figure TS.20, Box TS.3 Figure 1,4.3.1, 4.5.1, 4.6.1, 8.4.1}

[START TABLE TS.6 HERE]

Table TS.6: Projected precipitation changes (%) relative to averages over 1995–2014 for selected future periods, regions and SSPs. The multi-model averages across the individual models and the 5 to 95% ranges (based on multiplying the CMIP6 ensemble standard deviation by 1.645) are given in parentheses. Also shown are land precipitation changes at the time when global increase in GSAT relative to 1850–1900 exceeds 1.5°C, 2.0°C, and 3.0°C, and the percentage of simulations for which such exceedances are true (to the right of the parentheses). Here, the time of GSAT exceedance is determined as the first year at which 11-year running averages of GSAT exceed the given threshold. Land precipitation percent anomalies are then computed as 21-year averages about the year of the first GSAT crossing. {Table 4.3, 4.3.1} *[PURPOSE: Projected precipitation changes, parallel and complementary to Table TS.5. Shows clear increase signal across scenarios]*

Units = %	SSP1-1.9	SSP1-2.6	SSP2-4.5	SSP3-7.0	SSP5-8.5
Land: 2021–2040	2.6 (0.9, 4.2)	2.1 (0.6, 3.5)	1.6 (0.1, 3.0)	1.1 (-0.6, 2.8)	1.8 (-0.2, 3.7)
2041–2061	2.9 (0.9, 5.0)	2.7 (0.5, 5.0)	2.8 (0.7, 4.8)	2.4 (-0.3, 5.1)	3.8 (0.7, 6.8)
2081–2100	2.7 (0.6, 4.8)	3.2 (0.7, 5.6)	4.7 (1.8, 7.7)	5.5 (0.5, 10.4)	8.2 (2.5, 13.8)
Global: 2081–2100	2.2 (0.6, 3.8)	2.7 (0.9, 4.5)	4.1 (1.7, 6.4)	4.8 (1.8, 7.8)	6.3 (2.6, 10.0)
Ocean: 2081–2100	2.0 (0.5, 3.6)	2.5 (0.7, 4.4)	3.8 (1.3, 6.4)	4.6 (1.5, 7.6)	5.8 (1.9, 9.7)
Land: ΔT > 1.5°C	2.1 (-0.4, 4.6) 60	2.2 (-1.7, 6.0) 95	1.9 (-2.3, 6.1) 100	1.3 (-2.8, 5.3) 100	1.8 (-2.1, 5.8) 100
ΔT > 2.0°C	3.9 (1.0, 6.7) 40	3.1 (-0.2, 6.4) 64	3.1 (-1.5, 7.7) 100	2.3 (-2.7, 7.3) 100	3.2 (-1.5, 7.9) 100
ΔT > 3.0°C	- (-, -) 0	- (-, -) 0	4.2 (-0.2, 8.6) 67	4.3 (-2.3, 10.9) 100	4.9 (-1.2, 11.1) 100

[END TABLE TS.6 HERE]

The geographical pattern of annual mean precipitation is projected to change in response to anthropogenic forcings (Figure TS.19). With increased global warming, a larger land area will experience statistically significant increase or decrease in precipitation (*medium confidence*). The increase of area fraction with significant precipitation increase will be larger over land than over the ocean, but the increase of area with significant decrease will be larger over the ocean than over land (*medium confidence*). Precipitation will increase in large parts of the tropics and in the high latitudes, but decrease over the Mediterranean and large parts of the subtropics (*high confidence*). Beyond precipitation, there is *high confidence* that increased evaporation due to growing atmospheric water demand will dry soils in many water-limited regions. There is *medium* to *high confidence* in an expansion of arid areas towards the midlatitudes, and in pronounced drying in the Mediterranean, southern Africa, southern Australia, southern North America, Central America and northeastern Brazil. {4.5.1, 4.6.1, 8.4.1}

[START FIGURE TS.19 HERE]

Figure TS.19: CMIP6 multi-model mean projected changes (%) in near-term (left column), mid-term (middle column) and long-term (right column) annual mean precipitation under three SSP scenarios: SSP1-2.6 (top row), SSP2-4.5 (middle row) and SSP5-8.5 (bottom row) relative to 1995–2014. Stippling indicates regions where the multi-model mean change exceeds two standard deviations of pre-industrial internal variability and where at least 90% of the models agree on the sign of change, as a measure of robustness. Hatching indicates regions where the multi-model mean signal is less than one standard deviation of internal variability. Top-right panel numbers indicate the number of CMIP6 models used for estimating the ensemble mean. *[PURPOSE: Emphasize the robustness of the geographical pattern of projected precipitation changes, and highlight the time and scenario dependence of their magnitude.]*

[END FIGURE TS.19 HERE]

In response to greenhouse-gas-induced warming, it is very likely that global land monsoon precipitation will increase irrespective of the emission scenario and time horizon, particularly in the Northern Hemisphere although Northern Hemisphere monsoon circulation will weaken (high confidence). In the long-term, monsoon rainfall changes will feature regional disparities (see Box TS.6) although global projections indicate an overall extension of the length of the wet season and an enhancement of the interannual variability (medium confidence) {4.4.1, 4.5.1, 8.2.1, 8.2.3, 8.4.1, 8.4.2}.

There is high confidence that water cycle variability is projected to increase in most regions of the world (cf. lower panels in Figure TS.20). Intraseasonal precipitation variability is projected to increase with less rainy days over the Mediterranean, Amazonia and the maritime continent, but increased daily mean precipitation intensity over many regions over land (high confidence). The seasonality of precipitation, runoff, streamflow and water availability will increase over many regions (high confidence). There is also high confidence that earlier snowmelt will bring forward the timing of peak streamflow and reduce summer streamflow, with medium con*fidence* that reduced snow volume and less energy for melt earlier in the season will also reduce the most intense snowmelt flows. Interannual variability of precipitation and runoff over land is projected to increase, at a faster rate than changes in mean precipitation in the tropics and in the summer extratropics of both hemispheres (*medium confidence)*. {Cross-section Box 1, Figure 3, 8.2.3, 8.4.1, 8.4.2}

[START FIGURE TS.20 HERE]

Figure TS.20: Summary of long-term (2081-2100) projected annual mean water cycle changes (%) relative to present-day (1995-2014) in the SSP2-4.5 emission scenario for: precipitation (P), surface evapotranspiration (E), Precipitation minus - Evapotranspiration (P-E), total runoff, surface soil moisture, sea surface salinity, number of dry days, precipitation seasonality index (red shading highlights areas with increased rainfall seasonality), precipitation interannual variability (as estimated by the relative change in the standard deviation of annual precipitation). Top-right panel numbers indicate the number of CMIP6 models used for estimating the ensemble mean. *[PURPOSE: Synthetic overview of changes in multiple components/features of the global water cycle, with the following important key messages: 1) long-term changes in runoff, soil moisture and sea surface salinity result from changes in both P and E, 2) they are generally less robust than changes in P or E, 3) changes in P seasonality and variability (intraseasonal and interannual) can be more pronounced or robust than changes in annual mean P at the regional scale.]*

[END FIGURE TS.20 HERE]

The amplitude of most projected water cycle changes will increase with increasing concentrations of greenhouse gases and global warming levels (*high confidence*). For a given emissions scenario or global warming level, variable model response and internal variability contribute to a substantial range in projections of large-scale and regional water cycle changes (*high confidence*). Uncertainties related to the model response are particularly strong at the transition between wet and dry regions and seasons. Internal climate variability strongly affects near-term water cycle responses for all emission scenarios, and mid-term water cycle changes in high-mitigation scenarios, especially for those related to regional summer monsoons and winter mid-latitude storm tracks (*medium confidence*). {8.5.1, 8.5.2}

TS.2.5.4 Summary of water cycle changes

The effect of anthropogenic forcings on the observed water cycle is generally less clear than on temperature, given the larger observational uncertainties and the larger relative magnitude of internal variability. It is however *likely* that human influence has contributed to observed large-scale precipitation changes since 1950, with the response to greenhouse gases having been partly offset over some regions by the response to increasing anthropogenic aerosols (*high confidence*). Global mean precipitation and evapotranspiration are *very likely* to increase over the 21st century under all scenarios considered, and water cycle variability is projected to increase in most regions at both intraseasonal and interannual timescales (*high confidence*). Future climate change will also increase both geographical and seasonal contrasts between wet and dry regimes (*medium confidence*).

TS.2.6 The Carbon Cycle

Changes in the abundance of greenhouse gases (GHGs), including CO_2, CH_4 and N_2O, in the atmosphere play a large role in determining the Earth's radiative properties and its climate. Since 1950, the human-induced increase in these atmospheric GHGs has been the dominant cause of the observed climate change. While the main driver of changes in atmospheric GHGs over the past 200 years are the direct emissions from human activities, the net accumulation of GHGs in the atmosphere, the airborne fraction, is also controlled by physical and biogeochemical source–sink dynamics. These are processes, mainly physical in the ocean, and mainly biospheric on land, that drive the exchange of quantities between multiple carbon reservoirs on land, ocean and atmosphere. For instance, the combustion of fossil fuels and land-use change for the period 1750–2018 resulted in the release of an estimated 675 ± 80 PgC (1 PgC = 10^{15} g of carbon) to the atmosphere, of which about 44% remains in the atmosphere today. This underscores the important role of terrestrial and ocean carbon dioxide (CO_2) sinks in regulating atmospheric CO_2 and driving feedbacks that may influence the airborne fraction. This section also assesses the changes in the ocean and land carbon cycle processes that are relevant as drivers, indicators and feedback elements of global climate change and their attribution to human and natural influences. {5.1.2}

TS.2.6.1 Emissions and reservoir changes

It is unequivocal from multiple lines of evidence using atmospheric gradients of CO_2 concentrations, isotopes, and inventory data that the atmospheric growth in GHGs since the beginning of the Industrial Era is due to the direct emissions from human activities. However, the accumulation of GHGs in the atmosphere is determined by the balance of human GHG emissions and biogeochemical source-sink dynamics. {5.2.1, 5.2.2, 5.2.3, Figure 5.4}

The fate of the carbon emitted from human activities during the decade of 2009–2018 (decadal average 11.0 PgC yr^{-1}) was: 44% accumulated in the atmosphere (4.9 ± 0.02 PgC yr^{-1}), 23% was taken up by the ocean (2.5 ± 0.6 PgC yr^{-1}) and 29% was removed by terrestrial ecosystems (3.5 ± 0.7 PgC yr^{-1}) (*high confidence*). The sum of these quantities has an imbalance of 0.4 PgC suggesting an underestimation of the sinks, or an overestimation of the emissions, or combination of both. During the last measured decade, average annual anthropogenic emissions of CO_2, CH_4, and N_2O, reached the highest levels in human history at 11.8 ± 0.8 PgC yr^{-1} (2009–2018), 348–392 Tg CH_4 yr^{-1} (2018–2017), and 4.2– 11.4 TgN yr^{-1} (2007–2016), respectively (*high confidence*). {5.2.1, Figure 5.4, 5.2.2, 5.2.3}.

Of the total anthropogenic CO_2 emissions, the combustion of fossil fuels was responsible for about 81–91% and the remaining from land use change (e.g., deforestation, degradation, peat drainage). {5.2.1, Table 5.1}

The multi-decadal growth trend in atmospheric CH_4 is *very likely* dominated by anthropogenic activities, and there is *medium confidence* that the growth since 2007 is largely driven by emissions from fossil fuels and livestock for food production. The multi-year variability is predominantly driven by El Niño Southern Oscillation cycles during which biomass burning and wetland emissions play an important role. {5.2.2}

Agricultural N_2O emissions have increased by about 80% since the early 1900s, and by 30% since the 1980s. There is *high confidence* that increased use of nitrogen fertiliser and manure contributed to about 70% of the increase during the 1980–2016 period. {5.2.3}

It is unequivocal that the ocean and land uptake of anthropogenic CO_2 have continued to grow as anthropogenic CO_2 emissions have increased over the past six decades but the airborne fraction has remained constrained around 44%. There is, however, *high confidence* that the combined rates of CO_2 removal by ocean and land per unit of excess anthropogenic CO_2 in the atmosphere have declined. Interannual and decadal variability of the ocean and land sinks indicate that these sinks are sensitive to climate variability and therefore, sensitive to climate change (*high confidence*). {5.2.1, Figure 5.5, Figure 5.8, Figure 5.9, Figure 5.11}.

TS.2.6.2 Changing Mechanisms that Influence Carbon Feedbacks on Land and in the Ocean

Carbon uptake by vegetation photosynthesis exerts a first-order control over the net land CO_2 sink. Several lines of evidence show enhanced vegetation photosynthesis (*medium to high confidence*) over the past decades. For instance, the length of the terrestrial growing season has increased over much of the extratropical Northern Hemisphere since mid-20th century (*high confidence*), and vegetation greenness indicators such as green leaf area and photosynthetic activity have increased since satellite observations began in the 1980s (*high confidence*). The observed increased amplitude of the seasonal cycle of atmospheric CO_2 since the 1960s is *likely* attributable to fertilisation of plant growth, and therefore higher plant growth activity. Increasing strength of global net land CO_2 sink since 1980s is mainly driven by the fertilisation effect from rising atmospheric CO_2 concentrations (*medium to high confidence*), but increasing nitrogen deposition or the synergy between increasing nitrogen deposition and increasing atmospheric CO_2 concentration could have also contributed to the increased global net land CO_2 sink. The contribution of climate change to changes of the global net land CO_2 sink is so divergent that even the signs of the effects are not the same across dynamic global vegetation models. {5.2.1, Figure 5.9}.

It is unequivocal that the continuing ocean uptake of CO_2 both mitigates global warming and is beginning to drive observable large-scale changes to ocean carbonate chemistry associated with ocean acidification and reducing ocean carbonate buffering capacity. The latter process is the major projected driver of future weakening of the ocean CO_2 uptake. The effect of these changes on carbon–climate feedbacks in the contemporary period is still undetectable. However, the observed reduced CO_2 buffering capacity and the increased impact of warming on ocean pCO_2 are modifying the seasonal cycle characteristics of pCO_2 and thereby that of air-sea CO_2 flux (*high confidence*). There is *medium to high confidence* that the global trends in changing ocean CO_2 chemistry during the historical period are driving the increasing rates of change in the amplitude of the seasonal cycle of ocean pCO_2 of 2.2 ± 0.4 μatm per decade for 1982–2015 poleward of 10º latitude. It is also *likely* to amplify the seasonal cycle of surface-water hydrogen ion concentration (+81 ± 16%) while attenuating that of pH by 16 ± 7%, on average, during the 21st century. {5.2.1, 5.4.2}

TS.2.6.3 Future changes to the ocean and terrestrial carbon cycles

Oceanic and terrestrial carbon sinks will continue to grow in response to increasing atmospheric concentrations of CO_2 (Figure TS.21a,b), but emerging feedbacks will weaken those sinks (*high confidence*). It is *very likely* that the global ocean and land sinks will stop taking up more CO_2 from the second part of the century under any emission scenario. Ocean and land sinks show a similar future behaviour under low and high emission scenarios, but the land sink has a much higher inter-annual variability and wider model spread. The latter is due to both the inclusion of different processes in different models (e.g., plant growth limitation by nitrogen availability), and by different model sensitivity to key processes such as the CO_2 fertilization effect on plant growth or the response of soil organic matter decay to climate change resulting from lacking observations to constrain these long-term dynamics at large spatial scales. {4.3.2, 5.4}
In the ocean, the sink will stop growing at a maximal level varying from about 4 to 6 PgC yr^{-1}, primarily due to the reduced ocean carbonate buffering capacity, ocean warming and altered ocean circulation. The net uptake of carbon by the ocean from 2014 to the end of the 21st century (Figure TS.21c) varies from about 145 ± 25 PgC under SSP1-2.6 to about 355 ± 30 PgC under SSP5-8.5 based on the CMIP6 models (high confidence). {5.4}

The land carbon sink is projected to saturate at around 5 ± 3 PgC yr^{-1} under SSP5-8.5, and to decline to less than 0.3 ± 0.8 PgC yr-^{1} by 2100 under SSP1-2.6. Cumulative land carbon uptake from 2014 is projected to reach 280 ± 130 PgC by 2100 under SSP5-8.5, and to saturate at approximately 160 ± 35 PgC under SSP1-2.6 (Figure TS.21d). It is very likely that the land carbon sink will decline from mid-century onwards under high-emissions scenarios, but it is very unlikely that the land will switch from being a sink to a source. {5.4.5}

The probability of crossing regional thresholds (e.g., forest dieback) increases with climate change, but there is no one particular threshold of global warming or atmospheric CO_2 identified in Earth system model projections. There is *medium confidence* that carbon-climate feedbacks can have a discernible effect on global atmospheric GHG concentrations, but do not lead to runaway changes over the next 100 years.

{5.4.8}

For global warming of no more than 2°C, paleoclimate records do not provide strong support for abrupt changes in the carbon cycle (*low confidence*). In response to climate forcing, paleoclimate records show changes of a magnitude larger than 100 ppm in atmospheric CO_2 over several millennia and abrupt smaller changes of about 10 ppm over centuries. However, the annual CO_2 emissions rates from any of these paleoclimate changes are one order of magnitude slower than the contemporary perturbation from anthropogenic emissions suggesting caution when using the paleo record as an analogue for contemporary and future carbon-climate feedbacks. Paleoclimate records also indicate that carbon uptake from living organisms in the ocean is sensitive to climate and directly decreases the CO_2 ocean sink in periods of increased warming (*medium confidence*). {5.1.3, 5.4.4, Figure 5.2}

Large uncertainties remain on the possibility of additional feedbacks not represented in many current models (e.g., fires, frozen landscapes collapse) which could lead to departures from the current modelled trajectories. {5.4.8}

Despite the wide range of model responses, the overall uncertainty in projections of atmospheric CO_2 by 2100 is dominated by uncertainties in emissions pathways rather than uncertainties in carbon-climate feedbacks. {4.3.2, 5.4}

[START FIGURE TS.21 HERE]

Figure TS.21: Projections of: (a) atmosphere-to-ocean carbon flux; (b) atmosphere-to-land carbon flux; (c) change in ocean carbon storage; (d) change in land carbon storage; from the CMIP6 ensemble of ocean and land for SSP 2.6 (green) and 8.5 (purple). Shaded regions indicate the ensemble spread. *[PURPOSE: To show projections of future changes in carbon uptake and storage for ocean and land in CMIP6 ensemble.]*

[END FIGURE TS.21 HERE]

TS.2.6.4 Summary of observed, present and projected carbon cycle changes

There is unequivocal evidence that the continued growth of atmospheric CO_2, CH_4 and N_2O is largely due to emissions from human activities, and that the ocean and land anthropogenic CO_2 sinks slows the rise of CO_2 in the atmospheres. With *high confidence*, the magnitude of carbon-climate feedbacks over the last six decades was too small to influence the airborne fraction of CO_2. However, there is *medium to high confidence* that changes to processes that govern carbon-climate feedbacks are already modifying the variability and magnitude of the ocean and land sinks. There is *high confidence* that ocean and land sinks will stop growing in the second half of the century. For global warming of no more than 2ºC, paleoclimate records provide little evidence of abrupt biogeochemical change on a global scale. However, there is high confidence that biogeochemical responses to anthropogenic CO_2 emissions lead to abrupt impacts at the regional scale and irreversible on decadal to century time scales. Atmospheric CO_2 changes comparable to the anthropogenic period have occurred in the past but the rates of change are at least a magnitude slower than the historical equivalent *(low confidence*).

TS.2.7 Extremes

This subsection summarizes assessments of weather and climate extremes, including observed and projected changes, as well as their attribution. Regional changes are summarized in TS.4.3. Reliable observations with global coverage are available only after 1950, and for this reason, assessments of past changes and their causes are generally also from 1950 onward, unless indicated otherwise. Evidence of observed changes in extremes and their attribution to human influence have strengthened since the AR5, leading to higher confidence in the assessment compared with AR5, in particular for extreme precipitation, droughts, tropical cyclones, marine extremes, and compound extremes. Summaries of the assessments are provided in the

Table TS.7 and Table TS.8, as well as in Figure TS.22.

TS.2.7.1 Temperature extremes

It is *virtually certain* that there has been an increase in the likelihood and severity of hot extremes and a decrease in the likelihood and severity of cold extremes on global scale since 1950. Evidence of changes include an increase in the number of warm days and nights, an increase in the intensity and duration of heatwaves, and a decrease in the number of cold days and nights (*virtually certain*). Both the coldest extremes and hottest extremes display increasing temperatures (*virtually certain*). Trends in temperature extremes are generally larger (by about 50% to 200%) than those in global mean temperature, due to larger warming on land and additional feedback effects (*high confidence*). Trends on regional to continental scales are generally consistent with the global-scale trends (*high confidence*). {Table TS.7, 11.3.2, 11.9}

It is *extremely likely* that human influence is the main contributor to the observed increase in the likelihood and severity of hot extremes and the observed decrease in the likelihood and severity of cold extremes on global scales. It is *very likely* that this also applies on continental scale. The available evidence suggests that some recent extreme events could not have occurred without human influence (*medium confidence*). The effect of increased greenhouse gas concentrations on extreme temperature are moderated, counteracted or amplified at the regional scale due to feedbacks or forcings such as regional land-use and land-cover changes, or aerosols. Urbanization has exacerbated the effects of global warming in cities (*high confidence*). Changes in aerosol concentrations have affected trends in hot extremes in some regions, with the presence of aerosols leading to attenuated warming, in particular from 1950-1980. Irrigation and crop expansion have attenuated increases in summer hot extremes in some regions, such as the central North America (*medium confidence*). {Figure TS.22, Table TS.7, 1.3, Cross Chapter Box 3.2, 11.1.4, 11.3.4}

It is *virtually certain* that further increases in the likelihood and severity of hot extremes and decreases in the likelihood and severity of cold extremes will occur throughout the 21st century. Such changes are expected at both global and continental scales, and in nearly all inhabited regions, if global warming increases to 1.5°C or higher above the pre-industrial level, with stronger increases at higher levels of global warming. It is *virtually certain* that the number of hot days and hot nights and the length, frequency, and/or intensity of warm spells or heat waves (defined with respect to late 20th century conditions) will increase over most land areas. {Box TS.1 Figure 1, Box TS.2 Figure 3, Table TS.8, 11.3.5, 11.9}

TS.2.7.2 Heavy precipitation and floods

There is *high confidence* that heavy precipitation has intensified on global scale over land regions. It is *likely* that, since 1950, the annual maximum amount of precipitation falling in a day or over five consecutive days has increased in more regions than it has decreased, over land regions with sufficient observation coverage for assessment. This is also the case at the continental scale over three continents: North America, Europe, and Asia. Larger percentage increases in heavy precipitation have been observed in the northern high-latitudes in all seasons, as well as in the mid-latitudes in the cold season (*high confidence*). {Table TS.7, 11.4.2, 11.9}

There is *high confidence* that the seasonality of flood has changed in cold regions where snow-melt is involved. There is *high confidence* that significant trends in peak streamflow have been observed in some regions. {Table TS.7, 11.5.2}

It is *likely* that anthropogenic influence is the main cause of the observed intensification of heavy precipitation in land regions. The evidence includes attribution of the observed global increase in annual maximum one-day and five-day precipitation to human influence (*high confidence*), a large fraction of land showed enhanced extreme precipitation, and larger probability in record-breaking one-day precipitation. At continental and regional scales, human influence on extreme precipitation is less detectable because of higher variability, but evidence is emerging. {Figure TS.22, Table TS.7, Cross-Chapter Box 3.2, 11.2.5, 11.4.4}

Over almost all land regions, it is *very likely* that extreme precipitation will be more intense and more frequent in a warmer world. The increase in the magnitude of extreme precipitation will be, in general, proportional to the global warming level, with an increase of 7% and a slightly smaller rate in the 50-yr event of annual maximum 1-day and 5-day precipitation per 1°C warming, respectively (*high confidence*). There can be large differences in the increase regionally. {Cross-Section Box TS.1 Figure 1, Cross-Section Box TS.2 Figure 3, Table TS.8, 11.4.5}

There is *high confidence* in an increase in flood potential in urban areas where extreme precipitation is projected to increase, especially at high global warming levels. Global hydrological models project a larger fraction of the land areas to be affected by an increase in river floods than by a decrease in river floods (*medium confidence*). {Table TS.8, 11.5.5, 12.4.1.2}

TS.2.7.3 Droughts

Different drought types (related to prolonged negative anomalies of precipitation, soil moisture, streamflow or increased atmospheric evaporative demand) are associated with different impacts and respond differently to increased greenhouse gas forcing. Observed trends in drought measures are highly regional, with increases in some regions and decreases in others. Atmospheric evaporative demand displays a global drying tendency over continents, and there is an observed tendency towards increased drying in the dry season since the beginning of the 20th century, when aggregated on global scale (*high confidence*). There is *medium confidence* that trends in potential evaporation have exceeded trends in precipitation in some regions and seasons. There is overall *medium confidence* in the ability of available models (climate, land surface or hydrological models) to simulate trends and anomalies in precipitation deficits, soil moisture deficits, streamflow deficits, or atmospheric dryness on global and regional scales. {Table TS.7, 11.6.1, 11.6.2}

There is *high confidence* that human influence has increased drought potential and increased the tendency towards drying in the dry season since the beginning of the 20th century, when aggregated on the global scale. The drying tendency is dominated by warming- and radiation-induced increase in evaporative demand rather than by changes in precipitation. {Table TS.7, 11.6.4}

There is *high confidence* that atmospheric evaporative demand will continue to increase with increasing global warming and lead to further drying tendencies in some regions. There is *medium confidence* in projected increases in the frequency and severity of prolonged negative anomalies in precipitation, soil moisture, and streamflow in some regions. While there is high agreement among climate models, there are uncertainties in drought representation in climate models, the use of drought metrics in projections, and a lack of observations in several regions to evaluate models. In addition, there is *medium confidence* that prolonged negative anomalies in soil moisture and streamflow may also be affected by physiological CO_2 effects on plants' transpiration under enhanced CO_2 concentrations. Projections of soil moisture change show stronger increases in prolonged negative anomalies in drought area and severity than projections of changes in prolonged negative precipitation anomalies (*medium confidence*). These projections are strongly dependent on the warming scenario considered, with stronger drought trends for higher warming levels, even for changes as small as 0.5°C in global warming (*high confidence*). Some regions with humid or transitional climate characteristics in the 20th century are projected to become drier (*medium confidence*). {Table TS.8, 11.6.5}

TS.2.7.4 Tropical cyclones

There is *medium confidence* that the global proportion of stronger tropical cyclones (TCs) has increased detectably over the past 40 years. The average location of peak TC wind-intensity has migrated poleward in the western North Pacific Ocean since the 1940s, substantially increasing TC exposure at higher latitudes. It is *unlikely* that the observational evidence for migration is the result of data artifacts, and there is *medium confidence* that it cannot be explained by natural variability. There is *medium confidence* that TC forward motion (translation speed) has slowed detectably over the U.S. since 1900, but *low confidence* for a global signal because of the potential for data heterogeneity. There is *low confidence* in the cause of the slowdown in any region due to a lack of robust agreement among models that simulate TCs, although the slowdown is consistent with theory and modelling studies that indicate a general slowing of atmospheric circulation with warming. There is *low confidence* in past trends in characteristics of severe convective storms such as hail and severe thunderstorm winds. {Table TS.7, 11.7}

There is *high confidence* that average peak TC wind speeds and the proportion of Category 4-5 TCs will increase globally with warming. There is *medium confidence* that the average location where TCs reach their maximum wind-intensity will migrate poleward in the western North Pacific Ocean as the tropics expand with warming. There is *medium confidence* that the global frequency of TCs over all categories will decrease or remain unchanged. There is *medium confidence* that wind speeds associated with extratropical cyclones will change following changes in the storm tracks, with increases/decreases depending on the region being considered. There is *medium confidence* that the frequency of springtime severe convective storms will increase, leading to a lengthening of the severe convective storm season. {Table TS.7, 11.7}

There is *high confidence* that the average and maximum rain-rates associated with tropical and extratropical cyclones, atmospheric rivers and severe convective storms will increase as atmospheric water vapour increases with warming. There is *medium confidence* that peak TC rain-rates will increase at greater than the Clausius-Clapeyron scaling rate of 7% per °C of warming in some regions due to increased low-level moisture convergence caused by regional increases in TC wind intensity. There is *high confidence* that the magnitude of the increase in precipitation depends on the horizontal resolution and the specific representation of convective processes in climate models due to the effect of fine-scale dynamical feedbacks. {Table TS.8, 11.7}

TS.2.7.5 Marine extremes

Marine heatwaves (MHWs) have become more frequent since 1982 (*high confidence*) with more intense warming (*medium confidence*), longer duration (*medium confidence*) and larger spatial extent associated with the long-term ocean warming trend (*high confidence*) {Figure TS.8, 9.6.4, Cross-Chapter Box 9.1}

Under further global warming, MHWs are *very likely* to increase in frequency, duration, spatial extent and intensity in all ocean basins, but with differential magnitudes in space {Cross-Chapter Box 9.1}. The largest changes are projected to occur in the tropical ocean and the Arctic Ocean (*high confidence*), with moderate increases are projected for midlatitudes, and only small increases are projected for the Southern Ocean (*medium confidence*). {Cross-Chapter Box 9.1, Figure TS.8}

There is *high confidence* in increases in extreme still water levels over the 20th century, largely driven by regional sea level rise, and with the median high-tide flooding increasing by 165%. {9.6.4}

There is *high confidence* that the frequency of current 1% probability extreme sea level events will increase under continued global warming. By 2050, 1% average annual probability extreme water levels are projected to occur 11 and 14 times more frequently under SSP1-2.6 and SSP5-8.5 respectively, becoming an annual event at about 20% of the tide gauge stations (*high confidence*). {Box TS.3 Figure 2, 9.6.4}

TS.2.7.6 Compound events

There is *high confidence* that concurrent heatwaves and droughts have become more frequent and that this trend will continue under higher levels of global warming. There is *high confidence* that concurrent extreme events at different locations, but possibly affecting similar sectors (e.g. breadbaskets) in different regions, would become more frequent at higher levels of warming, in particular above 2°C of global warming. There is *medium confidence* that likelihood of compound flooding (storm surge, extreme rainfall and/or river flow) has increased in some locations, and will continue to increase due to both sea level rise and increases in heavy precipitation. There is *medium confidence* that wildfire (compound hot and dry event) risk has increased in some regions over the last century. There is *medium confidence* that various risks of other compound events will increase under higher levels of global warming. {Table TS.7, Table TS.8, 11.8}

[START FIGURE TS.22 HERE]

Figure TS.22: Summary figure on confidence in global-scale projected trends in extreme types at +3°C vs confidence in attribution of global-scale observed trends in extremes types. [*Purpose: Show that confidence in projected changes in extremes is linked (and typically slightly higher) than confidence in attribution of observed trends in extremes.]*

[END FIGURE TS.22 HERE]

[START TABLE TS.7 HERE]

Table TS.7: [Summary table on observed changes in extremes and their attribution on global and continental scale. More detailed information, particular on regional scales, is found in Table 11.1 which is a more detailed version of this table. *[Purpose : Provide a synthetic overview of observed changes in extremes and their attribution to human activity, on large scales]*

Phenomenon and direction of trend	Observed/detected trends since 1950 (for ca. +0.5°C global warming)	Human contribution to the observed trends since 1950 (for ca. +0.5°C global warming)
Warmer and/or more frequent hot days and nights over most land areas	*Virtually certain* on global scale Regional information : Table 11.1	*Extremely likely* main contributor on global scale Regional information : Table 11.1
Warmer and/or fewer cold days and nights over most land areas	*Virtually certain* on global scale Regional information : Table 11.1	*Extremely likely* on global scale
Warm spells/heatwaves; Increases in frequency or intensity over most land areas	*Virtually certain* on global scale Regional information : Table 11.1	*Very likely* on global scale
Cold spells/cold waves: Decreases in frequency or intensity over most land areas	*Virtually certain* on global scale Regional information : Table 11.1	*Very likely* on global scale
Heavy precipitation events: increase in the frequency, intensity, and/or amount of heavy precipitation	*Likely* more regions with positive than negative trends	*Likely* main contributor to the observed intensification of heavy precipitation in land regions
Drought events: Increases in frequency, intensity and/or duration	*High confidence* that atmospheric evaporative demand displays a global drying tendency over continents, and that there is an observed tendency towards increased drying in the dry season since the beginning of the 20th century, when aggregated on global scale (*high confidence*). *Medium confidence* that trends in potential evaporation have exceeded trends in precipitation in some regions and seasons.	*High confidence* that human influence has increased the drought potential and increased the tendency towards drying in the dry season since the beginning of the 20th century, when aggregated on the global scale
Floods and water logging: Increases in intensity and/or frequency	*Low confidence* in the majority of the world regions with the exception of increases in the Amazon (*high confidence*), Northwest US and UK (*medium confidence*). *High confidence* in changes of flood seasonality, mostly in snow dominated regions.	*Low confidence* due to little evidence and high seasonality.

Increase in precipitation associated with tropical cyclones	*Low confidence* for detectable global trend in tropical cyclone (TC) rain rates, due to data limitations. *Low confidence* for detectable global change in TC translation speed.	*Low confidence* for global TC rain rates and changes in translation speed. *Low to medium confidence* for contribution of TCs to detectable anthropogenic contribution to extreme rainfall events. *Medium confidence* for detectable anthropogenic contribution to global near-surface water vapour increases, which is expected to increase TC rainfall, all other things equal. Regional information : Table 11.1
Increase in tropical cyclone intensity (maximum surface wind speed)	Generally *low confidence* in detection of trends in historical tropical cyclone intensity in any basin or globally due to lack of confidence resulting from data inhomogeneities.	Generally *low confidence* in attribution of any anthropogenic influence on historical changes in tropical cyclone intensity in any basin or globally due to lack of confidence resulting from data inhomogeneities, with exception of North Atlantic (see Table 11.1).
Changes in frequency of tropical cyclones	*Low confidence* in detection of trends in historical tropical cyclone frequency in any basin or globally due to lack of confidence resulting from data inhomogeneities. Furthermore, physical process understanding is still unclear and there is no clear expectation for an increase in overall frequency with increasing greenhouse gas concentration.	*Low confidence* in attribution of any anthropogenic influence on historical changes in tropical cyclone frequency in any basin or globally due to lack of confidence resulting from data inhomogeneities, with exception of North Atlantic (see Table 11.1).
Poleward migration of tropical cyclones	*Low confidence* for a detectable global signal. Regional information : Table 11.1	*Low confidence* for global migration. Regional information : Table 11.1
Slowdown of tropical cyclone translation speed	*Low confidence* due to a present limited literature and lack of consensus on model results.	*Low confidence.*
Severe convective storms (tornadoes, hail, rainfall, wind, lightning)	*Low confidence* in past trends in hail and winds and tornado activity due to short length of high-quality data records.	*Low confidence*.
Increase in compound events	*Medium confidence* that likelihood of compound flooding as increased along the US coastline. *High confidence* that co-occurrent heatwaves and droughts are becoming more frequent under enhanced greenhouse gas forcing at global scale. *Medium confidence* that wildfires have become more intense and that their frequency has increased in some fire-prone regions.	*Low confidence* that human influences has contributed to changes in compound events leading to flooding. *High confidence* that human influence has increased the frequency of co-occurrent heatwaves and droughts. *Medium confidence* that human influence has increased wildfire occurrence in some regions.

[END TABLE TS.7 HERE]

[START TABLE TS.8 HERE]

Table TS.8: [Summary table on projected changes in extremes on global and continental scale. Table 11.2 is a more detailed version of this table, containing in particular an additional column for projected changes at +2°C global warming.] [*Purpose: Provide an overview of observed changes in extremes and their attribution to human activity on large scales*]

Phenomenon and direction of	Projected changes at +1.5°C global warming (unless specified: compared to	Projected changes at +3°C global warming (unless specified: compared to pre-industrial

trend	pre-industrial conditions)	conditions)
Warmer and/or more frequent hot days and nights over most land areas	*Virtually certain* on global scale *Extremely likely* on all continents *Virtually certain* larger increases at +1.5°C compared to +1°C in most land regions Frequency of very hot days (1% probability) ~3 times larger on global scale compared to present (*high confidence*; Box on Global warming levels) Decadal average warming of hottest days of up to +3°C in mid-latitudes (*medium confidence*)	*Virtually certain* on global scale *Extremely likely* on all continents *Virtually certain* larger increases at +3°C compared to +2°C in most land regions Decadal average warming of hottest days of up to +6°C in mid-latitudes (*medium confidence*)
Warmer and/or fewer cold days and nights over most land areas	*Virtually certain* on global scale *Extremely likely* on all continents *High confidence* in larger decreases at +1.5°C compared to +1°C in most land regions Warming of coldest nights of up to +4.5°C (e.g. Arctic) (*medium confidence*)	*Virtually certain* on global scale *Extremely likely* on all continents *Extremely likely* larger decreases at +3°C compared to +2°C in most land regions Warming of coldest nights of up to +9°C (e.g. Arctic) (*medium confidence*)
Warm spells/heatwaves; frequency and/or duration increases over most land areas	*Virtually certain* on global scale *Extremely likely on* all continents	*Virtually certain* on global scale *Extremely likely* on all continents
Increase in marine heatwave (MHW) frequency, intensity and duration	*Very likely* in all ocean basins, but with differential magnitudes in space. *High confidence* that a permanent MHW state can be avoided.	*Very likely* in all ocean basins, but with differential magnitudes in space. *Medium confidence* of a near permanent MHW state in many parts of the ocean
Cold spells/cold waves: Decreases in frequency, intensity and/or duration over most land areas	*Very likely* on global scale	*Very likely* on global scale
Heavy precipitation events: increase in the frequency, intensity, and/or amount of heavy precipitation	*Very likely* on global scale *Very likely* increase at +1.5°C compared to +1°C on global scale Regional information : Table 11.2	*Very likely* on global scale *Very likely* in most continents but *low confidence* in Australasia, Central and South America *Very likely* increase at +3°C compared to +2°C on global scale
Increases in floods and water logging	*Medium confidence* in a larger fraction of land area affected by flood hazard at global scale compared pre-industrial time and compared to present	*High confidence that* flood hazard would be even more widespread at +3°C compared to +2°C given projected changes in heavy precipitation; in part lack of literature to quantitatively assess projected changes.
Increases in intensity and/or duration of drought events	*High confidence* that atmospheric evaporative demand will continue to increase and lead to further drying tendencies in some regions *Medium confidence* in increase in drought probability in subtropical regions Regional information : Table 11.2	*High confidence* that atmospheric evaporative demand will continue to increase and lead to further drying tendencies in some regions *Medium confidence* in increase in drought probability in subtropical regions, with higher probability of intense/frequent droughts than at 2°C of global warming ; *Medium confidence* in expansion of drought probability outside these

		regions given increased radiative forcing, with probability of intense droughts being higher than at 2°C of global warming Regional information : Table 11.2
Increase in precipitation associated with tropical cyclones (TC)	*High confidence* in a projected increase of TC rain rates at the global scale; the median projected rate of increase is about 11%. *Medium confidence* that rain rates will increase in every basin.	*High confidence* in a projected increase of TC rain rates at the global scale; the median projected rate of increase is about 21%. *Medium confidence* that rain rates will increase in every basin.
Increase in mean tropical cyclone lifetime-maximum wind speed (intensity)	*Medium-to-high confidence* for a 3.75% increase.	*Medium-to-high confidence* for a 7.5% increase.
Changes in frequency of tropical cyclones	*Medium-to-high* confidence for an increase in the proportion of TCs that reach the strongest (Category 4-5) levels. The median projected increase in this proportion is about 10%.	*Medium-to-high confidence* for an increase in the proportion of TCs that reach the strongest (Category 4-5) levels. The median projected increase in this proportion is about 20%.
Severe convective storms	M*edium confidence* that the frequency of severe convective storms increases in the spring with enhancement of CAPE, leading extension of seasons of occurrence of severe convective storms. *High confidence* of future intensification of precipitation associated with severe convective storms.	
Increase in extreme sea levels	*High confidence* for substantial frequency increases in the current 1% annual probability event.	*High confidence* for further frequency increases in the current 1% annual probability event.
Increase in compound events (frequency, intensity)	*High confidence* that co-occurrent heatwaves and droughts will continue to increase under higher levels of global warming, with higher frequency/intensity with every additional 0.5°C of global warming. *Medium confidence* that humid heatwaves will continue to increase under higher levels of global warming, with higher frequency/intensity with every additional 0.5°C of global warming. *Medium confidence* that compound flooding at the coastal zone will increase under higher levels of global warming, with higher frequency/intensity with every additional +0.5°C of global warming.	

[END TABLE TS.8 HERE]

[START BOX TS.4 HERE]

Box TS.4: Irreversibility, Abrupt Change and Tipping Points

The concepts

Under modest anthropogenic forcing (e.g., cumulative carbon dioxide emissions), the response of many aspects of the climate system is proportional to the strength of the forcing (Figure TS.29, Cross-Section Box 2). However, the paleoclimate record indicates that past changes, such as deglaciation after ice ages, can make abrupt shifts toward new regimes. Models that exhibit such behaviour are characterised by tipping points or thresholds that, once crossed, make a return to the former state difficult or change irreversible over centuries. As climate, since the Holocene, has been stable enough to avoid any significant global climate regime shifts, it is difficult to estimate in which climate processes such thresholds exist, what value of forcing will commit the system to crossing them, and the rate of change after they are crossed.

A familiar and common example of a tipping point is when a population shrinks to the extent that extinction becomes unavoidable: an irreversible process caused by strong detrimental changes to species' niche or habitat. The abrupt shift in behaviour after crossing a threshold implies a new scaling or regimes not representative of responses typical before the threshold was crossed. Thus, a reduction in ice sheet mass or ocean overturning under forcing does not necessarily imply an abrupt shift - it is a sudden change toward higher sensitivity that does. A variety of climate processes are examined in this assessment to see if tipping points exist, can be predicted, have what threshold, and if they have been crossed. Many of the slow to respond systems such as the deep ocean and its overturning circulation or the responses of the Greenland and Antarctic ice sheets are suspected of having tipping points, and their slow response to climate change strongly hinders our ability to observe imminent thresholds or even to know if we have already committed to change that will cross a threshold already.

Faster responding earth system components can have tipping points ruled out observationally in the past or near future. Thus, the ocean and ice sheet response on multi-decadal to centennial timescales under strong forcing retains uncertainty due to potential tipping points. However, monitoring systems are being put into place to observe if mechanisms associated with tipping in models are occurring or increasing in frequency. This network will reduce the uncertainty associated with tipping, by selecting among different probabilities--those before the tipping point and those beyond. Marine Ice Sheet Instability (MISI) and the Marine Ice Cliff Instability (MICI) are examples--recent observations indicate that MISI may have begun, which is reducing the potential future uncertainty by sharpening rate estimates. A large part of model spread in ice sheet contributions to sea level rise involves whether or not MICI will be significant during this or coming centuries. Many other processes in ice sheets, ice shelves and ocean are undergoing similar study. The slow timescale response of ocean & cryosphere elements mean that tipping points are hidden observationally or potentially lie in wait even at low sustained warming levels (~2°C).

From observational evidence to models

An *abrupt climate change* is defined in this report as a regional to global scale change that occurs much faster than the rate of change of the external climate forcing. By this definition, abrupt climate change implies significant non-linearity in the response of the large-scale climate to forcing. In some cases, abrupt change occurs because the current state actually becomes unstable, such that the subsequent rate of change is independent of the forcing. We refer to this class of abrupt climate change as a *tipping point*. Some of the abrupt changes and tipping points discussed in this report (see, e.g., Sections 4.7.2, 5.4.5, 8.6) could have severe local impacts, such as extreme temperature, droughts and forest fires. There is good evidence of abrupt change and even of tipping points in the paleoclimate record, fuelling concerns that anthropogenic greenhouse gases could tip the climate into a permanent hot-house state. However, there is no evidence of such non-linear responses at the global scale in climate projections for the next century, which indicate a near-linear dependence of global temperature on cumulative greenhouse gas emissions (Section 1.3; Chapter 5). However, at the regional scale, abrupt changes and tipping points have been detected in Earth System Models. Tipping points occur in narrow regions of parameter space (e.g. CO_2 concentration or temperature increase), and for specific climate background states. This makes them difficult to predict using mechanistic ESMs. In some cases, it is possible to detect forthcoming tipping points through time-series analysis that identifies increased sensitivity to perturbations as the tipping point is approached (e.g. 'critical slowing-down'). {1.3, 1.4.5}

The AR5 assessments on post-2100 zero-emission commitment trajectories and reversibility based on Earth system models of intermediate complexity have now largely been confirmed with comprehensive Earth system models (*high confidence*). Particularly important among these advances has been the reduction in uncertainty in the requirement for net-zero emissions for temperature stability. Long-term reversibility has been substantiated for many atmospheric, land surface and sea ice climate metrics following sea surface temperature recovery. Some metrics such as Atlantic Meridional Overturning Circulation intensity have been found to undergo recovery even without reversal of sea-surface temperature change. Substantial irreversibility is further substantiated for cryosphere and ocean warming. {4.7.2}

Assessment of potential future irreversibility, abrupt change and tipping points

For global warming up to 2ºC above preindustrial levels, paleoclimate records do not provide strong support for abrupt changes in the carbon cycle (*low confidence)*. In response to climate forcing, paleoclimate records show changes of a magnitude larger than 100 ppm in atmospheric CO_2 over several millennia and abrupt smaller changes of about 10 ppm over centuries. However, the annual CO_2 emissions rates from any of these paleoclimate changes are one order of magnitude slower than the contemporary perturbation from anthropogenic emissions, suggesting caution when using the paleo record as an analogue for contemporary and future carbon-climate feedbacks. {5.1.3, Figure 5.2}

The response of biogeochemical cycles to human forcing may be abrupt at regional scales, and irreversible on decadal to century timescales (*high confidence*). There is *high confidence* that thawing terrestrial permafrost will lead to carbon release, but the timing, magnitude and the relative roles of CO_2 versus CH_4 as feedback processes are known with *low confidence*. An ensemble of models project feedbacks due to CO_2 release from permafrost of 20 ± 13 PgC per degree of global warming by 2100. However, the incomplete representation of important processes such as abrupt thaw, combined with weak observational constraints, only allow *low confidence* in both the magnitude of these estimates and in how linearly proportional this feedback is to the amount of global warming. Because of water-saturated soils and a lack of oxygen in thawing permafrost regions, part of the carbon is released as CH_4, which leads to the combined radiative forcing being larger than from if there were CO_2 emissions only. {5.4.3, 5.4.8}

The probability of crossing regional thresholds (e.g., forest dieback) increases with climate change, but there is no one particular threshold of global warming or atmospheric CO_2 identified in Earth system model projections. There is *medium confidence* that carbon-climate feedbacks can have a discernible effect on global atmospheric GHG concentrations, but do not lead to runaway changes over the next 100 years. Large uncertainties remain on the possibility of additional feedbacks not represented in many current models (e.g., fires) which could lead to departures from the current modelled trajectories. {5.4.8}

It is *very likely* that positive land surface feedbacks and potential remediation measures such as solar radiation modification can drive abrupt changes in the water cycle globally and regionally. At the regional scale, non-linear responses and even reversals in the rate of change cannot be excluded. Observations and model simulations suggest that there are strongly positive land surface feedbacks that cause abrupt changes in the water cycle, including changes in vegetation cover, dust, and snowpack. Such changes can facilitate rapid onset of drought, increased rainfall, and water availability on a regional scale. Continued Amazon deforestation, combined with a warming climate, raises the probability that this ecosystem will cross a tipping point into a dry state. However, there is *low confidence* that such a change will occur by 2100. It is *very likely* that abrupt water cycle changes will occur if solar radiation modification techniques are implemented rapidly or terminated abruptly. The impact of solar radiation modification is *likely* heterogeneous and will affect different regions in diverse and potentially disruptive ways. {8.5.3, 8.6.2, 8.6.3}

Uncertainties and past non-linear or abrupt responses of hydrologic systems mean that low probability, high impact changes to the water cycle cannot be excluded. There is evidence of abrupt change in some high emissions projections, but there is no overall consistency regarding the magnitude, speed, and timing of such changes in currently available model simulations. There is *low confidence* that abrupt changes in acidification and rainfall will occur by 2100, although the possibility of abrupt events cannot be ruled out. The paleoclimate record shows that a collapse in Atlantic Meridional Overturning Circulation (AMOC) can cause abrupt and large-magnitude shifts in the water cycle (*high confidence*) such as a southward shift in the ITCZ, weakening of the African and Asian monsoons and strengthening of Southern Hemisphere monsoons. Some model projections suggest that if AMOC collapses in the future, a similar response in the water cycle will occur, although the pattern of change would be compounded by the effects of higher atmospheric CO_2. While it is *unlikely* that AMOC will collapse by 2100, it is *very likely* that there would be abrupt, regional changes in the water cycle if AMOC collapsed. {8.6.1}

Robust observed changes in the Atlantic Meridional Overturning Circulation (AMOC) are not presently linked to anthropogenic causes, but the AMOC will *likely* decline in response to human-induced climate change for all scenarios. The weakening of the AMOC between 2007 and 2011 is within the range of natural variability inferred from reanalysis, reconstructions and model simulations of the historical period (*high confidence*). Projected AMOC decline by 2100 is only weakly dependent on emission scenario ranging from 40% in SSP1-1.9 to 50% in SSP5-8.5 (*medium confidence*). An abrupt collapse of the AMOC before 2100 is *unlikely* with deep uncertainty beyond 2100 associated with meltwater fluxes from Greenland and Antarctica. Detecting long-term changes in other large-scale circulation systems remains challenging due to observation limitations, but the Southern Ocean overturning circulation, eastern boundary upwelling systems and Indonesian Throughflow are predicted to respond to changes in the atmospheric circulation. (*high* *confidence*) {9.2.3}

For future warming levels between 2 and 3°C, there is *medium confidence* that the Greenland Ice Sheet will pass a threshold where long-term mass loss becomes irreversible over centennial timescales. {9.4.1, 9.4.2}

Knowledge gaps

There are currently several knowledge gaps associated with assessments on changes in the dynamics driving extreme events in past and future. Some topics are still insufficiently investigated such as hail, and there are some remaining uncertainties regarding changes in some extremes such as droughts and tropical cyclones, although evidence have become much more robust in these areas compared to the AR5. Also, there is *low confidence* regarding the global warming levels at which possible changes associated with global and regional tipping points (low-probability high-impact events) related to extremes would occur, but these cannot be excluded, especially at high global warming levels (>3°C). Finally, there are still remaining important data and literature gaps in several regions of the world, in particular in Africa and South America. {11.10}

[START BOX TS.4, FIGURE 1 HERE]

Box TS.4, Figure 1: The idea is to show probability distributions together with a decision tree--probability without tipping vs. probability after tipping. Inspirational Chapter figures--1.12, 9.19, 9.27, 9.32. This figure is from the cited paper listed, and it shows some of the key aspects of compiling sea level models with different physics/tunings/sensitivity. Modified to suggest the conditional probability distribution of MICI vs. no MICI (an example, but could also be AMOC collapse, methane clathrates, etc.). This figure could be made quantitative for Marine Ice Cliff Instability using Figure 9.27 data from literature ranges. *[PURPOSE: The idea is to show probability distributions together with a decision tree-probability without tipping vs. probability after tipping. Inspirational Chapter figures: 1.12, 9.19, 9.27, 9.32. Suggestions for additional figure ideas to illustrate/combine other elements of Irreversibility, Abrupt Change and Tipping Points].*

[END BOX TS.4, FIGURE 1 HERE]

[END BOX TS.4 HERE]

TS.2.7.7 Summary of observed and projected changes in extremes

Changes in extremes are widespread since the 1950s, including a *virtually certain* increase in extreme air temperature and marine heatwaves (*high confidence*), intensification in extreme precipitation (*high confidence*), and the potential for worsening of drought conditions in the dry season when aggregated on the global scale (*high confidence*). There is *high confidenc*e that concurrent hot and dry extremes have increased on a global scale. It is *extremely likely* that human influence is the main contributor to the observed increase in the likelihood and severity of hot extremes (including marine heatwaves) and the observed decrease in the likelihood and severity of cold extremes. {11.8.2}

An additional half degree of global warming would be sufficient to cause further detectable changes in temperature extremes (*virtually certain*) and precipitation extremes (*very likely*) at the global scale. Projected changes in the magnitude of temperature and precipitation extremes are proportional to the magnitude of global warming at the global scale. The frequency of extreme temperature and precipitation events in the current climate will change with warming, with warm extremes becoming more frequent (*virtually certain*), cold extremes becoming less frequent (*extremely likely*) and precipitation extremes becoming more frequent in most locations (*very likely*). It is *likely* that the frequency of rarer events will be multiplied by a much larger factor than that of less rare events under higher warming. There is *high confidence* that the highest category tropical cyclones will be associated with increased maximum wind speed and precipitation with increasing warming levels. There is *high confidence* that concurrent extreme events affecting similar sectors (e.g., breadbaskets) in different regions, will become more frequent.

TS.2.8 Changes across the global climate system

Directly observed atmospheric, oceanic, cryospheric and biospheric changes provide unequivocal evidence of a warming world. Many key climate indicators are now in states not experienced for centuries to millennia or longer (Table TS.9), and since 1900 several key indicators of the global climate system have changed at a rate unprecedented over at least the last two thousand years. {2.3.5}

[START TABLE TS.9 HERE]

Table TS.9: Three large-scale climate indicators (GMST/GSAT, CO_2, sea level) across paleo, present and future from observations and simulations. *[PURPOSE: Summary table that integrates past, present and future based on both observations (direct and indirect) and simulations. This puts recent and future changes in context of the full range of climate variability and illustrates how long it's been since the climate was similar to recent/projected states. This table includes the three biggest-picture indicators, but could be expanded with additional columns (or transposed to include more rows). This complements the figures with time-series data in TS1 and TS2 because it avoids breaks/shifts in x-axis time scales, which can be difficult to comprehend, and because it calls out the values (not just graphical). Colours or graphics could be used to improve the presentation.]*

	Age[1]	**Global mean temp. (°C)**[2]			CO_2 **(ppm)**[3]			**Global sea level (m)**[4]		
Period	**(CE or years ago)**	***2.6***	***4.5***	***8.5***	***2.6***	***4.5***	***8.5***	***2.6***	***4.5***	***8.5***
Future 2	2280-2300	2.4 ± 0.4	4.3 ± 1.1	10.7 ± 4.3	363	543	2171	0.4 ± 0.1	0.7 ± 0.1	1.4 ± 0.1
Future 1	2081-2100	2.0 ± 0.6	3.0 ± 0.9	4.8 ± 1.6	426	535	1000	0.30 ± 0.02	0.35 ± 0.03	0.44 ± 0.07
Present	1995-2014	0.78 – 1.05 / x.xx – x.xx			360 – 397			0.16 ± 0.04		
PI reference	1850-1900	0 ± 0.06 / 0 ± 0.xx			287 – 297			-0.01 ± 0.02		
Mid Holocene	6,000	0.5 ± 0.3 / -0.3 ± 0.3			264 ± x			-3 ± 0.5		
Last glacial maximum	20,000	-6 ± 1.5 / -3.8 ± 0.3			187 – 195			-130 ± 5		
Last interglacial	125,000	1.5 ± 0.5 / 0.0 ± 0.6			272 – 280			7 ± 4		
Mid Pliocene	3,000,000	3 ± 1 / 2.8 ± 1.8			350 – 425			15 ± 10		
Early Eocene	50,000,000	14 ± 2 / xx ± x			1000 – 1800			72.5 ± 3		

Black font = observed or reconstructed; orange font = simulated
Values reported as either range of best values across the reference period (a – b), or as indicative value for the period, with 2 SD uncertainty (a ± b)
[1]Ages are rounded for paleo reference periods (CCB 2.1)
[2]Global mean surface temperature (GMST) is used for paleo reference periods; global surface air temperature (GSAT) is used for the instrumental period. Values for Future 2 GSAT are ± one half of model range.
[3]Values for Future 1 and 2 CO_2 are mid-points of range over interval.
[4]Values for Future 1 and 2 global sea level are ± one half of model range.

[END TABLE TS.9 HERE]

For most large-scale indicators of climate change, the ability to simulate the observed mean climate has improved in the latest-generation climate models underpinning this assessment compared to the models assessed in the AR5 (*high confidence*). Compared with the models used for paleoclimate simulations in the

AR5, the polar amplification simulated in more recent models is now more consistent with paleoclimate observations of past warm climates. High-resolution models exhibit reduced biases in some but not all aspects of surface and ocean climate (*medium confidence*). While a broad range of warming rates across models and a lengthening observational record mean that significant differences between the climate response in individual models and observations can often be identified, the multi-model mean captures most aspects of observed climate change well (*high confidence*). {3.8.2, 7.2.2, 7.4.4}

The IPCC Second Assessment Report (1995) identified a discernible human influence on the climate. Since then, and throughout subsequent assessments (TAR, 2001; AR4, 2007 and AR5, 2013), the evidence for human influence on the climate system has progressively strengthened. The AR5 concluded that human influence on the climate system is clear, evident from increasing greenhouse gas concentrations in the atmosphere, positive radiative forcing, observed warming, and physical understanding of the climate system. This evidence is now even stronger (Figure TS.23, Table TS.10). Synthesizing evidence from observed changes across the climate system and knowledge of changes in ERF, it is unequivocal that human activities have warmed the climate system. Combining the evidence from across the climate system increases the level of confidence in the attribution of observed climate change to human influence and reduces the uncertainties associated with assessments based on single variables. Large-scale indicators in the atmosphere, ocean and cryosphere show clear responses to anthropogenic forcing consistent with those expected based on model simulations and physical understanding. {3.3, 3.4, 3.5, 3.6, 3.7, 3.8, 7.3.5, Cross-Chapter Box 7.1}

Emissions reductions as represented in the low-emissions scenarios SSP1-1.9 and SSP1-2.6 are *virtually certain* to limit globally averaged surface warming in the latter half of the 21st century, but the effect of emissions reductions on the globally averaged warming rate in the near term (2021-2040) will be hard to detect due to masking by natural internal variability (*high confidence*). {4.6.3}

[START FIGURE TS.23 HERE]

Figure TS.23: Summary figure showing simulated and observed changes in key large-scale indicators of climate change across the climate system, for continental, ocean basin and larger scales. Black lines show observations, red lines and shading show the multi-model mean and 5-95th percentile ranges for CMIP6 historical simulations including anthropogenic and natural forcing, and green lines and shading show corresponding ensemble means and 5-95th percentile ranges for CMIP6 natural-only simulations. (Updated from Figure 3.7) *[PURPOSE: To compare the observed and simulated changes over the historical period for a range of variables are regions, with and without anthropogenic forcings, for attribution. Suggestions for alternative ways to present this information are welcome.]*

[END FIGURE TS.23 HERE]

[START TABLE TS.10 HERE]

Table TS.10: Assessments of observed changes in global-scale indicators of climate change across climate system components, and their attribution to human influence. Colour coding of attribution assessments: *virtually certain* anthropogenic main driver/substantial contribution; extremely *likely* anthropogenic main driver/substantial contribution; *very likely* anthropogenic main driver/substantial contribution; *virtually certain* anthropogenic contribution; extremely *likely*/*very likely*/*likely* anthropogenic contribution/*likely* attributable; medium confidence anthropogenic contribution. Note that observational assessments without confidence or likelihood qualifiers are statements of fact. *[PURPOSE: To provide a summary of the observed changes across all sections of TS2 alongside statements of attribution to human influences.]*

Change in indicator	**Assessment of observed change**	**Assessment of human contribution to the observed change**
Atmosphere and water cycle		
Warming of global mean surface	The estimated change in GSAT from	*extremely likely* that human influence is the main

air temperature since 1850-1900	1850-1900 to 2009-2018 is 1.10°C (0.97 – 1.25°C) {2.3.1, Cross-Chapter Box 2.3}	driver {3.3.1}
Warming of the troposphere since 1979	The troposphere has warmed since at least the 1950s {2.3.1}	*very likely* that human influence, dominated by greenhouse gases, was the main driver {3.3.1}
Cooling of the lower stratosphere since 1979	*virtually certain* that the stratosphere has cooled {2.3.1}	*extremely likely* that human influence, dominated by stratospheric ozone depletion, was the main driver {3.3.1}
Large-scale precipitation changes since 1979	*likely* that global land precipitation has increased since 1950, with a faster increase since the 1990s (*medium confidence*) {2.3.1}	*likely* that human influence has contributed to observed large-scale precipitation changes {3.3.2, 3.3.3}
Expansion of the zonal mean Hadley Circulation	*very likely* that the Hadley Circulation has widened and intensified since at least the 1980s, mostly in the Northern Hemisphere. {2.3.1}	*medium confidence* that greenhouse gas increases and stratospheric ozone depletion have contributed in the Southern Hemisphere {3.3.3}
Ocean		
Ocean heat content increase over the historical period	The global ocean has warmed since at least 1971 {2.3.3, 2.3.4, Cross-Chapter Box 2.4}	*extremely likely* that anthropogenic forcing has made a substantial contribution {3.5.1}
Salinity changes since the mid-20th century	*virtually certain* f that large-scale changes in near-surface salinity patterns (fresh get fresher, saltier get saltier) have occurred since at least 1950. {2.3.3, 2.3.4, Cross-Chapter Box 2.4}	*extremely likely* that human influence has contributed {3.5.2}
Global mean sea level rise since 1979	GMSL is now rising at a higher rate than anytime in at least the last 3000 years. {2.3.3}	*very likely* that anthropogenic forcings are the main driver {3.5.3, 3.5.1, 3.4.3}
Cryosphere		
Arctic sea ice loss since 1979	*very high confidence* that since the late 1970s, Arctic sea-ice area has decreased in both summer and winter and it has become thinner {2.3.2, Cross-Chapter Box 2.1, Cross-Chapter Box 2.4}	*very likely* that anthropogenic forcing was the main driver {3.4.1}
Reduction in Northern Hemisphere springtime snow cover since 1950	*very high confidence* that reductions in spring snow cover extent have occurred across the Northern Hemisphere since at least 1978. {2.3.2, Cross-Chapter Box 2.1, Cross-Chapter Box 2.4}	*very likely* that anthropogenic influence contributed {3.4.2, 3.4.3}
Retreat of glaciers	*very high confidence* that, with few exceptions, glaciers worldwide have retreated, since the cessation of the Little Ice Age, and continue to retreat. {2.3.2, Cross-Chapter Box 2.1, Cross-Chapter Box 2.4}	*very likely* that anthropogenic influence contributed {3.4.2, 3.4.3}
Biosphere		
Increased amplitude of the seasonal cycle of atmospheric CO_2	*medium confidence* in an enhanced seasonal cycle in the atmospheric burden of CO_2 {2.3.4.6}	*likely* attributable to fertilisation of plant growth by increased CO_2 {3.6.1}
Acidification of the global ocean	*high confidence* that ocean	*virtually certain* that the uptake of anthropogenic

	acidification is strengthening as a result of the ocean continuing to take up 23 ± 6% of the global anthropogenic CO_2 emissions {5.3.2, 5.3.3,Figure 5.20, Figure 5.21}	CO_2 has substantially contributed {3.6.2}
Synthesis		
Warming of the global climate system	Directly observed atmospheric, oceanic, cryospheric and biospheric changes provide unequivocal evidence of a warming world {2.3.5}	*virtually certain* that human influence has warmed the global climate system {3.8.1}

[END TABLE TS.10 HERE]

In conclusion, a wide range of indicators across all components of the climate system are changing rapidly. Many are in states unseen in millennia, and surface temperature is now in a state *as likely as not* unseen in at least 100,000 years, even if decades or centuries with similar temperatures cannot be ruled out. The combination of many independent observations showing that the Earth system changing in a way that is consistent with our understanding of the effects of greenhouse gas emissions provides irrefutable evidence of the impact of human activities on the global climate system (*very high confidence*). Based on fundamental understanding of the climate system (see also the following section TS3) that is confirmed by ever accumulating evidence of ongoing rapid change predicted already several decades ago, and on continuously improving climate models, the many facets of observed climate change are expected to continue or even accelerate in the coming decades unless there are dramatic reductions in emissions of greenhouse gases. Internal variability will continue to modulate rates of change on interannual-to-decadal timescales with greater importance at regional scales (TS4). Neglecting effects of potential large volcanic eruptions that could induce global-scale cooling on annual time scales, and notwithstanding decadal-scale climate variability limiting the capacity to predict the near-term evolution of the climate system, it is *virtually certain* that rapid implementation of substantial global GHG emission reductions as represented in the low-emissions scenarios SSP1-1.9 and SSP1-2.6 will limit globally averaged surface warming, globally averaged land precipitation increase and ice loss in the latter half of the 21st century (see also Cross-Section Box1 and Cross-Section Box 2). These fast responses contrast with the slow response of the ocean and ice-sheets to changes in GHG emissions, which will result in substantial committed sea-level rise under all scenarios for at least the next century. Failure to implement reductions in GHG emissions greatly enhances the risk of potentially irreversible changes in the global climate system (see Box TS.4), implying multi-millennial commitment in particular with respect to the contribution of ice sheets to global sea level change. {2.3.5, 3.3, 3.4, 3.5, 3.6, 3.7, 3.8, 4.6.3, 7.2.2, 7.3.5, 7.4.4, Cross-Chapter Box 7.1}

[START CROSS-SECTION BOX 1 HERE]

Cross-Section Box 1: Scenario-based future climate system changes across timescales

This Cross-Section Box presents findings of scenario-based climate model projections with the intent to discuss the evidence base underlying the assessment of future climate at different timescales. Selected indicators of global climate change are presented at reference time periods assessed in this report (near-term: 2021–2040, mid-term: 2041–2060, long-term: 2081-2100) and beyond 2100, where relevant. The temporal evolution of these key variables is presented in Cross-Section Box 1 Figure 1. This Cross-Section Box complements findings presented in Cross-Section Box 2 on global warming levels, Climate change as function of the level of global warming, including an assessment of the likelihood and timing of achieving specific warming levels during the 21st century.

The use of different scenarios for climate change projections introduces a ‘scenario-uncertainty’ in the projections (see Section TS1.3.1). Depending on the spatial and time scales of the projection, and on the variable of interest, the relative importance of scenario uncertainty compared to other sources of uncertainty like model structural choices and internal variability may vary substantially. {1.4.3, 1.6}

[START CROSS-SECTION BOX 1, FIGURE 1 HERE]

Cross-Section Box 1, Figure 1: Selected indicators of global climate change from CMIP6 historical and scenario simulations. (a) Global surface air temperature changes relative to the 1995–2014 average (left axis) and relative to the 1850–1900 average (right axis); the axes differ by 0.87°C. (b) Global land precipitation changes relative to the 1995–2014 average. (c) September Arctic sea-ice area. (d) Global sea level change relative to the 1995–2014 average. Curves with shading are global mean sea level (GMSL) and curves without shading are the contributions due to thermal expansion. (a), (b) and (d) are annual averages, (c) are September averages. In (a), the assessed time series of 20-year averages are shown from 2015 onwards, combining multiple lines of evidence. In (b) and (c), the curves show averages over the r1 simulations contributed to the CMIP6 exercise, the shadings around the SSP1-2.6 and SSP5-8.5 curves show 5 to 95% ranges (i.e., mean ± standard deviation times 1.645), and the numbers near the top show the number of model simulations. In (d), the contribution from ocean thermal expansion (thermosteric) is based on the r1 simulations in CMIP6; the contributions from land-ice melt have been computed using an emulator as in Chapter 9. [Note: In (a), the offset between the left and the right y-axes use the GMST instead of GSAT change, from 1850–1900 to 1995–2014. The axes thus assume an offset of 0.87°C, rather than 0.91°C, between these two time periods. The figure will be updated with the proper GSAT offset in the FGD.] {Figure 4.1}

[END CROSS-SECTION BOX 1, FIGURE 1 HERE]

Changes in global surface air temperature (GSAT)

The AR6 assessment of future GSAT is based on multiple lines of evidence, combining new projections forced by the core set of illustrative SSP scenarios (Section TS1.3) with observational constraints based on past simulated warming as well as the AR6-updated assessment of equilibrium climate sensitivity and transient climate response. Including lines of evidence in addition to the projection simulations has been possible through substantial research progress since previous IPCC assessments and has both reduced the assessed uncertainty ranges and increased the confidence in them. Internal variability in GSAT change, for example, can now be estimated robustly from several initial-condition large ensembles. The assessed future ranges of projections are constrained through the assessment of forcings, feedbacks and responses, which inform likelihood statements. {4.3.1, 4.3.4, 4.4.1}

Averaged over the near term (2021–2040), GSAT is *very likely* to be higher than during the recent past (1995–2014) by about 0.7°C (0.4°C, 0.9°C), across all scenarios assessed here (Cross-Section Box 1, Table 1). This corresponds to a *very likely* warming of 1.6°C (1.3°C, 1.8°C) relative to the period 1850–1900. Uncertainty in near-term projections of annually averaged GSAT arises in roughly equal measure from natural internal variability and model uncertainty (*high confidence*). By contrast, near-term projections exhibit only minor dependence on the scenario chosen, consistent with the AR5 assessment. Internal variability in GSAT change can now be estimated robustly from several initial-condition large ensembles. Predictions initialized from recent observations simulate annually averaged GSAT changes for the period 2019–2028 relative to the recent past that are consistent with the assessed *very likely* range (*high confidence*). These assessments assume that there will be no large volcanic eruption in the near term. Volcanic eruptions would increase the frequency of globally extremely cold individual years and the likelihood of decades with cooling trends in GSAT (*high confidence*). {4.4.1, 4.4.4, BOX 4.1, 7.5}

The *very likely* GSAT changes averaged over the mid-term period (2041–2060) show a clear separation between high- and low-emission scenarios. For SSP1-1.9, GSAT is *very likely* to be higher than during the recent past (1995–2014) by 0.8°C (0.5°C, 1.1°C); for SSP5-8.5, GSAT is very *likely to* be higher by 1.6°C (1.1°C, 2.0°C). {4.3.4}.

The average GSAT over the period 2081–2100 is *very likely* to be higher than in the recent past (1995–2014) by 0.3°C–0.9°C in the low-emission scenario SSP1-1.9 and by 2.6°C–4.7°C in the high-emission scenario SSP5-8.5. For the scenarios SSP1-2.6, SSP2-4.5, and SSP3-7.0, the corresponding *very likely* ranges are

0.6°C–1.4°C, 1.3°C–2.5°C, and 2.0°C–3.8°C, respectively. For a given scenario, the uncertainty ranges for the period 2081–2100 continue to be dominated by the uncertainty in equilibrium climate sensitivity and transient climate response (*very high confidence*). {4.3.1, 4.3.4, 4.4.1, 7.5}

The CMIP6 multi-model ensemble range of projected warming by the end of the 21st century, relative to the period 1995–2014, is approximately 20% larger than the CMIP5 range. The range increases mainly because the upper end of the projected warming range increases, due to models with higher equilibrium climate sensitivity in CMIP6, compared to CMIP5 (*high confidence*). {4.3.1, 4.3.4, 7.6}

[START CROSS-SECTION BOX 1, TABLE 1 HERE]

Cross-Section Box 1, Table 1: Assessment results for GSAT change, based on multiple lines of evidence. The change is displayed in °C relative to the 1995–2014 reference period for selected time periods (near term 2021–2040, mid-term 2041–2060, and long-term 2081–2100), and as the time when certain temperature thresholds are crossed, relative to the period 1850–1900. The observed warming in 1995–2014 relative to 1850–1900 is 0.91°C (0.78–1.05°C) (Box TS.4, Table 1). The timing of crossing a threshold does not include the uncertainty arising from natural internal variability. The entries give both the best estimate and, in parentheses, the *very likely* (5–95%) range. There is *high confidence* in the changes over the twenty-year periods relative to 1995–2014, which combine constrained CMIP6 projections and emulator results (Cross-Chapter Box 7.1). There is *medium confidence* in the timings when certain global warming levels are reached, which are based on a combination of emulator results and one set of constrained CMIP6 projections for SSP1-2.6, SSP2-4.5, and SSP5-8.5 but solely on emulator results for SSP1-1.9 and SSP3-7.0. An entry n.a. means that the global warming level is not attained during the period 2021–2100. [Note: This table is identical to Table 4.6 in Section 4.3.4, where the timing entries for when certain global warming levels are reached use the GMST instead of GSAT change, from 1850–1900 to 1995–2014. The table thus assumes an offset of 0.86°C, rather than 0.91°C, between these two time periods. The table will be updated with the proper GSAT offset in the FGD.] [PLACEHOLDER: Table is a duplication of Table TS.5. This duplication will be resolved for the FGD]

	SSP1-1.9	SSP1-2.6	SSP2-4.5	SSP3-7.0	SSP5-8.5
Near term, 2021–2040, relative to 1995–2014	0.7 (0.4, 0.9)	0.6 (0.4, 0.8)	0.7 (0.4, 0.9)	0.7 (0.4, 0.9)	0.7 (0.5, 1.0)
Mid-term, 2041–2060, relative to 1995–2014	0.8 (0.5, 1.1)	0.9 (0.6, 1.2)	1.1 (0.8, 1.5)	1.3 (0.9, 1.8)	1.6 (1.1, 2.0)
Long-term, 2081–2100, relative to 1995–2014	0.6 (0.3, 0.9)	1.0 (0.6, 1.4)	1.9 (1.3, 2.5)	2.9 (2.0, 3.8)	3.6 (2.6, 4.7)
1.5°C, relative to 1850–1900	2028 (2022, n. a.)	2033 (2024, 2053)	2031 (2024, 2042)	2029 (2023, 2038)	2028 (2022, 2036)
2°C, relative to 1850–1900	n.a. (n.a., n.a.)	n.a. (2047, n.a.)	2050 (2040, 2073)	2046 (2036, 2060)	2042 (2035, 2051)
3°C, relative to 1850–1900	n.a. (n.a., n.a.)	n.a. (n.a., n.a.)	n.a. (2074, n.a.)	2074 (2058, 2098)	2064 (2054, 2078)
4°C, relative to 1850–1900	n.a. (n.a., n.a.)	n.a. (n.a., n.a.)	n.a. (n.a., n.a.)	2100 (2079, n.a.)	2082 (2069, 2100)

[END CROSS-SECTION BOX 1, TABLE 1 HERE]

Changes in precipitation

Global-mean land and global-mean ocean precipitation are *very likely* to increase as global surface air temperature increases over the 21st century under all five SSP scenarios (Cross-Section Box 1, Table 2). Based on multiple lines of evidence, global-mean land precipitation is *very likely* to increase approximately 1–3% per 1°C warming in globally averaged surface air temperature. {4.5.1, 4.6.1, 8.4.1}

Near-term projected changes in precipitation are uncertain mainly because of natural internal variability and uncertainty in natural and anthropogenic aerosol forcing (*medium confidence*). In the near term, no discernible differences in precipitation changes are projected between different SSP scenarios (*high confidence*). The anthropogenic aerosol forcing decreases in most scenarios, contributing to increasing global-mean surface air temperature (*medium confidence*) and global-mean land precipitation (*low confidence*). Observational and modelling studies show that a large volcanic eruption is *likely* to substantially alter precipitation changes for up to a few years following the eruption (*medium confidence*). Volcanic eruptions generally result in decreased global-mean land precipitation for up to a few years following the eruption, with climatologically wet regions drying and dry regions wetting (*medium confidence*). {4.3.1, 4.4.1, 4.4.4}

In the mid-term (2041-2060) SSP1-1.9, SSP1-2.6, SSP2-4.5 and SSP3-7.0 project similar changes in precipitation averaged over land of respectively 2.9% (0.9, 5.0), 2.7% (0.5, 5.0), 2.8% (0.7, 4.8), 2.4% (-0.3, 5.1) while SSP5-8.5 shows some separation in the upper range of its projections already from this time period with 3.8% (0.7,6.8). {4.3.1, Table 4.3}

By 2081-2100, precipitation over land increases on average by 2.7% (0.6, 4.8) under SSP1-1.9, 3.2% (0.7, 5.6) under SSP1-2.6, 4.7% (1.8, 7.7) under SSP2-4.5, 5.5% (0.5, 10.4) under SSP3-7.0 and 8.2% (2.5, 13.8) under SSP5-8.5. Globally averaged, precipitation increases by the same period are 2.2% (0.6, 3.8), 2.7% (0.9, 4.5), 4.1% (1.7, 6.4), 4.8% (1.8, 7.8) and 6.3% (2.6, 10.0) under the same scenarios, respectively. {4.3.1, Table 4.3}

[START CROSS-SECTION BOX 1, TABLE 2 HERE]

Cross-Section Box 1, Table 2: Projected precipitation changes (%) relative to averages over 1995–2014 for selected future periods, regions and SSPs. The multi-model averages across the individual models and the 5 to 95% ranges (based on multiplying the CMIP6 ensemble standard deviation by 1.645) are given in parentheses. Also shown are land precipitation changes at the time when global increase in GSAT relative to 1850–1900 exceeds 1.5°C, 2.0°C, and 3.0°C, and the percentage of simulations for which such exceedances are true (to the right of the parentheses). Here, the time of GSAT exceedance is determined as the first year at which 11-year running averages of GSAT exceed the given threshold. Land precipitation percent anomalies are then computed as 21-year averages about the year of the first GSAT crossing. [PLACEHOLDER: Table is a duplication of Table TS.6. This duplication will be resolved for the FGD] {Table 4.3, 4.3.1}

Units = %	SSP1-1.9	SSP1-2.6	SSP2-4.5	SSP3-7.0	SSP5-8.5
Land: 2021–2040	2.6 (0.9, 4.2)	2.1 (0.6, 3.5)	1.6 (0.1, 3.0)	1.1 (-0.6, 2.8)	1.8 (-0.2, 3.7)
2041–2061	2.9 (0.9, 5.0)	2.7 (0.5, 5.0)	2.8 (0.7, 4.8)	2.4 (-0.3, 5.1)	3.8 (0.7, 6.8)
2081–2100	2.7 (0.6, 4.8)	3.2 (0.7, 5.6)	4.7 (1.8, 7.7)	5.5 (0.5, 10.4)	8.2 (2.5, 13.8)
Global: 2081–2100	2.2 (0.6, 3.8)	2.7 (0.9, 4.5)	4.1 (1.7, 6.4)	4.8 (1.8, 7.8)	6.3 (2.6, 10.0)

Ocean: 2081–2100	2.0 (0.5, 3.6)	2.5 (0.7, 4.4)	3.8 (1.3, 6.4)	4.6 (1.5, 7.6)	5.8 (1.9, 9.7)
Land: ΔT > 1.5°C	2.1 (-0.4, 4.6) 60	2.2 (-1.7, 6.0) 95	1.9 (-2.3, 6.1) 100	1.3 (-2.8, 5.3) 100	1.8 (-2.1, 5.8) 100
ΔT > 2.0°C	3.9 (1.0, 6.7) 40	3.1 (-0.2, 6.4) 64	3.1 (-1.5, 7.7) 100	2.3 (-2.7, 7.3) 100	3.2 (-1.5, 7.9) 100
ΔT > 3.0°C	- (-, -) 0	- (-, -) 0	4.2 (-0.2, 8.6) 67	4.3 (-2.3, 10.9) 100	4.9 (-1.2, 11.1) 100

[END CROSS-SECTION BOX 1, TABLE 2 HERE]

Changes in ocean temperature, ocean circulation and sea ice

Long time-scale processes associated with ocean circulation commit the ocean to *virtually certain* warming until 2040 regardless of emissions. It is *likely* that ocean warming will continue at least to 2300 even for low-emission scenarios because of ocean inertia, but with a rate dependent on the scenario. After 2040, similar spatial patterns of present warming will continue to warm at a rate dependent on present and future emissions. (*high confidence*). Ocean heat content in the 0–2000 m layer will increase by 1410, 1700, 1960, or 2300 ZJ from 1995-2014 to 2081-2100 under scenarios SSP1-2.6, SSP2-4.5, SSP3-7.0, and SSP5-8.5, respectively. The strength of the Atlantic meridional overturning circulation (AMOC) is *very likely* to decrease by 2100, and larger decreases in volume transport are expected by 2100-2300 in high emissions scenarios. {9.2.2, 9.2.3}

It is *likely* that the Arctic Ocean will become effectively ice-free (coverage below 1 million km^2) in September, averaged over 2081-2100 in the SSP2-4.5, SSP3-7.0, and SSP5-8.5 scenarios. For CMIP6 models, including those models whose ensemble spread across their individual realizations due to internal variability include the observational range of uncertainty, the vast majority of simulations show an ice-free Arctic for the first time in September before 2050, and before future cumulative anthropogenic CO_2 emissions reach 1000Gt CO_2 (*high confidence*). {4.3.2}

Changes in global mean sea level (GMSL)

It is *virtually certain* that GMSL will continue to rise beyond 2100 with heat continuing to accumulate in the Earth system over the 21st century (*high confidence*) and *medium confidence* that the Earth system will continue to accumulate heat after 2100 for another century or more under any scenario (see Box TS.3). GMSL rise is highly dependent on emissions scenario after 2050. {Box TS.3 Table 1, 7.2.2, Box 7.2, Table 7.1, 9.6.3, Cross-Chapter Box 9.2 , Box 9.3}

In addition to scenario uncertainty, sea-level rise is subject to deep uncertainty in the ice-sheet response with the Antarctic ice sheet contribution to long-term sea-level rise currently highly uncertain. In addition to the possibly already initiated marine ice sheet instability leading to increased mass loss of the West Antarctic Ice Sheet, marine ice cliff instability is a poorly understood and currently debated process that could, in principle, lead to rapid irreversible mass loss once initiated {Box TS.3 Table 1, Box 9.3}

In spite of uncertainty in the future ice-sheet contribution, a few integrated sea-level rise projection studies have examined projections of GMSL rise along the extended scenarios (currently only RCPs) beyond 2100. Based on the available projections, GMSL rise through 2300 under RCP2.6 is assessed to be *likely* between 0.3 and 2.9 m, the range defined by the lowest 17th and highest 83rd percentile projection. There is *medium confidence* in the upper plausible limit of 4.7m suggested by the 95th percentile of the projections. There is *low confidence* in central projections of GMSL rise under higher emissions scenarios, and *medium confidence* that GMSL in the projection results which suggest a 99% chance that GMSL rise through 2300 will be less than 7.0 m under RCP4.5 and less than 15.5 m under RCP8.5. {9.6.3, Box 9.3}

[START CROSS-SECTION BOX 1, TABLE 3 HERE]

Cross-Section Box 1, Table 3: Global mean sea-level projections for the core set of 5 illustrative SSP scenarios, median values, (*likely*) and [*very likely*] ranges of the process-based model ensemble, relative to 1995-2014 in meters.

	2040	2050	2090	2100	2150	2300
SSP1-1.9						
SSP1-2.6	0.14 (0.10--0.17) [0.08--0.20]	0.19 (0.15--0.23) [0.12--0.27]	0.39 (0.28--0.52) [0.19--0.65]	0.47 (0.33--0.64) [0.21--0.84]		
SSP2-4.5	0.14 (0.10--0.17) [0.08--0.19]	0.19 (0.15--0.24) [0.12--0.28]	0.45 (0.35--0.58) [0.26--0.71]	0.55 (0.40--0.71) [0.28--0.89]		
SSP3-7.0	0.14 (0.11-- 0.17) [0.08--0.20]	0.19 (0.15--0.24) [0.12--0.27]	0.51 (0.41--0.64) [0.33--0.75]	0.65 (0.51--0.81) [0.41--1.00]		
SSP5-8.5	0.14 (0.11-- 0.18) [0.08--0.22]	0.21 (0.16--0.26) [0.13--0.30]	0.59 (0.48--0.71) [0.39--0.83]	0.73 (0.60--0.90) [0.50--1.07]		

* Trends in the 17th-83rd percentile and 5th-95th percentile estimates are reported as the *likely* and *very likely* ranges. This approach effectively assumes perfect temporal correlation over 20 year periods, and may therefore underestimate uncertainties.

[END CROSS-SECTION BOX 1, TABLE 3 HERE]

Polar amplification

It is now well understood that the Arctic warms more quickly than the Antarctic due to a combination of asymmetries in radiative feedbacks and ocean heat uptake between the poles, but that surface warming will eventually be amplified in both poles (*very high confidence*). Since AR5, progress has been made to understand the mechanisms of polar amplification and its uncertainty. A variety of factors all contribute to Arctic amplification, including positive surface-albedo and lapse-rate feedbacks as well as increases in poleward atmospheric latent heat transport and ocean heat transport, making it a ubiquitous feature of climate model simulations and observations. The Antarctic warms slower than the Arctic owing primarily to upwelling in the Southern Ocean. Compared with the models used for paleoclimate simulations in AR5, the polar amplification simulated in more recent models is now more consistent with paleoclimate observations of past warm climates. There is *high confidence* that the rate of Arctic surface warming will continue to exceed the global average over the 21st century. There is also *high confidence* that Antarctic amplification will emerge as the Southern Ocean surface warms on centennial timescales, although only *low confidence* of the feature emerging this century. Polar amplification is thus a time- and pathway-dependent pattern not uniquely dependent on global warming levels. {7.2.2, 7.4.4}

Connecting scenarios and time periods to warming levels

After presenting changes in GSAT according to the near-, mid- and long-term periods for the five core SSP-scenarios, Cross-Section Box 1 Table 1 also reports the time periods at which GSAT reaches the individual warming levels under the same core scenarios. Cross-Section Box 1 Figure 2 synthesises this information and provides the link between SSP annual CO_2 emissions, the SSP projected GSAT ranges for the end of the 21st century and the time periods at which the specific warming levels are reached (see also Cross-Section Box 2).

[START CROSS-SECTION BOX 1, FIGURE 2 HERE]

Cross-Section Box 1, Figure 2: Combining ranges of projected temperature change and the time when particular warming levels are reached: time series of SSP-based annual CO_2 emissions from fossil fuel combustion and land use change for the core set of five illustrative SSP scenarios used in this report. SSP-based temperature projections for two time periods in the 21st century (vertical bars to the right of the panel). Time when particular warming levels are reached in the SSPs (horizontal bars at the top of the panel). [*PURPOSE: This figure combines key dimensions of integration (scenarios and warming levels) used across the WGI report and presents them along a time-axis in a single figure. The figure illustrates the relationship between scenario, projected warming, and time of reaching a particular temperature level.]*

[END CROSS-SECTION BOX 1, FIGURE 2 HERE]

[END CROSS-SECTION BOX 1 HERE]

[START CROSS-SECTION BOX 2 HERE]

Cross-Section Box 2: Global warming levels

This box presents findings on changes to the climate system at various levels of global mean surface warming above pre-industrial conditions, ranging from 1°C (or approximately present conditions) and up to 5°C, as well as a discussion of linearities and non-linearities in the response of the climate system. The results presented include large-scale changes and regional changes in extreme events. Several of these metrics represent hazards (detrimental climatic impact drivers, including changes to extremes, ocean circulation, hydrological cycle, cryosphere and others) that have been found relevant to characterizing risks synthesized in the Reasons for Concern. {4.6, 11.1, 11.2, 12.5.2}

Levels of warming are defined based on two main methodologies; time periods consistent with a given level of warming for model-based projections (see Table TS.5) and literature-based assessments. Compared to previous assessment reports, the core set of illustrative marker SSP scenarios used in this report (see TS.1) also cover lower emission pathways, including scenarios potentially consistent with a 1.5°C warming as envisaged in the Paris Agreement. This allows for seamless assessments of the climate implications of levels of global mean surface warming ranging from present conditions and through to the upper range of what is possible if climate mitigation measures were not implemented by 2100. {1.6, 4.6}

For each level of global warming, changes are projected in annual mean properties as well as extreme conditions (Cross-Section Box 2 Figure 1). Cross-Section Box 2 Figure 2 highlights types of extreme weather events in AR6 regions that have been attributed (1°C) and are projected to change at subsequent warming levels with high and medium confidence. With increasing warming level, relatively larger mean warming is projected for land regions (*virtually certain*). It is also *virtually certain* that global mean precipitation will increase with increased global mean surface temperature. The sparseness of observing networks, variable model response and internal variability however contribute to a substantial range in projections of water cycle changes, especially on regional scales (*high confidence*). Model limitations such as unresolved small-scale processes still preclude a strong model consensus about future water cycle changes regardless of global warming level. {1.5, 1.7, 4.6, 8.5}

Based on multiple lines of evidence, global-mean land precipitation is *very likely* to increase approximately 1-3% per 1°C warming in globally averaged surface air temperature. For scenarios where the individual CMIP6 simulations unanimously agree on a global warming above 1.5°C, 2°C, and 3°C relative to 1850-1900, the ensemble-mean increase in annual global-mean land precipitation is about 1.7%, 2.9%, and 4.6%, respectively, relative to 1850-1900 *(high confidence)*. {4.3, 4.5, 4.6}

For extremes, even a comparably small incremental increase in global mean temperature (0.5°C) is found to lead to significant changes, on both the global scale and for large regions. This is the case both for observed changes over the historical era, and for projected changes e.g. at +2°C vs 1.5°C of global warming. Many of the observed changes in extremes will continue in the future. An additional half degree of global warming would be sufficient to cause further detectable changes in temperature extremes (*virtually certain*) and precipitation extremes (*very likely*) at the global scale. {11.1, 11.3, 11.4, 11.5, 11.6, 11.7}

It is *virtually certain* that further increases in the likelihood and severity of hot extremes and decreases in the likelihood and severity of cold extremes will occur throughout the 21st century. Such changes are expected at both global and continental scales, and in nearly all inhabited regions, if global warming increases to +1.5°C or higher above the preindustrial level, with stronger increases at higher levels of global warming. It is *virtually certain* that the number of hot days and hot nights and the length, frequency, and/or intensity of warm spells or heat waves (defined with respect to late 20th century conditions) will increase over most land areas. In most regions, changes in the magnitude of temperature extremes are proportional to global warming levels *(high confidence)*. The likelihood of temperature extremes generally increases exponentially with increasing global warming levels *(high confidence)*. {11.3, 11.9}

[START CROSS-SECTION BOX 2, FIGURE 1 HERE]

Cross-Section Box 2, Figure 1: Large scale changes as function of the level of global mean surface warming relative to 1850-1900. Left to right: Surface temperature (GSAT), precipitation, annual daily maximum temperature (TXx), annual daily maximum 1-day precipitation (Rx1day), number of days per year with maximum temperature exceeding 35 °C, and consecutive dry days. Warming levels (bottom to top) are 1°C (close to present day conditions), 1.5°C, 2°C, 3°C and 4°C. Results are based on the full CMIP6 ensemble, one member per model, and combining simulations of SSP1-1.9, SSP1-2.6, SSP2-4.5, SSP3-7.0, and SSP5-8.5. *[Purpose: Show the regional distribution of changes across a range of indicators, as function of warming level. The figure is essentially a "lookup-table" of changes at a given location and level of warming.]*

[END CROSS-SECTION BOX 2, FIGURE 1 HERE]

[START CROSS-SECTION BOX 2, FIGURE 2 HERE]

Cross-Section Box 2, Figure 2: Overview of changes attributed to anthropogenic influences under present warming, and their expected evolution to higher levels of global mean surface warming. Bars show the evolution of regional annual mean values based on the maps in Cross-Section Box 2 Figure 1. [*Purpose: Show what attributable changes are expected at different levels of global warming, starting with existing assessments of attributed changes at current warming. Also, provide continuous bar charts of changes in support of the Reasons For Concern assessed in WG2.]*

[END CROSS-SECTION BOX 2, FIGURE 2 HERE]

Warming of 1 °C

Representative of current conditions. Taking a baseline of 1850-1900, which approximates pre-industrial conditions, global mean surface temperature change for the modern reference period (1995-2014) is 0.87 °C (0.77 – 0.97 °C), or close to a warming level of 1 °C. At this level, large scale changes are observed throughout the climate system (TS.2). A wide range of observed changes have also been attributed to human influence, including extreme precipitation, droughts, tropical cyclones, and compound extremes (TS Cross-Section Box 2 Figure 2). Changes in aerosol concentration and irrigation and crop expansion have affected trends in hot extremes and the water-cycle. There is further evidence of an increase in the land area affected by concurrent extremes. {1.2, 1.3, 2.3, 8.3.1, 8.3.2, Box 8.1, 10.6.3, 11.1, 11.3, 11.4, 11.5, 11.6, 11.7, 11.8, Box 11.3}

Warming of 1.5 °C

This level of global warming, approximately in line with the Paris Agreement target to pursue best efforts to limiting warming to 1.5°C, implies higher mean temperatures compared to the preindustrial levels across the globe, with generally higher warming over land compared to ocean areas *(virtually certain)* and larger warming in high latitudes compared to low latitudes. {1.6, 4.6}

A warming level of 1.5°C in globally averaged surface air temperature, relative to the period 1850–1900, is, in the near-term period 2021–2041, *very likely* to be reached in scenarios SSP3-7.0 and SSP5-8.5, *likely* to be reached in scenarios SSP1-2.6 and SSP2-4.5, and *more likely than not* to be reached in Scenario SSP1-1.9 *(high confidence)*. The best estimate for reaching a global warming level of 1.5°C – neglecting the influence of natural internal variability – is around 2028-2033, across all scenarios assessed in this report *(medium confidence)*. There is *medium confidence* that a combination of equilibrium climate sensitivity and transient climate response near the lower end of the assessed *very likely* range delays reaching 1.5°C to about year 2050 for scenario SSP1-2.6 and avoids it altogether for scenario SSP1-1.9. This broader assessment of when 1.5°C is reached encompasses the SR1.5 assessment of 1.5°C *likely* being reached in the period 2030–2052, with year 2040 as the best estimate, assuming that the current warming rate continues. However, the best estimate for when a global warming level of 1.5°C relative to 1850–1900 will be reached is assessed here in Chapter 4 to be about ten years earlier than the best estimate of the SR1.5 *(medium confidence)*. The dominant cause of this re-assessment is the provision of enhanced estimates of the historical observational record. {2.3.1, 4.3.1, 4.4.1, Box 4.1, Table TS.2}

Warming of 2 °C

A climate future that is close to, but ultimately missing, the Paris Agreement "well-below" 2.0°C target. Reached by 2042-2050 (*very likely* 2035-2075), depending on emission scenario. Not reached before 2100 under SSP1-19 or SSP1-2.6. {1.6, TS.5}

Global warming of 1.5°C–2°C will result in increases in precipitation over most high-latitude regions, as well as in the tropics *(high confidence)*. {4.6}

If future warming levels remain between 1.5°C and 2°C, the Arctic Ocean will *likely* remain partly sea-ice covered all year round in most years and Northern Hemisphere spring snow cover extent decrease will *likely* remain below 3 × 106 km^2. If this level is reached for decades and longer, all small low-latitude glaciers will *very likely* melt; however, 10-60% of glacier volume will remain in the polar regions; permafrost volume decrease in the top 3 meters will remain limited to less than 40%; the Greenland and the West Antarctic ice sheet will decline *(medium confidence)*. In pathways leading to about 2°C of warming, GMSL rise is *likely* to be 0.33-0.65 m between 1996-2014 and 2100. The committed sea level after two millennia will be 1 to 3 m GMSL rise per °C peak warming *(low confidence)*. {9.2, 9.3, 9.4, 9.5, 9.6,}

After a stabilization at 2 °C of global mean warming, global ocean heat content will continue to increase for thousands of years, peaking more than 1000 years after GMST peaks, and eventually increasing by 5 times more than the 1971-2018 accumulation *(low confidence)*. {9.2}

It is *likely* that the Atlantic Meridional Overturning Circulation (AMOC) will decrease in strength through the 21st century *(medium confidence)*. It is *likely* that under stabilization of global warming at 1.5°C, 2.0°C, or 3.0°C relative to 1850-1900, the AMOC will continue to weaken for several decades and then strengthen to historical values over several centuries *(medium confidence)*. {4.3}

Warming of 3 °C

Climate future that would result if the Paris Agreement "well-below" 2.0°C target were to be missed by at least 1°C, resulting in 3°C warming relative to pre-industrial levels. Several studies considering climate outcomes of current NDC pledges suggest temperature outcomes in this vicinity. Reached by 2064-2074 (*very likely* 2054-2098), depending on emission scenario. Not reached by 2100 under SSP1-19, SSP1-2.6 or SSP2-45. {Table TS.5, 1.2, 1.6}

There is *high confidence* that concurrent heatwaves and droughts have become more frequent and that this trend will continue under higher levels of global warming (TS Box.1 Figure 3). There is *high confidence* that concurrent extremes events at different locations, but possibly affecting similar sectors (e.g., breadbaskets) in different regions, will become more frequent at higher levels of warming, in particular above 2°C of global warming. {12.4}

For future warming levels between 2 and 3°C, there is *medium confidence* that the Greenland Ice Sheet will pass a threshold where long-term mass loss becomes irreversible over centennial timescales. There is *high confidence* that Antarctic ice shelf basal melting will increase, but *low confidence* in the projected melt rates. {9.4}

Warming of 4 °C and beyond

Global warming level by the end of the century under high emission scenarios, or reference scenarios that assume little or no climate policy implementation. Reached by 2082-2100 (*very likely* 2069-2100), depending on emission scenario. Not reached by 2100 under SSP1-19, SSP1-2.6 or SSP2-45. {1.6. Table TS.5}

Permafrost warming is very *likely* a pan-Arctic phenomenon. Active layer thickness increase is a pan-Arctic phenomenon, subject to interannual variations. Global permafrost volume in the top 3 m will decrease by about 25±5% per °C if global air temperature remains below 4°C above preindustrial levels. (*medium confidence*) {9.5}.

If future warming levels remain between 3° to 5 °C for decades or longer, the Arctic Ocean will *very likely* become sea-ice free throughout several summer months in most years and the Antarctic Ice Sheet will continue to lose mass due to ocean-forced dynamic thinning and acceleration (*high confidence*). The Greenland ice sheet will disappear after multiple millennia; most of the glaciers in the world will *very likely* melt, only the largest glaciers will persist at 10-20% of their present size; Northern Hemisphere winter snow cover will *likely* be less than 40 × 106 km^2 and spring snow cover extent decrease will *likely* exceed 6 × 106 km^2; permafrost volume decrease in the top 3 meters will exceed 60% compared to the present (*medium confidence*). Furthermore, for pathways leading to about 4°C of warming, GMSL rise is *likely* to be 0.54-0.85 m between 1996-2014 and 2100. The committed sea level after two millennia will be about 16 m GMSL rise for 4°C peak warming (*low confidence*). {9.2.2, 9.3.1, 9.5.1, 9.5.2, 9.5.3, 9.6.3}

There is *low confidence* regarding the global warming levels at which possible changes associated with global and regional tipping points (low-likelihood, high-impact events) related to extremes would occur, but these cannot be excluded, especially at high global warming levels (>3°C). {11.10}

[START CROSS-SECTION BOX 2, TABLE 1 HERE]

Cross-Section Box 2, Table 1: *[The purpose here is to deliver quantitative information on the changes to (primarily) a subset of compound events as function of warming level.]* Examples of changes in extreme conditions (single extremes, compound events) potentially challenging adaptation at different global warming levels {Box 11.4 Table 1}

	+1°C (present-day)	+1.5°C	+2°C	+3°C	+4°C
Risk ratio for annual hottest daytime temperature (TXx) with 1% of probability under present-day warming (+1°C) (Kharin et al., 2018): Global land	1	3.3 (i.e. 230% higher probability)	8.2 (i.e. 720% higher probability)	Not assessed	Not assessed
Risk ratio for heavy precipitation events (Rx1day) with 1% of probability under present-day warming (+1°C) (Kharin et al., 2018): Global land	1	1.2 (i.e. 20% higher probability)	1.5 (i.e. 50% higher probability)	Not assessed	Not assessed
Probability of "extreme extremes"– hot days with 1/1000 probability at the end of 20th century (Vogel et al., submitted, a): Global land	~20 days over 20 years in most locations	about ~50 days in 20 years in most locations	about ~150 days in 20 years in most locations	about ~500 days in 20 years in most locations	Not assessed
Probability of co-occurrence in the same week of hot days with 1/1000 probability and dry days with 1/1000 probability at the end of 20th century (Vogel et al., submitted, a): Amazon	0% probability	~1 week within 20 years	~4-5 weeks within 20 years	>9 weeks within 20 years	Not assessed

Projected soil moisture drought duration per year (Samaniego et al., 2018): Mediterranean region	41 days (+46% compared to late 20th century)	58 days (+107% compared to late 20th century)	71 days (+154% compared to late 20th century)	125 days (+346% compared to late 20th century)	Not assessed

[END CROSS-SECTION BOX 2, TABLE 1 HERE]

Linearity of the climate response

Not all changes to the climate system can be directly projected through the level of global warming. As the net anthropogenic climate influence comes through the sum of both long and short lived forcers, and acts in parallel with natural (forced and unforced) variability, the climate at a given warming level will depend on the particular combination of forcings. At the higher levels assessed here, however, the influence of long lived greenhouse gases increasingly dominates, meaning that this ambiguity is primarily a focus for lower warming levels (1.5°C-2°C). {4.6, 6.6, Cross-Section Box 2}

While many indicators of change are projected to respond linearly with changes in GSAT, a number have non-linear dependencies, for a range of physical reasons. Non-linear processes include the rates of extreme events and Arctic sea ice in September (Cross-Section Box 1 Figure 1), and the transient response of the midlatitude jets to forcing in the North Atlantic, North Pacific and Southern Hemisphere. Cross-Section Box 1 Figure 3 synthesizes information on the response of indicators with GMST from a range of chapters, using several lines of evidence, although the main bulk of information comes from CMIP6 simulations using the SSP scenarios. {4.6.1}

Projections of sea level rise show a 2000-year commitment of ~1.1 m associated with 1.0°C of peak warming, increasing to ~3 m/°C between 1.0 and 2.0°C of peak warming, and to ~6 m/°C at higher levels of peak warming. Sea-level rise continues to increase after 2,000 years, leading to a 10,000-year commitment of 1.9 m associated with 1.0°C of peak warming, 5 m associated with 1.5°C of peak warming, and 12 m associated with 2.0°C of peak warming, with an average slope of about 8 m/°C between 2.0°C and 6.0°C of peak warming. These estimated commitments are substantially higher than that assessed by AR5, which concluded with *low confidence* that the multi-millennial commitment was about 1 to 3 m/°C). {9.6}

[START CROSS-SECTION BOX 2, FIGURE 3 HERE]

Cross-Section Box 2, Figure 3: Several fundamental indicators change near-linearly with GSAT, indicating a near pathway independence of changes for fast-reacting indicators, reducing the dependence of projections of future changes on scenario details. Yellow box: How the rate (A, B) and frequency (C, D) of warm (A, C) and wet (B, D) extremes change with WL. Rates scale nearly linearly, while frequency increases more strongly, and with larger percentage increases for less frequent events, for each step in global surface warming. Clockwise from top right: E: Arctic sea ice extent in March and September. March ice scales linearly, while September ice reaches zero in most scenarios between warming of 2 °C and 3 °C. F: Global permafrost volume scales linearly until around 3 °C, then shows signs of accelerated melt in CMIP6 models. G: Spring snow cover in the Northern Hemisphere scales linearly with WL. H: Precipitation and runoff, mean and variability. I: Rate of sea level rise, at present and future levels of surface warming, compared to observed or reconstructed rates since the Last Glacial Maximum. [Panels will be harmonized for the FGD. In particular, the reference periods will all be 1850-1900; in the present draft they vary between panels. The evolution of large scale changes with global warming level (WL). The purpose of this figure is to show how a range of indicators scale with warming level; some linearly, some not.]

[END CROSS-SECTION BOX 2, FIGURE 3 HERE]

[END CROSS-SECTION BOX 2 HERE]

TS.3 Forcing, Feedbacks and Responses

The assessment of forcing, feedback and climate responses is summarized in this section. Human activities are changing the Earth's surface and atmospheric composition which is changing the Earth's energy balance and thereby driving changes in the climate system. Since the AR5, the scientific understanding of the total Earth system warming and its changes through time has improved. The Effective Radiative Forcing (ERF) framework, introduced in the AR5 and built upon the concept of radiative forcing, quantifies the net change in the energy balance of the Earth system due to an imposed perturbation with positive ERF leading to a warming and negative ERF to cooling. Since the AR5, important revisions in ERF estimates have been made. Climate feedbacks represent those processes that change the energy budget in response to a change in surface temperature. AR6 adopts new approaches to the quantification and treatment of feedbacks that improve the understanding of their nature and time-evolution, leading to better understanding of how these feedbacks relate to climate metrics, including Equilibrium Climate Sensitivity (ECS). Climate metrics are used in this report to evaluate how the Earth system response varies with atmospheric gas concentration or change in radiative forcing, while emission metrics evaluate how radiative forcing or surface temperature is affected by the emissions of a certain amount of gas. Metrics, such as the Transient Climate Response to Emissions (TCRE), are used for determining future surface temperature change under specific emission scenarios, and to estimate remaining carbon budgets that are used to inform mitigation policies. {7.1, Box 7.1}

Since AR5, there have been improvements in our understanding of the response of the global water cycle to drivers of change. Limiting further climate change will require substantial and sustained reductions of CO_2 and other anthropogenic forcing agents. Since AR5, methodological improvements have led to updates in the carbon budget estimates required for mitigating warming to specific levels (Cross-Section Box 2). Reductions in SLCFs[5] including aerosols and non-methane ozone precursors, would lead to improvements in air quality but would lead to near-term warming without simultaneous stringent CO_2 mitigation. Solar Radiation Modification could potentially offset GHG-induced global mean warming but the compensation is identified to be imperfect on regional and seasonal scales.

TS.3.1 Radiative forcing and energy budget

Changes in atmospheric composition, like those caused by anthropogenic greenhouse gas and aerosol emissions (assessed in TS2), influence climate through perturbations to the Earth's energy budget. The effective radiative forcing (ERF) framework provides a way to quantify these perturbations. Since being introduced in the AR5, the ERF framework has become well established and has been shown to provide a useful way of estimating temperature response. {7.3.1}

Since the AR5, total Earth system warming, that is, the total change in heat energy of the atmosphere, land, ice and ocean, has become a more established indicator of global climate change, representing a more reliable measure of the Earth system response to radiative forcing than globally averaged near surface temperature (GSAT), because it exhibits less natural internal climate variability. Total Earth system warming, that is the total change in heat energy of the atmosphere, land, ice and ocean (Figure TS.24), increased by 406 ± 84 Zetta Joules over 1971-2018 and by 144 ± 24 ZJ over 2006-2018. For comparison world primary energy production was around 7 ZJ over the 2006-2018 period. Ocean heat uptake represents more than 90% of the total, with roughly 5% associated with heating of the land surface, about 2% with the melting of ice and less than 1% in heating of the atmosphere. The decadal rate of Earth system warming has roughly doubled since the 1970s. (*high confidence*) {7.2.2, Box 7.2, Table 7.1}

[START FIGURE TS.24 HERE]

[5] SLCFs include aerosols, also called particulate matter, (sulphate, nitrate, ammonium, carbonaceous aerosols, mineral dust, and sea salt) and chemically reactive gases (methane, ozone, halogenated species, nitrogen oxides, carbon monoxide, non-methane volatile organic compounds, sulphur dioxide, and ammonia). Methane is both a well-mixed greenhouse gas as well as a SLCF as its atmospheric lifetime is much shorter than that of long-lived climate forcer but is long enough to result in a spatially homogeneous distribution in the atmosphere.

Figure TS.24: Estimates of the net cumulative energy change (ZJ = 1021 Joules) for the period 1971-2018 associated with: (a) Total Earth System Warming; (b) Effective Radiative Forcing; (c) Earth System Radiative Response. Shaded regions indicate the 5th to 95th percentile uncertainty range. The grey lines indicate equivalent heating rates in W m^{-2}, expressed relative to Earth's surface area. Panel (d) shows the breakdown of components, as indicated in the legend, for Total Earth System Warming. Forcing and Response timeseries are computed using a baseline period of 1850-1900. Panel (e) shows changes in ERF. The global annual mean temporal evolution since 1750 is shown as the central assessment value. ERF of changes to the atmospheric composition are shown for the gases carbon dioxide (CO_2), methane (CH_4), nitrous oxide (N_2O), synthetic greenhouse gases, and tropospheric ozone (O_3). Aerosol changes include the sum of the ERF due to aerosol – radiation and aerosol – cloud interactions. Other anthropogenic forcings include stratospheric ozone, stratospheric water vapour, land use / land cover changes, black carbon deposition on snow, and contrails. The two other key ERFs shown are for variability in TSI and in volcanic forcing. The sum of the best estimates for all forcings is shown as the total forcing. The inset in the lower right shows the rate of change (linear trend) in total anthropogenic ERF (total without TSI and volcanic ERF) for the periods 1850–1900, 1900–1950, 1950–2000 and 2000–2019. Panel (f) shows the Earth Energy Budget assessed for the period 1971-2018, i.e., the consistency between Total Earth System Warming and the implied heat storage from Effective Radiative Forcing plus Earth System Radiative Response. Shading represents the 5% to 95% uncertainty range. Forcing and Response timeseries are computed using a baseline period of 1850-1900. . [placeholder: Total Earth System Warming components to be updated to 2018 for final draft. Reported values for sum of components in main text are based on extrapolation of 2006-2015 rate to 2018. The aerosol ERF estimate is based on AR5 and will be updated for the final draft.]

[END FIGURE TS.24 HERE]

The rate of total Earth system warming corresponds to an Earth's energy imbalance of 0.54 ± 0.11 W m^{-2} for the period 1971-2018, increasing to 0.81 ± 0.14 W m^{-2} for the period 2006-2018 expressed relative to Earth's surface area (*high confidence*). Consistent estimates of the sea-level rise across different lines of evidence for the period 1971-2018 promotes greater confidence in the planetary heating rate since the AR5. Heat will continue to accumulate in the Earth system over the 21st Century driving future sea-level rise (*high confidence*) and there is *medium confidence* this will continue beyond 2100 for another century or more, even under strong mitigation of greenhouse gas emissions. {7.2.2, Box 7.2, Table 7.1, Cross-Chapter Box 9.2}

The total anthropogenic ERF (Figure TS.24) over the industrial era (1750-2018) was 2.53 W m^{-2} (1.58 to 3.34 Wm^{-2} *very likely* range). This is an 11% increase over AR5 estimates for 1750-2011. Changes in atmospheric concentrations of greenhouse gases since 2011 and upwards revisions of their forcing efficiencies have led to a 15% increase in their ERF. This is partly offset by a new assessment of total aerosol ERF that is 22% more negative compared to the AR5. (*high confidence*) {7.3.5}

Greenhouse gases contribute an ERF of 3.63 Wm^{-2} (3.27 to 3.97 Wm^{-2} *very likely* range) over the industrial era (1750-2018). 90% of this comes from the well-mixed greenhouse gases, with ozone and stratospheric water vapour changes contributing the remainder. Carbon dioxide contributes the largest part of this forcing with a value of 2.15 Wm^{-2} (1.89-2.41 Wm^{-2} *very likely* range). There has also been an increase in the estimated shortwave forcing from methane (*high confidence*). {7.3.2, 7.3.5}

The reactive well-mixed greenhouses gases (methane, nitrous oxide, halocarbons) cause additional chemical adjustments to the atmosphere through changes in ozone and aerosols (Figure TS.25a). The ERF due to methane emissions is 0.99 Wm^{-2} (0.8-1.17 Wm^{-2} range) of which 0.45 Wm^{-2} (0.34-0.56 W m^{-2} *very likely* range) is attributed to chemical adjustments. The net ERF attributable to halocarbons is smaller than the direct ERF due to their effect on ozone depletion, such that the range includes zero (0.0 to 0.16 W m^{-2}) (*high confidence*). {7.3.2, 7.3.5}

[START FIGURE TS.25 HERE]

Figure TS.25: (A) Components of radiative forcing from 1850 to 2014 by emitted species based on CMIP6 models. "VOC" includes CO as well as other non-methane hydrocarbons. WMGHGs are from analytical formulae, H2O (stratosphere) is unchanged since AR5. Other components are multi-model means and are based on model simulations where one species at a time is increased from 1850 levels to 2014. Error bars are 5-95% and account for uncertainty in radiative efficiencies and multi-model error in the means. IRFari and cloud effects are calculated from separate radiation calls for clear-sky and aerosol free conditions. "Cloud" includes cloud adjustments (semi-direct effect) and ERFaci. The aerosols (SO2, organic carbon, black carbon) components are scaled to sum to −0.25 W m−2 for IRFari and −0.95 W m−2 for "cloud". (B) Net aerosol ERFari+aci from different lines of evidence. Green bars show the assessment based on satellite observations. Blue bars show the assessment based on climate models, with individual models from CMIP5 and CMIP6 depicted. Both the satellite- and model-based assessments are for 1750-2014. Individual assessed best-estimate contributions from ERFari and ERFaci are shown with darker and paler shading respectively. Overlaid black diamond and black lines show the best estimate and very likely range of satellite- and model-derived ERFari+aci Grey shading shows the very likely range consistent with energy budget constraints. Purple bars show the assessed very likely range (thin), likely range (thick), and best estimate (black diamond) from all lines of evidence in this assessment for 1750-2018. *[Purpose**:** The intent of this figure is to show advances since AR5 in the understanding of (A) emissions-based ERF for SLCFs (SOD Figure 7.10) and (B) Aerosol ERFari+aci from different lines of evidence (satellite-based, model based and overall assessment of aerosol ERF; SOD Figure 7.8)]*

[END FIGURE TS.25 HERE]

The AR6 assessed value of ERF due to changes in stratospheric ozone for 1750-2018 remains the same as AR5 value but with reduced upper bound –0.05 (–0.15 to 0.0) W m^{-2} and that for changes in tropospheric ozone is +0.35 (0.18 to 0.52, *very likely* range) Wm^{-2}. Due to discrepancies in satellite and *in situ* records, there is *low confidence* in stratospheric water vapour change and the ERF of water vapour changes due to methane oxidation over 1750 to 2018 remains the same as in AR5 with a mean value of 0.07 Wm^{-2} (0.02 - 0.12 Wm^{-2} *very likely* range). There is *medium confidence* that historical changes in land use increased terrestrial albedo since 1850 with an ERF of –0.12 W m^{-2} (–0.21 to –0.03 W m^{-2}, *very likely* range). {2.2.5, 2.2.7, 7.3.2}

Aerosols contribute an ERF of −1.1 W m^{-2} (−2.0 to −0.4 W m^{-2} *very likely* range) over the industrial era (1750-2018). The ERF due to aerosol-cloud interactions (ERFaci) contributes most (about 3/4) to the magnitude of the total aerosol ERF, with the remainder due to the forcing associated with aerosol-radiation interactions (ERFari). There has been an increase in the estimated magnitude but a marked reduction in the uncertainty of the total aerosol ERF relative to the AR5, supported by a combination of increased process-understanding, and progress in modelling and observational analyses. Observation-based and modelling-based estimates are now consistent with each other (Figure TS.25b), in contrast to the AR5. Compared to the AR5, there has been a doubling of the magnitude of ERFaci, and a downward revision of the magnitude of ERFari (*high confidence*). {7.3.3, 7.3.5}

In summary, since the AR5 confidence in estimates of the Earth's heating rate and ERF has improved owing to better observations, especially for the sea-level budget, and better understanding of the physical and chemical processes governing the radiative forcing of the climate system, especially for methane and aerosol ERF. There is *high confidence* that Earth has accumulated heat by 144 ± 24 ZJ (equivalent of 0.81 ± 0.14 W m^{-2}) over 2006-2018, at a rate roughly doubled since the 1970s. Total anthropogenic ERF has increased further since the AR5 estimates and is 2.53 W m^{-2} (1.58 to 3.34 Wm^{-2} *likely* range) over the industrial era (1750-2018). {2.2.5, 2.2.7, 7.2.2, 7.3.2, 7.3.3, 7.3.5, Box 7.2, Table 7.1, Cross-Chapter Box 9.2}

TS.3.2 Feedbacks and metrics of climate response

The magnitude of global temperature change primarily depends on the strength of the radiative forcings (Section TS3.1) and feedbacks, or self-reinforcing cycles in the climate system. These feedbacks are those processes that modify the global energy budget in response to a change in global surface temperature, which in turn amplifies (positive feedback) or diminishes (negative feedback) the initial climate perturbation. The Earth system feedbacks are numerous but can be loosely categorised into three groups: physical feedbacks, biogeochemical feedbacks, and long-term feedbacks associated with ice sheets. In previous assessments, the equilibrium climate sensitivity (ECS) has been associated with a distinct set of physical feedbacks (Planck response, water vapour, lapse rate, surface albedo, and cloud feedbacks). In this assessment, a more general definition of ECS is adopted whereby all biogeochemical feedbacks that do not affect the atmospheric concentration of CO_2 are included. These include changes in natural methane emissions, natural aerosol emissions, nitrous oxide, ozone, and vegetation, which all act on timescales of years to decades and are therefore relevant for temperature change over the 21st century. The biogeochemical feedbacks that affect the atmospheric concentration of CO_2 and the long-term feedbacks associated with ice sheets are not included in the ECS. {6.3, 7.4, Box 7.1}

The AR5 assessed the net cloud feedback to be positive (Figure TS.26a) with *medium confidence*. Major advances in the understanding of cloud processes leads to a *high confidence* assessment that the net cloud feedback is positive and halved its uncertainty range. Process understanding of tropical-marine low cloud feedbacks within GCMs has been complemented by a better understanding of cloud-climate interactions, satellite-based evidence, and explicit simulations using large-eddy simulations and cloud-system resolving models, altogether leading to strong evidence that the total cloud feedback amplifies global climate warming. The net cloud feedback is assessed to be +0.4 W m^{-2} $°C^{-1}$ (–0.1 to 0.9 W m^{-2} $°C^{-1}$ *very likely* range). The CMIP5 and CMIP6 ranges of cloud feedback are similar to this assessed range, with CMIP6 having a slightly more positive median cloud feedback. (*high confidence*) {7.4.2, Figure 7.14, Table 7.10}

The surface albedo feedback and combined water vapour-lapse rate feedback are positive (Figure TS.26a) with *high confidence* in the estimated value of each based on multiple lines of evidence including observations, models and theory. The sum of cloud, albedo, water vapour, lapse rate, and non-CO_2 biogeochemical feedbacks is positive, thus amplifying the climate response to a forcing relative to the black body (Planck) response (*very high confidence*). Including Planck response, the net climate feedback is assessed to be –1.25 W m^{-2} $°C^{-1}$ (–1.9 to –0.6 W m^{-2} $°C^{-1}$ *very likely* range). {7.4.2, Figure 7.14, Table 7.10}

Natural sources and sinks of non-CO_2 greenhouse gases such as methane (CH_4) and nitrous oxide (N_2O) respond both directly and indirectly to atmospheric CO_2 concentration and climate change, and thereby give rise to additional biogeochemical feedbacks in the climate system. Many of these feedbacks are only partially understood and are not yet fully included in ESMs. Additional radiative forcing arising from climate-CH_4 and climate-N_2O feedbacks at multidecadal to centennial timescales will be small (<10%) compared to the forcing from the direct anthropogenic GHG emissions in the 21st century (*medium to high confidence*). There is large uncertainty about the magnitude and timing of the responses of each individual process involved. {5.4.7}

The carbon cycle provides for additional feedbacks on climate owing to the sensitivity of land-atmosphere and ocean-atmosphere carbon fluxes and storage to changes in climate and atmospheric CO_2. With *high confidence*, increased atmospheric CO_2 will lead to increased land and ocean carbon uptake, acting as a negative feedback on climate change (Figure TS.26c). However, a reduction in the CO_2 buffering capacity of seawater and possible nutrient limitation in terrestrial ecosystems reduce the efficiency of land and ocean carbon uptake (*high confidence*). A warming climate will weaken the land and ocean carbon sinks, due to a variety of factors, which include: reduced photosynthetic uptake; elevated rates of plant (autotrophic) and soil (heterotrophic) respiration; changes to plant mortality and disturbance rates; reduced CO_2 solubility of seawater and changes in ocean circulation (*medium* to *high confidence*). Uncertainty in the magnitude and geographic pattern of these feedbacks remains high, but it is *likely* that the land and ocean sink in a warmer climate will act as a positive feedback that will enhance global warming {Figure TS.26, 5.4}

There is *high confidence* that thawing terrestrial permafrost will lead to carbon release, but the timing, magnitude and the relative roles of CO_2 versus CH_4 as feedback processes are known with *low confidence*. An ensemble of models project feedbacks due to CO_2 release from permafrost of 20 ± 13 PgC per degree of global warming by 2100 leading to warming strong enough that it must be included in estimates of the remaining carbon budget but weaker than the warming from fossil fuel burning. However, the incomplete representation of important processes such as abrupt thaw, combined with weak observational constraints, only allow *low confidence* in both the magnitude of these estimates and in how linearly proportional this feedback is to the amount of global warming. Because of water-saturated soils and a lack of oxygen in thawing permafrost regions, part of the carbon is released as CH_4, which leads to the combined radiative forcing being larger than from if there were CO_2 emissions only. {5.4.3, 5.4.8}

Natural emissions of SLCFs including dust, biogenic volatile organic compounds (BVOCs), dimethyl sulphide (DMS), methane, lightning NOx and sea-salt respond to changes in climate, amplifying or diminishing the initial climate perturbation (Figure TS.26a). Since the AR5, global Earth System Models have advanced to include a consistent representation of biogeochemical cycles and atmospheric chemistry, facilitating the assessment of non-CO_2 biogeochemical feedbacks on climate, induced by changes in atmospheric abundances or lifetimes of SLCFs mediated by natural processes or atmospheric chemistry. While models have advanced, uncertainties in the understanding of processes that influence natural SLCF emissions remain high, resulting in *low confidence* in the magnitude and sign of most of these feedbacks. {6.2.1, 6.3.6}

The sum of all non-CO_2 biogeochemical feedbacks is negative with *low confidence* (Figure TS.26b). For the purposes of estimating the net climate feedback, the total non-CO_2 biogeochemical feedback is assessed to have a zero-mean value and a *likely* range from –0.1 to +0.1 W m^{-2} $°C^{-1}$ because there is insufficient evidence to support a central estimate (Figure TS.26a). {6.3.6, 7.4, Table 7.10}

[START FIGURE TS.26 HERE]

Figure TS.26: An overview of physical and biogeochemical feedbacks in the climate system. a) Synthesis of physical and non-CO2 biogeochemical feedbacks that are included in the definition of ECS assessed in this Technical Summary. These feedbacks have been assessed using multiple lines of evidence including observations, models and theory. "WV+LR" stands for water vapour and lapse rate feedback. The net feedback is the sum of the Planck response and water vapour, lapse rate, surface albedo, cloud, and non-CO2 biogeochemical feedbacks. Positive feedbacks (red bars) amplify and negative feedbacks (blue bars) diminish the initial climate response to radiative forcing. Bars denote the mean feedback values and uncertainties represent *very likely* ranges assuming variance between individual components are independent; b) Estimated values of individual non-CO2 biogeochemical feedbacks. The atmospheric methane lifetime and other non-CO2 biogeochemical feedbacks have been calculated using global Earth System Model simulations from AerChemMIP, while the CH4 and N2O source response to climate have been assessed for the RCP8.5 scenario in year 2100, using simplified radiative forcing equations. There is insufficient evidence to support a central estimate of the total non-CO2 biogeochemical feedback so it is assessed to have zero-mean value in panel (a). Note the different x-axis scale for panel (b). c) carbon-cycle feedbacks as assessed by models participating in the C4MIP of CMIP6. An independent estimate of the additional positive carbon-cycle climate feedbacks from fire and permafrost thaw, which is not considered in most C4MIP models is added. Note that these feedbacks act through modifying the atmospheric concentration of CO2 and thus are not included in the definition of ECS, which assumes a doubling of CO2. *[Purpose: The intent of this figure is to show the physical and biogeochemical feedbacks on global temperature (new, based on Chapters 5, 7).]*

[END FIGURE TS.26 HERE]

Cloud feedbacks are the dominant source of uncertainty in this century's transient global warming under emission scenarios with continued CO_2 emissions (Figure TS.26a), whereas uncertainty is dominated by aerosol ERF in scenarios reaching net zero CO_2 emissions. Global ocean heat uptake is a relatively minor source of uncertainty in centennial warming. Carbon cycle feedbacks provide an increasing fraction of uncertainty on longer timescales (*high confidence*). {7.5.7}

Equilibrium climate sensitivity (ECS) and transient climate response (TCR) are useful metrics summarising the global temperature response to an externally imposed ERF. ECS is defined as the equilibrium annual mean and global mean GSAT response to a sustained doubling of atmospheric CO_2 concentration from a pre-industrial reference state. It is a measure of the multi-century to millennial temperature response to an atmospheric CO_2 doubling, excluding the long-term response of the ice-sheets which may take multiple millennia to reach equilibrium. TCR is defined as the change in the annual mean and global mean GSAT for the hypothetical scenario in which CO_2 increases at 1% yr^{-1} from pre-industrial to the time of a doubling of atmospheric CO_2 concentration (year 70). It is a measure of transient warming accounting for the strength of climate feedbacks and ocean heat uptake. While idealized metrics of climate response, both ECS and TCR help explain the variation in warming projected by GCMs across a range of concentration-driven future scenarios. In emission-driven scenarios the carbon cycle response is also important. The proportion of variance explained by ECS and TCR varies with scenario and the time period considered, but both past and future surface warming are highly correlated with both metrics. {7.1, 7.5, Box 7.1, Figure 7.1}

Constraints on ECS and TCR are based on four main lines of evidence (Figure TS.27), including feedback process understanding, climate change and variability seen within the instrumental record, paleoclimate evidence, and so-called "emergent constraints". In reports up until and including AR4, raw values of ECS and TCR derived from GCMs were a primary line of evidence but in the AR5 historical warming and paleoclimates provided additional constraints. In the AR6, various numerical models are used where they are considered accurate evidence, or in some cases the only available source of information, and thereby support all four lines of evidence. For example, GCMs are essential for producing emergent constraints, whereby a relationship between an observable quantity and either ECS or TCR established within an ensemble of models is combined with observations to derive a constraint on ECS or TCR. However, AR6 differs from previous reports in not directly using climate model values of ECS and TCR in the assessed ranges of climate sensitivity. {1.5, 7.5}

When estimating ECS and TCR, the dependence of feedbacks on time scales and the climate state must be accounted for. Radiative feedbacks will become less negative (more amplifying) in the future as the spatial pattern of surface warming evolves, leading to an ECS that is substantially higher than has been traditionally inferred from warming over the historical record (*high confidence*). This new understanding, along with updated estimates of historical temperature change, ERF, and energy imbalance, reconciles previously disparate ECS estimates. However, there is currently insufficient evidence to quantify a *likely* range of the magnitude of future feedback changes. {7.4.4, 7.5.2, 7.5.3, Figure 7.18, Figure 7.19, Figure 7.20}

Based on multiple lines of evidence the best estimate of ECS is 3 °C, the *likely* range is 2.5 to 4 °C and the *very likely* range is 2 to 5 °C. It is *virtually certain* that ECS is larger than 1.5 °C. There is a high level of agreement among the four main lines of evidence, and all lines help rule out ECS values below 1.5 °C. Emergent constraint evidence, process evidence, and paleoclimate evidence help rule out ECS values above 5 °C, but it remains challenging to rule out low-probability but high-impact upper-end ECS, which is indicated by the notable asymmetry of the assessed ranges. (*high confidence*) {7.5.5}

Based on process understanding, warming over the instrumental record, and emergent constraints, the best estimate of Transient Climate Response (TCR) is 1.8°C, the *likely* range is 1.4° to 2.2°C and the *very likely* range is 1.2° to 2.4°C. There is a high level of agreement among the different lines of evidence (*high confidence*). {7.5.5}

The distribution of ECS and TCR from CMIP6 models show higher values than from CMIP5 models and the assessed ranges of ECS and TCR (*high confidence*). The higher ECS and TCR values in many CMIP6 models can be traced to changes in extra-tropical cloud feedbacks that have emerged from efforts to reduce biases in these clouds compared to satellite observations (*medium confidence*). The ranges of ECS and TCR from CMIP6 span the assessed *very likely* ranges, in contrast to previous assessment reports where models only sampled the middle of the range. The CMIP6 models with the highest ECS and TCR values are useful to provide insights into high-risk, low-likelihood futures, which cannot be excluded based on currently available evidence. {7.5.6}

[START FIGURE TS.27 HERE]

Figure TS.27: Evolution of the uncertainty range is ECS as assessed by the Charney report and a succession of IPCC Assessment Reports. Reports are coloured according to the lines of evidence considered in the assessment, those lines of evidence being listed in the same colour below each group. Best estimates are marked by horizontal bars, *likely* ranges by thick vertical bars, and *very likely* ranges by whiskers. [*Purpose: This figure shows how the uncertainty range in ECS derived from different lines of evidence as assessed by the Charney report and successive IPCC Assessment Reports. This figure will be a replacement for SOD Figure 7.23.]*

[END FIGURE TS.27 HERE]

Since AR5, alternative methods for comparing the warming effects of greenhouse gases have been developed. Some of these give a more faithful simulation of the temperature effects of a portfolio of gases, especially under mitigation scenarios, such as those implied by successful attainment of the temperature goals set out in Article 2 of the Paris Agreement. As was pointed out in the AR5, ultimately, it is a matter for policymakers to decide which emission metric to use, because they have the social licence to make the normative judgements regarding timescale, variable choice and functional form that underpin emission metric choice. Physical science can only form a subset of the inputs to those choices. Global warming potentials (GWPs) have been developed to compare the radiative effects of different radiative forcing agents relative to the radiative effects of CO_2. Because the concentrations and radiative effects in the Earth's atmosphere can evolve due to chemical, biogeochemical, and physical interactions with the rest of the climate system, the GWPs are calculated as a function of time horizon from a hypothetical instantaneous emission of each agent. GWPs for each agent are defined as the ratio of the time-integrated radiative forcing from the pulsed emission of 1 kg of that agent relative to the time-integrated radiative forcing from 1 kg of CO_2 over a specified time horizon. GWPs have been calculated on time horizons of 100 and 500 years for N_2O and several SLCFs and decrease by factors ranging between 3 to 4 as the horizon increases from 100 to 500 years. GWPs for the entire suite of GHGs assessed in the AR6 have been calculated on 100-year time horizons. {7.6.3, 7.6.2, Table 7.15, Table 7.SM.2}

Global temperature change potentials (GTPs) compare the global mean surface temperature at a specified time horizon change due to the pulsed emission of a radiatively active compound relative to that of the reference gas CO_2. GTPs quantify the temperature change in response to the radiative forcing quantified by GWPs. The GTPs for SLCFs decrease with time horizon due to the decrease in SLCF concentrations following a single pulse of emissions. Global Warming Potentials and Global Temperature change Potentials are larger compared to AR5, due to the methodological change of accounting for carbon-cycle responses (*high confidence*). GWP* is a new metric which compares pulse emissions of long-lived climate forcers (LLCFs) like CO_2 and N_2O against changes in emissions of SLCFs, such as CH_4. Metrics like CGTP and GWP* provide a more accurate way than either GWP or GTP of assessing the temperature implications of a time-series of emissions. In summary, specifying short and long-lived greenhouse gases separately in emission scenarios generally improves the quantification of surface warming, compared to approaches that aggregate greenhouse gases using CO_2 equivalent emission metrics (*high confidence*). New metrics comparing pulse emissions of long-lived greenhouse gases with sustained emission changes in short-lived gases can lead to more equivalence in surface temperature response (*high confidence*). {7.6.3}

The transient climate response to cumulative carbon emissions (TCRE) is the globally averaged surface temperature change per unit emissions of atmospheric CO_2. TCRE is computed from the product of the change in global temperature due per total change in carbon dioxide accumulated in the Earth's atmosphere times the ratio of total accumulated carbon to total carbon emissions over the same time period. The utility of this metric is predicated on the long lifetime of CO_2 varying from decades to millennia, the approximate linearity of temperature change with cumulative emissions and the resulting near-constancy of TCRE. {5.5.1}

Medium evidence with *high agreement* underpins the near linear relationship during the 21st century between cumulative CO_2 emissions and maximum global mean temperature increase caused by CO_2 for the range of temperatures included in the Paris Agreement (*medium confidence*). This relationship implies that halting global warming requires global net anthropogenic CO_2 emissions to become zero, and no significant warming occurs afterwards. TCRE is assessed to be *likely* in the 1.0°-2.2°C per 1000 PgC range (*high confidence*). This is slightly narrower than the 0.8°-2.5°C per 1000 PgC assessment of the AR5 due to a better integration of different lines of evidence. Additional Earth system feedbacks that operate on century timescales, such as permafrost thawing, have the potential to weaken the linearity of cumulative carbon-climate relationship. This could result in potentially higher warming, further warming after net zero CO_2 emissions are reached, or a path dependency of warming as a function of cumulative emissions of CO_2 but there is *low confidence* in their precise quantitative influence on TCRE because of the large uncertainties in projections of these Earth system feedback processes and the limited number of studies. There is *high agreement* between multiple lines of evidence resulting in *high confidence* that TCRE remains constant for the domain of increasing cumulative CO_2 emissions until roughly 1500 PgC, which has earlier been assessed to be broadly consistent with warming significantly beyond 2°C. There is *medium evidence* yet *high agreement* resulting in *medium confidence* that TCRE can be considered constant when applied in the context of emission reduction pathways, provided that the Zero Emissions Commitment and long-term Earth system feedback are adequately accounted for. The *limited evidence* and its *low agreement* on the overall effect of additional Earth system feedbacks on TCRE results in *low confidence* in the reversibility assessment of TCRE, particularly for time scales beyond centuries. {5.5.1}

In summary, since the AR5 additional constraints from observations and paleoclimate studies combined with an improved understanding of feedback processes allow an assessment of ECS that is much less dependent on climate models than in past assessments. New understanding of the dependence of radiative feedbacks on the pattern of surface warming has also helped reconcile previously disparate ECS estimates. Estimates of TCR have also improved thanks to a high level of agreement among different lines of evidence. In terms of metrics, specifying short- and long-lived greenhouse gases separately in emission scenarios generally improves the quantification of surface warming, compared to approaches that aggregate greenhouse gases using CO_2-equivalent emission metrics *(high confidence*). New metrics comparing pulse emissions of long-lived greenhouse gases with sustained emission changes in short-lived gases can lead to more equivalence in surface temperature response (*high confidence*). Global Warming Potentials and Global Temperature change Potentials are larger compared to AR5, due to the methodological change of accounting for carbon-cycle responses (*high confidence*). {7.6.1, 7.6.2, 7.6.3, Box 7.3}

TS.3.3 Drivers of Water Cycle Change

Water vapour is *virtually certain* to increase on average globally due to thermodynamic constraints that increase atmospheric evaporative demand and determine a 6-7% increase per ℃ in near-surface moisture for constant relative humidity. Prevalent increases in atmospheric water vapour drive powerful amplifying climate feedbacks (TS3.2), intensify atmospheric moisture transport and associated heavy precipitation events (TS4.3.2) and increase the atmospheric absorption of sunlight and emission of infrared radiation to the surface. Additionally, there is a direct interaction between the water and carbon cycles as elevated atmospheric CO_2 levels influence plant water-use efficiency. The evolving atmospheric and surface energy budgets determine global-scale evaporation and precipitation responses.

Global mean evaporation and precipitation are *virtually certain* to increase as the energy budget evolves with warming of the climate system. The increase is driven by slow changes in the energy budget that scale with surface temperature but the rate of increase is reduced by fast atmospheric adjustments to radiative forcing agents that directly alter the atmospheric energy budget (Figure TS.28). Removing fast adjustment effects, there is *high confidence* based on robust physics and idealised CO_2 forcing experiments that global mean precipitation increases at 2.1-3.1% per ℃ of global mean warming—this rate of increase is referred to as hydrological sensitivity (η) (Figure TS.28). The actual global mean rate of precipitation change per °C of surface warming, referred to as apparent hydrological sensitivity (ηa), is reduced compared to hydrological sensitivity by the direct influence of radiative forcing agents on the atmospheric energy balance. Therefore, global precipitation appears more sensitive to drivers that do not directly impact the atmospheric energy budget, such as sulphate aerosols (ηa =2.8±0.7 % per °C) compared with responses to GHGs (ηa=1.4±0.5 % per °C). The response to black carbon aerosols can be negative (ηa=–3.5±5.0 % per °C) due to the effects of strong atmospheric solar absorption. Present-day increases in global mean evaporation and precipitation with global annual mean surface warming are partly offset by rapid atmospheric adjustments to radiative forcings from GHGs and absorbing aerosols, but these counteracting effects will diminish in relative importance in the future (*high confidence*). {8.2.1, 8.2.2, 8.2.3}

[START FIGURE TS.28 HERE]

Figure TS.28: Schematic representation of rapid and slow responses of the atmospheric energy balance and global precipitation to radiative forcing. (SOD Figure 8.3)

[END FIGURE TS.28 HERE]

There is *high confidence* that mechanisms driving declining continental near-surface relative humidity suppress precipitation response to warming over land relative to the ocean. It is *very likely* that hydrological sensitivity for CO_2-induced warming over the global land (1.6±0.7 %/°C) is smaller in magnitude but with a larger range than for the global ocean (2.8±0.2 %/°C). The CO_2-induced warming and near-surface relative humidity decline over land drives an increase in atmospheric water demand (*high confidence*) and annual mean land surface evapotranspiration (*medium confidence*) until soil moisture availability becomes a strong limitation in drying areas. There is *high confidence* that increasing atmospheric CO_2 enhances photosynthesis and rates of plant growth while also increasing stomata regulation and water-use efficiency but only *low confidence* in how these factors will combine in driving precipitation and soil moisture changes regionally. Land use change and irrigation also drive detectable water cycle changes in some regions through their influence on land surface water and energy budgets (*high confidence*). {2.3.1, 5.2.1, 5.4.1, 5.4.3, 8.2.1, 8.2.2, 8.2.3}

Anthropogenic aerosols alter the water cycle through their regionally dependent surface radiative cooling effect (*high confidence*) and variable atmospheric heating effects that influence global precipitation response and drive changes in large-scale atmospheric circulation patterns including monsoons (TS2.2.3, TS4.2, Box 8.1). Aerosol also affects cloud development through absorption of solar radiation that suppresses light rainfall and delays convection, while the supply of cloud condensation nuclei suppresses light rainfall from shallow and short-lived clouds but is compensated by heavier rainfall from deep clouds. {8.2.1, 8.2.2, Box 8.1}

Well-understood increases in low-level moisture of 6-7% per °C of warming explain a similar magnitude of intensification of heavy precipitation during wet events (*high confidence*). The increase in precipitation intensity with warming can vary significantly from the mean water vapour response due to less well-understood cloud microphysical and convective processes but there is *medium confidence* that these processes amplify more than suppress precipitation intensification. Changes in large-scale atmospheric circulation patterns also modulate the frequency of wet extremes, the seasonality and variability of which are expected to increase with global mean temperature (*medium confidence*). Based on improved understanding of thermodynamic drivers from multiple lines of evidence, there is *high confidence* that the contrast between wet and dry weather regimes, seasons and prolonged climate events will increase in a warming climate. An overall increase in the severity of flood events in response to more intense wet extremes (from sub-daily up to seasonal time-scales) is *very likely* at the global scale (*high confidence*). However, local factors including catchment conditions, seasonal melt characteristics and direct human influence on the land surface and water resources will dominate changes in hydrology and flood frequency in some regions. {8.2.2, 8.2.3, 8.4.1, 8.5.1}

Overall, there is more evidence that warming of the climate intensifies the global water cycle through increased atmospheric water vapour transport and exchange of water between the atmosphere and surface through precipitation and surface evaporation. There is improved understanding of the response of global precipitation and evaporation to radiative forcing agents. The cooling effects of anthropogenic aerosols and rapid atmospheric adjustments to increases in GHGs and absorbing aerosols are currently suppressing global precipitation increases. However, these effects will diminish as warming dominates future responses. It is *likely* that increases in multi-annual mean precipitation together with warming over land will be smaller than over the ocean due to declining near-surface relative humidity driven by increasing land-ocean thermal contrast and surface feedbacks. There is *high confidence* based upon multiple lines of evidence that the contrast between wet and dry weather regimes will increase in a warming climate. Well-understood increases in water vapour drive corresponding intensification of heavy precipitation events and the severity of associated flooding. However, regional water cycle drivers are less well understood since they depend upon changes in atmospheric circulation and local-scale processes, such as seasonal melt characteristics, the modification of cloud development as a result of aerosol pollution, vegetation feedbacks and direct responses to elevated CO_2 levels, as well as human modification of the land surface and water resources.

TS.3.4 Climate Stabilization, Net-Zero Emissions and Carbon Budgets

Limiting further climate change will require substantial and sustained reductions of greenhouse gas emissions. Without net-zero or net-negative CO_2 emissions, and a stabilization or decrease in the non-CO_2 net forcing, the climate system will continue to warm. The concept of a cumulative carbon emission budget associated with stabilizing global temperatures at particular levels was established in AR5. While quantifying the remaining carbon budgets precisely is sensitive to various assumptions, reaching net-zero carbon emissions remains a prerequisite for halting warming at 1.5°C, well below 2°C, or higher levels. {1.3.5, Box 1.2, Cross-Section Box 2}

TS.3.4.1 Carbon budgets and climate stabilization

There is *high confidence* that mitigation requirements for limiting warming to specific levels can be quantified using a carbon budget that relates cumulative CO_2 emissions to global mean temperature increase (Figure TS.29). Since the year 1850, a total of 2,363 Gt (645 ±65 PgC) of anthropogenic CO_2 has been emitted. The remaining carbon budgets, starting from the year 2020, for limiting warming to 1.5°C, 1.7°C, and 2.0°C with a probability of at least 66% are 310 $GtCO_2$, 570 $GtCO_2$, and 960 $GtCO_2$, respectively (Table TS.11). For a probability of at least 50%, the budgets for the same temperature targets are 390 $GtCO_2$, 690 $GtCO_2$, 1140 $GtCO_2$. Since the AR5, estimates have been updated with methodological improvements, resulting in larger, yet consistent estimates. Using 42 $GtCO_2$ (11.5 ±0.9 PgC, the estimated global CO_2 emissions in 2018) as a starting level and following a linear downward trajectory from today onwards, the values for a 50% probability of limiting warming to 1.5°C, 1.7°C or 2°C correspond to reaching net zero emissions in about 20, 35, and 55 years, respectively. If a specific remaining carbon budget is exceeded, carbon dioxide removal will be required to return warming to a certain temperature level. {Table TS.6, 5.5.2, 5.6, Box 5.1}

[START FIGURE TS.29 HERE]

Figure TS.29: Illustration of relationship between cumulative emissions of CO2 and global mean surface air temperature increase (left) and conceptual schematic of the assessment of the remaining carbon budget from its constituting components (right). Historical data in the left-hand panel (thin black line data) shows historical CO2 emissions together with the assessed global surface air temperature increase from 1850-1900. Orange-brown range with its central line show the human-induced share of historical warming. The circle and vertical line show the assessed range of historical human-induced warming for the 2010–2019 period relative to 1850-1900. The grey cone shows the assessed range for the transient climate response to cumulative emissions of carbon dioxide (TCRE) assessed to fall *likely* in the 1.0–2.2 °C/EgC range, starting from 2015. The red range and thin red lines within it represent CMIP6 simulations of the SSP5-8.5 scenario, starting from 2015. {Updates: to include an additional cone showing future GSAT change versus cumulative emissions for assessed GSAT ranges following the SSP5-8.5 scenario.}. [*Purpose**:** The proportionality between cumulative CO2 emissions and global surface air temperature in observations and models (left) as well as the assessed range of TCRE and the right-hand panel shows how information is combined to derive remaining carbon budgets consistent with limiting warming to a specific level. Update to AR5 SPM.10, SOD Figure 5.31.]*

[END FIGURE TS.29 HERE]

[START TABLE TS.11 HERE]

Table TS.11: The assessed remaining carbon budget and corresponding uncertainties. Assessed estimates are provided for additional human-induced warming expressed as global average surface air temperature since the recent past (2010–2019), which amounted to 1.1°C ± 0.2°C relative to the 1850–1900 period. {Chapter 5 Table 5.8}]

Additional warming since 2010-2019 (°C)*(1)	Approx. warming since 1850-1900 (°C)*(1)	Remaining carbon budget*(2)			Key uncertainties and variations						
		Percentiles of TCRE*(3)			Earth-system feedbacks *(4)	Non-CO_2 scenario variation* (5)	Non-CO_2 forcing and response uncertainty	TCRE distribution uncertainty*(7)	Historical temperature uncertainty*(1)	Zero Emissions Commitment (ZEC)*(8)	Recent emissions uncertainty*(9)
		33rd ($GtCO_2$)	*50th ($GtCO_2$)*	*67th ($GtCO_2$)*	*($GtCO_2$)*	*($GtCO_2$)*	*($GtCO_2$)*	*($GtCO_2$)*	*($GtCO_2$)*	*($GtCO_2$)*	*($GtCO_2$)*
0.2	1.3	140	90	50							
0.3	1.4	320	240	180							
0.4	1.5	500	390	310							
0.5	1.6	670	540	440	Already included in left-hand table*(10)	±250	-400 to +200 TBC*(6)	+60 to +110 $GtCO_2$ per °C of additional warming	±450	±410	±20 TBC
0.6	1.7	850	690	570							
0.7	1.8	1030	840	700							
0.8	1.9	1210	990	830							
0.9	2.0	1390	1140	960							
1.0	2.1	1570	1290	1090							
1.1	2.2	1740	1440	1220							
1.2	2.3	1920	1590	1350							
1.3	2.4	2100	1740	1480							
1.4	2.5	2280	1890	1610							

*(1) Human-induced global surface air temperature increase between 1850-1900 and 2010-2019 is assessed at 0.9-1.3°C (*likely* range; Chapter 3) with a central estimate of 1.1°C.
*(2) Historical CO_2 emissions since the middle of the 1850-1900 reference period (mid-1875) until and including 2019 are estimated at 2120 $GtCO_2$ (±15% one standard deviation range) until end 2014. Since 1 January 2015, an additional 210 $GtCO_2$ has been emitted until the end of 2019 (Friedlingstein et al., 2019).
*(3) TCRE: transient climate response to cumulative emissions of carbon, assessed to fall *likely* between 1.0-2.2 °C/EgC, considering a normal distribution consistent with AR5 (Stocker et al., 2013b). Values are rounded to the nearest 10 $GtCO_2$.
*(4) Earth system feedbacks include CO_2 released by permafrost thawing as shown in Figure 5.28, and discussed in Section 5.5.2.2.4. This uncertainty contribution is included in the left-hand part of the table. The 135 $GtCO_2$ reduction per °C of additional warming comes with a ±100% one standard deviation range.
*(5) Variations due to different scenario assumptions related to the future evolution of non-CO_2 emissions in mitigation scenarios reaching net zero CO_2 emissions (Huppmann et al., 2018; Rogelj et al., 2018).
*(6) Remaining carbon budget variation due to geophysical uncertainty in forcing and temperature response of non-CO_2 emissions. Currently still based on (Forster et al., 2018; Rogelj et al., 2018).
*(7) The distribution of TCRE is not precisely defined. Here the influence of assuming a lognormal with a 1.0-2.2 °C/EgC central 66% range instead of a normal distribution with a 0.6 °C/EgC 1-sigma range centred around 1.6°C is shown.
*(8) The variation due to the ZEC is estimated for a central TCRE value of 1.6 °C/EgC and a 1-sigma ZEC range of 0.18°C
*(9) Historical emissions uncertainty reflects the uncertainty in historical emissions since 1 January 2015.
*(10) The contribution of these additional Earth system feedbacks was estimated at a 135 $GtCO_2$ reduction of the carbon budget per °C of additional warming.

[END TABLE TS.11 HERE]

There is *medium confidence* that several factors, including estimates of historical warming, future emissions from thawing permafrost, and variations in projected non-CO_2 warming, affect the precise value of carbon budgets but do not change the need for global CO_2 emissions to decline to net zero to halt global warming. Geophysical uncertainties related to the climate response to non-CO_2 emissions and the transient temperature response to cumulative CO_2 emissions distribution result in an uncertainty of at least ±300 $GtCO_2$. Uncertainties in the level of historical warming result in a ±450 $GtCO_2$ uncertainty, and estimates may vary by ±250 $GtCO_2$ depending on median the amount of warming caused by past and future non-CO_2 emissions at the time global anthropogenic CO_2 emissions reach net zero levels. The latter uncertainty will be further assessed in the AR6 Working Group III Contribution. {5.4, 5.5.2}

Initial results from idealized numerical experiments that specifically explore the response to CO_2 emissions are inconclusive as to whether the change in globally averaged surface air temperature following the cessation of all CO_2 emissions (known as the Zero Emissions Commitment) will be positive or negative on decadal timescales of about half a century, with values spanning from approximately −0.4°C to 0.2°C after cumulative CO_2 emissions broadly consistent with global warming in the range of 2°C. For lower cumulative CO_2 emissions, the range would be smaller yet with equal uncertainty about the sign. There is therefore *low confidence* in the sign and magnitude of the Zero Emissions Commitment. If the Zero Emissions

Commitment is in fact positive on decadal timescales, this would further reduce remaining carbon budgets, and vice versa if it would be negative. {4.7.2, 5.5.2}

The combined effect of all additional Earth system feedbacks is assessed to result in a reduction of the remaining carbon budget of about 135 $GtCO_2$ per °C of additional warming relative to the recent past (2010-2019, with a 1-sigma range of a ±135 $GtCO_2$). This contribution is already included in the estimates of the here reported remaining carbon budget. Of this overall range of additional Earth system feedback contributions, the release of CO_2 from thawing permafrost alone is estimated to be responsible for about 75 $GtCO_2$ (±50 $GtCO_2$, 1-sigma range) per degree of additional warming. Due to limited studies, the assessment of the size of these contributions has *very low confidence*. Despite the large uncertainties surrounding the understanding and quantification of the impact of these processes, they represent identified additional risk factors that scale with additional warming and mostly increase the challenge of limiting warming to specific temperature thresholds. {5.4, 5.5.2}

The impact on global mean temperature following a climate mitigation measure that affects emissions of both short- and long-lived climate forcers depends on their lifetimes, how fast the emissions are reduced and the inertia of the climate system itself. Mitigation of SLCFs is often implemented through new legislation or technology standards for the different emission sectors and components, implying that reductions are sustained over time. AR5 found that the largest contributors to warming on 50-100-year time scales are the energy, industrial and on-road transportation sectors. Attribution of global temperature changes to emissions from sectors and regions represents the mitigation potential inherent in current emissions, as shown in Figure TS.30 and indicates that SLCFs have substantial short-term impacts, especially from CH_4, BC and SO_2. In AR6, considering current emissions of CO_2 and SLCFs, the largest warming sectors are energy, agriculture, waste/landfill and residential on a 10-year time scale and energy, industry and land transportation on a 100-year time scale (*high confidence*). Current emissions of CO_2 and SLCFs from East Asia and North America are the largest regional contributors to global warming on both short (*medium confidence*) and long-time scales (10 and 100 year) (*high confidence*). Because the effect of the SLCFs decays rapidly over the first few decades after emission, the net long-term temperature effect is predominantly determined by CO_2. CO_2 emissions also cause an important contribution to warming on short 10-20-year time scales (*high confidence*). {6.5.1, 6.5.2}

[START FIGURE TS.30 HERE]

Figure TS.30: Global Surface Air Temperature (GSAT) effect for 10 and 100 years after one year pulse of present-day emissions (year 2014 in Community Emissions Data Systems (CEDS) emissions (Hoesly et al. 2018)) of short-lived climate forcers (SLCFs) and CO2 for: a) global total emissions, and b) emissions from 10 major economic sectors sorted by total net effect on the 10-year timescale. The temperature response is broken down by individual species. Error bars in the top panel show uncertainty (±1 standard deviation) in net temperature impact due to uncertainty in radiative forcing of the individual species (calculated using a Monte Carlo approach and best estimate uncertainties from the literature - see Lund et al. (2020) for details). The CO2 emissions from biomass burning and biofuel use in residential sector (RES) are not considered. HFCs are not yet part of the chart. Sectoral split is based on Hosely et al. 2018, Höglund-Isaksson et al. (2020) and Klimont et al. (2017).{Ideas from Joeri: I would like to highlight that reductions in CO2 emissions result in an almost instantaneous change in the rate of warming. I think the figure probably needs a more direct visualisation of the "thought experiment" of simply looking at current emissions for one year, and then basically switching all emissions off and wait for 10 and 100 years, respectively. The bars can maybe also be distributed on a global map for the regional contributions and linked to icons that represent the various sectors for the sectorial emissions.} *[Purpose: This figure shows the sectoral contribution to present-day climate change by specific climate forcers including CO2 as well as SLCFs. {Figure 6.16}*

[END FIGURE TS.30 HERE]

Reductions in aerosols and non-methane ozone precursors to improve air quality but without simultaneous stringent CO_2 mitigation would lead to additional near-term warming with a *likely* range of 0.1-0.2°C (considering the SSP3.7.0 plus additional SLCF mitigation following the SSP3-7.0-low NTCF scenario but no CH_4 mitigation). Methane mitigation stands out as an option that combines near and long-term benefits for surface temperature (*high confidence*). However, across the SSPs, it is *unlikely* that methane mitigation alone can fully cancel out the near-term warming from reduction of non-methane cooling SLCFs. In decarbonisation scenarios, additional CH_4 and BC mitigation would contribute to offset the warming associated with SO_2 reduction that accompany decarbonisation (*high confidence*). {6.6.3, 6.6.4, 6.5.3, Box 6.2}

Assuming the Kigali Amendment and national regulation are implemented and efficiently enforced, the estimated reduction of global warming due to hydrofluorocarbons (HFCs) would be less than 0.07 °C by 2050 and between 0.2°C -0.4°C by 2100, relative to scenarios without HFCs regulation (*medium confidence*). This results from both HFC substitution and CO_2 reduction driven by energy efficiency improvements in refrigeration and air-conditioning equipment. {6.5.3, 6.6.3}

TS.3.4.2 Carbon Dioxide Removal

Carbon dioxide removal (CDR) refers to anthropogenic activities that seek to remove CO_2 from the atmosphere and durably store it in geological, terrestrial or ocean reservoirs, or in products. CO_2 is removed from the atmosphere by enhancing biological or geochemical carbon sinks or by direct capture of CO_2 from air and storage. Emission pathways that limit globally averaged warming to 1.5°C or 2°C typically assume the use of CDR approaches in combination with emissions reductions. CDR approaches could be used to offset emissions from sectors that are difficult or costly to decarbonize. CDR could also be implemented at a large scale to generate global 'net negative' emissions, which could compensate for earlier emissions as a way to meet long-term climate stabilization targets after overshoot. This report assesses the effects of CDR on the carbon cycle and climate, whereas a detailed assessment of the socio-economic dimensions of these options is presented in the AR6 WGIII. {4.6.3, 5.6}

There is *high confidence* that land- and ocean-based CDR methods have the potential to sequester CO_2 from the atmosphere. However, a given amount of CO_2 sequestered by CDR results in a smaller amount of CO_2 reduction in the atmosphere due to the redistribution of CO_2 between carbon pools (e.g., degassing from the ocean) and Earth system feedbacks (*medium confidence*). The effectiveness of CDR, defined as the reduction in atmospheric CO_2 per unit CO_2 sequestered, is largely independent of the magnitude and rate of CDR but varies strongly with the background atmospheric CO_2 concentration from which CDR is applied (*medium confidence*). Due to asymmetries in the climate-carbon cycle response, CO_2 emissions are more effective at raising atmospheric CO_2 than CO_2 removals are at lowering atmospheric CO_2, particularly for large emissions/removals (>100 PgC). This asymmetry implies that an extra amount of CDR is required to offset a positive emission of a given magnitude (*low confidence*). {5.6.2, Figure 5.32, Figure 5.34, Figure 5.36}

The sequestration potential of many land- and ocean-based CDR methods is weakened by associated Earth system feedbacks by decreasing either the land or ocean carbon uptake or through effects on climate (*medium confidence*). CDR methods can have positive or negative biogeochemical (e.g., non-CO_2 emissions) and biophysical side-effects (e.g., changes in hydrology or surface reflectivity) (*high confidence*) and other side-effects related to water, food and biodiversity (*high confidence*). The level of *confidence* in the direction and magnitude of multiple side effects of CDR methods varies from *low* to *medium* and is often project and region specific. The effects of terminating CDR are expected to be small for the deployment of CDR that is applied at scales as large as currently deemed possible (*medium confidence*). {4.6.3, 5.6.2}

Simulations with ESMs indicate that in scenarios with CO_2 emissions gradually declining and becoming net negative (meaning that removals exceed emissions) during the 21st century (e.g., RCP2.6) suggest that land and ocean carbon sinks begin to weaken in response to declining atmospheric CO_2 and eventually turn to sources (Figure TS.31). For the land carbon sink, the sink-to-source transition occurs decades to a few centuries after CO_2 emissions become net negative. The ocean remains a sink of CO_2 for centuries after emissions become net negative. This sink-to-source transition lags the time CO_2 emissions become net negative, as carbon sinks respond much later to the prior atmospheric CO_2 concentration and continue to take up CO_2 for decades to centuries. While the general response is robust across models, the magnitude of CO_2 fluxes and the timing of the sink-to-source transition vary between models, particularly for the land sink. These uncertainties reflect the large spread in simulated terrestrial carbon cycle responses under positive CO_2

emissions. There is *low confidence* in the strength and timing in the sink-to-source transition in scenarios with net negative emissions. {5.6.2}

[START FIGURE TS.31 HERE]

Figure TS.31: Carbon flux components during different stages of ESM simulations driven by RCP2.6. (a) Large positive CO2 emissions, (b) Small net positive CO2 emissions, (c) Net negative CO2 emissions (short-term response), (d) Net negative CO2 emissions (long-term response). Fossil fuel and land use emissions as well as emissions from negative emission technologies are from the RCP2.6 scenario. Due to small differences between the compatible CO2 emissions diagnosed from the ESMs and the emissions in RCP2.6, emissions and land and ocean carbon fluxes over each 50-year period do not balance precisely. [*Purpose: This figure shows how atmospheric CO2 evolves under negative emissions and its dependence on the negative emissions technologies. It also shows the evolution of the ocean and land sinks (SOD Figure 5.33).]*

[END FIGURE TS.31 HERE]

The near-linear relationship between cumulative CO_2 emissions and maximum global mean temperature increase caused by CO_2 implies that stabilizing global temperature requires net anthropogenic CO_2 emissions to become zero. While mitigation of SLCF has the potential to reduce the rate of warming in the short-term, the net long-term temperature effect is predominantly determined by CO_2. Because of the linear relationship between cumulative CO_2 emissions and global mean temperature increase, mitigation requirements for limiting warming to specific levels can be quantified in terms of a carbon budget (*high confidence*). Carbon budget estimates since the AR5 have been updated with methodological improvements, resulting in larger, yet consistent estimates. Several factors, including estimates of historical warming, future emissions from thawing permafrost, variations in projected non-CO_2 warming, and the global mean temperature increase after cessation of emissions affect the exact value of carbon budgets (*medium confidence*). Deliberate removal of CO_2 from the atmosphere (CDR) has the potential to offset residual CO_2 emissions or to generate net-negative emissions. The effectiveness of CDR in reducing atmospheric CO_2 is dependent on the emission scenario and Earth system feedbacks that redistribute CO_2 between carbon pools and affect the specific CDR method's sequestration potential (*medium confidence*). There is *high confidence* that CDR methods can have unintended biogeochemical and biophysical side-effects and other side-effects related to water, food and biodiversity, but the level of confidence in the direction and magnitude of multiple side effects of CDR methods varies from *low confidence* to *medium confidence*.

TS.3.5 Climate and Air Quality Response to SLCFs in SSP Scenarios

This section summarizes the assessment of the climate and air quality responses to SLCF emission trajectories in the SSP scenarios. In the SSP scenarios, SLCF emissions (except methane) evolve from 2015 to 2100 following different air pollution control storylines consistent with SSP narratives (TS1.3.1). Climate response to SSP SLCF trajectories are driven by the offsetting effects of changes in emissions of climate forcers that cause cooling versus warming.

Across the SSP scenarios, it is *very likely* that SLCFs will cause warming in the near term (2040) relative to 2020. The net near term effect of SLCFs on GSAT is *likely* a warming of 0.05-0.3°C. This near-term warming is quite insensitive across the SSPs due to compensating effects of warming (methane, ozone) and cooling (aerosols) agents (Figure TS.32). There is greater diversity near the end of the century response among the scenarios. It is *likely* that SLCFs in the low climate mitigation scenarios (SSP3-7.0 and SSP5-8.5) will cause a warming in the range of 0.3-0.9°C in 2100 relative to 2020 due to increase in methane and tropospheric O_3 levels. For these scenarios, methane, tropospheric ozone and HFCs are the main warming agents. For the strong climate and pollution mitigation scenarios SSP1-1.9 and SSP1-2.6, after 2040 the reduced warming from reductions in methane, ozone and HFCs dominates and at the end of century the temperature change due to reductions in emissions of SLCFs is close to zero. The middle of the road scenario, SSP2-4.5, gives a warming in 2100 by the SLCFs of 0.1-0.4°C, with the largest warming from reductions in aerosols. {6.6.3, 6.6.4}

Projections of air quality (near surface ozone and PM) at global and local scales will be predominantly driven by changes in precursor emissions rather than climate (*high confidence*). There is *high confidence* that reduced emissions from strong air quality and climate mitigation measures (SSP1-2.6 and SSP1-1.9) will lead to substantial reductions in global surface ozone and PM while increases in emissions from weak climate and air pollution mitigation will lead to strong increases throughout the whole century (SSP3-7.0) (Figure TS.32). High methane levels can offset the decline in global surface ozone from strong pollutant emission controls in the near term (SSP5-8.5) (*high confidence*). There is *high confidence* that rapid decarbonisation strategies, beyond those considered in SSP scenarios, lead to air quality improvements but are not sufficient to achieve, in the near term, air quality guideline values set by the World Health Organization (WHO) in some highly polluted regions. Additional policies (e.g., access to clean energy, waste management) envisaged to attain SDG goals bring complementary SLCF reduction. {6.2.1, 6.4, 6.5.3, 6.6, Box 6.2}

[START FIGURE TS.32 HERE]

Figure TS.32: Effect of 5 groups of short-lived climate forcers (SLCFs) (net aerosols, tropospheric ozone, Hydrofluorocarbons (HFCs), methane and black carbon (BC) on snow) and total forcing across the main Shared Socio-Economic Pathway (SSP) scenarios on future Global Surface Air Temperature (GSAT) for 2040 and 2100 relative to year 2021. The GSAT changes are based on calculations of historic and future of Effective Radiative Forcing (ERF) evolution from three simple climate models/emulators participating in the Reduced Complexity Model Intercomparison Project (RCMIP). The temperature response to the ERFs are calculated with one common impulse response function for the climate response, equal to the Instantaneous Radiative Forcing (IRF) used for metric calculations in Chapter 7. The IRF has an equilibrium climate sensitivity of 3.3°C (feedback parameter of 0.885 C (Wm-2)-1). The uncertainties are the intra-model standard deviation. The scenario total (grey bar) includes all anthropogenic forcings (LLCFs, SLCFs and Land Use Changes). The global changes in air pollutant concentrations (ozone and PM2.5) are based on multimodel simulations (AerChemMIP) and represent change in annual mean surface continental concentrations for the near and long-term relative to 2021. *[Purpose: The intent of this figure is to show the climate and air quality (surface ozone and PM2.5) response to SLCFs in the SSP scenarios (new figure based on Figures 6.17, 6.18, and 6.19) for near and long-term.]*

[END FIGURE TS.32 HERE]

Overall, reductions in cooling aerosols, primarily sulfate, due to air pollution regulation are inexorably unmasking the ongoing climate change, though the magnitude of the cooling effect of aerosols remains the largest uncertainty in the effect of SLCFs in future climate projections. The peak near-term warming of 0.3°C due to reductions in emissions of SLCFs will *likely* occur before 2040. This warming due to reductions in emissions of SLCFs can only be partially compensated by controlling methane in the near term. Methane mitigation, which induces global surface ozone reduction and thus contributes to air quality improvements, also offers climate benefits in the longer term, whereas only LLCF reductions allow long term climate stabilization.

TS.3.6 Solar Radiation Modification

Solar radiation modification (SRM) refers to a category of deliberate large-scale climate engineering or intervention options that have been proposed to offset some of the warming effects of greenhouse gas emissions on climate by intentional modification of the Earth's radiative budget. Following SR1.5, the SRM in this report refers to changes in both shortwave and longwave radiation. The other category of climate engineering option, carbon dioxide removal (CDR), involves the removal of carbon dioxide that is already in the atmosphere by accelerating natural carbon cycle processes or by industrial means (TS 3.4.2). SRM contrasts with climate mitigation and CDR, as it introduces additional human induced perturbations to the planet, rather than attempting to remove existing ones. By masking only the climate effects of greenhouse gas emissions, it does not address other issues related to atmospheric CO_2 increase, such as ocean acidification. SRM approaches are largely hypothetical at present and there are important considerations over their implementation, cost, governance, trans-boundary issues relationship to the SDGs and ethics which the WGII and WGIII reports will address. The WGI report assesses physical understanding of the earth system response to proposed SRM approaches. The assessment is based primarily on idealized climate model simulations. {4.6.3}

SRM options include those that increase surface albedo (e.g., by engineering crops to be brighter in near-infrared wavelengths), brighten marine clouds (e.g., by increasing the amount of sea-salt cloud condensation nuclei), or even reduce the amount of sunlight incident at the top of the Earth's atmosphere (e.g. using hypothetical space mirrors). However, the most commonly studied approaches attempt to mimic the cooling effects of volcanoes by injecting reflective aerosols (e.g., sulfates) or their precursors (e.g., sulphur dioxide) into the stratosphere. {5.6.3}

SRM could potentially offset the GHG-induced global mean warming, but the offset is *likely* to be imperfect at regional scales and seasonal timescales (*high confidence*) and varies substantially across different SRM options. There are large uncertainties in important climate processes associated with SRM options and the interactions among these processes (*high confidence*). Since the AR5, more modelling work has been conducted on SRM with more sophisticated treatment of aerosol-based SRM approaches, such as stratospheric aerosol injections, marine cloud brightening and cirrus cloud thinning, but the uncertainties in cloud-aerosol-radiation interactions are still large (*high confidence*). Modelling studies suggest that it is possible to meet multiple large-scale temperature and precipitation stabilization goals simultaneously by tailoring the deployment strategy of SRM options (*medium confidence*) but with large residual or overcompensating regional and seasonal climate changes. The effect of SRM on global temperature and precipitation has been found to be detectable after one to two decades which is similar to the timescale for the detection of mitigation effects. There is *high confidence*, as assessed in AR5, that a sudden and sustained termination of SRM would cause a rapid increase in temperature, but a gradual phase-out of SRM combined with mitigation and CDR is *likely* to avoid large rates of warming. {4.6.3}

SRM approaches targeting shortwave radiation (sulfate injection, surface albedo modification, cloud brightening) are *very likely* to reduce global mean precipitation (*high confidence*) relative to future CO_2 emissions scenarios. In contrast, cirrus cloud thinning, a longwave technique, results in increased global mean precipitation because it causes enhanced cooling in the troposphere (*high confidence*). When shortwave approaches are used to offset global mean warming, the magnitude of reduction in regional precipitation minus evaporation (P-E) which is more relevant to freshwater availability is smaller than precipitation decrease because of simultaneous reduction in both precipitation and evaporation (*medium confidence*). It is *very likely* that an implementation or termination of strong SRM can drive abrupt changes in the water cycle globally and regionally, especially in the tropical regions by shifting the ITCZ and Hadley cells. At the regional scale, non-linear responses cannot be excluded as changes in evapotranspiration can lead to strong regional non-linearities. {4.6.3, 8.6.3}

SRM acts to cool the planet relative to unmitigated climate change, which reduces plant and soil respiration, and also reduces the negative effects of warming on ocean carbon uptake (*medium confidence*). As a consequence, SRM is *likely* to reduce the atmospheric CO_2 concentration by enhancing global land and ocean sinks. SRM will not counteract ocean acidification. Rapid termination of SRM would cause rapid increase in global warming with return of positive and negative effects of warming on carbon sinks (*low confidence*). {5.6.3}

In summary, solar radiation modification (SRM) acts to mask but not to undo greenhouse gas-induced warming and it does not address other issues related to atmospheric CO_2 increase. There has been much progress in the understanding of the climate effects of and responses of biogeochemical and water cycles to SRM since AR5. However, despite that progress, important climate processes associated with specific SRM approaches and the interactions between these processes still suffer from large uncertainties (*high confidence*). {4.6.3, 5.6.3, 8.6.3}

TS.4 Regional change

Previous IPCC assessment reports underlined the urgent need for regional climate information that is useful and relevant to the decision scale. To help fill this gap, the AR6 WGI provides foundational knowledge of key factors that frame the formulation, interpretation and application of regional messages of change. Regional climate change is addressed through the introduction of a unified WGI Reference Set of Land and Ocean Regions, as well as the use of Typological regions such as monsoon regions, mountains, urban/megacities in addition to continental regions mainly used for links with WGII. {1.4.6}

This section provides the rationale for generating messages of regional climate change and the relevance of these messages for climate services (TS4.1), followed by a global overview of the drivers of regional climate variability and change and how they are being affected by anthropogenic factors (TS.4.2). It concludes with a region-by-region assessment of past and projected changes in climate means, extreme events and climatic impact drivers (TS.4.3). The climatic impact drivers can take the form of hazards when they lead to negative impacts, or can lead to beneficial impacts, or both, depending on sector and/or region. {12.1, 12.2}

TS.4.1 Construction of regional climate information and messages

Given the large number of types of regional climates, the broad range of spatial and temporal scales, and the variety of users needs (TS.4.1.3), several methodologies and approaches have been developed worldwide to construct climate information and distil climate messages to inform adaptation and policy decisions (Figure TS.33). Approaches to synthesize climate information use multiple lines of evidence including process understanding, the analysis of observed trends and changes and their attribution to large- and regional-scale anthropogenic and natural drivers and forcings (TS.4.2), the application of different model types, and other methodologies to address uncertainties in model projections, like ensemble construction and storylines approaches (TS.4.1.1). Translating climate information into the user context, taking into account the values of the actors involved, including climate services, results in the generation of climate message (TS.4.1.2, TS.4.1.3) aiming at providing actionable information and aiding decision making.

TS.4.1.1 Sources and methodologies to generate regional climate change information

Climate change information at the regional scale is usually generated from a large variety of sources. These include regional observations and a hierarchy of different model types, including high-resolution and variable resolution global climate models (GCMs), dynamical downscaling using regional climate models (RCMs), statistical downscaling and bias adjustment techniques.

Good quality observations allow monitoring the regional aspects of climate, are used to adjust inherent model biases, and are the basis for assessing model performance. {10.1.1}

There is *very high confidence* that the availability of multiple observational records is fundamental for assessing climate model performance at regional scale. However, observational records for data sparse regions, mountainous areas, and cities cause difficulties that pose limits to the assessment of regional climate change. For instance, there is *very high confidence* that precipitation measurements, especially of solid precipitation, in mountainous areas are strongly affected by the gauge location and setup. There is *high confidence* on elevation-dependant warming in most of the mountain ranges but field measurements are extremely limited at high elevations. It is *virtually certain* that the scarcity and decline of observations (e.g., in southern Mediterranean, Africa, or India) increase the uncertainty of long-term temperature and precipitation estimates. Gridded products of temperature and precipitation are strongly affected by interpolation methods over complex orography and data scarce regions such as the southern Mediterranean. {10.2.2, 10.6.2, 10.6.3, 10.6.4, Cross-Chapter Box 10.3}

There is *high confidence* that to assess whether a climate model realistically simulates required aspects of present-day regional climate, and to increase confidence of future projections of these aspects, evaluation needs to be based on diagnostics taking into account multiple variables and process-understanding. {10.3.3}

There is *very high confidence* that GCMs are an important source of future climate information at the regional scale. There is *medium confidence* that increasing GCM resolution helps reduce systematic errors, although there is *high confidence* that higher resolution per se does not solve all performance limitations. Reducing errors in the model formulations of GCMs is fundamental for improving both global climate model performance at the regional scale and the boundary conditions for dynamical downscaling. {10.3.1, 10.3.3, 10.4.1, Box 10.2}

RCMs are dynamical models similar to GCMs that are run over a limited area, but with a resolution higher than that of standard GCMs. They are the basis for dynamical downscaling but are also often used for process understanding. In the construction of global/regional climate model ensembles, computational costs can be reduced by selecting a small number of global/regional climate model combinations such that climate response uncertainty is spanned as comprehensively as possible. Including all relevant forcings in RCMs, including aerosols, land-use change and ozone concentrations, is a prerequisite for reproducing historical trends and to ensure fitness for purpose for future projections in certain regions (*medium confidence*). Dynamical downscaling using RCMs adds value in representing many regional weather and climate phenomena, in particular over complex terrain (*very high confidence)*, in spite of errors in model formulation that affect performance. Simulations at kilometre-scale resolution add value to the representation of convection *(high confidence*) and many local-scale phenomena such as land-sea breezes and influences of soil moisture (*medium confidence*), which are, in turn, relevant for triggering convection. {10.3.1, 10.3.3, 10.3.4, 10.4.1, Box 10.2}

An alternative or addition to dynamical downscaling is the use of statistical approaches to generate regional projections, such as statistical downscaling and bias-adjustment. Since AR5, several initiatives have been launched to improve the understanding of these statistical approaches. Statistical downscaling methods with carefully chosen predictors and an appropriate model structure for a given application realistically represent many characteristics of present-day daily temperature and precipitation (*high confidence*), and plausibly simulate future changes in daily mean temperature (*medium confidence*). There is, however, a lack of research about which predictors are required for plausibly simulating future daily precipitation. Statistical downscaling of spatial fields remains a challenge, especially for daily precipitation. {10.3.1, 10.3.3, Cross-Chapter Box 10.2}

Bias adjustment has proven beneficial as an interface between climate model projections and impact modelling, yet it cannot correct for unresolved or misrepresented processes that lead to model errors *(high confidence*). Applying bias adjustment to models that misrepresent relevant physical processes leads to severe problems (*medium confidence*). Using bias adjustment as statistical downscaling, in particular of coarse-resolution GCMs, may lead to substantial misrepresentations of regional climate and climate change (*medium confidence*). Instead, dynamical downscaling may be required to resolve relevant local processes prior to bias adjustment. {10.3.3, Cross-Chapter Box 10.2}

Multi-model ensembles (MMEs) are simulations typically performed by separate models set up with consistent boundary conditions and forcings, as in the series of Coupled Model Intercomparison Project. MMEs, while excluding models that simulate processes relevant for a given purpose unrealistically, are required to assess regional climate response uncertainty (*very high confidence*), although model spread is in general not a full measure of projection uncertainty. At the regional scale, multi-model means and ensemble spreads may not sufficiently capture low-probability, high-impact changes, and they may obscure situations where different models simulate changes that are substantially different in magnitude or even differ in direction (*high confidence*). {10.3.4}

Since the AR5, increase in computing power has made it possible to investigate simulated internal variability and to provide robust estimates of forced model responses, using large initial condition ensembles (ICEs). ICEs are required to separate internal variability from forced changes (*high confidence*). {1.5.4, 10.3.4}

Sometimes using different tools can result in different and potentially conflicting information; for instance, GCM- and RCM-based ensembles can disagree concerning the future projections for some key variables even over large areas. Similarly, different GCM-RCM combinations can produce contrasting results {Section 10.5.1}. When assessing future climate change, documenting, understanding and taking into account these inconsistencies are required to create a comprehensive and effective narrative on regional climate change. {10.5.1, 10.3.4, Atlas.6.3}

Storyline approaches are a complementary instrument to aid the representation of climate projection uncertainties and they can also be used to assess risks associated with low-likelihood but high-impact events. In fact, storylines make it possible to consider the physically self-consistent unfolding of past events, or of plausible future events or pathways which would be masked in a probabilistic approach. These aspects are important as the greatest risk need not occur at the highest likelihood outcome and can occur at low-likelihood outcomes because of the nature of the impact. {1.4.4}

Attributing observed changes to large- and regional-scale anthropogenic and natural drivers and forcings is also an important source of climate information. {TS.4.2, 10.1.1}

TS.4.1.2 Methodologies and approaches for generating regional climate change messages

Climate information is the basis for the development of a regional climate message that translates the factual information into the context and values of the user (Figure TS.38). Climate messaging is inherently influenced by the values of all parties: those constructing the message, those communicating the message, those receiving the message, and critically those who construct the problem statement which the message seeks to inform.

An important element of the process for developing the AR6 has been a strong emphasis on communication and the transfer and integration of information between the Working Groups (handshake). Important elements of this effort included the use of a consistent risk framework and the use of storylines and the Reasons for Concerns (TS.4.2.3). Key aspects of these elements are addressed in this section.

The choices made to generate climate messages have typically been part of a linear supply chain, starting from the generation of climate data transformed into maps or derived data products. This methodology has proven to be valuable in many cases, but it is equally fraught with dangers of not communicating important assumptions, estimating the relevant uncertainty, and possibly causing misunderstandings in the hand-over from one community to another one. This has led to the emergence of new pathways to generate user-oriented climate messages, many in the context of emerging climate services (TS.4.1.3).

It is *virtually certain* that complex climate change information is understood differently by different groups of people. Best-practice guidance is emerging to achieve greater consistency in the understanding and use of climate information. There is *high confidence* that involving diverse expertise from climate scientists and decision makers in the production of regional climate information results in better integration of scientific evidence into decision making. There is *high confidence* that including users ensures the correct context in forming the message. {10.5}

Communication of scientific understanding to policymakers and other users occurs in the context of implicit and explicit values and beliefs, including pre-existing understanding of weather and climate in diverse cultures. Science has values of its own, including objectivity, openness, well-defined methods, and well-documented evidence. Values are often implicit in choices made during the construction, assessment, and communication of information. {2.3.3, 2.3.4, Cross-Chapter Box 2.4}

For a message on regional climate change to be effective it needs to recognize and respond to the values of all parties (Figure TS.33). Part of the challenge with climate messages, especially for messages of impactful change, is that they can be based on a variety of disciplines and target people with a variety of backgrounds, which could give them differing sets of experiences, capabilities, and values, so that the messages may need to accommodate a range of normative lenses. Lack of this recognition can make the message ineffective even if the climate information it is based on is of the highest quality.

[START FIGURE TS.33 HERE]

Figure TS.33: Effective messaging requires shared development of the actionable information that engages all parties involved and the values that guide their engagement. Participants in the development of climate messages come from varying perspectives, based in part on their professions and communities. Each of the three broad categories shown in the Venn diagram (U, P, R) is not a homogenous group, and often has a diversity of perspectives, values and interests among its members. The subheadings in each category are illustrative and not all-inclusive. The arrows connecting those categories represent the distillation process of providing context and sharing climate relevant information. The arrows that point toward the centre represent the distillation of climate messages that involves all three categories.

[END FIGURE TS.33 HERE]

Climate change becomes relevant for regional impact management and for risk assessment when trends or episodic events affect particular natural and societal assets and can thus become climatic hazards or benefits. Decision makers, policymakers, risk managers, and impacts scientists therefore benefit from climate information that tracks key trends and thresholds that represent crucial challenges for natural and human systems. While useful indices and precise threshold values for a given sector can vary widely and are often unknown, categories and progressions of threshold levels emerge within many sectors to form coherent messages concerning altered regional impacts and risk profiles under climate change.

Given the complex context of climate understanding, special care is required when communicating findings and uncertainties, including in IPCC assessments that inform high-stakes decisions. {1.2.3}

Use of a narrative structure that converges with the values and experiences of audiences rather than presenting lists of facts *likely* improves understanding in the face of this complexity. {Atlas.1.2}

TS.4.1.3 Climate Services

A climate service can be considered as the provision of climate information to assist decision-making. IPCC AR5 WGII introduced climate services as institutions that bridge generation and application of climate knowledge and described the history and concepts of climate services. Since AR5, there has been considerable progress in understanding climate information user needs, better facilitation of user engagement and an appreciation of climate scientists to involve communication specialists and social scientists to support the co-design and co-development process that is fundamental to a successful climate service. With the link between WGI and WGII becoming stronger, there is a greater focus in WGI on regional information. Regional information is constructed through multiple lines of evidence (Box TS.5, Figure 2) and can form the basis for the development of regional climate message (TS.4.1.2) and climate services, taking account the specific context of the question at stake, the values of all parties involved, and the challenge of communicating across different communities (Figure TS.33). It is *virtually certain* that complex climate change information is understood differently by different groups of people. {10}

Climate services include the synthesis of context-relevant climate information addressing a wide range of time scales that go beyond operational weather services. From this point of view, climate services are an instrument for the production of climate information in a co-production process that is inclusive, collaborative and flexible. {10.5.1}

In general, climate services involve the generation, provision, and contextualization of information and knowledge derived from climate research for decision making at all levels of society. Climate services generally involve user engagement and there are various forms of how climate information and data is delivered or communicated to the users. There are different levels of user engagement from passive engagement, to interactive group activities to focused relationships between climate service provider and users, which yield in different types of climate service products from websites, capacity building, and tailored climate indices. {12.6.1, 12.6.2}

The climate services landscape is fast growing and very broad as reflected in the vast diversity of practices and products that can be found in the peer-reviewed literature (*high confidence*). {12.6.2}

Climate services are being developed across regions, sectors (e.g., agriculture, water, energy, health), timescales (from sub-seasonal to multi-decadal) and target users (*high confidence*). User needs and decision-making contexts are very diverse and there is no 'one size fits all' solution to climate services (*very high confidence*). While there exists a diversity of perspectives around what constitutes co-production of climate information there is a *medium evidence and high agreement* that processes that support collaborative learning and knowledge production involving a diversity of expertise including both climate scientists and decision makers, results in enhanced integration of science evidence into decision. {10.5.1}

Climate services requires communication of climate information and the mode of knowledge production and transfer by scientists, as a fluid understanding is required between academic and non-academic professionals to co-design and co-produce useful decision-relevant information and tools (*high confidence*). {12.6}

Climate services also set new scientific challenges to research *(high confidence*). Many questions have appeared over at least the last decade in terms of, for instance, how to best estimate changes and uncertainties from projections of model ensembles, optimize the ensemble, or how to adjust model biases without harming trends, cross-variable, time and space consistencies, to downscale information at the local scale, are currently the object of intense research. {12.6.1}

There are recurring challenges related to successful climate service applications: 1) climate services are scarcely visible and poorly understood by 'end users', 2) data quality, overabundance and accessibility and 3) users are unsure how they would set about procuring climate services that are pertinent to their needs. These challenges relate to climate services development, provision of climate services, generation of climate service products, engagement and communication with users, and evaluation of the quality and socio-economic value of climate services. {12.6.2}

TS.4.1.3.1 Summary

Climate change information at regional scale is usually generated from a large variety of sources, including regional observations and a hierarchy of different model types and statistical methodologies. There is *high confidence* that multiple sources of observations and tailored diagnostics are needed to evaluate climate model performance and to increase confidence in future projections of regional climate. However, limited observational records for mountainous regions, data-sparse regions and cities cause difficulties that pose limits to the assessment of regional climate change.

Overall, there is *high confidence* that increasing model resolution, downscaling and adding relevant model components can increase the fitness for purpose of some aspects of regional projections when they are accompanied by a process-understanding analysis.

At the regional scale, multi-model mean and ensemble spread are not sufficient to characterise low-probability high-impact changes or situations where different models simulate changes that are substantially different or are even contradictory (*high confidence*). Storyline approaches are a complementary instrument to aid the representation of climate projection uncertainties. Grand ensembles of many realisations of internal variability are required to separate internal variability from forced changes (*high confidence*).

It is *virtually certain* that complex climate change information is understood differently by different groups of people. The development of a regional climate message translates the factual information into the context of the user. Climate messaging is inherently influenced by the values of all parties. There is *high confidence* that involving diverse expertise from climate scientists and decision makers in the production of regional climate information results in better integration of scientific evidence into decision making. There is *high confidence* that regional climate-change messages are influenced by the values of those constructing, communicating, and receiving the message. There *is high confidence* that including users ensures the correct context in forming the message.

Climate services are becoming more and more widely established as a way to tailor climate information to specific decision-making needs, often related to adaptation. User-driven climate services have become a key aspect of meteorological and environmental agencies. This provides opportunities for making the science assessed in IPCC reports more relevant for regional and local adaptation and risk management. However, it also introduces new scientific challenges with respect to climate model evaluation, data accessibility and communication. These challenges can only be met through close collaboration between practitioners and scientists working towards co-production of knowledge, which is particularly relevant for the risk and solution-oriented framing adopted in AR6 that seeks to move the risk question from the prediction space to the decision-making space. The cross-WG integration and communication efforts in the AR6 process are an example of such co-production process and provide the basis for further collaboration between scientific communities and stakeholders to produce useful and relevant climate information for decision making.

[START BOX TS.5 HERE]

Box TS.5: The Interactive Atlas and multiple lines of evidence for constructing regional climate change message.

A significant innovation in the AR6 WGI report is the inclusion of the Atlas chapter with part of its remit to visualise, expand on, collate, and synthesize results from the other WGI chapters. An important component of this is the development of an online interactive tool, the Interactive Atlas, with flexible spatial and temporal analyses of much of the observed and projected climate change information underpinning the WGI assessment. This includes the ability to generate maps and regional averages of observed and projected climate change using a range of different datasets including from the three most recent coordinated climate projection experiments, CMIP5, CMIP6 and CORDEX (Box TS.5, Figure 1). Projection information can be displayed and summarised for different global warming levels, under a range of SSP-RCP scenarios and future timeslices relative to several different baseline periods. The maps and various statistics can be generated for annual mean trends and changes or for any user-specified season. A new set of WG I reference regions (Box TS.5, Figure 2) is used for generating the regional summary statistics and these are widely used throughout the report.

[START BOX TS.5, FIGURE 1 HERE]

Box TS.5, Figure 1: Screen shots from the Interactive Atlas showing the main interface and WGI Reference regions (top map) and various formats for displaying summary information over the reference regions (bottom four graphics panels). Other details of model ensembles, resolutions and the summary statistics available are displayed in the text of the figure.

[END BOX TS.5, FIGURE 1 HERE]

[START BOX TS.5, FIGURE 2 HERE]

Box TS.5, Figure 2: AR6 WG I reference regions used for the regional analysis of atmospheric variables and land surface variables in the several WG I chapters including the Atlas and the Interactive Atlas. The definition of the regions and companion notebooks and scripts are available at the ATLAS GitHub (TS4).

[END BOX TS.5, FIGURE 2 HERE]

There is *high confidence* that distilling climate messages derived from multiple, potentially contrasting, lines of evidence such as observed, paleoclimate proxy and simulated data, theoretical understanding, diverse analysis methods and expert judgment increases confidence in regional climate change messages. {10.5.4, 10.6}.

As an example, Box TS.5, Figure 3 shows how the Interactive Atlas products together with other lines of evidence are used to distil the message of the Mediterranean warming exceeding Northern Hemisphere mean warming. The lines of evidence include the projected temperature by global and regional climate models, agreement between observational records and understanding of mechanisms. The mechanisms include dynamic and thermodynamic processes and the impact of aerosols. Despite the robust information of enhanced Mediterranean warming, uncertainties about future amplitude and regional distribution due to differences between the models about the relative contribution of those mechanisms remain. The yet unresolved discrepancy between the warming in the CMIP5 and CMIP6 experiments is an example of this uncertainty, which highlights the need for further investigation and distillation of all available evidence. {10.6.4}

[START BOX TS.5, FIGURE 3 HERE]

Box TS.5, Figure 3: Example of constructing regional climate message from multiple lines of evidence for the case of Mediterranean summer warming. (a) Mechanisms and feedbacks involved in enhanced Mediterranean summer warming. (b) Locations of observing stations in E-OBS v19e (Cornes et al., 2018) and Donat et al. (2014). (c) Differences in temperature observational data sets with respect to E-OBS for the land points between the Mediterranean Sea and 46°N and west of 30°E. (d) Observed summer (June to August) surface air temperature trends (°C per decade) over the 1960–2014 period from BEST (Rohde et al., 2013) dataset. (e) Time series of area averaged (25°N–50°N, 10°W–40°E) land point summer temperature anomalies (°C, baseline 1995–2014). Black, brown, orange and violet lines show low-pass filtered temperature of BEST, CRU TS v4.02 (Harris et al., 2014), HadCRUT4 (Morice et al., 2012) and the MPI-GE (Maher et al., 2019), respectively. Dark blue, red and light blue lines and shadings show low-pass filtered ensemble means and standard deviations of CMIP5 (30 members), CMIP6 (15 members) and HighResMIP (7 members), respectively. The filter is the same as the one used in Figure 10.11. (f) Distribution of 1960–2014 summer temperature trends (°C per decade) for observations (black crosses), the MPI-GE (violet histogram) and for ensemble means and single runs of CMIP5 (dark blue circles), CMIP6 (red circles) and HighResMIP (light blue circles). (g) Bias in ensemble mean 1960–2014 trends (°C per decade) of CMIP5, CMIP6, HighResMIP and CORDEX in reference to BEST. (h) Projections of ensemble mean 2014–2050 trends (°C per decade) of CMIP5, CMIP6, HighResMIP and CORDEX. All trends are estimated using ordinary least-squares.

[END BOX TS.5, FIGURE 3 HERE]

[END Box TS.5 HERE]

TS.4.2 Multiple drivers of regional climate variability

This section assesses the multiple physical causes or drivers of observed and future changes at regional scale in the context of ongoing anthropogenic influence on the global climate. Regional climate is determined by a complex interplay between the interannual-to-multidecadal variation of large-scale modes of variability and associated remote impacts (teleconnections), external forcings with both global and local expression, and regional-scale climate processes and related feedbacks. Modes of variability are defined as recurrent space-time structures of variability of the climate system with preferred spatial patterns, seasonality and time scales. They can arise though the dynamical characteristics of the atmospheric circulation but also through coupling between the ocean and the atmosphere with some interaction with land, sea-ice surfaces, all being mostly driven by natural internal processes. Foundations for interpreting past and projected regional climate are given here, including assessments of the regional fingerprint of anthropogenic and natural external forcing and the influence of modes of variability. A representative example is then provided to illustrate the inherent complexity of interpreting past regional climate variability and of generating comprehensive and reliable information for the future, which must account for the combined influences of all the drivers and their interactions as well as multiple lines of evidence. {Annex VI.1}

TS.4.2.1 Regional fingerprint of external forcing

Since the IPCC Third's Assessment report in 2001, the signal of climate change attributable to human influence has been unequivocally detected at the global scale in the observations, and the anthropogenic forced response is increasingly emerging on smaller regional spatial scales and in a range of climate variables relative to the amplitude of local natural variations. {1.4.2}

TS.4.2.1.1 Anthropogenic forcing (GHG, aerosols, other SLCFs, stratospheric ozone depletion, land use)

For temperature over the historical period, anthropogenic forcing has been a major driver of changes since 1950 in many sub-continental regions of the world (*high confidence*). Net effective radiative forcing (ERF) from anthropogenic aerosols, despite different influences from individual species, is opposite in sign to that from GHGs in several regions leading to counteracting effects, for example on the monsoon circulations in South Asia, East Asia and West Africa during the second half of the century. In response to local and remote aerosol forcings, global climate model simulations show qualitatively similar continental-scale patterns of temperature change that extend across much of the Northern Hemisphere and amplification of the temperature response toward the Arctic (*medium confidence)*. Aerosol ERF has offset part of the Arctic sea ice loss induced by GHG and has offset the strengthening of monsoon precipitation in response to GHG-induced warming in South Asia, East Asia and West Africa (*very likely*). Aerosol influence has attenuated hot extremes in some regions. There is *medium confidence* that a reduction of aerosol concentrations over the European part of the Mediterranean region, an outcome of air pollution control legislation, has been a dominant factor for the recent enhanced warming. At the regional scale at the regional scale extreme temperature are moderated, counteracted or amplified due to feedbacks or forcings such as regional land use and land cover changes. Irrigation and crop expansion have attenuated increases in summer hot extremes in some regions, such as the central North America (*medium confidence)*. {1.3, 3.4.1, 6.3.4, 8.3.1, 8.3.2, 10.4.1, 10.6.4, Box 8.1}

For precipitation over the historical period, anthropogenic forcing has contributed to multi-decadal precipitation changes in several regions (*medium confidence*). Large observational uncertainty and natural internal variability as well as model errors lead to *low confidence* with regard to a well-constrained quantification (best estimate and confidence interval) of the total anthropogenic contribution to precipitation changes as well as the relative contributions of GHGs, ozone, and different aerosol species. Land use change and irrigation also drive detectable water cycle changes in some regions through their influence on land surface water and energy budgets (*high confidence*). {8.2.1, 8.2.2, 10.4.1}

TS.4.2.1.2 Natural forcing (solar, volcanic aerosols)

Solar forcing, particularly its 11-yr variability, affects the leading atmospheric circulation modes of variability of the North Atlantic region yielding continental impacts on wintertime temperature over Eurasia and North America, thus allowing for potential near-term predictability. The magnitude of the forced solar response with respect to internal variability however remains weak and solar-forced signals not detectable in the historical period {3.7.1, 10.1.4.1, AVI.1}

Volcanic eruptions impact regional climate through their spatial heterogeneous effect on the radiative budget as well as the dynamical responses they trigger through phase-locking of certain modes of climate variability. Nevertheless, the statistical significance of the regional response remains difficult to evaluate over the historical era due to the small sampling of large volcanic eruptions over this period and the fact that the signal is superimposed upon relatively large internal variability. Overall, observational and modelling studies show that volcanic eruptions generally result in decreased global-mean land precipitation for up to a few years following the eruption, with climatologically wet regions drying and dry regions wetting (*medium confidence*). Major volcanic eruptions can have discernible impacts on the water cycle at the regional scale enhancing regional drought (*medium confidence*). Similar future large explosive volcanic eruptions are *likely* to substantially alter precipitation changes in the same way (*medium confidence*). {3.7.1, 3.7.3, 10.1.4, AVI.3, 4.3.1, 4.4.1, 4.4.4, 8.5.3}

TS.4.2.2 Internal modes of variability and regional teleconnections

The variability of the climate system at ocean- or continental-basin scales, and in particular on seasonal and longer time scales, is largely affected by the occurrence and often combination of several modes of variability leading to local impacts or remote responses through teleconnection processes. Many modes arise from internal processes and external forcing can either affect the temporal properties (occurrence, variance, seasonality, etc.) and/or the spatial properties of the mode itself and/or the associated teleconnections (strength, location, etc.).

This subsection integrates information related to the model representation of the main modes of variability and teleconnections on interannual to interdecadal time scales as well as attribution statements when applicable to interpret the observed changes over the historical period. Projected changes are also described, and assessments are summarized in Table TS.12 for all the modes addressed in AR6 and introduced in Technical Annex AVI: Modes of Variability. Detailed assessments are given for five specific modes of variability including El Niño and Southern Oscillation (ENSO), Southern Annular Mode (SAM), Northern Annular Mode (NAM), Atlantic Multidecadal Variability (AMV) and Pacific Decadal Variability (PDV). {2.4, 3.7, 4.3.3, 4.4.3, 8.3.2, 8.4.2, 10.4, Cross-Chapter Box 2.2}

[START TABLE TS.12 HERE]

Table TS.12: Summary table for modes of variability and teleconnection. Model performance, table of the modes and related teleconnection at regional scale. Evidence which is found in a chapter executive summary (ES) statement is identified by its code, e.g. [CH05P010] which denotes the tenth ES statement from Chapter 5.

Name	Short name	Time-scale	Teleconnections	Teleconnections	Observed trend	Model evaluation	Simulated trend	Attribution	Projected trend
			Temperature (warm; cold)	Precipitation (wet; dry)					
North Atlantic Oscillation & Northern Annular Mode	NAO/ NAM	intra-seasonal to multi-decadal	North America, Northern Europe/Siberia, Greenland/Northern Canada {AVI.2.2}	Eastern North America, Mediterranean; Northern Europe {8.3.2.9; 8.4.2.9; AVI.2.2}	[1958-2014] Strongly positive [1995-2014] Not significant [CH02P15] {2.4.1.1} ***High confidence***	Medium-to-high performance in CMIP5 & CMIP6 [CH03P16] {3.7.1} ***High confidence***	No significant trends in ensemble mean of historical simulation for both NAO and NAM {3.7.1}	No attribution because of overly dominance of internal variability [CH03P16] {3.7.1; 8.5.2} ***High confidence***	**21st century:** slightly positive NAM in SSP5-8.5 and SSP3.70 [CH04P14] ***High confidence***
Southern Annular Mode	SAM	intra-seasonal to multi-decadal	East Antarctica, southern South America, South Africa, southeastern Australia; {AVI.3.2}	southern South America; South Africa; southeastern Australia - {8.3.2.9; 8.4.2.9; 10.4.2.2.3; 10.4.3.2.3; AVI.3.2}	[1979-2014] Strongly positive [1995-2014] Weakly positive [CH02P15] {2.4.1.2} ***High confidence***	CMIP6 better than CMIP5 in austral summer [CH03P16] ***Medium confidence***	Significantly positive [CH03P16] ***Medium confidence***	Yes. [CH03P16] Combined response to stratospheric ozone depletion & GHG forcing in austral summer {4.4.3} ***High confidence***	**Near-term:** positive but weaker than late 20th century (***high***) **Mid-to-long-term:** increased wrt 1995-2014 in SSP5-8.5 and SSP3.70 (*medium*) [CH04P12]; [CH04P13] {4.3.3.1}; ***High confidence***
El Nino Southern Oscillation	ENSO	mostly interannual	Wintertime: Northwestern North America, northern South America, south Asia/Europe; northern Asia/Europe, southern North America	Eastern Australia, South Africa, northeastern South America; SESA, southern North America {8.3.2.9; 8.4.2.9; 10.4.1.2.3; AVI.3.2}	no SST trend but increased amplitude and increased frequency of high-amplitude events [CH02P15] {2.4.2} ***Medium confidence***	Medium performance and CMIP6/CMIP5 better than CMIP3 {3.7.3}	no trend; {3.7.3}	no evidence of anthropogenic influence in amplitude change [CH03P16]	**21st century:** no-consensus about systematic change **(medium)**; **Long-term:** enhanced rainfall variability associated with ENSO **(high)** Strengthening of ENSO-Indian Summer relationship in future high scenarios; [CH04P15]
Indian Ocean Basin and Dipole Modes	IOB/ IOD	mostly interannual	IOB: southeast Asia; Maritime Continent; northern Australia; northern South America; central America; east Asia. IOD:	IOB: Maritime Continent, south Africa, north Australia; East Asia. IOD: Maritime Continent; southeastern Australia; south Asia; east Africa {AVI.5.2}	low agreement on trends due to observational uncertainties [CH02P15]	Medium performance, good skill for IOB amplitude {3.7.4} ***Medium confidence***	n/a	Limited evidence of anthropogenic influence {3.7.4}	**Mid-to-long term:** stronger persistence of IOB/IOD variability related to ENSO (*high*) {4.5.3.4} ***High confidence***

			India, central South America, southern Australia {AVI.5.2}						
Atlantic meridional and zonal modes	AMM/ AZM	mostly interannual	AZM: western Africa, eastern South America; {AVI.6.2}	AZM: Indian summer monsoon {AVI.6.2}	low agreement on trends due to observational uncertainties [TBC] [CH02P15]	Low performance in both CMIP5/CMIP6 models {3.7.5}	n/a	No evidence of anthropogenic influence {3.7.5}	**Mid-to-long term:** changes with high uncertainty [To be rephrased] {4.5.3.5}
Atlantic meridional and zonal modes	AMM/ AZM	mostly interannual	AZM: western Africa, eastern South America; {AVI.6.2}	AZM: Indian summer monsoon {AVI.6.2}	low agreement on trends due to observational uncertainties [TBC] [CH02P15]	Low performance in both CMIP5/CMIP6 models {3.7.5}	n/a	No evidence of anthropogenic influence {3.7.5}	**Mid-to-long term:** changes with high uncertainty {4.5.3.5}
Pacific Decadal Variability	PDV	multi-decadal	northwestern North America, western South America, Australia, Africa, northern Asia/Europe {AVI.7.2}	India, eastern Australia, northeastern South America, southern South America, southern North America {AVI.7.2}	no trend [CH02P15] ***High confidence***	Moderate performance; (underestimation of variance and crude representation of associated tropical-extratropical basin-wide structure [CH03P16]	no trend {3.7.6}	Anthropogenic influence inconsistent among models (*low*) {3.7.6}	**Near-term:** shift to positive phase (*low*) {4.4.3.3} **Mid-to-long term:** no clear consensus on the change (*low*) {4.5.3.3}
Atlantic Multidecadal variability	AMV	multi-decadal	northeastern North America, Siberia, north Africa; southern Australia, eastern Central Asia {AVI.8.2}	Central America, Maritime Continent, India, Western Africa; southeastern North America, southern South America {AVI.8.2}	no trend [CH02P15] ***High confidence***	Moderate performance; crude representation of associated tropical-extratropical basin wide structure [CH03P16]	no trend {3.7.7}	Anthropogenic influence on AMV cold phase from mid-60s to mid-90s (*medium*) {3.7.7}	**Near-term:** no clear consensus on the sign {4.4.3.5} **Mid-to-long term:** no change expected {4.5.3.5}
Madden-Julian Oscillation	MJO	sub-seasonal	Arctic warming; North America/Europe - {10.3.3.4; AVI.9.2}	tropical cyclones &. monsoons; deep tropics; southeast Asia; SESA/SACZ - {8.3.2.9; 12.4.4; Atlas.5.3.4; Atlas.5.5.2 AVI.9.2}	Positive trend in variance {8.3.2.9} ***Medium confidence***	moderate skill but advances in recent decades {10.3.3.4} ***High confidence***	n/a	n/a	increases in global warming conditions {8.4.2.9}

[END TABLE TS.12 HERE]

Over the historical period, there is *no robust evidence* that anthropogenic forcing has affected the principal modes of interannual climate variability and associated regional teleconnections beyond the range of internal variability, with the exception of the SAM (see below). Further assessment since the AR5 confirms that climate and Earth system models are able to reproduce most aspects of the spatial structure and variance of the interannual modes of variability, which are intrinsic to the atmosphere (North Atlantic Oscillation -NAO, NAM) and coupled to the ocean (ENSO and Indian Ocean Basin and Dipole modes), although some underlying processes are still misrepresented. Biases exist in the details in spatial structure, magnitudes, and seasonality in CMIP6 despite slight improvement. In the Tropical Atlantic basin, major errors in mean state and variability remain. For all of these modes, internal variability overwhelms the influence of anthropogenic forcing in the simulation of their changes over the historical era (*high confidence*). {Table TS.12, 3.7.1, 3.7.2, 3.7.3, 3.7.4, 3.7.5}

ENSO

Instrumental record, paleo proxy evidence through the Holocene and coupled models all suggest that the ENSO phenomenon can display considerable modulations in amplitude, pattern and period. Paleo-proxy evidence indicates that ENSO activity in the 20th century and early 21st century was greater than any time between 1400 and 1850 (*medium confidence*). Over the historical period, ENSO has exhibited fluctuations in mean state, frequency and amplitude at interdecadal timescales, without exhibiting sustained trends since the late 19th century. Coupled models display large changes of ENSO behaviour in the absence of external forcing changes and little-to-no variance sensitivity to anthropogenic forcing. Therefore, there is *no robust evidence* that human perturbation has had an impact on ENSO activity and ENSO spatio-temporal properties. {Figure TS.34a, 2.4, 3.7.3}

It is *virtually certain* that ENSO will remain the dominant mode of interannual variability in a warmer world (*high confidence*). There is no consensus from models for a systematic change in amplitude of ENSO-related SST variability over the 21st century in any of the SSP scenarios assessed (*medium confidence*). However, it is *very likely* that ENSO-induced rainfall variability over the central eastern Pacific, which is used for defining extreme El Niño and La Niña events and which corresponds to the source of worldwide teleconnection through diabatic heating release in the atmosphere, will be enhanced significantly regardless of amplitude changes in ENSO SST variability by the latter half of the 21st century in the scenarios SSP2-4.5, SSP3-7.0, and SSP5-8.5 (*high confidence*). {Figure TS.34b, 4.3.3, 4.5.3, 8.4.2}

The degree of agreement between modelled teleconnection patterns and observed ones over the historical period in most of the regions impacted by ENSO in boreal winter is shown. There is *high confidence* that the models simulate both the sign and amplitude of the ENSO-related anomalies over land and there is also *high confidence* that because of overwhelming internal atmospheric variability, the observed modulation of the ENSO teleconnections is not attributable to any external forcing. {Figure TS.34c, 3.7.3}

For the future, because of increased and displaced ENSO-related diabatic heating in the Central-Eastern Pacific in high warming level scenario at mid-to-long term (*high confidence*), changes in strength of the ENSO related teleconnection is expected to occur. Reinforced ENSO influence on land along the western Pacific basin in both precipitation and temperature is expected, as well as diminished influence along the North Pacific North American coast due to both local reduced snow feedback and eastward shift of the Aleutian Low deepening (*high confidence*) and enhanced links with the North Atlantic atmospheric dynamics leading to reinforced teleconnection over the Mediterranean basin (*medium confidence*) {8.4.1}

[START FIGURE TS.34 HERE]

Figure TS.34: **a.** Observed, modelled and projected evolution of annual ENSO SST variability over the Nino 3.4 region from 1880 to 2100. Thick lines stand for multi-model ensemble mean for historical and four SSP runs and shading is the 5-95% range across CMIP6 models for historical simulation (grey), SSP1-2.6 (mid blue) and SSP5-8.5 (pink), respectively. The amplitude of ENSO variability is defined as the standard deviation of the Nino 3.4 SST index over backward 30-year running windows. Values are normalized with respect to the 1995-2014 period. The number of available models is listed in parentheses. The observed change (green line) based on ERSST version 5 is also shown from 1881-2014. **b.** Same as **a.** except for rainfall over the Nino 3.4 region. The green line indicates the rainfall variability change based on 20C ERA reanalysis from 1881-2014. **c.** Observed, simulated and projected ENSO teleconnections for 2m-temperature and precipitation during December--February. Teleconnections are identified by linear regression with the Niño 3.4 SST index based on ERSSTv5 during the period 1958-2014. Maps show observed patterns for temperature from the Berkeley Earth dataset over land and from ERSSTv5 over ocean (top) and for precipitation from GPCC over land and GPCP over ocean (contour, period: 1979-2014). Distributions of regression coefficients for regional means drawn from 261 historical simulations from 30 CMIP6 models in grey and for 113 SSP5-8.5 projections in light pink are provided for a subset of pre-defined AR6 regions in Atlas for temperature (top) and precipitation (bottom). Multi-model multi-member ensemble means are indicated by thick vertical coloured lines (black for historical and red for SSP5-8.5). Green vertical lines stand for observational estimates based on Berkeley Earth and GISTEMP datasets for temperature and from GPCC and GPCP datasets for precipitation.

[END Figure TS.34 HERE]

NAM/NAO

The positive trends for the NAM/NAO winter indices were observed from the 1960s to the early 1990s and then have weakened since the mid-1990s (*high confidence*). The NAO variability in the instrumental record was *very likely* not unusual in the millennial and multi-centennial context *(high confidence*). Models have *medium-to-high* performance in simulating the spatial features and the variance of the NAM/NAO and related teleconnection over the adjacent continents. However, models tend to systematically underestimate the level of multidecadal versus interannual variability of the winter NAM and NAO (*medium confidence* –to be confirmed with Chap3). Despite some models suggest that anthropogenic forcings influence the NAM/NAO and despite biases in simulating the NAM/NAO variance at decadal timescale that appears underestimated, there is *limited evidence* for a significant role for anthropogenic forcings in driving the observed multidecadal variations of the winter NAM/NAO over the entire instrumental period (*medium confidence* - to be confirmed with Chap3). There is however *very high confidence* that the associated teleconnections have contributed to a significant fraction of observed multidecadal variability over the Northern Hemisphere continents and have modulated human-induced changes at regional scale. {Figure TS.35, 2.4.1, 3.7.1}

The future boreal wintertime NAM estimated from Mean Sea Level Pressure is *very likely* to become more positive but with substantial inter-model variability by the end of 21st century under SSP3-7.0 and SSP5-8.5 (*high confidence*) . NAM-induced teleconnections over North East Canada and Northern Europe are expected to decrease in winter in high warming levels scenarios due to the reduced positive feedbacks associated with sea-ice and snow loss (*virtually certain*) in the subarctic basins and over Arctic land, respectively. Despite changes in NAM-related teleconnection for precipitation are marginal over Europe in terms of mean, variance is increased in high warming levels by the end of the 21st century as a common pattern for most of regions {Figure TS.35a, 4.5.1, 8.2.3, 8.4.1, 8.4.2}

[START FIGURE TS.35 HERE]

Figure TS.35: Evolution of observed, simulated and projected NAM and SAM indices and associated teleconnection for boreal winter/austral summer (Dec.-Feb. average). a. Observed, modelled and projected evolution of the NAM index defined as the latitudinal difference of the zonally averaged mean sea level pressure between 35ºN and 65ºN (Jianping and Wang, 2003) from 1958 to 2100, with respect to 1995-2014 used as a reference period. Thick lines stand for multi-model ensemble mean for historical and four SSP runs and shading is the 5-95% range across CMIP6 models for historical simulation (grey), SSP1-2.6 (mid blue) and SSP5-8.5 (pink), respectively. The number of available models/members is listed in parentheses. b. Histogram of the 1958-2014 trends built from all historical members (grey). The black vertical line indicates the multi-model multi-member ensemble mean; green lines stand for observational estimates. [Placeholder: because the effect of O3 recovery is important, flattening trend when computing over 2000-2014 should be shown. A PDF of the 2000-2014 trend will be added in the final version] c. Observed, simulated and projected NAM teleconnections for 2m-temperature and precipitation during December-January-February. Teleconnections are identified by linear regression with the NAM index. Maps show observed patterns for temperature from the Berkeley Earth dataset over land and from ERSSTv5 over ocean (top) and for precipitation from GPCC. Distributions of regression coefficients for regional means drawn over 1995-2014 from 373 historical simulations from [XX] CMIP6 models in grey and for 133 SSP5-8.5 projections over 2081-2100 in light pink are provided for a subset of pre-defined AR6 regions in Atlas for temperature (top) and precipitation (bottom). Multi-model multi-member ensemble means are indicated by thick vertical coloured lines (black for historical and red for SSP5-8.5). Green vertical lines stand for observational estimates based on Berkeley Earth and GISTEMP datasets for temperature and from GPCC and GPCP datasets for precipitation. Efg. Same for SAM based on latitudinal difference of the zonally averaged mean sea level pressure (between 40ºS and 65ºS as defined in Gong and Wang (1999). Only teleconnections for precipitation are assessed over Southern Hemisphere continents for SAM.

[END FIGURE TS.35 HERE]

SAM

The SAM has become systematically more positive since the late 19th century (*high confidence*). Since the AR5, further model evidence supports the assessment that ozone depletion and greenhouse gas increases have contributed to a positive trend of the SAM, particularly during austral summer in the last several decades (Figure TS.35e). There is *medium confidence* that climate models reproduce the spatio-temporal features and trends of the summertime SAM observed during recent decades, with CMIP6 models outperforming CMIP5 models. {2.4, 3.3.3}

In the near term (2021-2040), the SAM trend in austral summer is *likely* to be weaker than observed during the late 20th century under all five SSPs assessed (*high confidence*). This is because of the opposing influence in the near- to mid-term from stratospheric ozone recovery and increases in other greenhouse gases on the Southern Hemisphere summertime mid-latitude circulation (*high confidence*). Natural internal variability will therefore *likely* obscure forced trends in the SAM in the near term. {4.3.3, 4.4.3}

In the long term (2081-2100), it is *likely* that the SAM will increase associated with a poleward shift and strengthening of the Southern Hemisphere mid-latitude jet under SSP5-8.5 and SSP3-370 relative to the recent past (1995-2014) (*medium confidence*). {4.5.1, 4.5.3}

Decadal modes

Modes of decadal and multidecadal variability over the Pacific and Atlantic Ocean, including PDV and AMV, exhibit no significant trends over the period of direct observational records (*high confidence*). {2.4}

There is new evidence that anthropogenic aerosol changes have contributed to the observed phasing of the AMV, but there is *low confidence* in the magnitude of this influence. Large uncertainties remain in the identification of the human influence on AMV and PDV due to the brevity of the observational records, difficulty in separating externally and internally driven decadal phenomena in observations, inconsistencies among proxy reconstructions, moderate model performance in reproducing these modes, and limited process understanding. In addition to the models' moderate skills in reproducing the decadal-to-multidecadal modes of variability and underlying mechanisms, there is *medium evidence* for an underestimation of the magnitude of PDV and for a crude representation of the intrinsic tropical-extratropical relationships associated with both PDV and AMV. {3.7.6, 3.7.7}

Based on paleoclimate reconstructions and model simulations, AMV is *unlikely* to change its behaviour in the future. However, AMV fluctuations over the coming decades are *likely* to influence regional climates, enhancing or offsetting some of the regional effects of global warming. Over the Pacific, there is *low confidence* on how PDV would evolve in the future in response to global warming. {4.5.3}

TS.4.2.3 Interplay between drivers of climate variability at regional scales

Some feedbacks in the climate system originate at, or have impacts at, regional rather than global scales. They potentially interact with all drivers of climate variability and their relative importance with respect to the magnitude of anthropogenic signals and the natural internal variability is essential for reliability and utility of model projections that can vary very much at the regional level. This section explores these important considerations.

TS.4.2.3.1 Regional feedbacks

Feedback mechanisms including land-atmosphere feedbacks strongly modulate regional- and local-scale changes in temperature extremes (*high confidence*). This effect is particularly notable in the mid-latitude regions where drying of soil moisture amplifies high temperatures. The soil moisture-temperature feedback was shown to be relevant for past and present-day heatwaves based on observations and model simulations. {11.1.6, 11.3.1}

Feedbacks related to individual or combined effects of natural dust (mineral, sea-salt) remain largely uncertain in terms of sign and magnitude at both local and regional scale. The surface direct radiative effect of dust is *likely* negative over land and ocean, especially when the assumed solar absorption by dust is large. Surface temperature and precipitation adjust to the direct radiative effect over the extent of the perturbed circulation in complicated ways, and their sign and magnitude depend sensitively upon the assumed dust absorptive properties. {10.1.4}

Polar amplification, which is mostly explained by feedbacks related to snow and sea ice, is better simulated in the most recent models compared to AR5 for paleoclimates with better consistence with paleoclimate observations of past warm climate. For future climate, there is *high confidence* that the rate of Arctic surface warming will continue to exceed the global average over the 21st century. There is also *high confidence* that

Antarctic amplification will emerge as the Southern Ocean surface warms on centennial timescales but there is *low confidence* as to whether Antarctic amplification will emerge this century. {7.2.2, 7.4.4}

TS.4.2.3.2 Relative importance of the drivers and implication in terms of uncertainties

For temperature in future climate, based on regional-scale detection and attribution studies over the historical period and climate projections including those from multi-model large ensembles, temperature change due to anthropogenic forcing will be the dominant factor to future multi-decadal temperature trends in most land regions of the world under the high-end (SSP5-8.5 and RCP8.5) GHG emission scenarios (*high confidence*). {10.4.2}

The anthropogenic aerosol forcing decreases in most scenarios, contributing to increasing global-mean surface air temperature (*medium confidence*) and global-mean land precipitation *(low confidence)*. In general, however, the quantification of all SLCF effects on regional climate remain of *low confidence*. Although cloud feedbacks are the dominant source of uncertainty in 21st century's transient global warming under emission scenarios with continued CO_2 emissions, uncertainty is dominated by aerosol ERF in scenarios reaching net zero CO_2 emissions. {4.3.1, 4.4.1, 4.4.4, 6.3.4, 7.5.7, 10.4.2}

For precipitation, it is *very likely* that internal variability will still significantly influence future multi-decadal precipitation trends in many land regions (except Antarctica) until at least the mid-21st century (TS.4.1.1) and beyond for some regions, such as the South-east South American region (Figure TS.36) showing all the involved drivers for precipitation changes (Figure TS.36).

In the near term, projected changes in precipitation are uncertain mainly because of natural internal variability and uncertainty in natural and anthropogenic aerosol forcing (*medium confidence*) and no discernible differences are projected between different SSPs (*high confidence*). In the long term, the contrast between late 21st century increases in Indian monsoon rainfall and actual declining rainfall in the observational record can be explained using multiple lines of evidence. The observational record and future projections are not contradictory since the trends are attributed to different mechanisms, namely aerosols and greenhouse gases, respectively. {4.3.1, 4.4.1, 4.4.4, 10.4.2, 10.6.3}

For a given emissions scenario, variable model response and internal variability contribute to a substantial range in projections of water cycle changes, especially on regional scales (*high confidence*). Internal climate variability strongly affects near-term water cycle responses for all emission scenarios, and mid-term water cycle changes in high-mitigation scenarios, especially for those related to regional summer monsoons and winter mid-latitude storm tracks (*medium confidence*). In many land regions, uncertainties in projected water cycle changes remain large even at the decadal timescale due to limitations in both observations and models and the high variability of atmospheric circulation (*high confidence*). Improvements in the quantification and understanding of observed water cycle changes are needed to identify the most reliable models and help distinguish forced responses from internal variability. {Figure TS.36, 8.5.1, 8.5.2}

[START FIGURE TS.36 HERE]

Figure TS.36: a. Identification of the climate drivers and their influences on climate phenomena contributed through teleconnection to Southeastern South America summer (Dec.-Feb.) precipitation trends observed over 1950-2014. Drivers include modes of variability such as AMV, ENSO, PDV and SAM [placeholder: as well as external forcing (GHGs and ozone depletion) – currently not shown and to be added schematically]. Observed anomalous SST patterns of the oceanic modes are shown (red-blue colour bar in °C) as well as mean sea level pressure anomalies for SAM (brown contour every 0.5 hPa) as displayed in Technical Annex VI. Observed precipitation linear trend from GPCC is shown on continents (green-brown colour bar in mm/month/decade) and the SESA AR6 WG I reference region is outlined with the thick black contour. Climate phenomena leading to local impact on SESA (moisture convergence, changes in ascending motion and storm-track location) are schematically presented and include the Hadley Cell, the Southern Hemisphere polar vortex as well as the forced Rossby waves related to large-scale SST anomalies. b. Timeseries of decadal precipitation anomalies for DJF SESA simulated from 7 large ensembles of historical + RCP8.5 simulations over 1950-2100. Shading corresponds to the 5th-95th range of climate outcomes given from each large ensemble for precipitation (in mm/month) and thick coloured lines stand for their respective ensemble mean. The thick timeseries in white corresponds to the multi-model multi-member ensemble mean with model contribution being weighted according to their ensemble size. GPCC observation is shown in light black line with squares over 1950-2014 and the 1995-2014 baseline period has been retained for calculation of anomalies in all datasets. c. Fractional contribution of individual sources of uncertainties (internal in orange, model in blue and scenario in green) to total uncertainty for SESA DJF precipitation following Hawkins and Sutton (2009). All computations are done with respect to 1995-2014 taken as the reference period and the scenario uncertainty is estimated from CMIP5 using the same set of models as for the large ensembles that have run different RCP scenarios following Lehner et al. (2020). Near-term and long-term temporal windows defined in AR6 are highlighted in b. and c.

[END FIGURE TS.36 HERE]

TS.4.2.4 Summary

Changes in effective radiative forcing due to variations in solar radiation and volcanic activity have been small in comparison to the anthropogenic drivers and were not unusual in a multi-millennial context *(high confidence)*. Climate responses to natural forcing are therefore difficult to detect and to extract at regional scale and they often occur though dynamical interactions with modes of variability. {2.2, 3.3, 3.7, 5.1, 5.2, 7.3, 10.1, AVI.6.1, AV.6.3, Figure 5.1, Figure 5.2, Figure 5.4}

Anthropogenic forcing including GHG, aerosols, other SLCFs and land use that are all responsible for radiative perturbations and are all involved in various climate feedbacks have affected observed regional climate changes *(high confidence)* and will continue to do so in the future (*high confidence*) with various degrees of influence depending on lead-times, warming levels and the nature of the forcing (e.g., well mixed gases versus aerosols). Anthropogenic forcing has been a major driver of temperature change since 1950 in many sub-continental regions of the world (*high confidence*) and will continue to drive regional temperature increased under all SSPs (*virtually certain*). In response to the combination of GHG and aerosol forcings, global climate model simulations show qualitatively similar continental-scale patterns of temperature change. Anthropogenic forcing has contributed to multi-decadal precipitation changes in several regions (*medium confidence*). However, internal variability largely controlled by the excitation of the modes will still significantly influence future multi-decadal precipitation trends in many land regions until at least the mid-21st century. Consequently, in the near term, no discernible differences in precipitation changes are projected between different SSPs (*high confidence*).

Over the historical period, strong internal variability associated with all the modes of variability limits any attribution of the observed changes to external forcing except for SAM *(high confidence)*. It is *likely* that the SAM has become systematically more positive since the late 19th century in summertime (*high confidence*) and that the late 20th century trend is attributable to the combined effect of ozone depletion and GHG increase (*high confidence*). In the near term, there is *high confidence* that ozone recovery and GHG influence will cancel each other thus stopping the past decade observed positive trend of SAM whatever the scenarios, which is expected to restart in high warming levels in late 21st century (*medium confidence*).

Positive trends for the NAM in winter were observed over 1960 to the early 1990s and then have weakened since the 1990s (*high confidence*) which does not support a significant role for anthropogenic forcings in driving the observed multidecadal variations of the NAM/NAO over the instrumental period. There is, however, *high confidence* that the associated teleconnections have contributed to a significant fraction of observed multidecadal variability over the Northern Hemisphere continents and have modulated the human-induced changes at regional scale. The future boreal wintertime NAM is very *likely* to become more positive but with substantial inter-model variability by the end of 21st century (*high confidence)*.

There is *no robust evidence* that anthropogenic influence has had an impact on ENSO activity and ENSO spatio-temporal properties. However, it is *very likely* that ENSO-related rainfall variability in the tropics will increase significantly regardless of amplitude changes in ENSO-related SST variability in the latter half of the 21st century in the scenarios SSP2-4.5, SSP3-7.0, and SSP5-8.5 (*high confidence*) leading to changes in strength and location of regional teleconnection.

In spite of uncertainties, regional climate has been, is being, and will continue to be affected by ERF. Depending on warming levels, regions which have a larger signal of change relative to the background variations will potentially face greater risks than other regions as they will see unusual or unprecedented climates more quickly.

To increase confidence in the interpretation of both observed changes and projections for the future at regional timescales, it is essential to account for the interplay of multiple drivers, including the feedbacks, which can amplify or limit the direct influence of external forcing, and the modes of variability, which determine the full range of climate outcome being superimposed and/or interacting with the anthropogenic forced response. Narratives including such complexity are valuable in the generation of regional climate information.

[START BOX TS.6 HERE]

Box TS.6: Monsoons

The global monsoon is the primary emergent response of the coupled climate system to the annual cycle of solar insolation, manifesting in transitions between seasonal regimes of atmospheric circulation and the redistribution of moist static energy, favouring the dominance of summer precipitation in much of the tropics. The global monsoon domain and its precipitation can be controlled on climate time scales by global mean temperature, inter-hemispheric temperature contrasts and internal decadal or multi-decadal modes of climate variability. Embedded within the global monsoon is a series of regional monsoons (see the global and regional domains in Box TS.2: Figure 1, South and Southeast Asia, East Asia, Australia and the Maritime Continent, West Africa, South Africa, North America and South America) which are themselves controlled by these large-scale drivers as well as being modulated by more local factors such as regional patterns of land-use/land-cover or aerosol emissions. Large populations in the monsoon regions heavily depend on freshwater supply from monsoon rainfall for agriculture, water resources, industry, transportation and other socio-economic activities. This Box integrates assessments of changes in the global and regional monsoons in the past, present, and future. {2.3.1, 3.3.3, 4.4.1, 8.3.2]}

Global monsoon

In the instrumental records, global summer monsoon precipitation intensity (measured by summer precipitation averaged over the monsoon domain) decreased from the 1950s to 1980s, followed by an increase (*medium confidence*), mainly due to Northern Hemisphere land contributions. It is *likely* that the decreasing precipitation trend in the Northern Hemisphere monsoon regions is partly attributable to anthropogenic aerosols from the mid-to-late 20th century (*medium confidence*) [Box TS.2: Figure 1]. Natural multi-decadal variability such as Atlantic Multidecadal Variability and Pacific Decadal Variability has *likely* contributed to the recent increase of global monsoon precipitation (*medium confidence*). {2.3.1, 3.3.2, 3.3.3}

In response to future greenhouse-gas-induced warming, it is *very likely* that global land monsoon precipitation will increase, particularly in the Northern Hemisphere, although Northern Hemisphere monsoon circulation will weaken (*high confidence*). In the long-term, monsoon rainfall change will feature a robust north-south asymmetry characterised by a greater increase in the Northern Hemisphere than in the Southern Hemisphere and an east-west asymmetry characterised by enhanced Asian-African monsoons and a weakened North American monsoon (*high confidence*). In the near-term and mid-term, changes in global monsoon precipitation and circulation may be disguised by natural internal variability such as Atlantic Multidecadal Variability and Pacific Decadal Variability (*medium confidence*). {4.4.1, 4.5.1, 8.4.1}

Regional monsoons

The 20th century water cycle response to global warming has been partly offset over some regions due to increasing anthropogenic aerosol loadings in the atmosphere *(high confidence*). It is *very likely* that Northern Hemispheric anthropogenic aerosols have caused a weakening of the regional monsoon circulations in South Asia, East Asia and West Africa during the second half of the 20th century, thereby offsetting a strengthening monsoon precipitation in response to GHG-induced warming. Areas in South America and Australia have experienced a detectable influence of anthropogenic aerosols on precipitation patterns. Remote effects far from emission regions have resulted from large-scale circulation responses to spatially heterogeneous changes in surface temperatures (*high confidence*). There is *medium confidence* that the recent partial recovery and enhanced intensity of monsoon precipitation over West Africa is related to the growing influence of anthropogenic greenhouse gases with an additional contribution from the transition from a dimming to a brightening overall radiative effect of anthropogenic aerosols, emitted largely from North America and Europe. {8.3.1, 8.3.2, Box 8.1}

Projections of regional monsoons indicate contrasting (region-dependent) and uncertain changes in total precipitation, but an overall extension of the length of the wet season. For the North American monsoon, projections indicate a decrease in precipitation, whereas increased monsoon rainfall is projected over South and Southeast Asia, East Asia and West Africa (*medium confidence*). For the South American monsoon, the CMIP6 projections do not indicate a clear increase in precipitation during the 21st century. There is *medium confidence* that a delayed wet season in the Sahel is driven by intensifying Sahara heat low, but only *low confidence* in the projected changes in the wet season onset and cessation in many other tropical regions. {8.2.1, 8.4.2}

The contrast between long-term future increases in South Asian monsoon rainfall and declining rainfall in the observational record can be explained using multiple lines of evidence. The observational record and future projections are not contradictory since the trends are attributed to different mechanisms (aerosols and greenhouse gases, respectively). The long-term future changes are generally consistent across global (including at high resolution) and regional climate models and supported by theoretical arguments. While there are subtle differences found in paleoclimate analogues of the future climate (i.e., like the mid-Holocene), different physical mechanisms at play suggest that paleoclimate evidence does not reduce confidence in the future projections. {10.6.3}

It is *likely* that, since 1950, the frequency and/or the intensity of heavy rainfall has increased in most of the monsoon regions including Asia, north west Australia, southeast South America, north South America (*high confidence*) and west and South Africa (*medium confidence*). In the future, the frequency of precipitation extremes and annual maximum five-day precipitation (Rx5day) will increase over many monsoon regions, particularly East Asia, central India, and West Africa if global warming continues (*high confidence*). {11.4, 11.9, Atlas}

Limitations to the assessment

Large natural variability of monsoon precipitation across different timescales poses an inherent challenge for robust quantification of future changes in precipitation at regional and smaller spatial scales. Additionally, climate model simulations exhibit large biases and uncertainties in representing the observed characteristics of monsoon precipitation. The representation of monsoon warm rain processes organized tropical convection, heavy orographic rainfall and cloud-aerosol interactions in state-of-the-art climate models remains a major research gap. {4.5.1, 8.3.2, 10.3.3}

Nonlinear abrupt response of hydrological systems to climate change is a source of uncertainty for future projections of monsoon rainfall. There is *medium evidence* of abrupt change in monsoon system in some high emissions projections, but there is no overall consistency regarding the magnitude, speed, and timing of such changes. There is *low confidence* that abrupt changes in rainfall and aridification will occur by 2100, although the possibility of abrupt events cannot be ruled out. Paleoclimate evidence suggests that a collapse of the Atlantic Meridional Overturning Circulation (AMOC) can cause abrupt and large-magnitude shifts in the water cycle (*high confidence*), including weakening of the African and Asian monsoons and strengthening of Southern Hemisphere monsoons. An AMOC collapse by 2100 is *unlikely*, but the consequence of such an occurrence is *very likely* to generate abrupt regional changes in the water cycle and monsoon system. {8.6.1}

Summary

It is *very likely* that global monsoon precipitation increases with lengthening of the wet season in response to anthropogenic global warming yet accompanied with substantial regional contrast (*high confidence*). There is *high confidence* that precipitation will increase in South Asia and East Asia but decrease in North America and equatorial South America during local summer. There is *medium confidence* that precipitation will increase (decrease) in West Africa in the Eastern Sahel (Western Sahel) and will increase in the Australian and Maritime Continent monsoons during local summer. {2.3.1, 3.3.2, 3.3.3, 4.4.1, 4.5.1, 8.2.1, 8.3.1, 8.3.2, 8.4.1, 8.6.1, 10.3.3, 10.6.3, 11.4, 11.9, Atlas, Box 8.1}

[START BOX TS.6, FIGURE 1 HERE]

Box TS.6, Figure 1: (a) **Global monsoon domain and regional land monsoon domains**: Global monsoon domain (contour) is defined by the local summer-minus-winter precipitation rate exceeds 2 mm day^{-1}, and the local summer precipitation exceeds 55% of the annual total. The regional monsoon domains are defined based on published literature and also accounting for the fact that the climatological summer monsoon rainy season varies across the individual monsoon regions *viz.,* South and Southeast Asia *(**SAsiaM**, Jun-Jul-Aug-Sep)*, East Asia *(**EAsiaM**, Jun-Jul-Aug)*, West Africa *(**WAfriM**, Jun-Jul-Aug-Sep),* North America *(**NAmerM**, Jul-Aug-Sep)*, South America *(**SAmerM**, Dec-Jan-Feb)*, Australia and Maritime Continent Monsoon *(**AusMCM**, Dec-Jan-Feb)*. Also shown are regions in equatorial South America *(**EqSAmer**)* and South Africa *(**SAfri**)*, which receive seasonal rainfall although the qualification of monsoon is subject to discussion. (b) Regional mean monsoon precipitation based on seven CMIP6 models from all anthropogenic radiative forcings (ALL) GHG only radiative forcings (GHG) aerosol only radiative forcings (AER) and natural only experiment. Mean value of observation is from CRU and GPCP data. Precipitation averaged over global monsoon area (GMA) is also shown. (c) Percentage change in projected seasonal mean precipitation over regional monsoon and global monsoon domain in the near-term (2021-2040), mid-term (2041-2060), and long-term (2081-2100) under SSP 2-4.5 based on seven CMIP6 models.

[END BOX TS.6, FIGURE 1 HERE]

[END BOX TS.6 HERE]

TS.4.3 Regional climate change and its implications for climate extremes and climatic impact drivers

The regional signature of global climate change has significant variations as demonstrated in Figure TS.37. These result from the complex interplay of global and regional drivers and modes of variability as discussed in TS.4.2 which also result in similar variations in the many climate statistics and indices of relevance to human and natural systems. These changes are explored region by region (following the WGII continental scale regions augmented by polar regions and ocean) and for selected typological domains in the latter section of TS.4.3. These are preceded by a section on construction of regional climate change information and generic changes in climatic impact drivers. The final section provides a summary of the regional findings including summary tables of observed, attributed and projected changes in climatic impact drivers across the WGI reference regions and where the assessment of these changes can be found in the chapters.

[START FIGURE TS.37 HERE]

Figure TS.37: Demonstrating the spatial variation in annual mean observed and projected climate change for different future time periods, warming levels and emissions scenarios.
Top map: Consensus on the observed temperature trends from the three observational datasets (CRU TS, BERKELEY and EWEMBI). Hatching indicates regions where no or only one dataset provides a significant trend. Linear trends are calculated for the common 1980–2014 period and expressed in °C per decade (temperature) with respect to the climatological mean over this period.
Middle four maps: Global temperature changes projected for mid-century (left-hand column) under RCP4.5 (top) and RCP8.5 (bottom) compared to, in the right column, a global mean warming level of 2°C (top) and at the end of the century under RCP8.5 emissions (bottom) from an ensemble of nine CMIP5 GCMs. Note that the future period warmings are calculated against a baseline period of 1986–2005 whereas the global mean warming level is defined with respect to a 'pre-industrial' baseline of

1861–1890. Thus, the other three RCP-based maps would show greater warmings with respect to this earlier baseline.
Bottom six maps: Future projected changes of annual mean precipitation in the CMIP5 (left-hand column) and CMIP6 (right-hand column) ensembles. Projected changes are calculated as the climatology differences for near-term (2021-2040), medium-term (2041-20160| and long-term (2081-2100) periods for the emissions scenario RCP8.5 (SSP5-8.5 for CMIP6) with respect to the historical period (1986-2005); values are expressed relative differences (%). Hatching indicates lack of model agreement (less than 80% of agreement) and the black lines mark out the WGI reference regions defined in Box TS.5, Figure 2. Similar analysis for other indices and scenarios (including warming levels) are available at the Interactive Atlas (http://ipcc-atlas.ifca.es).

[END FIGURE TS.37 HERE]

TS.4.3.1 Construction of regional climate change information

Attribution techniques are now offering clearer insights into the links between human influence on the climate system and climate and weather events. Attribution methods are applied across all three working groups in the AR6 and are fundamental to determining how climate change has contributed to observed changes, such as a long-term trend or an extreme event. If anthropogenic forcing is found to be a major driver of such an observed change, then it can be used to illustrate a narrative of the near future. Attribution methods are also applied to quantify the influence from a range of drivers on observed impacts or changes and can include the results of adaptation or mitigation actions. {1.4.4, Cross-Chapter Box 1.4}

Since the AR5, the increased availability of coordinated ensemble regional climate model projections and improvements in the level of sophistication and resolution of global climate models have enabled the investigation of past and future evolution of a range of sector-relevant climatic impact drivers in many regions of the world. {12.1, 12.2}

To increase confidence in future projections of regional climate, there is *high confidence* that multiple sources of observations and tailored diagnostics are needed. Limited observational records in data-sparse regions cause difficulties that pose limits to the assessment of regional climate change. At the regional scale, multi-model mean and ensemble spread are not sufficient to characterise low-probability high-impact changes or situations where different models simulate substantially different or even opposite changes (*high confidence*). Storyline approaches are a complementary instrument to aid the representation of climate projection uncertainties. Grand ensembles of many realisations of internal variability are required to separate internal variability from forced changes (*high confidence*). Overall, there is *high confidence* that increasing model resolution, downscaling and adding relevant model components can increase the fitness for some aspects of regional projections when these are accompanied by a process-understanding analysis. {10.3.3}

The subset of CMIP6 results project more pronounced warming in many regions than CMIP5, with these differences clearest in high latitude regions. There is a broadscale consistency in the patterns of mean temperature and precipitation change in the CMIP5 and CMIP6 ensembles models over all regions.

TS.4.3.2 Generic changes in climatic impact drivers

Climate change induces a spatially heterogeneous pattern of changes in the magnitude, occurrence frequency, duration, spatial extent and intensity of extremes and climatic impact drivers which have a wide range of consequences (*high confidence*). In many cases, understanding these consequences requires different, tailored indices to characterise weather or climate conditions affecting the system or sector involved. These indices can be based on thresholds that vary by specific region, system and sector. {12.3}

There is *high confidence* that several climatic impact drivers have either increased or decreased in almost all regions of the world in recent decades and are expected to continue increasing or decreasing over the 21st century regardless of the climate scenario. {12.4, 12.5}

Changes in surface temperature exceeding levels of interannual variability have emerged in virtually all regions, with tropical regions exhibiting the most clearly distinguishable anthropogenic warming signals (*high confidence*). It is *very likely* that most land areas have warmed by at least 0.1°C per decade over the past 50-100 years with many areas warming faster in recent decades. The latter include most areas of Central and South America, West Antarctica and Western Europe (0.2-0.3°C per decade), the Arabian Peninsula, Central Asia and Eastern Europe (0.3-0.5°C per decade) and Arctic land regions warming up to 1°C per decade (or more in a few areas).

Both the rate of long-term change and the amplitude of interannual variability differ between regions and across climate variables, and from global to regional to local scales, so influencing when a signal of long-term change emerges. The tropical regions have experienced less warming than most other regions, but have smaller interannual variations, meaning the signal of change is more apparent than in regions with larger warming but larger interannual variations. Regional changes in climate states that are amplified or opposite in sign compared to the long-term trend are expected to occur on decadal timescales, especially in regions with large interannual climate variability. {1.4.2, 1.4.3, FAQ1.2}

Anthropogenic forcing has been a major driver of temperature change since 1950 in many sub-continental regions of the world (*high confidence*). Consistent with this annual mean warming has been an increase in hot extremes which have shown to be *virtually certain* attributed to anthropogenic climate change in regions such as Europe where a range of extreme event attribution methods have been applied (*high confidence*). {10.4.2}

Warming trends observed in recent decades are projected to continue over the 21st century (*high confidence*) and over most land regions at a rate higher than the global average. Under an RCP8.5 high emissions future it is *likely* that most land areas will experience a further warming of at least 4°C and in some areas significantly more; West, Central and Northern Asia and the Arabian Peninsula (8-10°C) and the Arctic up to 12°C. Climatic impact drivers associated with hot temperatures become more adverse everywhere, although the amount of change differs between regions (see Figure TS.38). {12.5.1}

[START FIGURE TS.38 HERE]

Figure TS.38: Projected change in the mean number of days per year with maximum temperature exceeding 35°C and 40°C. The map shows the median change in the number of days for 35°C between the mid-century (2041-2060) and historical (1995-2014) periods for the CMIP6 ensemble and Scenario SSP5-8.5. The ensemble includes 10 CMIP6 models. Stippling indicates areas where more than 2/3 of models agree on the sign of change. Plots in the “satellite boxes” show the median (dots) and the 5-95% range of model ensemble values across each model ensemble and for each time period (historical [modern], mid-century [mid] and end of century [long]) for the regional mean of the index over land areas for the AR6 regions (defined in Chapter 1 and grouped here by continent). Two exceedance thresholds are considered: 35°C (light colours) and 40°C (dark colours). Both extreme scenarios are shown for CMIP6 only (red; SSP1-2.6 [circled dots] and SSP5-8.5 [open dots]) while for CMIP5 only one scenario is shown (blue; RCP8.5). Available CORDEX results are also shown for RCP8.5 (green) [*Placeholder: here only for Europe and Africa, will be extended*]; [*Placeholder: no bias adjustment is applied here, but it will be used in the FGD*]. {Figure 12.4}

[END FIGURE TS.38 HERE]

Over most land areas no significant trends in annual mean precipitation have been observed. Regions where significant positive trends have been observed include most of North Asia and parts of Central and Southeast Asia (*medium or high confidence*). Significant negative trends have been observed in the Horn of Africa and south-west Australia (*high confidence*) and southern Africa with the latter attributed to anthropogenic warming of the Indian Ocean. Increases in precipitation intensity have been observed in the Sahel and over Southeast Asia (*medium confidence*). Precipitation-related indicators show increases in hazard in some regions but decreases in others, broadly following the geographical distribution of change in precipitation. {12.4, 12.5}

Anthropogenic forcing has contributed to multi-decadal precipitation changes in several regions (*medium* *confidence*). Large observational uncertainty and internal variability as well as model errors lead to *low confidence* with regard to a well-constrained quantification (best estimate and confidence interval) of the total anthropogenic contribution to precipitation changes as well as the relative contributions of greenhouse gases, including ozone, and different aerosol species.. It is thus *very likely* that internal variability will still significantly influence future multi-decadal precipitation trends in many land regions (except Antarctica, Section 9.4.2) until at least the mid-21st century. {10.4.2}

There is *high confidence* that in response to global warming the precipitation climatology will change in most regions, either through changes in mean values or the characteristics of rainy seasons or daily precipitation statistics. Regions where mean rainfall is *likely* to increase include East and North Asia, southeast and southern South America, northern Europe and North America and the polar regions. Regions were mean rainfall is *likely* to decrease include Indonesia, northern Arabian Peninsula, Central America, southwest South America, and southern Europe. Changes in monsoons are *likely* to result in increased precipitation in northern China, increases during the summer monsoon but decreases during the winter monsoon in South Asia (*medium to high confidence*). There is also *high confidence* that precipitation intensity and extremes will increase in many areas, also in regions with reductions in mean precipitation.

The 20th century water cycle response to global warming has been partly offset over some regions due to increasing anthropogenic aerosol loadings in the atmosphere (*high confidence*). It is *very likely* that Northern Hemispheric anthropogenic aerosols have caused a weakening of the regional monsoon circulations in South Asia, East Asia and West Africa during the second half of the 20th century, thereby offsetting a strengthening monsoon precipitation in response to GHG-induced warming. Areas in South America and Australia have experienced a detectable influence of anthropogenic aerosols on precipitation patterns. {8.3.1, 8.3.2.4, Box 8.1}

It is *very likely* that shifts in the average regional and seasonal characteristics of the water cycle will occur by 2100, with the magnitude of change scaling to the emissions scenario. However, the robustness of these changes varies spatially, and in many regions projections are still model-dependent. Among the robust signatures, there is *high confidence* that increased evaporation due to growing atmospheric water demand will dry soils in many water-limited regions. It is *virtually certain* that snow cover and tropical mountain glaciers will diminish with increased emissions. There is *medium to high confidence* in an expansion of arid areas towards the midlatitudes, and in pronounced drying in the Mediterranean, southern Australia, southern North America, Central America and northeastern Brazil. {8.4.1}

Projections of regional monsoons indicate contrasting (region-dependent) and uncertain changes in total precipitation but an overall extension of the length of the wet season. For the North American monsoon, projections indicate a decrease in precipitation, whereas increased monsoon rainfall is projected over South and Southeast Asia, East Asia and West Africa (*medium confidence*). For the South American monsoon, the CMIP6 projections do not indicate a clear increase in precipitation during the 21st century. There is *medium confidence* that a delayed wet season in the Sahel is driven by intensifying Sahara heat low, but only *low confidence* in the projected changes in the wet season onset and cessation in many other tropical regions. {8.2.1, 8.4.2.}

For a given emissions scenario, variable model response and internal variability contribute to a substantial range in projections of water cycle changes, especially on regional scales (*high confidence*). With increased warming, a larger land area will experience statistically significant increase or decrease in precipitation (*medium confidence*). With additional warming, the increase of area fraction with significant precipitation increase will be larger over land than over the ocean, but the increase of area with significant decrease will be larger over the ocean than over land (*medium confidence*). The change in global-mean (land plus ocean) precipitation will be constrained by global energy balance, whereas regional precipitation changes will be dominated by thermodynamic moisture convergence and dynamical processes (*high confidence*). Precipitation will increase in large parts of monsoon region, tropics and high latitudes, but decrease over the Mediterranean and large parts of the subtropics in response to greenhouse-gas-induced warming (*high confidence*). Interannual variability of precipitation over many land regions will be strengthened in a warmer world (*medium confidence*). {4.5.1, 4.6.1, 8.4.1}

Internal climate variability strongly affects near-term water cycle responses for all emission scenarios, and mid-term water cycle changes in high-mitigation scenarios, especially for those related to regional summer monsoons and winter mid-latitude storm tracks (*medium confidence*). In many land regions, uncertainties in projected water cycle changes remain large even at the decadal timescale due to limitations in both observations and models and the high variability of atmospheric circulation (*high confidence*). {8.5.1, 8.5.2}

Model deficiencies and unresolved small-scale processes still preclude a strong model consensus about future water cycle changes whatever the scenario, time horizon or global warming level is. Model response range is particularly strong at the transition between wet and dry regions and seasons, and for soil moisture and freshwater reservoirs that are sensitive to small differences in precipitation or evapotranspiration changes, poor representation of land surface processes or lack of consideration of land use change and irrigation.

There is *high confidence* that sea surface temperature will increase in the ocean, excepting the North Atlantic region. Relative sea level rise is *very likely* to continue along the 21st century, contributing to increased coastal flooding in low-lying coastal areas (*high confidence*) (see Figure TS.39) and coastline recession along most sandy coasts (*high confidence*), while ocean acidification is also expected to increase (*high confidence*).

[START FIGURE TS.39 HERE]

Figure TS.39: Projections of extreme sea level (1:100 yr return period total water level). Central map: change in extreme sea level (ESL) for the year 2100 relative to 1980-2014 from Vousdoukas et al. (2018)'s CMIP5 based dataset. Satellite plots: regional mean ESL values for the modern period (1979/1980 - 2014), mid-term (2050) and long term (2100) for the Vousdoukas et al. (2018) (light blue), and the (Kirezci et al., submitted) (dark blue) CMIP5 based datasets, for the AR6 regions. Data represent RCP8.5, except circled dots which represent RCP4.5. Dots represent the median estimate (regionally averaged), and bars the 5-95th percentiles representing the uncertainty associated with the projections for the AR6 sub-regions (defined in Chapter 1 and grouped here by continent). [*Placeholder: A CMIP6 estimate will also be added, and the central map and RCP4.5 or 2.6 will come from this instead.*] Units m. {Figure 12.7}

[END FIGURE TS.39 HERE]

Future changes in surface ozone and PM concentrations at global and local scales will be predominantly driven by changes in precursor emissions rather than climate (*high confidence*). Future climate change is expected to have a small effect on surface particulate matter (PM) concentrations and more generally on the aerosol global burden **(***medium confidence). *Warmer climate is expected to reduce surface ozone in unpolluted regions (*high confidence*) and to increase surface ozone by a few ppb over polluted regions of North America, Europe and East Asia, with regional discrepancies over South Asia for the monsoon season (*medium confidence*). However, there is *low to medium confidence* in the response of surface ozone and PM to future climate change due the uncertainty in the response of the natural processes (stratosphere-troposphere exchange, natural precursor emissions, including biogenic VOCs, land and marine aerosols, and lightning NO_x) to climate change. There is *low confidence* in the response of air pollution extremes due to climate-driven changes in the meteorological regimes such as atmospheric blockings or extreme events such as heatwaves or heavy precipitation. {6.2.1, 6.4, 6.6}

TS.4.3.3 Summary of regional changes in climatic impact drivers (CIDs)

The sections below provide an assessment of the overall state of knowledge regarding continental and regional-scale changes in Climatic Impact Drivers (CIDs) resulting from changing climate characteristics. These include temperature and precipitation related CIDs as well as wind, cryosphere and oceanic indicators. Assessments are organized first per continent or geographic region, followed by sub-continental regional discussions. Mountains, monsoon areas and urban characteristics are summarized in the section on specific zones.

Changes in key large-scale indicators can be assessed using a combination of *in situ*, paleo, and satellite data, often fused with models e.g. via reanalysis of various types. Each of these observation types has its own advantages and limitations. Both in-situ and in particular paleo data extend farther back in time, but coverage is less complete spatially, resulting in systemic knowledge gaps across multiple indicators for large regions (e.g., Africa and South America concerning *in situ* data over land, and the Southern Hemisphere for paleo data).

In the regional assessment sections below, summary tables are included displaying the assessment of increases and decreases of changes in region-specific CIDs. These assessments are based on multiple lines of evidence, including observed trends, attribution statements and future projections. TS Annex 1 provides references to sections in the AR6 report supporting the CID assessment statements displayed in these summary tables.

In the AR6 report a number of specific case studies are discussed, underlining the use of multiple lines of evidence, constructing regional messages, or attributing changes to specific processes or drivers. Box TS.7: provides a cross-reference to these case studies.

[START BOX TS.7 HERE]

Box TS.7: Box on Case Studies

AR6 includes a variety of case studies that provide details on methods, physical processes, and assessment procedures that are relevant to regional or local contexts. A description of these case studies and their main purposes is summarized in the table below.

[START BOX TS.7, TABLE 1]

Box TS.7, Table 1: Regional Case Studies

#	Name of case study	Geographical domain	Mean purpose	Section in AR6
	Exploring regional climate drivers			
1	Europe aerosol	Central & South Europe	Communicating regional climate change in a case of inconsistency between various lines of evidence	Atlas.6.3.1
2	East Asia	East Asia, including east China, Japan and Korea	To provide a concrete, detailed assessment for a consequential climate hazard using the example of the 2013 East Asia Heat extreme. Severe Heat extremes with multiple impacts are not only hazards for the distant future, they are occurring today	CH12 Cross-Chapter Box 12.1
3	Influence of the Arctic on mid-latitude climate	Arctic	Assessing the influence of the Arctic on mid-latitude climate	Cross-Chapter Box 10.1
4	Climate Change over the Hindu Kush Himalaya	Hindu Kush Himalaya	Assessing climate change, including extreme precipitation events over the Hindu Kush Himalaya region, including observational uncertainty, model performance and process understanding (Elevation-dependent warming),	Cross-Chapter Box 10.3 Atlas 5.10.1
5	Urban climate	Urban (various cities across the world)	Assessing various aspects of urban climate including observational issues, observed climate in cities, future climate projections and urban parameterization schemes in climate models	Box 10.2
6	Marine heatwaves	All basins	Under further global warming, MHWs are *very likely* to increase in frequency, duration, spatial extent and intensity in all ocean basins, but with	Cross-Chapter Box 9.1

			distinct spatial magnitudes	
7	Greenland ice sheet dynamics	Greenland	Describe paleo-analogues for rapid GrIS response	Box 9.2
8	West- and East Antarctica ice sheet dynamics	Antarctica	Describe paleo-analogues for rapid WAIS and EAIS response	Box 9.2
9	Global-scale concurrent climate anomalies at the example of the 2015/2016 Super El Niño and the 2018 boreal spring/summer extremes	Global (2015/2016 Super El Niño; 2018 Northern Hemisphere summer heatwaves)	Interplay between natural variability and human-induced climate change in leading to concurrent extremes across large fractions of the globe	Box 11.3
10	Glaciers in the Arctic	Arctic and Greenland	This section then describes examples of generating climate change assessments relevant to these typological domains	Atlas.5.10.2
11	Snow on sea ice in Arctic	Arctic and Greenland	This section then describes examples of generating climate change assessments relevant to these typological domains	Atlas.5.10.3
Regional attribution studies				
12	The Sahel and the West African monsoon drought and	West Africa	Interplay between anthropogenic change and internal variability: attribution of the Sahel and the West African monsoon decline (1955-1984) and recovery (1985-2014)	CH.10.4.1.2.1
13	The East Asia summer monsoon weakening and recovery	East Asia	Interplay between anthropogenic change and internal variability: attribution of the East Asia summer monsoon weakening and recovery	CH10.4.1.2.2
14	The southern Australian rainfall decline	Australia	Interplay between anthropogenic change and internal variability: attribution of the southern Australian rainfall decline	CH10.4.1.2.3
15	The south-eastern South America summer wetting	South America	Interplay between anthropogenic change and internal variability: the south-eastern South America summer wetting	CH10.4.1.2.4
16	The central and eastern Eurasian winter cooling	Eurasia	Interplay between anthropogenic change and internal variability: the central and eastern Eurasian winter cooling	CH10.4.1.2.5
17	Western Europe summer warming	Europe	"Interplay between anthropogenic change and internal variability	CH10.4.1.2.6
Constructing a regional climate message				
18	Cape Town Drought	Cape Town	Integrated assessment of the Cape Town drought including observational issues, attribution of anthropogenic and natural drivers, global and regional models simulations of past and future climate change, and regional climate message distilled from multiple lines of evidence.	CH10.6.2
19	Indian summer monsoon	India	Integrated assessment of the Indian summer monsoon including observational issues, attribution of anthropogenic and natural drivers, global and regional models simulations of past and future climate change, and regional climate message distilled from multiple lines of evidence.	CH10.6.3
20	Mediterranean summer warming	Mediterranean	Integrated assessment of the Mediterranean summer warming, including observational issues, attribution of anthropogenic and natural drivers, global and regional models simulations of past and future climate change, and regional climate message distilled from multiple lines of evidence.	CH10.6.4

[END BOX TS.7, TABLE 1]

[END BOX TS.7 HERE]

Figure TS.40 shows an illustrative collection of changes in regional CIDs, discussed in more detail in the regional sections below.

[START FIGURE TS.40 HERE]

Figure TS.40: Projected changes in selected climate impact driver indices for selected regions. (a) coastal recession for sandy coasts by the year 2100 relative to 2010 (meters; negative values indicate recession) from the CMIP5 based data set presented by (Vousdoukas et al., 2020); (b) change of extreme runoff in Asia.; (c) change in 1/100jr river discharge in Europe (from CORDEX); (d) 99th percentile of daily precipitation (mm day^{-1}); (e) 98th percentile of daily maximum wind (m s^{-1}) ; (f) number of days with snow water equivalent (SWE) over 100 mm between (from CORDEX). {Figure 12.8, Figure 12.9, Figure 12.10, Figure 12.11, Figure 12.12, Figure 12.13}

[END FIGURE TS.40 HERE]

TS.4.3.4 Africa

The rate of temperature increase has generally been more rapid in Africa than the global average (*high confidence*). Minimum temperatures have increased more rapidly relative to maximum temperatures over inland southern Africa (*medium confidence*). {Atlas.5.2} Mean temperature over East Africa has shown an increasing trend since 1980, but a decreasing trend in the decades before (*medium confidence*). Mean temperatures over northern Africa and West Africa have increased over the last 50 years (*high confidence*). The distillation of several lines of evidence provides confidence in the Mediterranean warming exceeding Northern Hemisphere mean warming. {Figure TS.33, 10.6.4, Atlas.5.2}

Relative to the 1995-2014 baseline, annual mean temperature over Africa is projected to rise faster than the global average *(very high confidence)* with the increase *likely* to exceed 4°C by the end of the century under the SSP5-8.5 scenario. Under this scenario all parts of Africa will have increased maximum and minimum temperatures with a commensurate increase in the number of warm days in all seasons (*high confidence*) with North Africa, central interior of southern Africa and West Guinea *likely* to warm at a faster rate (*high confidence*). {Atlas.5.2.}

There is a *high confidence* that West Africa experienced the wettest decade (1950s and early 1960s) in the twentieth century (*high confidence*), followed abruptly by the driest years (1970-1989), with a deficit in annual rainfall falling to 60% of the long-term century mean. Wetter conditions prevailed from the mid-to-late 1990's, but with less spatial coherence and temporal persistence, in the Guinean coastal region (*medium confidence*) and in the Sahel (*high confidence*). {8.3.2}

There is *high confidence* that precipitation deficits have increased since the mid-20th century in Southern Africa. There is *medium confidence* that the southern Africa region shows more frequent hydrological droughts. Also the Horn of Africa has experienced significant rainfall decreases during the long rains season March to May (*high confidence*). Drying trends in this region can be attributed to oceanic influences (*high confidence*), both internal variability and human-induced. The drying trends in parts of Africa during each monsoon season is attributable to oceanic influences. In particular, drying over the Sahel is attributed to an increase in the South Atlantic Sea Surface Temperature (SST) and over southern Africa as a response to anthropogenically forced Indian Ocean warming. Drying over East Africa is associated with decadal natural variability in SSTs over the Pacific Ocean. The enhanced rainfall intensity over the Sahel in the last two decades is associated with anthropogenic warming (*medium confidence*). {11.6.2, Atlas.5.2.}

Heatwaves, deadly heat stress and the frequency of exceedance of hot temperature thresholds (e.g. 35°C or 40°C) will drastically increase by the end of the century (*high confidence*) under RCP8.5/SSP5-8.5. {12.4.1}

In regions of high or complex topography, such as the Ethiopian Highlands, downscaled projections indicate *likely* increases in rainfall by the end of the 21st century. However, the Northern Africa and the south-western parts of southern Africa are *likely* to have a reduction in precipitation. Over West Africa, rainfall will *likely* decrease in the Western Sahel subregion (*medium confidence*) and increase in the central Sahel subregion (*low confidence*) and along the Guinea Coast subregion (*medium confidence*). Rainfall amounts over the western part of East Africa is *likely* to reduce but increase in the eastern part of the region (*medium confidence*). Southern Africa is projected to have a reduction in annual mean rainfall, and there is *medium confidence* for an increase in hydrological droughts, but intensity of extreme rainfall is *likely* to increase by 2100 (*medium confidence*). {11.6.5, 12.4.1, Atlas.5.2}

Increasing climatic impact drivers will also include heavy precipitation inducing pluvial flooding (*high confidence*) and fluvial flooding (*low confidence*) in West, central, North and South Eastern Africa and Southern Sahara. {12.4.1}

There is *high confidence* that *for high warming levels by the end of the 21st century* increased evaporation due to growing atmospheric water demand will dry soils in southern Africa. There is *medium to high confidence* in an expansion of arid areas towards the midlatitudes, and in pronounced drying in southern Africa. {8.4.1}

A case study carried out in Cape Town (see Box TS.3) shows that climate messages on drier future conditions are supported by the use of several consistent lines of evidence: the projected change in precipitation by both global and regional climate models of different spatial resolutions, and the observed and projected changes of circulation patterns consistent with drier conditions. However, lack of information still persists about certain physical relationships, such as whether or not a relationship between Cape Town precipitation and large-scale circulation processes also occurs over longer historical periods than only the post-1979 decades, and how compensating changes in greenhouse gases and Antarctic ozone will influence circulation changes over the twenty-first century. {10.6.2}

There is *medium confidence* that a delayed wet season in the Sahel is driven by intensifying Sahara heat low, but only *low confidence* in the projected changes in the wet season onset and cessation in many other tropical regions. {8.2.1, 8.4.2}

There is *medium confidence* of a decrease in mean wind speed in North Africa and in increase in Southern African regions by the end of the century under RCP8.5/SSP5-8.5. {12.4.1}

Sea level rise is *very likely* to continue at a higher than the global average in Africa contributing to increased coastal flooding in low-lying areas (*high confidence*) and coastline recession along most sandy coasts (*high confidence*) (see Figure TS.39). {12.4.1}

Table TS.13 shows a summary of changes in CIDs for Africa, derived from a combination of evidence from observed trends and projected future conditions. TS. Appendix A provides references to the locations in the underlying chapters which support the assessment shown in this table.

[START TABLE TS.13 HERE]

Table TS.13: Summary of confidence in projected directional changes for climatic impact drivers for Africa. The colours represents their aggregate characteristic changes for mid-century RCP8.5 within each AR6 WG I reference region. Dark purple: *high confidence* of increase; light purple: *medium confidence* of increase; white: *low confidence* of increase or decrease; light brown: *medium confidence* of decrease; dark brown: *high confidence* of decrease; grey: CID not broadly relevant. Arrows indicate *medium to high confidence* trends derived from observations and asterisks indicate low, medium and high confidence in attribution of observed changes (which are of the same sign as the projected changes unless stated otherwise).

Climatic Impact Driver	Heat and Cold				Wet and Dry							Wind			Snow and Ice						Coastal and Oceanic					Other			
Africa	Mean temperature	Extreme heat	Cold spell	Frost	Mean precipitation	River flood	Pluvial flood	Landslide	Aridity	Drought	Wildfire	Mean wind speed	Severe wind storm	Sand and dust storm	Snow and land ice	Permafrost	Lake, river and sea ice	Heavy snow and ice storm	Hail	Snow avalanche	Relative sea level	Coastal flood	Coastal erosion	Marine heatwave	Ocean and lake acidity	Air pollution	Atmospheric CO_2	Radiation at surface	*Notes on attribution evidence*
North Africa*	↗	↗ *	↘						↗ *	↗											↗		↗	↗	↗		↗		
Sahara	↗	↗	↘																		↗		↗	↗	↗		↗		*WAF: medium confidence that*
West Africa	↗	↗	↘		**		↗ **			↗											↗		↗	↗	↗		↗		*GHG and aerosols caused the*
North East Africa	↗ **	↗	↘							o					↘	↘					↗		↗	↗	↗		↗		*drought and the recovery*
Central East Africa	↗ **									o					↘	↘					↗		↗	↗	↗		↗		
Central Africa	↗																				↗		↗	↗	↗		↗		*SEAF: ** for decrease in*
South West Africa	↗	↗	↘		**				↗	↗ **											↗		↗	↗	↗		↗		*extreme rainfall*
South East Africa	↗	↗	↘		**		**		↗	↗ **											↗		↗	↗	↗		↗		

Key for observational trend evidence

↗	Past upward trend (*medium or high confidence*)
↘	Past downward trend (*medium or high confidence*)

Key for level of confidence in future changes

	High confidence of increase
	Medium confidence of increase
	Low confidence in direction of change
	Medium confidence of decrease
	High confidence of decrease
	Not broadly relevant

Key for attribution evidence

***	High confidence
**	Medium confidence
*	Low confidence
x	Mixed signal
o	No signal

Note: There are several region-specific qualifiers/exceptions attached to some of the directions of change/confidence levels indicated above. Please refer to Table.3 of TS.A1 for details.

[END TABLE TS.13 HERE]

TS.4.3.5 Asia

In Asia, temperatures have warmed along the last century (*high confidence*) and extreme heat episodes have become more frequent in most regions (*medium confidence*). Extreme cold spells have become less frequent, with *medium agreement* due to high variability and possible interactions with Arctic amplification in Siberia (*medium confidence*). It is *virtually certain* that there has been an increase in the number of warm days and nights and a decrease in the number of cold days and nights since 1950. Both the coldest extremes and hottest extremes display increasing temperatures. It is *very likely* that this also applies in regions in Asia where data are available. In Asia, there is *high confidence* in the increase of daily temperature extremes during the last decades over most of the Asian continent. It is *very likely* that there has been an increase in the intensity and duration of heatwaves and in the number of heatwave days in Asia. {11.3.2, 12.4.2, Table 11.1, Table 11.5}

Under the RCP8.5 high emissions future it is *likely* that further warming in West, Central and Northern Asia and the Arabian Peninsula will exceed the global mean land warming and reach 8-10°C at the end of the 21st century. It is *likely* that cold spells will become less frequent in future scenarios and that high heat thresholds (e.g. Tmax > 40°C) will be crossed at least several days per year in regions where they are currently recorded only rarely, such as in Siberia. In Asia, increases in hot events and decreases in cold events are projected with *high confidence* over most of the continent. Particularly, in southern Asia, more intense heatwaves of longer durations and occurring at a higher frequency are projected with *medium confidence*. {11.3.5, 12.4.2, Table 11.5}

Regional increases in the frequency and/or in the intensity of heavy rainfall have been observed in most parts of Asia (*high confidence*). There is *high confidence* in the observed increase in daily precipitation extremes over Central Asia, most of South Asia; the northwest Himalaya, and parts of East Asia, whereas no trend is observed or contrasting evidence exists over the eastern Himalayas. {11.4.2}

It is *very likely* that Northern Hemispheric anthropogenic aerosols have caused a weakening of the regional monsoon circulations in South and East Asia during the second half of the 20th century, thereby offsetting a strengthening monsoon precipitation in response to GHG-induced warming. There is *limited evidence* of an effect of climate change on air pollution in Asia. {8.3.1, 8.3.2, Box 8.1, 12.4.2}

Regions where mean rainfall is *likely* to increase include East and North Asia. Regions were mean rainfall is *likely* to decrease include Indonesia and the northern Arabian Peninsula. Changes in monsoons are *likely* to result in increased precipitation in northern China, increases during the summer monsoon but decreases during the winter monsoon in South Asia (*medium to high confidence*). Projections of regional monsoons indicate contrasting (region-dependent) and uncertain changes in total precipitation but an overall extension of the length of the wet season. Increased monsoon rainfall is projected over South, Southeast, and East Asia (*medium confidence*). There is *high confidence* in increasing extreme precipitation and *medium confidence* in increasing river floods across most Asian regions, while decreased peak floods are projected in West Siberia (*medium confidence)*). {8.2.1, 8.4.2, 12.4.2}

Glaciers will continue to melt and permafrost to thaw (*high confidence*), inducing cascading impacts in river hydrology and mountain slopes stability. Droughts will have contrasted patterns with decrease in Siberia and increase in West Asia and East Asia (*medium confidence*). {12.4.2}

Sea level rise is *very likely* to continue at a higher than the global average in Asia contributing to increased coastal flooding in low-lying areas (*high confidence*) and coastline recession along most sandy coasts (*high confidence*). Marine Heatwaves and Ocean acidification are also expected to increase over the 21st century (*high confidence*). {12.4.2}

Tropospheric columns of nitrogen dioxide (NO_2) and sulphur dioxide (SO_2) declined over East Asia since 2011 (*likely*), and increased over South Asia (*likely*). {6.2, 2.2.4, 2.2.5, 2.2.6}

Warmer climate is expected to increase surface ozone by a few ppb over polluted regions of East Asia, with regional discrepancies over South Asia for the monsoon season (*medium confidence*). {6.2.1, 6.4, 6.6}

TS.4.3.5.1 Middle East Asia

Observations over the Arabian Peninsula for the period 1978–2018 exhibit an increase in annual surface air temperature estimated at 0.52°C per decade and *very likely* in the range of 0.21–0.73°C per decade *(high confidence)* and a decrease in annual precipitation estimated at 6.3 mm per decade and *likely* in the range –30 mm–9.0 mm per decade *(medium confidence).* The highest warming and precipitation decrease are observed in the northern Peninsula and the lowest warming and highest precipitation increase in the south.

As the annual precipitation total in the region comes mostly in a wet season from a few scattered extreme events, decrease in their frequency has resulted in a negative precipitation trend (*medium confidence*), Nevertheless intensity of extreme precipitation has increased (*low confidence*). {11.9, Atlas.5.3, Table 11.5,}

A strong increase of annual surface air temperature and precipitation amount continued over West and Central Asia in the last half century based on observational and gridded datasets including satellite products. The observed trend in the period 1960–2013 *very likely* was in the range 0.27°C–0.47°C per decade for temperature and 1.3–4.8 mm per decade for precipitation. In mountainous areas the scarcity of observation stations and the decline of observation sites after the collapse of the former Soviet Union in 1991 *very likely* increase the uncertainty of the long-term temperature and precipitation estimates. {Atlas.5.3}

Extensive land-use and land-cover changes had different impacts on the local temperature and precipitation in Central Asia *(medium confidence).* Agriculture intensification through oasis expansion in the Xinjian region has increased summer precipitation (*medium evidence*, *high agreement*). The shrinking of the Aral Sea has induced an increase of local surface air temperature in the range of 2°C to 6°C (*very high confidence*), but its impact on precipitation can be attributed only with *very low confidence*. {Atlas.5.3}

There is *medium evidence* about performance of RCMs in the Middle East region as publications on regional model evaluation have only recently emerged. Published studies have *medium to high agreement* for mean temperature and precipitation biases in RCMs. Regional models simulate colder temperatures than observed over mountainous and high plateau regions including the Himalayas and Plateau of Tibet (*limited evidence*, *high agreement*). Mean temperature bias of RCMs is within ± 3°C over West Asia (*high confidence*), but

RCMs have a tendency to overestimate precipitation amounts in almost all parts of the region (*low confidence*). {Atlas.5.3}

Over the Arabian Peninsula the highest rate of warming (0.98°C per decade) is projected for its northern part under the higher emission scenario during the 21st century *(high confidence).* Strong decreases in precipitation (–30% to –50%) are projected in the north-western part of the Arabian Peninsula with the area of largest increase (8.6% per decade) found over the southern part *(medium confidence).* Projected warming is between 1°C and 2°C for SSP1-2.6 and 4°C and 6°C for SSP5-8.5, while precipitation is projected to change by –3% to 41% for SSP1-2.6 and 12% to 126% for SSP5-8.5 (*medium confidence*). {Atlas.5.3}

Widespread warming over West and Central Asia is projected at the end of the 21st century compared to 1971–2000, varying from 2.5°C to 8°C depending on the season and scenario *(high confidence)* with the maximum warming rate in the northern part of the region in summer *(medium confidence)*. {Atlas.5.3}

Strong spatiotemporal differences with overall decreasing precipitation are projected over West Asia *(low confidence)* and in the central and northern parts of Central Asia in summer, while relatively stronger increasing rates are projected over north of Central Asia in winter *(medium confidence)*. {Atlas.5.3}

There is *high confidence* on the increase in frequency and magnitude of warm extremes and decrease in frequency and severity of cold extremes. For precipitation extremes and flooding and for aridity changes only *low confidence* can be assigned for both observations and projections across all subregions of the Middle East. {11.9, Table 11.5}

TS.4.3.5.2 North Asia

Annual surface air temperature *very likely* has increased over most territories of North Asia based on observational datasets. The most pronounced warming has been found in spring in East Siberia and over the Russian Far East, strengthening from the South to North territories of the sub-regions with a linear trend of 0.8°C-1.2°C per decade for the 1976–2014 period (*high confidence*). A temperature decrease was identified in winter in the southern part of Western and Eastern Siberia *likely* due to midlatitude circulation variability, but the decrease has moderated from –0.6°C per decade for 1976–2012 to –0.3°C per decade for the longer 1976–2018 period due to warmer winters in the more recent years (*high confidence*). {Atlas.5.3}

Annual precipitation sums *very likely* have increased over the most territory of North Asia based on observational datasets. The highest precipitation increase predominantly was observed over some regions of Siberia and the Russian Far East with estimated trends of 5–15 mm per decade for the 1976–2014 period (*medium confidence*). The decrease in annual precipitation sums was observed to be up to –20 mm per decade for the 1976–2014 period over the southern and north-eastern parts of the Russian Far East, namely over the Kamchatka and the Chukchi Peninsulas (*medium confidence*). {Atlas.5.3}

It is *likely* that, since 1950, the annual maximum daily or 5-daily precipitation amount has increased in Asia. In addition, regional increases in the frequency and/or in the intensity of heavy rainfall have also been observed in most parts of Asia with larger relative increases in the northern high-latitudes in all seasons, and in the mid-latitudes in the cold season (*high confidence*). {11.4, 11.9}

There is *high confidence* that in parts of northern Asia the seasonality of floods in cold regions where snow-melt is involved has changed with significant trends in peak streamflow increases. There is *low confidence* in attributing changes in the probability or magnitude of individual floods to human influences. {11.5}

Most of the CMIP5 GCMs overestimate the annual mean air temperature and precipitation over the North Asia region (*medium confidence*). The biases in the simulated annual mean surface air temperature are particularly apparent in the winter (DJF) season, while the model biases in other seasons are relatively smaller (*medium confidence*). Most of the GCMs are able to represent the observed decadal temperature trend (*medium confidence*), but CMIP5 GCMs fail to capture the decreasing temperature trend over the southern East Siberia in winter (*high confidence*). {Atlas.5.3}

Surface air temperature and precipitation in the North Asia region are projected to further increase based on

CMIP5/CMIP6 projections (*medium confidence*). Temperature change is projected in the range from 3°C in summer to 4.9°C in winter based on the RCP4.5 scenario, and from 5.6°C in summer to 9.7°C in winter based on the RCP8.5 scenario, whereas the projected precipitation increase is 9–22% (summer-winter in RCP4.5) and 9–56% (summer-winter in RCP8.5) for the 2080–2099 period compared to the 1981–2000 period (*medium confidence*). {Atlas.5.3}

There is *medium confidence* that river floods will increase in the northern Eurasia. Regional changes in river floods are more uncertain because complex hydrological processes are involved. {11.5}

TS.4.3.5.3 East Asia

In most East Asia areas annual mean temperature is increasing since the 1950s. It is *very likely* that the linear trend of annual mean surface air temperature exceeds 0.1°C per decade over most of East Asia from 1980 to2014. Annual mean precipitation over most East Asia does not show a significant change for the period of 1980-2014 (*high confidence*). {Atlas.5.3.1.2} There is *medium confidence* that soil moisture deficits have increased in east Asia. {11.6}

It is *very likely* that the surface temperature over East Asia will increase under global warming. Larger warming magnitudes will occur in the northern part of the region (*high confidence*). {Atlas.5.3}

GCMs still show a poor performance in simulating the mean rainfall and its variability over East Asia, especially over regions characterized by complex topography (*high confidence*). RCMs generally produce more detailed regional features, but do not always produce superior simulations compared with the driving GCMs (*medium confidence*). {Atlas.5.3}

Precipitation is projected to increase over land in most of East Asia at the end of the 21st century under the high emissions scenario (RCP8.5, SSP5-8.5). Stronger precipitation increase occurs in northern China, corresponding to the strengthened monsoon circulation in the lower troposphere. (*high confidence*) {Atlas.5.3}

Current emissions of CO_2 and SLCFs from East Asia is one of the largest regional contributors to global warming on both short (*medium confidence*) and long time scales (10 to100 years) (*high confidence*). {6.5.1, 6.5.2}

TS.4.3.5.4 South East Asia

El Niño events have strongly influenced observed warming over Southeast Asia (*medium confidence).* However, there is *low confidence* in the exact effect of El Niño on mean, extreme, and night time temperatures. {Atlas.5.3}

There is *high confidence* that RCMs can reproduce reasonably well seasonal climate patterns of temperature, precipitation and large-scale circulation over the different subregions of South East Asia. {Atlas 5.3}

Temperature is projected to increase over South East Asia by at least 3°C by the end of the 21st century under the RCP8.5 scenario (*very likely)*. This regional warming is consistent across CORDEX, CMIP5 and CMIP6 ensembles. {Atlas.5.3}

There has been an increase in maximum daily precipitation during La Niña events over Southeast Asia (*medium confidence*). Changes in daily mean precipitation are less spatially coherent (*low confidence*) and the effect of ENSO variability on extreme precipitation trends vary between subregions (one day extreme rainfall decreasing over the Maritime Continent and increasing over Indochina and Thailand) (*low confidence).* {Atlas.5.3}

Projected changes in rainfall over Southeast Asia will be season dependent with significantly drier conditions over most regions during boreal summer (JJA) at the end of the 21st century under the RCP 8.5 scenario (*medium confidence*). Over Indonesia, a 20-30% decrease in mean rainfall is *very likely*. During boreal winter (DJF) there will be an increase in mean rainfall over Indochina and the Philippines while there is a drying tendency over the Maritime Continent (*medium confidence*). {Atlas.5.3}

TS.4.3.5.5 South Asia

Minimum and maximum daily temperatures in South Asia are increasing and winters are warming faster than summers (*high confidence*). There is *high confidence* that there is an increasing trend in heat wave occurrence in many regions over South Asia. {Atlas.5.3}

It is *likely* that temperatures over South Asia will increase by 5.0±0.9°C during 2081-2100 relative to the 1995-2014 baseline period under both CMIP5 RCP8.5 and CMIP6 SSP5-8.5 scenarios. {Atlas.5.3}

The South Asian monsoon has shown contrasting behaviour over India and Pakistan (in the monsoon dominated region only), with a strengthening trend over the core monsoon zone in Pakistan (*low confidence*) and weakening trend over central north India (*high confidence*). {Atlas.5.3}

There is *medium evidence* and *high agreement* that representing irrigation is important for a realistic simulation of South Asian monsoon precipitation. There is *limited evidence* that including irrigation in climate models improves the simulation of maximum and minimum daily temperatures as well as precipitation outside of the South Asian monsoon region. {10.3.3}

Summer monsoon precipitation in South Asia is *likely* to increase by the end of the 21st century while winter monsoons are projected to be drier. Based on CMIP6 models available in the Interactive Atlas, an increase (> 22%) in mean annual precipitation is projected over South Asia under RCP 8.5 at the end of the century (*medium confidence*). {Atlas.5.3}

Atmospheric aerosol concentrations across the Northern Hemisphere mid-latitudes increased since 1700, but have declined in the past 20 years (*medium confidence*). Aerosol Optical Depth (AOD) has decreased since 2000 over Northern Hemisphere mid-latitudes mainly, but increased over South Asia (*high confidence*), and the trends in fine-mode AOD are more pronounced. {2.2.6}.

Table TS.14 shows a summary of changes in CIDs for Asia, derived from a combination of evidence from observed trends and projected future conditions. TS. Appendix A provides references to the locations in the underlying chapters which support the assessment shown in this table.

[START TABLE TS.14 HERE]

Table TS.14: Summary of confidence in projected directional changes for climatic impact drivers for Asia. The colours represents their aggregate characteristic changes for mid-century RCP8.5 within each AR6 WG I reference region. Dark purple: *high confidence* of increase; light purple: *medium confidence* of increase; white: *low confidence* of increase or decrease; light brown: *medium confidence* of decrease; dark brown: *high confidence* of decrease; grey: CID not broadly relevant. Arrows indicate *medium to high confidence* trends derived from observations and asterisks indicate low, medium and high confidence in attribution of observed changes (which are of the same sign as the projected changes unless stated otherwise).

Climatic Impact Driver

	Heat and Cold				Wet and Dry							Wind			Snow and Ice						Coastal and Oceanic					Other			
Asia	Mean temperature	Extreme heat	Cold spell	Frost	Mean precipitation	River flood	Pluvial flood	Landslide	Aridity	Drought	Wildfire	Mean wind speed	Severe wind storm	Sand and dust storm	Snow and land ice	Permafrost	Lake, river and sea ice	Heavy snow and ice storm	Hail	Snow avalanche	Relative sea level	Coastal flood	Coastal erosion	Marine heatwave	Ocean and lake acidity	Air pollution	Atmospheric CO_2	Radiation at surface	*Notes on attribution evidence*
West Siberia	↗	↗ *	↘ *				↗ *S			*		↘				↘											↗		*SAS: ch10 attribution on weakening*
East Siberia	↗	↗ *	↘ *				↗					↘				↘											↗		*monsoon to aerosols*
West Central Asia	↗	↗	↘								↗	↘			↘						↗		↗	↗			↗		
South Asia	↗	↗	↘ ***			*	↗ o*			*		↘			↘						↗		↗	↗					*SEA: low confidence of increase*
Southeast Asia	↗	↗ **					**			*											↗		↗	↗			↗		*of drought*
Russian Far East	↗	↗	↘				↗					↘				↘					↗		↗	↗	↗		↗		
East Asia	↗	↗ ***	↘ ***				↗ *			**		↘									↗		↗	↗			↗		
Tibetan Plateau	↗	↗ **	↘ **				↗ *					↘															↗		
Arabian Peninsula	↗	↗	↘																		↗		↗	↗			↗		

Key for observational trend evidence

↗	Past upward trend (*medium or high confidence*)
↘	Past downward trend (*medium or high confidence*)

Key for level of confidence in future changes

- High confidence of increase
- Medium confidence of increase
- Low confidence in direction of change
- Medium confidence of decrease
- High confidence of decrease
- Not broadly relevant

Key for attribution evidence

***	High confidence
**	Medium confidence
*	Low confidence
x	Mixed signal
o	No signal

Note: There are several region specific qualifiers/exceptions attached to some of the directions of change/confidence levels indicated above. Please refer to Table.3 of TS.A1 for details.

[END TABLE TS.14 HERE]

TS.4.3.6 Australasia

There is *very high confidence* that the climate of Australia warmed by just over 1°C and New Zealand by around 1°C since reliable records began in 1910 and 1909 respectively. It is *very likely* that there has been an increase in the intensity and duration of heatwaves and in the number of heatwave days in Australia. There is *high confidence* that human influence has been the dominant driver of the warming trend and has contributed to greater intensity and duration of atmospheric and marine heat events. {11.3.2, Atlas.5.4, Table 11.1, Table 11.6}

Detectable anthropogenic increases in precipitation in Australia have been reported particularly for north central Australia and for a few regions along the south-central coast for the period 1901-2010. In New Zealand, winter rainfall increased in several places, but trends are not statistically significant. {Atlas 5.4.2}

There is *high confidence* (*medium agreement and robust evidence)* that anthropogenic forcing has contributed to southwest Australia autumn and winter rainfall decline since the early 1970s. There is *low confidence* in the magnitude of the human influence and role of specific anthropogenic drivers on the autumn and winter precipitation decline. {10.4.1}

Regional increases in the frequency and/or in the intensity of heavy rainfall have also been observed in northwest Australia (*high confidence*), but there is *low confidence* of larger-scale regional increases of extreme precipitation in Australia. {11.4.2, Table 11.6}

There is *medium confidence* that model representation of aspects of the Australasian region has improved between CMIP5 and the CMIP6 ensemble in the Interactive Atlas, including temperature and rainfall climatology, ocean currents, ENSO and IOD and their teleconnection with Australian rainfall. {Atlas.5.4}

There is *high confidence* that dynamical downscaling and statistical downscaling have produced 'added value' in the climate change projected signals in regional temperature, rainfall and extremes related to topography and coasts in Australia and New Zealand. However, different downscaling methods and the limited sample size of CMIP and CORDEX simulations provide an incomplete picture of future conditions. {Atlas.5.4}

Warming is projected to continue with a magnitude roughly equal to or slightly more than the global average temperature, and proportional to the emissions pathway by the end of the century (around 2.5 to 5.5°C under SSP585 and 0.5 to 1.5°C for SSP126 for 1995-2014 to 2081-2100). Together with this warming, more frequent hot extremes (*very likely*), increasing heat stress (*high confidence*) and less frequent cold extremes (*very likely*) are projected. {12.4.3, Atlas.5.4}

Annual mean precipitation is projected to increase in Central and north east Australia and the west and south of New Zealand, while decreases are projected for south western and eastern Australia and the north and east of New Zealand (*medium confidence*).. By contrast, there is *high confidence* for a future rainfall decline in southwest Australia in the cool season (April-October) and a rainfall increase in parts of New Zealand in winter, with similar results in CMIP5 and CMIP6, other rainfall changes are less significant or less certain. {12.4.3, Atlas.5.4}

River flooding is projected to increase in northern Australia and New Zealand (*medium confidence*). There is *medium confidence* for an increase in hydrological droughts in South Australia. Weather conditions conducive for wildfires are projected to increase throughout Australasia (*high confidence* in Australia, *medium confidence* in New Zealand). {8.4.1, 11.6.5, 12.4.3}

CMIP5 projections of severe winds indicate a general increase in north eastern Australia, and decrease in some parts in the south (*high confidence*) and centre (*medium confidence*) of the country. However, projections based on CMIP6 are not consistent with the above CMIP5 based projections. A small (0.1 - 0.3 $m\ s^{-1}$) but robust decrease in the 98th percentile winds by mid-century (SSP5-8.5) over most of Australia, and a non-robust 0.1 – 0.2 $m\ s^{-1}$ increase (over Tasmania and the south island of New Zealand) are indicated. {12.4.3, Figure 12.10b}

Snow cover is expected to decrease at high altitudes in both Australia and New Zealand (*high confidence*). {12.4.3}

Marine heatwaves and ocean acidification are also expected to increase over the 21st century (*high confidence*). Sea level rise is *very likely* to continue at a higher than the global average in Australasia contributing to increased coastal flooding in low-lying areas (*high confidence*) and coastline recession along most sandy coasts (*high confidence*). {12.4.3}

Table TS.15 shows a summary of changes in CIDs for Australasia, derived from a combination of evidence from observed trends and projected future conditions. TS. Appendix A provides references to the locations in the underlying chapters which support the assessment shown in this table.

[START TABLE TS.15 HERE]

Table TS.15: Summary of confidence in projected directional changes for climatic impact drivers for Austalasia. The colours represents their aggregate characteristic changes for mid-century RCP8.5 within each AR6 WG I reference region. Dark purple: *high confidence* of increase; light purple: *medium confidence* of increase; white: *low confidence* of increase or decrease; light brown: *medium confidence* of decrease; dark brown: *high confidence* of decrease; grey: CID not broadly relevant. Arrows indicate *medium to high confidence* trends derived from observations and asterisks indicate low, medium and high confidence in attribution of observed changes (which are of the same sign as the projected changes unless stated otherwise).

Climatic Impact Driver	Heat and Cold				Wet and Dry							Wind			Snow and Ice						Coastal and Oceanic					Other		
Australasia	Mean temperature	Extreme heat	Cold spell	Frost	Mean precipitation	River flood	Pluvial flood	Landslide	Aridity	Drought	Wildfire	Mean wind speed	Severe wind storm	Sand and dust storm	Snow and land ice	Permafrost	Lake, river and sea ice	Heavy snow and ice storm	Hail	Snow avalanche	Relative sea level	Coastal flood	Coastal erosion	Marine heatwave	Ocean and lake acidity	Air pollution	Atmospheric CO_2	Radiation at surface
Northern Australia	↗	↗***	↘								*										↗		↗	↗	↗		↗	
Central Australia	↗	↗***	↘								*										↗		↗	↗	↗		↗	
Southern Australia	↗	↗***	↘		↘		*			**	↗ *				↘						↗		↗	↗	↗		↗	
New Zealand	↗		↘				**			*					↘						↗		↗	↗	↗		↗	

Key for observational trend evidence

↗	Past upward trend (*medium or high confidence*)
↘	Past downward trend (*medium or high confidence*)

Key for level of confidence in future changes

High confidence of increase
Medium confidence of increase
Low confidence in direction of change
Medium confidence of decrease
High confidence of decrease
Not broadly relevant

Key for attribution evidence

***	High confidence
**	Medium confidence
*	Low confidence
x	Mixed signal
o	No signal

Note: There are several region specific qualifiers/exceptions attached to some of the directions of change/confidence levels indicated above. Please refer to Table.3 of TS.A1 for details.

[END TABLE TS.15 HERE]

TS.4.3.7 Central and South America

TS.4.3.7.1 Central America

New literature has confirmed a continued increase in mean temperatures in a majority of regions of Central America since the beginning of the 20th century (*high confidence*). Significant warming trends between 0.2°C and 0.3°C per decade have been observed in all the subregions of Central America in the last 30 years, with the largest increases in the North America monsoon region (*high confidence*), with some local cooling trends reported for certain small regions. {12.4.4, Atlas.5.5}

Warming trends observed in recent decades are projected to continue to increase over the 21st century (*high confidence*). Under the middle emissions scenario (SSP2-4.5) surface warming is *likely* to exceed 1.5°C for continental Central America before the mid-century, becoming *very likely* by the end of the century. Under the high emissions scenario (SSP5-8.5), surface warming is *very likely* to exceed 1.5°C before the mid-century and 3°C before the end of the century, but it is *likely* to exceed 4.5°C by the end of the century.. It is *very likely* that most regions in Central America will frequently undergo extreme heat stress conditions by the end of century under the RCP8.5/SSP5-8.5 scenario. {12.4.4, Atlas.5.5, Figure Atlas.42}

Observed trends in precipitation are non-significant and highly variable in entire Central America. Regional increases in the frequency and/or in the intensity of heavy rainfall have been observed in Mexico (*medium confidence*). {11.4.2, Atlas.5.5}

Projected change in mean annual precipitation shows a large spatial variation across Central America. Mean annual precipitation is *likely* to decrease as an average in the whole Central America (*low confidence*). Under middle emissions scenario, there are overall negative but non-significant (*low confidence*) precipitation trends during the 21st century. Under high emissions scenario, average precipitation is *likely* to decrease in most of the region, particularly in part of continental Central America. {Atlas.5.5}

There is *medium confidence* in projected increases in the frequency and severity of precipitation deficits in

Central America. Climate projections indicate a decrease in frequency of tropical cyclones in Central America and an increase in mean wind speed and in wind power potential in most parts of the region (*medium confidence*) {11.6.5, 12.4.4}.

Regional mean sea level rise projections for the ocean around Central America range from 0.3-0.5 m under SSP1-2.6 to 0.6-1.0 m under SSP5-8.5 for 2081-2100 with respect to 1995-2014 (median values), which is around the projected Global Mean Sea Level change. Extreme sea level magnitude and occurrence frequency are expected to increase around the Caribbean islands (*high confidence*). Projections indicate that sandy coasts in Central America will experience coastline recession throughout the 21st century (*high confidence*).There is *high confidence* of increasing marine heat waves and increased ocean acidity in the nearshore ocean of Central America. {9.6.3, 12.4.4, Cross-Chapter Box 9.1}

TS.4.3.7.2 South America

Warming trends have been observed across most of South America (*high confidence*). It is *very likely* that the average temperatures across the continent have warmed almost 0.2°C per decade from 1980 to 2014, particularly in Central and Northern South America (*high confidence*), while the southern regions are warming at a slower rate (*low confidence*). {Atlas.5.5, Figure Atlas.42}

Warming trends observed in recent decades in South America are projected to continue over the 21st century (*high confidence*). There is *high confidence* that the surface temperature is *very likely* projected to exceed 1.5°C before mid-century under all emission scenarios (RCPs and SSPs). Warming is *likely* (*medium confidence*) to exceed 4°C by the end of the 21st century (2081–2100), in particular under a high-emission scenario (RCP8.5 and SSP5-8.5). {Atlas.5.5, Figure Atlas.42}

It is *very likely* (*high confidence*) that most regions in South America will frequently undergo extreme heat stress conditions by the end of the 21st century, and such conditions will prevail more than 200 days per year in Northern South America. There is *high confidence* that droughts and fire weather conditions will intensify in Northern South America, the South American monsoon region, and Northeastern South America while there is *medium confidence* in Southern South America. Also, there is *medium confidence* in changes in the intensity and duration of heatwaves and in the number of heatwave days in South America. The lower confidence in this assessment compared to other regions is due to reduced data availability and fewer studies in the region. {} Along with the observed increase of extreme heat, there is *high confidence* in a decrease in frequency of cold days and nights and there is *medium confidence* (*limited agreement*) of a decrease in frost days in Southeastern, Southwestern, and Southern South America. {11.3.2, 12.4.4}

Regional increases in the frequency and/or in the intensity of heavy rainfall have been observed in Southeastern South America and Northern South America (*high confidence*). Areas in South America have experienced a detectable influence of anthropogenic aerosols on precipitation patterns. Remote effects far from emission regions have resulted from large-scale circulation responses to spatially heterogeneous changes in surface temperatures (*high confidence*). {8.3.1, 8.3.2, 11.4.2, Box 8.1}

Projected change in mean annual precipitation shows a large spatial variation across South America. However, precipitation is *likely* projected to increase in Southeastern South America and decrease in Southwestern South America with increased levels of warming (*medium confidence*). For the period 2081–2100, compared to present day, Northern and Southwestern South America are *likely* (*medium confidence*) to experience a decrease in annual mean precipitation in the range of about –22 to –0.3 % (5–95% range of available CMIP6 projections). An increase (> 50%) in mean annual precipitation is projected over Southern South America (*medium confidence*). The projected change in rainfall exhibits a large spatial variation across other South American regions with larger uncertainty (*low confidence*). For the South American monsoon, the CMIP6 projections do not indicate a clear increase in precipitation during the 21st century. {8.2.1, 8.4.2, Atlas.5.5, Figure Atlas.42}

Among the robust signatures of shifts in the average regional and seasonal characteristics of the water cycle, there is *medium to high confidence* in an expansion of arid areas towards the midlatitudes, and in pronounced drying in Northeastern Brazil. Changes in the dry season in the central part of South America, and decreased precipitation over the Amazon and central Brazil are projected by the end of the 21st century under the

RCP8.5 scenario. There is *medium confidence* for an increase in hydrological droughts in Southern South America. Increases in extreme precipitation are projected for almost all of South America, except for the Southern Cone (*medium confidence).* {8.4.1, 11.6.5, 12.4.4}

There is *medium confidence* that river floods will increase in the western Amazon and the Andes. Regional changes in river floods are more uncertain because complex hydrological processes are involved. Increasing floods are expected in most of the continent (Southeastern, Southwestern, and Northwestern South America and the South American monsoon region) (*medium confidence*). {11.5.5, 12.4.4}

There is *high confidence* that glacier volume loss and permafrost thawing will continue in all climate scenarios. Reduced snowfall and decreased light rainfall amounts, combined with increased temperatures, have driven a rapid retreat of mountain ice caps all over the Andes. In the future, glacier volume loss and its concomitant meltwater runoff decrease will continue all across the Andes (*high confidence*), leading to significant changes in local hydrological conditions. {12.4.4}

There is limited evidence in trends in present-day wind speed and windstorms in South America. There is *high confidence* of increased intensity and frequency of marine heat waves and ocean acidity in the nearshore ocean of South America. Wind speeds are projected to increase in South America, enhancing wind power potential (*medium confidence*). Extreme sea level magnitude and occurrence frequency are expected to increase throughout the region, with higher increases along the coasts of Chile and Argentina, and slightly lower increases around the Amazon (*high confidence*). Projections indicate that sandy coasts in South America will experience coastline recession throughout the 21st century (*high confidence*). Regional mean sea level rise projections for the ocean around South America range from 0.3-0.5 m under SSP1-2.6 to 0.6-1.0 m under SSP5-8.5 for 2081-2100 with respect to 1995-2014 (median values), which is around the projected Global Mean Sea Level change. {9.6.3, 12.4.4, Cross-Chapter Box 9.1}

Table TS.16 shows a summary of changes in CIDs for Central and South America, derived from a combination of evidence from observed trends and projected future conditions. TS.A1 provides references to the locations in the underlying chapters which support the assessment shown in this table.

[START TABLE TS.16 HERE]

Table TS.16: Summary of confidence in projected directional changes for climatic impact drivers for Central and South America. The colours represents their aggregate characteristic changes for mid-century RCP8.5 within each AR6 WG I reference region. Dark purple: *high confidence* of increase; light purple: *medium confidence* of increase; white: *low confidence* of increase or decrease; light brown: *medium confidence* of decrease; dark brown: *high confidence* of decrease; grey: CID not broadly relevant. Arrows indicate *medium to high confidence* trends derived from observations and asterisks indicate low, medium and high confidence in attribution of observed changes (which are of the same sign as the projected changes unless stated otherwise).

Climatic Impact Driver

	Heat and Cold				Wet and Dry							Wind			Snow and Ice						Coastal and Oceanic					Other			
Central and South America	Mean temperature	Extreme heat	Cold spell	Frost	Mean precipitation	River flood	Pluvial flood	Landslide	Aridity	Drought	Wildfire	Mean wind speed	Severe wind storm	Sand and dust storm	Snow and land ice	Permafrost	Lake, river and sea ice	Heavy snow and ice storm	Hail	Snow avalanche	Relative sea level	Coastal flood	Coastal erosion	Marine heatwave	Ocean and lake acidit	Air pollution	Atmospheric CO_2	Radiation at surface	***Notes on attribution evidence***
Southern Central America	↗	↗ *	↘																		↗		↗	↗	↗		↗		*NWS: medium confidence for*
Northwestern South America	↗	↗	↘***				**								↘						↗		↗	↗	↗		↗		*decrease of extreme rainfall*
Northern South America	↗	↗	↘				↗ *														↗		↗	↗	↗		↗		
South American Monsoon	↗	↗	↘				*																				↗		*SWS * on increase of drought*
Northeastern South America	↗	↗	↘				↘ **			↗ o											↗		↗	↗	↗		↗		
Southwestern South America	↗	↗	↘	↘			*			↗ *					↘						↗		↗	↗	↗		↗		*SSA ** on increase of extreme*
Southeastern South America	↗	↗***	↘	↘			↗ **														↗		↗	↗	↗		↗		*precipitation*
Southern South America	↗		↘	↘			**								↘						↗		↗	↗	↗		↗		

Key for observational trend evidence

↗	Past upward trend (*medium or high confidence*)
↘	Past downward trend (*medium or high confidence*)

Key for level of confidence in future changes

	High confidence of increase
	Medium confidence of increase
	Low confidence in direction of change
	Medium confidence of decrease
	High confidence of decrease
	Not broadly relevant

Key for attribution evidence

***	High confidence
**	Medium confidence
*	Low confidence
x	Mixed signal
o	No signal

Note: There are several region specific qualifiers/exceptions attached to some of the directions of change/confidence levels indicated above. Please refer to Table.3 of TS.A1 for details.

[END TABLE TS.16 HERE]

TS.4.3.8 Europe

Like most land areas, the European continent is warming faster than the global mean. It is *very likely* that Western Europe has warmed by 0.2-0.3°C per decade and Eastern Europe by 0.3-0.5°C per decade.

In most European areas it is *very likely* that observed positive trends in extreme precipitation and warm temperatures are persistent. This is documented using new datasets with homogenized observations at higher spatial and temporal resolution. It is *very likely* that there has been an increase in the intensity and duration of heatwaves and in the number of heatwave days in Europe. A detectable anthropogenic increase in a summertime heat stress index over all regions of Europe has been identified based on wet bulb global temperature (WBGT) index trends for 1973-2012 (*medium confidence, limited evidence*), and heat stress due to both high temperature and humidity, affecting morbidity, mortality and labour capacity is projected to increase in all scenarios by the middle of the century. {11.3.3, 12.4.5, Atlas.5.6}

Regional increases in the frequency and/or in the intensity of heavy rainfall have also been observed in northern Europe (*high confidence*), eastern Mediterranean region and central Europe (*medium confidence*). {11.4.2}

Model representation of the climatology of European mean and extreme temperature and precipitation has improved compared to AR5 (*likely*). This is aided by continuous model development, the existence of new coordinated modelling initiatives dedicated to Europe such as Euro-CORDEX and Med-CORDEX, and the release of new (high-resolution) observational data sets and reanalysis data. {Atlas.5.6}

There is *medium confidence* that high-resolution, convection permitting RCMs have a better representation of characteristics of extreme precipitation (e.g., diurnal cycles, mesoscale convective events, extremes) and exhibit stronger responses in the tails of the precipitation distribution than coarser resolution models. {Atlas.5.6}

The subset of CMIP6 results available in the Interactive Atlas shows higher future warming in the European regions in December-January-February and June-July-August than CMIP5, corresponding to a larger climate sensitivity of the CMIP6 models (*likely*). June-July-August precipitation in NEU and EEU is *likely* lower in CMIP6 than in CMIP5. {Atlas.5.6}

It is *very likely* that strong winter warming in Northern Europe and strong summer warming in Southern Europe will continue. It is *likely* that the associated northern European increase in seasonal mean precipitation and reduced summer mean precipitation in southern Europe will continue. Different regional warming levels will be reached depending on the level of global warming. {12.4.5, Atlas.5.6}

There is *high confidence* that the frequency of extreme heat will increase. Extreme heat will make more frequent excursions above critical thresholds for health, agriculture and other sectors (*high confidence*) {12.4.5}. By the end of the century cold spells will virtually disappear in SSP5-8.5 (*high confidence*). {11.5.5, Atlas.5.6}

There is *high confidence* that river floods will increase in Central and Western Europe and *medium confidence* that they will decrease in Eastern and Southern Europe, with respective changes in the 1:100 years river flow being larger for higher warming levels (see Figure TS.39). There is *high confidence* that droughts are increasing in the Mediterranean region. There is *medium confidence* in projected increases in the frequency and severity of precipitation deficits in the Mediterranean region and associated trends in soil moisture deficits based on observations-driven land surface models. Most of Europe, especially Western, Eastern and Central regions, could experience an increase in the weather conditions favouring extreme wildfires by 2080 (current 100-yr. events will occur every 5 to 50 years) with a progressive in time increase in significance and model agreement. {11.6.2, 11.6.5, 12.4.5}

Projections of summer surface radiation, surface temperature and precipitation of RCMs and GCMs are frequently inconsistent. There is *limited evidence* that some of these inconsistencies can be attributed to the treatment of aerosols and that internal variability of large-scale atmospheric circulation also plays a role. {Atlas.5.6}

In the Alps, snow cover is *very likely* to drastically decrease below 1500-2000m elevation throughout the 21st century. Glaciers in Europe as in all mountain regions worldwide are *likely* to continue to lose mass throughout the 21st century due to temperature increase, and permafrost is *likely* to undergo increasing thaw and degradation. {9.5.1, 12.4.5}

Mean surface wind speeds have decreased in Europe as in many other areas of the Northern Hemisphere (AR5, WGI) (*medium confidence*) and detected tornadoes are increased in Europe, but its trend depends on density of observation. A slightly increased frequency and amplitude of strong winds and extra-tropical storms is projected for Northern and Central Europe (*medium confidence*). Medicanes are projected to decrease (*medium confidence*), but they will have a longer life cycle. There is *medium confidence* that severe convection environments and serial clustering of storms, inducing cumulated losses, in future climate will increase in many areas in Europe under climate projections. {11.7.3, 12.4.5}

Relative sea level rise is *very likely* to continue in Europe contributing to increased coastal flooding in low-lying areas (*high confidence*) and coastline recession along most sandy coasts (*high confidence*). Marine heatwaves and ocean acidification are also expected to increase over the 21st century (*high confidence*). {12.4.5}

The Atlantic coast of Europe is projected to undergo more acidification over the 21st century, as is the Mediterranean (*high confidence*), and surface atmospheric CO_2 will rise with greenhouse gas emissions. Ozone background concentration is *likely* to be augmented up to 5 ppb in areas of Europe from climate change by the middle of the century. {12.4.5}

Table TS.17 shows a summary of changes in CIDs for Europe, derived from a combination of evidence from observed trends and projected future conditions. TS.A1 provides references to the locations in the underlying chapters which support the assessment shown in this table.

[START TABLE TS.17 HERE]

Table TS.17: Summary of confidence in projected directional changes for climatic impact drivers for Europe. The colours represents their aggregate characteristic changes for mid-century RCP8.5 within each AR6 WG I reference region. Dark purple: *high confidence* of increase; light purple: *medium confidence* of increase; white: *low confidence* of increase or decrease; light brown: *medium confidence* of decrease; dark brown: *high confidence* of decrease; grey: CID not broadly relevant. Arrows indicate *medium to high confidence* trends derived from observations and asterisks indicate low, medium and high confidence in attribution of observed changes (which are of the same sign as the projected changes unless stated otherwise).

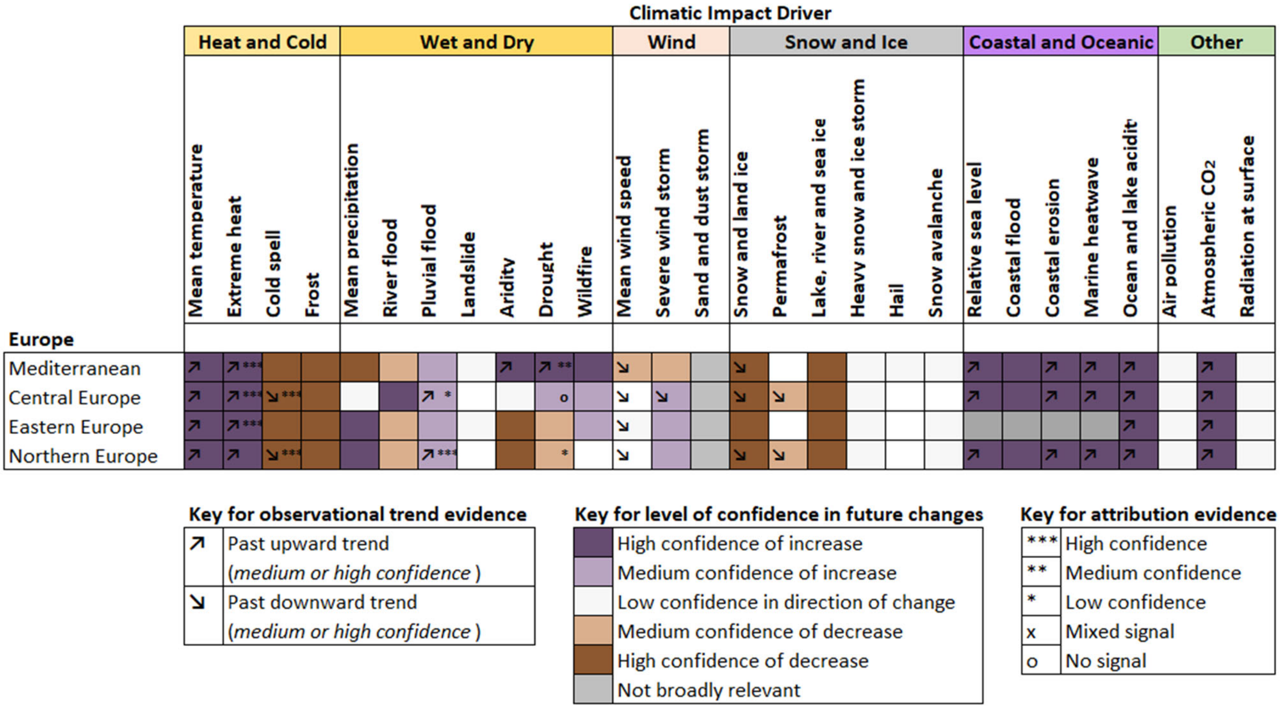

Note: There are several region specific qualifiers/exceptions attached to some of the directions of change/confidence levels indicated above. Please refer to Table.3 of TS.A1 for details.

[END TABLE TS.17 HERE]

TS.4.3.9 North America

Spanning the range of available climate sensitivities in CMIP ensembles is *very likely* critical for producing a representative range of dynamically downscaled projections. This is the case for both temperature and precipitation. The ability of models to reproduce the observed climatology of mean and extreme temperatures and precipitation in North America has *likely* improved compared to AR5. This is aided by continuous model development and the existence of new coordinated modelling initiatives such as NA-CORDEX. {Atlas.5.7, Figure Atlas.47}

There is *high confidence* in observed changes to climatic impact drivers over North America including mean precipitation, pluvial flooding, aridity, wildfire, and coastal flooding. Changes in wet and dry climatic impact drivers accentuate wetter conditions in the North and East and projections indicate drier conditions toward the Southwest with more widespread summertime drought, soil moisture deficits, and wildfire in summertime (*medium confidence*). Declines in snow season and ice are *very likely* in all but the highest elevations and portions of north-central Canada (*high confidence*). {12.4.6}

Climate change is *virtually certain* to shift the balance of temperature toward warming trends and away from cold extremes, with increases in the magnitude, frequency, duration, timing, and spatial extent of heat extremes driving impacts across North America. In most North American areas it is *very likely* that positive trends of warm temperatures are persistent. The observed trends in annual temperature indicate that across near-Arctic latitudes of North America surface air temperature increases are exceptionally pronounced (> 0.5°C per decade) and relatively well-defined as seen in the consistency across multiple data analyses *(high* *confidence*). The subset of CMIP6 results available in the Interactive Atlas project more pronounced warming in most North American regions compared to CMIP5 with this difference clearest in northern regions. {12.4.6, Atlas.5.7, Figure Atlas.45}

Extreme heat episodes in North America have increased in recent decades (*medium evidence, medium agreement*), and are projected to increase with climate change (*high confidence*). There is *robust evidence* and *strong agreement* that cold spells have decreased in recent decades. Cold spells are projected to decrease over North America under climate change, with largest decreases most common in the winter season (*high confidence*). An expansion of the frost-free season is underway and projections indicate a continuation of this trend in the future (*high confidence*). {12.4.6}

Changes in North American wet and dry climatic impact drivers are largely organized by the northeast (wet) to southwest (dry) pattern of mean precipitation change, although pluvial flood increases are more widespread and drought and wildfire can increase even where total precipitation increases (*medium confidence*). In most North American areas it is *likely* that no clear trends in precipitation are present in the period of 1980 to 2014. Since 1980, it is *likely* that precipitation has decreased in the south-western U.S. and north-western Mexico. Nearly everywhere else, there is no significant trend in precipitation. Regions where mean rainfall is *likely* to increase include North America, and mean rainfall is *likely* to decrease in Central America. It is *very likely*, based on global and regional model future projections, that annual mean precipitation will increase over North America north of about 40°N, and it is *likely* that the direction of change of precipitation is uncertain below 40°N. {12.4.6, Atlas.5.7}

There is *high confidence* in observed shifts in the timing of peak streamflow toward higher winter and earlier spring flows in snowmelt-driven basins in Canada and the United States. Regional increases in the frequency and/or in the intensity of heavy rainfall have also been observed in most of the United States (*high confidence*). Results from a large number of regional climate model experiments of varying spatial resolutions underscore that it is *very likely* that precipitation extremes will increase in the future, but also underscore the potential complexities based on model resolution and nature of the specific extreme event considered. Pluvial flooding is projected to increase across North America in future decades, particularly in Canada and Eastern North America (*high confidence*). {11.4.2, 12.4.6, Atlas.5.7}

Among the robust signatures of changes in the water cycle by 2100, there is *high confidence* that increased evaporation due to growing atmospheric water demand will dry soils in the southwestern USA, and there is *medium to high confidence* in pronounced drying in southern North America and Central America. There is *medium confidence* in trends in soil moisture deficits based on observations-driven land surface models, which suggest an increase in the frequency of soil moisture deficits in Northwest North America. There is *medium confidence* that southern North America shows more frequent hydrological droughts. Future aridity is projected to increases in the US Southwest and Mexico, with drier summer soil moisture across much of the continental interior (*medium confidence*). {8.4.1, 11.6.2, 12.4.6}

There is *medium confidence* in projected increases in the frequency and severity of precipitation deficits in Southern North America. All forms of drought are projected to increase across Mexico and meteorological drought decreases in Northwest North America, Northeast Canada, and Eastern North America (*medium confidence*). There is *low confidence* in changes in meteorological drought across Central and Western North America but *medium confidence* in increases for agricultural drought in these regions. Agricultural drought intensity is projected to increase even in places where its frequency decreases (*medium confidence*). There is *robust evidence* and *high agreement* that climatic conditions conducive to wildfire have increased over North America. Climate change drives future increases in North American wildfire weather (*medium confidence*), although shifts in exposure and vulnerability are needed to understand overall wildfire risks. {11.6.5, 12.4.6}

Mean wind speeds are expected to decline over much of North America (*medium confidence*). There is *medium confidence* that tropical cyclone translation speed has slowed detectably over the U.S. since 1900, but *low confidence* for a global signal because of the potential for data heterogeneity. It is *likely* that tornado activity has increased in the United States over the 2000s with a decrease in the number of days per year where tornadoes are observed. An increase in severe storms over Mexico and the Contiguous US is expected (*medium confidence*) although there remains a lack of regional specificity among studies that project an increase in atmospheric conditions conducive to severe storm outbreaks. {11.7.1, 11.7.3, 12.4.6}

Snow and ice climatic impact drivers over North America are characterised by reduction in glaciers and the seasonality of snow and ice formation, as well as shifts in the rain/snow transition line that alters the seasonal and geographic range of snow and ice hazards in the coming decades (*very high confidence*). The seasonal extent of snow cover has *very likely* reduced over North America in recent decades (*robust evidence, high agreement*). Climate change is expected to reduce the total snow amount and the length of the snow cover season over most of North America, with a corresponding decrease in the proportion of total precipitation falling as snow and a reduction in end-of-season snowpack (*high confidence*). There is *high confidence* of a reduction in snowfall where warming shifts precipitation to rain, but an increase where wintertime temperatures are well below freezing, including many higher elevations. It is *virtually certain* that the snow cover will experience a decline over most regions of North America during the 21st century, in terms of water equivalent, extent and annual duration. It is however *very likely* that some high-latitude regions will rather experience an increase in winter snow water equivalent, due to the snowfall increase impact prevailing over the warming impact. Glaciers in North America are expected to continue to lose mass and areal extent (*high confidence*). {12.4.6, Atlas.5.7}

Relative sea level rise is *very likely* to continue in North America (except around the Hudson Bay) contributing to increased coastal flooding in low-lying areas (*high confidence*) and coastline recession along most sandy coasts (*high confidence*). Marine Heatwaves and Ocean acidification are also expected to increase over the 21st century (*high confidence*). There is *medium confidence* that the probability of compound flooding has increased in some locations, including along the US coastline, over the last century. Observations show increasing ocean acidification and surface atmospheric CO_2 (*robust evidence, high agreement*), and it is *virtually certain* that future ocean acidification and atmospheric CO_2 in North America will increase given projected future increases in greenhouse gases {11.8.1, 12.4.6, Cross-Chapter Box 9.1}.

Table TS.18 shows a summary of changes in CIDs for North America, derived from a combination of evidence from observed trends and future projections. TS.A1 provides references to the locations in the underlying chapters which support the assessment shown in this table.

[START TABLE TS.18 HERE]

Table TS.18: Summary of confidence in projected directional changes for climatic impact drivers for North America. The colours represents their aggregate characteristic changes for mid-century RCP8.5 within each AR6 WG I reference region. Dark purple: *high confidence* of increase; light purple: *medium confidence* of increase; white: *low confidence* of increase or decrease; light brown: *medium confidence* of decrease; dark brown: *high confidence* of decrease; grey: CID not broadly relevant. Arrows indicate *medium to high confidence* trends derived from observations and asterisks indicate low, medium and high confidence in attribution of observed changes (which are of the same sign as the projected changes unless stated otherwise).

Climatic Impact Driver

North America	Heat and Cold				Wet and Dry							Wind			Snow and Ice						Coastal and Oceanic					Other		
	Mean temperature	Extreme heat	Cold spell	Frost	Mean precipitation	River flood	Pluvial flood	Landslide	Aridity	Drought	Wildfire	Mean wind speed	Severe wind storm	Sand and dust storm	Snow and land ice	Permafrost	Lake, river and sea ice	Heavy snow and ice storm	Hail	Snow avalanche	Relative sea level	Coastal flood	Coastal erosion	Marine heatwave	Ocean and lake acidity	Air pollution	Atmospheric CO_2	Radiation at surface
North Central America	↗	↗ *	↘							o	↗ **	↘		↗							↗	↗	↗	↗	↗		↗	
Western North America	↗ **	↗	↘			*	↗ **			**	↗ *	↘			↘		↘				↗	↗	↗	↗	↗		↗	
Central North America	↗ **	↗ **	↘ ***				↗ **			↗ **	*	↘			↘		↘				↗	↗	↗	↗	↗		↗	
Eastern North America	↗ **	↗ **	↘ ***				↗ **			↘ **		↘			↘ *		↘				↗	↗	↗	↗	↗		↗	
Northeastern Canada	↗	↗ **	**	↘			↗					↘			↘	↘	↘					↗	↗		↗		↗	
Northwest North America	↗	↗ **	↘ **	↘			↗ *			↘	*	↘			↘	↘	↘				↗	↗	↗	↗	↗		↗	

Key for observational trend evidence

↗	Past upward trend (*medium or high confidence*)
↘	Past downward trend (*medium or high confidence*)

Key for level of confidence in future changes

High confidence of increase
Medium confidence of increase
Low confidence in direction of change
Medium confidence of decrease
High confidence of decrease
Not broadly relevant

Key for attribution evidence

***	High confidence
**	Medium confidence
*	Low confidence
x	Mixed signal
o	No signal

Note: There are several region specific qualifiers/exceptions attached to some of the directions of change/confidence levels indicated above. Please refer to Table.3 of TS.A1 for details.

[END TABLE TS.18 HERE]

TS.4.3.10 Small Islands

Since IPCC AR5, there is *robust evidence* of significant warming trends in the small islands, such as those in the western Pacific and the Caribbean, particularly over the latter half of the 20th century. It is *very likely* that the tropical Western Pacific has warmed by 0.15-0.18°C per decade over the period 1953 to 2011 whilst daily maximum and minimum temperatures in the Caribbean region have increased by 0.19°C and 0.28°C per decade respectively during 1961 to 2010. {12.4.7, Atlas.5.8}

Western Pacific islands show warming trends, mostly significant, for all temperature extreme indices (*high confidence*). On the other hand, there is *medium confidence* in the warmer conditions over the north and cooler conditions over the eastern Caribbean. {Table 11.6, Table 11.7}

There are few significant trends in precipitation in these regions though some locations in the Caribbean have detectable decreasing trends, in part attributable to anthropogenic forcings (*medium confidence*). There is *medium confidence* in the negative trends in R95p over the northern and eastern Caribbean, as well as in positive trends in consecutive dry days over some locations in the northern and eastern Caribbean. Western Pacific Islands show decreases in both total and extreme precipitation (southwestern French Polynesia and the southern subtropics) (*low confidence*). {Atlas.5.8, Table 11.6, Table 11.7}

There is *limited evidence* and *low agreement* for the cause of the drying trend over the Caribbean in mid-summer since 1950 and whether this trend is mainly caused by either decadal-scale internal variability or anthropogenic forcing. Climate change will modify multiple climatic impact drivers in small islands in all ocean basins, most notably climatic impact drivers related to heat, dryness, and coastal and oceanic impacts. {10.4.1, 12.4.7}

Warming and heat stress are *very likely* to continue over the 21st century with *high confidence* of warming over small islands even at 1.5°C global warming levels. There is *high confidence* in the increase in the frequency of warm extremes, and a decrease in the frequency of cold extremes in the Caribbean. Massive heatwave events are projected in the Caribbean at the end of the 21st century (*high confidence*). {12.4.7, Atlas 5.8, Table 11.7}

Projections in rainfall indicate strong spatial variability across the small islands. Small island regions in the Western and equatorial Pacific, and Southern Ocean are projected to be wetter in the future but drier over parts of the Caribbean, central and eastern Pacific, Atlantic Ocean, and Indian Ocean by mid-21st century under SSP5-8.5 (*medium confidence*). There is *low confidence* in projected declines in R10mm, RX1day and R95p over central Caribbean with increases for northern Caribbean, as well as increases in consecutive dry days over most stations, with decreases over eastern Caribbean and Bahamas. Projected decreases in rainfall, groundwater extraction and saltwater intrusion associated with sea level rise will increase water stress in these areas (*medium confidence*). {12.4.7, Atlas.5.8, Table 11.7, Box 11.5}

Limited availability of literature prohibits a robust assessment on future changes in river flooding, landslides and fire weather in the small islands (*low confidence*). {12.4.7}

Projected changes in tropical cyclone track, frequency, intensity and associated rainfall can increase wind and coastal hazards faced by small islands, especially when compounded by rising sea levels, but there is spatial variability in the impacts (*medium confidence*). {12.4.7, Box 11.5}

The rise in regional sea levels is *very likely* to continue throughout the 21st century, increasing the coastal hazards faced by small islands. Increasing extreme sea levels will increase the frequency and magnitude of coastal floods at many locations (*high confidence*).There *is high confidence* that coastal erosion will increase along sandy coasts in small islands. {12.4.7, Box 11.5}

Table TS.19 shows a summary of changes in CIDs for small islands, derived from a combination of evidence from observed trends and projected future conditions. TS.A1 provides references to the locations in the underlying chapters which support the assessment shown in this table.

[START TABLE TS.19 HERE]

Table TS.19: Summary of confidence in projected directional changes for climatic impact drivers for Small Islands regions. The colours represents their aggregate characteristic changes for mid-century RCP8.5 within each AR6 WG I reference region. Dark purple: *high confidence* of increase; light purple: *medium confidence* of increase; white: *low confidence* of increase or decrease; light brown: *medium confidence* of decrease; dark brown: *high confidence* of decrease; grey: CID not broadly relevant. Arrows indicate *medium to high confidence* trends derived from observations and asterisks indicate low, medium and high confidence in attribution of observed changes (which are of the same sign as the projected changes unless stated otherwise).

Climatic Impact Driver

	Heat and Cold				Wet and Dry							Wind		
Small Islands	Mean temperature	Extreme heat	Cold spell	Frost	Mean precipitation	River flood	Pluvial flood	Landslide	Aridity	Drought	Wildfire	Mean wind speed	Severe wind storm	Sand and dust storm
Caribbean	High confidence of increase ↗	High confidence of increase	Not broadly relevant	Not broadly relevant	Medium confidence of decrease **	Low confidence	Medium confidence of decrease ↘	Low confidence	Medium confidence of increase	Medium confidence of increase ↗	Low confidence	Low confidence	Medium confidence of decrease **	Not broadly relevant
Pacific	High confidence of increase ↗	High confidence of increase	Not broadly relevant	Not broadly relevant	Medium confidence of increase	Low confidence	Medium confidence of increase	Low confidence	Medium confidence of decrease	Medium confidence of decrease	Low confidence	Low confidence	Medium confidence of increase	Not broadly relevant

	Snow and Ice						Coastal and Oceanic					Other		
Small Islands	Snow and land ice	Permafrost	Lake, river and sea ice	Heavy snow and ice storm	Hail	Snow avalanche	Relative sea level	Coastal flood	Coastal erosion	Marine heatwave	Ocean and lake acidity	Air pollution	Atmospheric CO_2	Radiation at surface
Caribbean	Not broadly relevant	Not broadly relevant	Not broadly relevant	Not broadly relevant	Not broadly relevant	Not broadly relevant	High confidence of increase ↗	High confidence of increase	High confidence of increase ↗	High confidence of increase ↗	High confidence of increase ↗	Low confidence	High confidence of increase ↗	Low confidence
Pacific	Not broadly relevant	Not broadly relevant	Not broadly relevant	Not broadly relevant	Not broadly relevant	Not broadly relevant	High confidence of increase ↗	High confidence of increase	High confidence of increase ↗	High confidence of increase ↗	High confidence of increase ↗	Low confidence	High confidence of increase ↗	Low confidence

Key for observational trend evidence

↗	Past upward trend (*medium or high confidence*)
↘	Past downward trend (*medium or high confidence*)

Key for level of confidence in future changes

High confidence of increase
Medium confidence of increase
Low confidence in direction of change
Medium confidence of decrease
High confidence of decrease
Not broadly relevant

Key for attribution evidence

***	High confidence
**	Medium confidence
*	Low confidence
x	Mixed signal
o	No signal

Note: There are several region specific qualifiers/exceptions attached to some of the directions of change/confidence levels indicated above. Please refer to Table.3 of TS.A1 for details.

[END TABLE TS.19 HERE]

TS.4.3.11 Polar regions

Many aspects of the cryosphere either have seen significant changes in the recent past and/or will see them during the 21st century (*high confidence*). Climate change has caused and will continue to induce enhanced warming trends, heat-related extremes, and reductions in snow cover, permafrost glaciers, and sea ice in the Arctic (*high confidence*). Warming trends are also occurring over the Antarctic ice sheet (*medium confidence*) but observations are sparse. The projected warming trends over high latitude regions is much stronger in CMIP6 than in CMIP5. {TS2.4.1, TS2.4.2, 2.3.2, Atlas 5.9, Cross-Chapter Box 2.1, Cross-Chapter Box 2.4}

Global water cycle enhancement in polar regions is projected to manifest as increased precipitation and higher river flood potential (*high confidence*). Higher relative sea levels and loss of coastal sea ice increase coastal flooding and coastal erosion (*high confidence*), although land uplift in some regions counteracts those changes. There is *high confidence* in decreasing permafrost and seasonal duration and extent of snow cover. A decrease in surface snow cover in polar regions is only partially compensated by current and projected increase in precipitation, with the proportion of precipitation falling as rain increasing. {4.5.1, 4.6.1, 8.2.3, 8.4.1, 8.5.1, 9.5.3, 12.4.9, Atlas 5.9}

Satellite altimetry data show that relative sea levels (with glacial isostatic adjustment) are rising in Arctic Europe and Northwest North America, declining in Arctic Northeastern Canada and no clear trend in Greenland and Arctic Russia. Projections indicate *high confidence* in future rises in relative sea level for all Arctic regions other than areas of substantial land uplift in Northeastern Canada, the west coast of Greenland, and narrow portions of West Antarctica. Higher sea levels and reduced coastal sea ice protection will increase future extreme sea levels and coastal erosion along Arctic coastlines, with erosion also accelerated by subsurface permafrost thaw (*high confidence*). Projections show increases in marine heatwave intensity, frequency, and duration will be larger over the Arctic Ocean than mid-latitude ocean (*high confidence*), with MHW days increasing 50-fold when global warming is 3.5°C in response to mean ocean warming and sea ice loss, with the smallest corresponding increase (~doubling) in the Southern Ocean around Antarctic {12.4.9, 12.9.4}.

TS.4.3.11.1 Antarctica

The annual mean surface air temperature in West Antarctica *likely* increased by up to 0.3°C per decade from 1958 to 2012, with the largest warming observed in austral winter (0.28 ± 0.27°C per decade) and spring (0.39 ± 0.21°C per decade) (*medium confidence* due to *limited evidence*). The Antarctic Peninsula *very likely* experienced the fastest warming with a rate of up to 0.5°C per decade since around 1950. East Antarctica *likely* showed no significant trends in temperature over the same period. {Atlas.5.9}

Since direct precipitation measurements in Antarctica are sparse, observations of surface mass balance (net snow accumulation on the surface) are considered as a proxy for precipitation. The surface mass balance in West Antarctica showed a significant increase in the eastern area and significant decrease in the west (respectively 5 to 15 mm water equivalent and -5 to -15 mm water equivalent per decade from 1957 to 2000). The Antarctic Peninsula has *very likely* experienced an increase in surface mass balance over the 20th century (beginning in about 1930 and accelerating during the 1990s). The surface mass balance in East Antarctica showed strong interannual variability over recent decades, masking any possible existing trends (*medium confidence* due to limited observations). It is *likely* that the increased surface mass balance has slightly compensated for the total Antarctic ice-sheet mass loss. {Atlas.5.9}

Under low-, intermediate- or high-emission scenarios during the 21st century, both West and East Antarctica will *likely* experience higher annual mean surface air temperatures and increased precipitation, which will have a dominant influence on future changes in the surface mass balance. The projected Antarctic mean increase in temperature and precipitation (median for CMIP6 models compared to the 1986–2005 baseline period) will *likely* be up to 1°C and 7% respectively by 2050, and 1.4°C and 7% respectively by 2100 under SSP1-2.6. Up to 2°C and 12% respectively by 2050, and 5°C and 30% respectively by 2100 are projected under SSP5-8.5. Although the projected increases in temperature and precipitation are largest over the interior of Antarctica, it is *likely* that the warming around the coastal margins by the end of the century under the high-emission scenario will lead to enhanced surface melting that has been historically leading to the ice-shelf collapse. {Atlas.5.9.}

The mass balance has not changed significantly across eastern Antarctica since the onset of modern measurements in the early 1990s, but has decreased rapidly in western Antarctica, accelerating 3-fold since the 1990s (*medium confidence*). . Antarctic sea ice has experienced interannual and decadal variability but no significant trend during the period of continuous satellite observations (1979-2018) (very *high confidence*). {2.3.2, 9.3.2, 9.4.2, Cross-Chapter Box 2.1, Cross-Chapter Box 2.4}

TS.4.3.11.2 Arctic

It is *very likely* that the Arctic has warmed at more than twice the global rate over the past 50 years. A variety of factors all contribute to this Arctic amplification, including positive surface-albedo and lapse-rate feedbacks as well as increases in poleward atmospheric latent heat transport and ocean heat transport. {7.4.2, Atlas.5.9}

Arctic annual precipitation has *likely* increased with the highest increases during the cold season. New attribution studies find anthropogenic influence in the increase of high latitude precipitation over the Northern Hemisphere. It is *likely* that the frequency of rainfall increased over the Arctic by 2.7–5.4% over the 2000–2016 period with more frequent rainfall events being reported for northern Europe and Svalbard. {3.3.2, 3.3.3, Atlas.5.9.2}

Reductions in spring snow cover extent have occurred across the Northern Hemisphere since at least 1978 (very *high confidence*). {2.3.2, Cross-Chapter Box 2.1, Cross-Chapter Box 2.4}

CMIP6 results show *likely* higher Arctic annual mean temperatures and precipitation compared to CMIP5, reaching 12.5 ± 2.9°C and 54.7 ± 13.7 mm over the 2081–2100 period (with respect to a 1995–2014 baseline) under the SSP5/RCP8.5 scenario, and 4.0 ± 1.4°C and 17.3 ± 6.6 mm under the SSP1/RCP2.6 scenario. Rain is projected to become the dominant form of precipitation in the Arctic region by the end of the 21st century due to projected higher temperatures (*high confidence*). Mid-winter snowpack extent increases in some tundra and high-elevation locations given sufficient cold and higher precipitation totals (*medium confidence*), but overall snow extent and duration are projected to continue recent declines (*high confidence*). {12.4.9, Atlas.5.9}

It is *virtually certain* that snow cover will experience a decline over most regions of North America during the 21st century, in terms of water equivalent, extent and annual duration.

There is high confidence that large polar mean warming will drive increases in local heat extremes as well as continuing declines in the magnitude and frequency of cold extremes, although dynamical effects can still bring cold air outbreaks over the Arctic. {12.4.9}

Observations and model projections indicate *high confidence* in increasing Arctic river runoff in response to increasing total precipitation, with changes in temperature leading to a shift toward earlier meltwater flooding. Higher Arctic precipitable water totals are also connected with observed increases in heavy precipitation (*high confidence*). Recent decades have seen a general decrease in aridity (high confidence) with increased moisture transport into the Arctic leading to higher precipitation, humidity and streamflow with a corresponding decrease in dry days. Fire weather index increases have already exceeded historical variability envelopes in boreal forests of Arctic Europe, and will emerge in portions of Arctic Russia and Northeast North America by the 2040s (*medium confidence*). Trends toward more frequent wildfires in tundra regions are expected to continue driven in particular by increasing potential evapotranspiration and changes in vegetation (*high confidence*). {12.4.9}

Arctic sea ice thickness, extent, and average age have significantly decreased over the past four decades with largest declines in September (when sea ice is at an annual minimum) (*high confidence*). Future declines in Arctic sea ice are *virtually certain*, although there is *low confidence* in declines of Antarctic sea ice given dynamical processes in the Southern Ocean and the recovery of stratospheric ozone. There is *high confidence* in observations of significant declines in seasonal ice cover thickness and duration over most Arctic lakes, with many lakes projected to lose more than month of ice cover by mid-century (*medium confidence*). {9.3.1, 12.4.9}

Arctic sea ice extent is projected to reduce during summer and open new maritime transport routes between North America, Europe, Russia and China but could affect impact marine ecosystem by pollution and short live climate forcers (*medium confidence*). Future ocean warming will assist the development of hypoxic zones, or minimal oxygen zones. {12.4.8}

Table TS.20 shows a summary of changes in CIDs for polar regions, derived from a combination of evidence from observed trends and projected future conditions. TS.A 1 provides references to the locations in the underlying chapters which support the assessment shown in this table.

[START TABLE TS.20 HERE]

Table TS.20: Summary of confidence in projected directional changes for climatic impact drivers for Polar regions. The colours represents their aggregate characteristic changes for mid-century RCP8.5 within each AR6 WG I reference region. Dark purple: *high confidence* of increase; light purple: *medium confidence* of increase; white: *low confidence* of increase or decrease; light brown: *medium confidence* of decrease; dark brown: *high confidence* of decrease; grey: CID not broadly relevant. Arrows indicate *medium to high confidence* trends derived from observations and asterisks indicate low, medium and high confidence in attribution of observed changes (which are of the same sign as the projected changes unless stated otherwise).

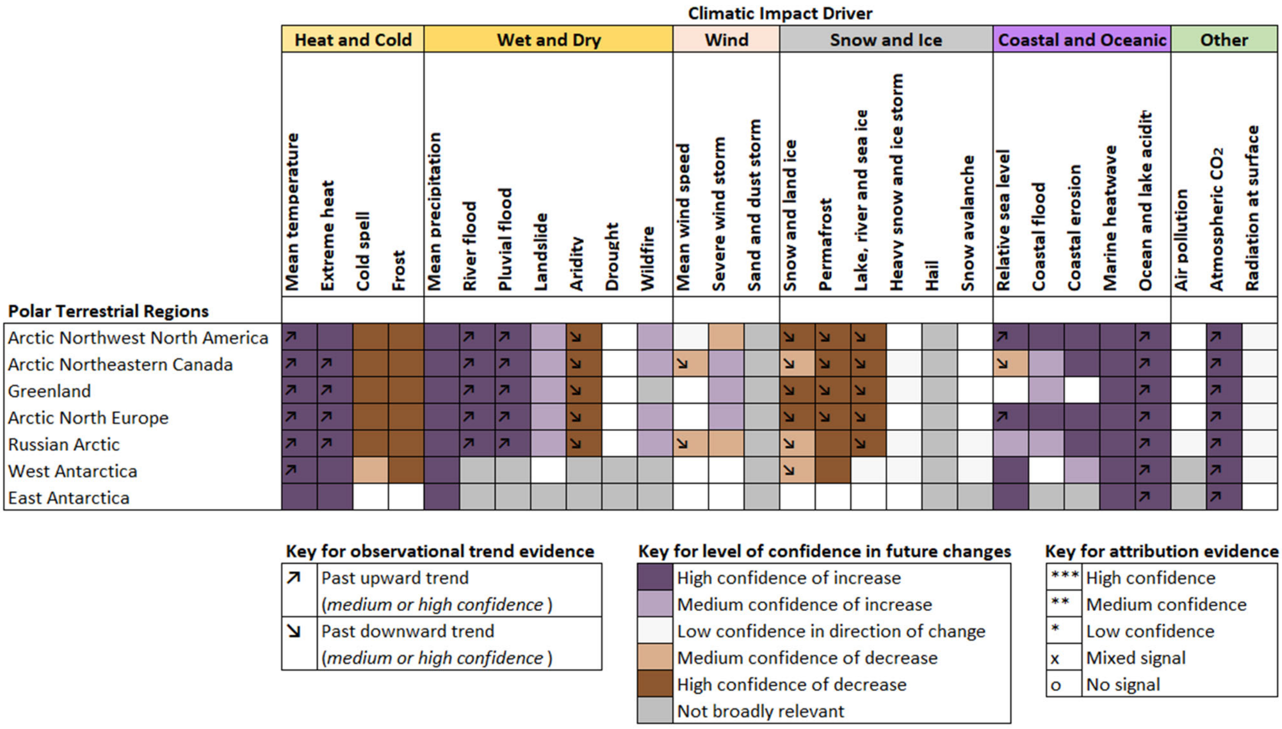

Note: There are several region specific qualifiers/exceptions attached to some of the directions of change/confidence levels indicated above. Please refer to Table.3 of TS.A1 for details.

[END TABLE TS.20 HERE]

TS.4.3.12 Open and deep ocean

While global average ocean surface temperature has increased about 0.05°C per decade over 1900-2017, portions of the Eastern Pacific Ocean, North Atlantic Ocean, and Southern Ocean have warmed slower than the average or even cooled due to regional ocean dynamics. Marine heatwaves have become more frequent (*high confidence*) and longer in duration (*medium confidence*) since 1982. Marine heatwaves are *very likely* to increase in frequency, duration, spatial extent and intensity in all ocean basins, but with distinct spatial magnitudes in the coming decades. The largest increase in marine heatwaves is projected in the tropics and in the Arctic ocean (*high confidence)* and smallest increase in the Southern Ocean (*medium confidence*), and there is *high confidence* that marine heatwave conditions conducive to coral bleaching events will become more intense and frequent in the future. {12.4.8, Cross-Chapter Box.9.1}

There is *high confidence* that sea surface temperature will increase regionally in the ocean throughout the 21st century, with the exception of slower or no warming in the subpolar North Atlantic. Climate model projections show that the largest part of global ocean heat uptake occurs in the Southern Ocean, due downward transport of heat by the large-scale circulation. More generally, the regional pattern of future warming at depth tends to follow known water mass pathways from surface formation regions to depth, primarily in the North Atlantic and Southern Ocean. {9.2.2}

During 1950-2018 regions of high salinity where evaporation dominates in the subtropics have become more saline, while regions of low salinity where precipitation dominates in the tropics and high-latitudes have become fresher, at the near-surface (*virtually certain*) and subsurface (*very likely*). Regionally, multidecadal freshening has been observed since the 1950s in the North Pacific subpolar gyre, Pacific and Indian intermediate waters, Pacific Ocean, Greenland Seas, and Southern Ocean. Future projections reproduce the fresh gets fresher, salty gets saltier paradigm on large scales (*high confidence*), including complex regional changes resulting in stronger freshening of the Pacific, Indian and Southern Ocean, with a saltier subtropical Atlantic (*medium confidence*). {2.3.3, 9.2.2}
It is *virtually certain* (*robust evidence, high agreement*) that ocean pH has consistently decreased over the past few decades even as regional rates vary. Ocean acidification is spreading downward into the ocean interior over time, having already reached depths surpassing 2000 meters. {5.3.2, 5.3.3}

Consistent with the current observed trend, climate models project that upper ocean stratification will continue to increase in the 21st century under increased radiative forcing (*high confidence*), primarily due to increased surface temperature and high-latitude surface freshening. There is *high confidence* that upper ocean stratification will continue to increase in the tropical and North Atlantic, Southern, North Pacific Ocean. There is *medium confidence* that the abysses are becoming less stratified due to the changes in temperature and salinity. {9.2.1, 12.4.8}

There is *medium confidence* that the average location where tropical cyclones reach their peak wind-intensity will migrate poleward in the western North Pacific Ocean as the tropics expand with warming. Future increases of storm waves are projected in the north Pacific and south Indian Ocean (*medium confidence*). {11.7.1, 12.4.8, Cross-Chapter Box 9.1}.

Table TS.21 shows a summary of changes in CIDs for ocean basins, derived from a combination of evidence from observed trends and projected future conditions. TS.A 1 provides references to the locations in the underlying chapters which support the assessment shown in this table.

[START TABLE TS.21 HERE]

Table TS.21: Summary of confidence in projected directional changes for climatic impact drivers for Ocean regions. The colours represents their aggregate characteristic changes for mid-century RCP8.5 within each AR6 WG I reference region. Dark purple: *high confidence* of increase; light purple: *medium confidence* of increase; white: *low confidence* of increase or decrease; light brown: *medium confidence* of decrease; dark brown: *high confidence* of decrease; grey: CID not broadly relevant. Arrows indicate *medium to high confidence* trends derived from observations and asterisks indicate low, medium and high confidence in attribution of observed changes (which are of the same sign as the projected changes unless stated otherwise).

Climatic Impact Driver

Oceans	Mean ocean temperature	Marine heatwave	Severe storm and waves	Sea ice	Sub-sea permafrost	Ocean acidification	Dissolved oxygen	Salinity
Arctic Ocean	↗			↘		↗		
South Pacific Ocean	↗	↗				↗		
Equatorial Pacific Ocean	↗	↗				↗		
North Pacific Ocean	↗	↗				↗		
South Atlantic Ocean	↗	↗				↗		
Equatorial Atlantic Ocean	↗	↗				↗		
North Atlantic Ocean	↗	↗				↗		
Equatorial Indian Ocean	↗	↗				↗		
South Indian Ocean	↗	↗				↗		
Arabian Sea	↗	↗				↗		
Bengal Gulf	↗	↗				↗		

Key for observational trend evidence

↗	Past upward trend (*medium or high confidence*)
↘	Past downward trend (*medium or high confidence*)

Key for level of confidence in future changes

High confidence of increase
Medium confidence of increase
Low confidence in direction of change
Medium confidence of decrease
High confidence of decrease
Not broadly relevant

Key for attribution evidence

***	High confidence
**	Medium confidence
*	Low confidence
x	Mixed signal
o	No signal

[END TABLE TS.21 HERE]

TS.4.3.13 Typological domains

TS.4.3.13.1 Mountain regions

Mountains cover about 30% of the land areas on earth (not counting the Antarctica continent) and are delivering a number of vital services to humanity. The change in the mountain climate is therefore of key relevance to society. {12.4.10}

There is *very high confidence* that precipitation measurements, especially of solid precipitation, in mountainous areas are strongly affected by the gauge location and setup, gridding procedure, interpolation methods and statistical homogenization. In mountainous areas, both the scarcity of observation stations and the decline of observation sites after the collapse of the former Soviet Union in 1991 *very likely* increase the uncertainty of the long-term temperature and precipitation estimates. It is *virtually certain* that uncertainties related to long-term warming estimates at regional scale are reduced using statistical homogenization methods. {10.2.2, 10.6.2, 10.6.3, 10.6.4, Cross-Chapter-Box 10.3, Atlas.5.3.2}

There is *high confidence* on elevation-dependent warming in most of the mountain ranges but field measurements are extremely limited at high elevations. Mountain permafrost has been lost and has warmed over recent decades (*medium confidence*). {9.5.2, 10.2.2, Cross-Chapter Box 10.3}

Regional models simulate colder temperatures than observed over mountainous and high plateau regions including the Himalayas and Plateau of Tibet (*limited evidence*, *high agreement*). Mean temperature bias of RCMs is within ± 3°C over West Asia (*high confidence*), but RCMs have a tendency to overestimate precipitation amounts in almost all parts of the region (*low confidence*).} Future temperature changes over HKH indicated projected by the CORDEX multi-RCM experiments provided additional topographic detail for the hilly sub-region within the Karakoram and north-western Himalaya, thereby increasing the confidence in the projections. {Atlas.5.3, Atlas.5.10}

The annual mean surface air temperature has increased significantly in the HKH at a rate of about 0.1°C per decade during 1901–2014, with a larger increase of more than 0.2°C per decade in the Tibetan Plateau (TP) and southern Pakistan. The observed annual and winter mean temperatures at high elevation sites (>2,000 m) of the eastern TP have increased at a rate of about 0.42°C per decade and 0.61°C per decade respectively during 1961–2006, while the low-elevation sites (<500 m) have warmed at a rate of about 0.2°C per decade during the same period. Minimum temperatures are increasing more than maximum temperatures with high values for winter temperatures (*high confidence*). {Atlas.5.10}

Glacier mass loss since the last decades of the 20th century cannot be explained without human induced warming (*high confidence*). Globally, glaciers are not in equilibrium with current climate and will diminish even if climate stabilizes (*very high confidence*).Glaciers in all mountain regions worldwide are *likely* to continue to lose mass throughout the 21st century due to temperature increase, and permafrost is *likely* to undergo increasing thaw and degradation. Under continued warming those mountain ranges characterized by small glaciers, such as the European Alps and low latitude mountains (Tropical Andes, Mountain areas of Africa, will lose most or all glaciers by 2100 (*high confidence*). The glacier mass is *likely* to decrease considerably under RCP 4.5 and 8.5 scenarios while the snowmelt is higher in central and eastern Himalaya than western Himalaya. Karakoram glaciers are in approximately balanced state, however elevation dependent warming is evident over the HKH region (*high confidence*). In High Mountain of Asia glaciers will continue to melt and permafrost to thaw (*high confidence*), and together with extreme precipitation, will inducing cascading impacts in river hydrology and mountain slopes stability. There is *high confidence* that the human induced retreat of the springtime snow cover and enhanced melting of glaciers has already contributed to changes in streamflow seasonality in high-latitude and mountain watersheds. Heavy precipitation events will intensify in future, which may cause more Glacial Lake Outburst Flood (GLOF events) (*medium confidence*). {8.3.1, 9.5.1, 9.6.3, 12.4.2, 12.4.4, 12.4.5, Atlas.5.10, Box 8.2}

Further global warming will lead to near-surface permafrost volume loss (*high confidence*). There is *high confidence* in changes in mountain permafrost with high spatial variability given local snow and temperature changes. Snow avalanche hazards generally decrease at low elevations given lower snowpack even as high elevations are increasingly susceptible to wet snow avalanches *(medium confidence).* {9.5.2, 12.4.6}

TS.4.3.13.2 Monsoons

Global monsoon intensity and precipitation have *likely* increased, being dominated by Northern Hemisphere summer trends (*medium confidence*). The South Asian monsoon has shown contrasting behaviour over India and Pakistan (in the monsoon dominated regions), with a strengthening trend over the core monsoon zone in Pakistan (*low confidence*) and weakening trend over central north India (*high confidence*). Vertically Integrated (0–500 hPa) Meridional Moisture Transport and extra-tropic connections are mainly forming this dipole like mechanisms since the 1950s. {2.3.1, Atlas.5.3}

It is *very likely* that Northern Hemispheric anthropogenic aerosols have caused a weakening of the regional monsoon circulations in South Asia, East Asia and West Africa during the second half of the 20th century, thereby offsetting a strengthening monsoon precipitation in response to GHG-induced warming. Areas in South America and Australia have experienced a detectable influence of anthropogenic aerosols on precipitation patterns. Remote effects far from emission regions have resulted from large-scale circulation responses to spatially heterogeneous changes in surface temperatures (*high confidence*). There is *medium confidence* that the recent partial recovery and enhanced intensity of monsoon precipitation over West Africa is related to the growing influence of anthropogenic greenhouse gases with additional contribution from the transition from a dimming to a brightening overall radiative effect of anthropogenic aerosols, emitted largely from North America and Europe. There is *very high confidence* (*robust evidence* and *high agreement*) that patterns of 20th century surface temperature variability have caused the Sahel drought and subsequent recovery, and that Saharan warming has contributed to this recovery. There is *medium confidence* (*robust evidence* and *medium agreement*) that patterns of SST variability are themselves driven by anthropogenic emissions. {8.3.1, 8.3.2, Box 8.1}

In response to greenhouse-gas-induced warming, it is *very likely* that global land monsoon precipitation will increase, particularly in the Northern Hemisphere, although Northern Hemisphere monsoon circulation will weaken (*high confidence*). In the long-term, monsoon rainfall change will feature a robust north-south asymmetry characterised by a stronger increase in the Northern Hemisphere than in the Southern Hemisphere and an east-west asymmetry characterised by enhanced Asian-African monsoons and weakened North American monsoon (*high confidence*). The near-term changes in global monsoon precipitation and circulation will be affected by natural internal variability such as Atlantic Multidecadal Variability and Interdecadal Pacific Oscillation (*medium confidence*). {4.4.1, 4.5.1, 8.4.1}

It is *virtually certain* that the pattern of projected precipitation changes will exhibit substantial regional and seasonal contrast in response to global warming (*high confidence*). Precipitation will increase in large parts of monsoon regions, tropics and high latitudes but decrease over the Mediterranean and large parts of the subtropics in response to greenhouse-gas-induced warming (*high confidence*). Interannual variability of precipitation over many land regions will be strengthened in a warmer world (*medium confidence*). {4.5.1, 4.6.1, 8.4.1}

For the North American monsoon, projections indicate a decrease in precipitation, whereas increased monsoon rainfall is projected over South and Southeast Asia, East Asia and West Africa with a statistically significant increase (decrease) of rainfall in central-eastern (western) Sahel (*medium confidence*). For the South American monsoon, the CMIP6 projections do not indicate a clear increase in precipitation during the 21st century. Changes in monsoons are *likely* to result in increased precipitation in northern China, increases during the summer monsoon but decreases during the winter monsoon in South Asia (*medium to high confidence*). There is *medium confidence* that a delayed wet season in the Sahel is driven by intensifying Sahara heat low, but *low confidence* in the projected changes in the wet season onset and cessation in many other tropical regions. {8.2.1, 8.4.2, Atlas 5.3}

The contrast between long-term future increases in Indian monsoon rainfall and declining rainfall in the observational record can be explained using multiple lines of evidence. The observational record and future projections are not contradictory since the trends are attributed to different mechanisms (aerosols and greenhouse gases, respectively). The long-term future changes are generally consistent across global (low and high resolution) and regional climate models, and supported by theoretical arguments; furthermore, while there are subtle differences found in paleoclimate analogues of the future climate (the mid-Holocene), different physical mechanisms at play suggest that paleoclimate evidence does not reduce confidence in the future projections. {10.6.3}

Uncertainties and past non-linear or abrupt responses of hydrologic systems mean that low probability, high impact changes to the water cycle cannot be excluded. There is evidence of abrupt change in some high emissions projections, but there is no overall consistency regarding the magnitude, speed, and timing of such changes in currently available model simulations. There is *low confidence* that abrupt changes in aridification and rainfall will occur by 2100, although the possibility of abrupt events cannot be ruled out. The paleoclimate record shows that a collapse in Atlantic Meridional Overturning Circulation (AMOC) can cause abrupt and large-magnitude shifts in the water cycle (*high confidence*) such as a southward shift in the Intertropical Convergence Zone, weakening of the African and Asian monsoons and strengthening of Southern Hemisphere monsoons. {8.6.1}

TS.4.3.13.3 Other typological domains

Biodiversity hotspots are located around the world. Heat, drought and length of dry season, wildfire weather, sea surface temperature and deoxygenation are relevant drivers to terrestrial and freshwater ecosystems, and have specific evolutions with marked increasing trends. There is *medium confidence* (*limited evidence, high agreement*) that in several regions the length of the dry season has already increased and is projected to further increase, such as Mediterranean areas, Amazonia and sub-Saharan areas. An extension both in length and space in the fire weather season is observed and probable in all future scenarios (*low confidence*, *limited evidence*). Ocean acidification and oxygen reduction are also major increasing hazards for marine biodiversity hotspots, and sea level change and floods have the potential to impact hotspots of biodiversity, with different effects depending on the region {5.3.2, 5.3.3, 12.4.8, 12.4.10}.

Desert and semi-arid areas are exposed to specific climatic impact drivers such as extreme heat, drought and dust storms. Heat hazards are *very likely* increasing in all future climate scenarios, but other climatic impact drivers future evolution remains uncertain. Despite large uncertainties on future changes in rainfall in arid and semi-arid zones, climate simulations show that the area of global drylands is projected to expand by ~10% by 2100 compared to 1961-1990 under high greenhouse gas emission scenario (*medium confidence*). It is *likely* that heat stress will be much more intense by the end of the century in many areas under all scenarios, such as arid zones in Asia, Australia and Africa, with consequences on labour productivity with respect to very high wet bulb temperature. {11.9, 12.4.10, Figure 12.5}

Tropical forests are mostly exposed to heat, drought and lengthening of dry seasons, fire weather and CO_2 increase climatic impact drivers. Patterns and amplitudes of heat hazard changes depend on thresholds and regions, but there is *medium confidence* that tropical forests will undergo an increase in most of these phenomena. There is *medium confidence* (*limited evidence*, *high agreement*) that in several tropical-forest regions the dry season length has increased (Amazonia, West Africa). There is generally *low confidence* in future projections of general fire weather risk evolution in tropical forests and evolutions depend on the region. {12.4.10}

[START BOX TS.8 HERE]

Box TS.8: Urban box

Observed and projected climate in cities

Urban areas extend typically from a few kilometres to hundreds of kilometres, but their internal features influence the air flow at scales down to the street-canyon scale of a few meters. Urban centres and cities are often several degrees warmer than the surrounding rural area due to what is known as the urban heat island effect. Urban heat islands have been observed to exacerbate extreme heat in large cities around the world, with effects often more evident at night time. Urbanization has also exacerbated the effects of global warming in cities (*high confidence*). Cities can also experience phenomena such as the urban dryness island (referring to conditions where lower relative humidity is observed in cities relative to nearby rural locations) and the urban wind island (where cities experience slower wind speeds compared to their adjacent suburbs and countryside). This box presents information about observed climate trends, extreme events, and climate change projection for cities. {11.3, Box 10.2}

At the city scale, there is *very high confidence* (r*obust evidence and high agreement*) that a percentage of the observed warming trend is linked to historical urbanization in rapidly industrialized countries. There is *very high confidence* that annual-mean maximum temperature is less affected by urbanization than the annual-mean minimum temperature. Observations indicate a positive trend in urban heat islands over many major cities among which a number are by the sea. There is *medium confidence* that urbanization modifies precipitation patterns near cities with an increase in mean but particularly in heavy precipitation over and downwind of the city in different climate regions of the world and especially in the afternoon and early evening. However, the global annual mean surface air temperature response to urbanization is negligible (*medium evidence*, *high agreement*). {12.3, 12.4, Box 10.2}

There is *very high confidence* (*robust evidence* and *high agreement*) that future urbanization will amplify the projected air temperature under different background climate, with a strong impact on minimum temperatures that regionally could be comparable in magnitude to the global warming. There is *very high confidence* (*robust evidence* and *high agreement*) that large impact is expected from the combination of future urban development and more frequent occurrence of extreme climatic events, such as heat waves. Urban heat islands are generally projected to intensify (*medium confidence*) in the future, with more hot days and warm nights adding to heat stress in cities. {12.4.10, Box 10.2}

Coastal cities and settlements are exposed to a number of climatic impact drivers and hazards that are changing with human influence on climate such as extreme heat, pluvial floods, coastal erosion, coastal floods (*high confidence*), potentially compounding with heavy rainfalls, and tropical cyclones (*low confidence*). Both sea and air temperatures are projected to rise in most coastal environments (*high confidence*). There is *high confidence* in an increase in flood potential in urban areas where extreme precipitation is projected to increase, especially at high global warming levels. Climate change related variations in oceanic drivers (e.g., relative sea level, storm surge, ocean waves) are expected to lead to more frequent and more intense coastal flooding and erosion (*high confidence*) impacting cities and settlements located especially in low elevation coastal zones. {11.5, 12.4.10}

There is *high confidence* in an increase in flood potential in urban areas where extreme precipitation is projected to increase, especially at high global warming levels. Global hydrological models project a larger fraction of the land areas to be affected by an increase in river floods than by a decrease in river floods *(medium confidence*). {11.5}

Methodologies for understanding interactions between climate change and cities

It is *virtually certain* that city-scale climate monitoring networks enhance the understanding of urban microclimate and their interaction with climate change, and provide key information for end-users such us urban planners, decision-makers such as city mayors, stakeholders and the general public. Particularly for cities in developing countries, limited data availability and scientific capacity remain major challenges. Over the past decade, more crowdsourcing data in real time is becoming available through the use of cheap sensors (using internet of things technology) that are incorporated in various platforms like cars, amateur weather stations, and smartphones. This technological trend could prove very useful and the regional climate community is making efforts to understand the extent to which these methods can be exploited as a complement to traditional datasets. {10.2.2, Box 10.2, Cross-Chapter-Box 10.3}

In the past decade urban models, with varying complexity, have been developed to calculate the exchanges of heat, water and momentum between the urban surface and its overlying atmosphere. Many regional modelling groups are now beginning to implement these urban modules within the land-surface component of their regional climate models. There is *very high confidence* that various urban parameterizations simulate radiation exchanges in a realistic way; they have, however, strong biases when simulating latent heat fluxes. There is *medium evidence but high agreement* that a simple single-layer parameterization is sufficient for use in climate modelling. Impact assessments and adaptation plans in cities will require, however, high spatial resolution climate projections along with models that represent urban processes, ensemble dynamical and statistical downscaling, and local-impact models. {Box 10.2}

[END BOX TS.8 HERE]

TS.4.3.14 Summary

In this section a summary is given for each continental region. Box TS.5 contains references to sections providing the multiple lines of evidence for the CID assessment included in the continental sections.

In nearly all assessed regions, observed warming is shown to be persistent and projected to continue in the future. Associated warm extremes and climatic impact drivers are also *very likely* to remain increasing, and cold spells and associated climatic impact drivers reducing. In some regions, and particularly for high-end scenarios, present-day extreme high temperature values and current heat stress thresholds will be exceeded very frequently at the end of the 21st century. While observed and projected changes in mean precipitation vary regionally, the likelihood of extreme rainfall and associated pluvial flooding is increasing in most regions. Drought intensity is decreasing at high latitudes in Asia, Europe and America, and increasing in the Mediterranean, Southern and Central America and selected regions in Africa. Sea level rise will continue around all continents and lead to increased likelihood of coastal floods. Climatic impact drivers will exceed critical thresholds relevant to specific sectors (e.g. agriculture, health, ecosystems) with increasing warming. Some regions may experience a regime shift, for instance in terms of exceeding critical thresholds that have not been experienced in that region before, or changes in seasonal precipitation. There will *likely* be compounding effects of climatic impact drivers co-occurring in the same region.

Africa

The rate of temperature increase has generally been more rapid in Africa than the global average *(high confidence)*. Relative to the late 20th century, annual mean temperature over Africa is projected to rise faster than the global average *(very high confidence)* with the increase *likely* to exceed 4°C by the end of the century if mitigation strategies are not implemented. West, East and Southern Africa have experienced decreased rainfall *(medium confidence*) that are attributable to oceanic influences both internal variability in some cases and human-induced in other cases. There are contrasting signals in the projections of rainfall over some parts of Africa until the end of 21st century *(high confidence)* though changes in any given region are projected *with medium confidence.* Northern Africa and Southern Africa are *likely* to have a reduction in precipitation. Over West Africa, rainfall will *likely* decrease in the Western Sahel subregion (*medium confidence*) and increase in the central Sahel subregion (*low confidence*) and along the Guinea Coast subregion (*medium confidence*). Rainfall amounts over western part of the East Africa is *likely* to reduce but increase in the eastern part of the region (*medium confidence*). Heatwaves, deadly heat stress and the frequency of exceedance of hot temperature thresholds will drastically increase (*high confidence*) for high warming levels. Heavy precipitation inducing pluvial flooding will increase (*high confidence*) for West, North East, Central East and Central Africa. Increased evaporation will dry out soils in southern Africa (*high confidence*) for high warming levels. Higher than global average sea level rise in Africa will lead to increased coastal flooding in low-lying areas (*high confidence*) and coastline recession along most sandy coasts (*high confidence*).

Central America

Trends of warming of 0.1°C per decade have *very likely* been observed in Central America and they increased in the recent decades. Projection indicate with *high confidence* a temperature increase that will reach 1.5°C before the mid-century for the SSP2-4.5 scenario. Mean precipitation is going to decrease resulting in a pronounced drought for the whole region (*medium to high confidence*). Extreme sea level magnitude and occurrence frequency are expected to increase around the Caribbean islands (*high confidence*). Projections indicate that sandy coasts in Central America will experience coastline recession throughout the 21st century (*high confidence).*There is *high confidence* of increasing marine heat waves and increased ocean acidity in the nearshore ocean of Central America.

North America

Observed temperature trend in North America are *very likely* persistent and precipitation trend are uncertain. Thanks to initiative like NA-CORDEX, the model ability to reproduce mean and extreme temperature and precipitation climatology is *likely* improved. The CMIP6 mean temperature projections show a more intense warming in northern North America compared to the CMIP5 ensemble. It is *very likely* that precipitation will increase in northern North America and there is *high confidence* of a drying of southern North America. Extreme heat episodes in North America are projected to increase and cold spells are projected to decrease with climate change with an expansion of the frost-free season (*high confidence*). Mean precipitation is projected to increase in Northwest North America, Northeastern Canada and Eastern North America (*very high confidence*). There is *high confidence* in observed shifts in the timing of peak streamflow toward higher winter and earlier spring flows in snowmelt-driven basins in Canada and the United States. Pluvial flooding is projected to increase across North America in future decades, particularly in Canada and Eastern North America (*high confidence*). There is *high confidence* that increased evaporation due to growing atmospheric water demand will dry soils in the southwestern USA. Climate change drives future increases in North American wildfire weather (*medium confidence*). Mean wind speeds are expected to decline over much of North America (*medium confidence*). Shifts in the rain/snow transition line that alters the seasonal and geographic range of snow and ice hazards in the coming decades (*very high confidence*). Climate change is expected to reduce the total snow amount and the length of the snow cover season over most of North America, with a corresponding decrease in the proportion of total precipitation falling as snow and a reduction in end-of-season snowpack (*high confidence*). Projected sea level rise will contribute to increased coastal flooding in low-lying areas (*high confidence*) and coastline recession along most sandy coasts (*high confidence*).

South America

It is *very likely* that South America has experienced a warming of at least 0.2-0.3°C per decade in recent decades (1980-2014). Surface temperature is projected to *very likely* exceed 1.5°C before mid-century (*high confidence*). There is *high confidence* that most regions in South America will frequently undergo extreme heat stress conditions by the end of the 21st century and droughts and fire weather conditions will intensify in Northern South America, the South American monsoon region, and Northeastern South America (*high confidence).* Mean rainfall will *likely* increase in southeastern South America and to decrease in southwestern South America (*medium confidence*). Areas in South America have experienced a detectable influence of anthropogenic aerosols on precipitation patterns. There is *medium to high confidence* in an expansion of arid areas in northeastern Brazil. There is *high confidence* of increased intensity and frequency of marine heat waves and increased ocean acidity in the nearshore ocean of South America. Projections indicate that sandy coasts in South America will experience coastline recession throughout the 21st century (*high confidence*). There are still remaining literature and data gaps in the continent.

Asia

It is *very likely* that temperatures over most of Asia have increased by at least 0.1°C per decade in the last 30-40 years, with more pronounced warming trends (of at least 0.5°C per decade) in North Asia (East Siberia and Russian Far East) and in East Asia (Northern China). Most of the observed changes in precipitation in the region are not significant (*high confidence)*, but for an increasing trend in North Asia and parts of Central and Southeast Asia (*medium confidence)*. Regional increases in the frequency and/or in the intensity of heavy rainfall have been observed in most parts of Asia (*high confidence*). Temperatures over Asia will continue to increase under both CMIP5 and CMIP6 scenarios (*high confidence*), and most of the region will be warmer by at least 2°C in the period 2041-2060 under the RCP8.5 high emissions scenario. The northern regions of North Asia will have a more pronounced warming of 5-7°C. There is *high confidence* on the increase in frequency and magnitude of warm extremes and decrease in frequency and severity of cold extremes in many regions in Asia. It is *likely* that precipitation will change with varying sign of change over Asia. Rainfall is projected to increase in East, North Asia, and the northern parts of Southeast Asia (*likely*) and projected to decrease in areas in the Maritime Continent and northern Middle East Asia (*likely).* Higher than global average sea level rise in Asia will contribute to increased coastal flooding in low-lying areas (*high confidence*) and coastline recession along most sandy coasts (*high confidence*). Marine Heatwaves and Ocean acidification are also expected to increase over the 21st century (*high confidence*).

Australasia

There is *very high confidence* in the observed warming over Australasia, where the temperature increase is projected to continue throughout the 21st century. While there is *high confidence* in the human influence on the warming trend, there is *medium to high confidence* in the anthropogenic role in the ongoing drying over southwest Western Australia in April to October (*high confidence*). Apart from the increase in winter rainfall in parts of New Zealand (*high confidence*), changes in other parts of Australasia are less significant. Warming is projected to continue with a magnitude roughly equal to or slightly more than the global average temperature. This will be accompanied by more frequent hot extremes (*very likely*), increasing heat stress (*high confidence*) and less frequent cold extremes (*very likely*). Annual mean precipitation is projected to increase in Central and north east Australia and the west and south of New Zealand, while decreases are projected for south western and eastern Australia and the north and east of New Zealand. There is *high confidence* for a future rainfall decline in southwest Australia in the cool season. Snow cover is expected to decrease at high altitudes in both Australia and New Zealand (*high confidence*). Marine heatwaves and ocean acidification are expected to increase over the 21st century (*high confidence*). Higher than global average sea level rise in Australasia will lead to coastal flooding in low-lying areas (*high confidence*) and coastline recession along most sandy coasts (*high confidence*). Improvements are noted in the representation of Australian climate and associated climate drivers in CMIP6 models (*medium confidence*), as well as in the downscaled projections (*high confidence*) but these do not yet fully sample the uncertainties in the CMIP and CORDEX runs.

Europe

Thanks to the improvement of available observations, there is *high confidence* that temperature and extreme precipitation trend persist over Europe. Compared to AR5, model ability to represent the temperature and precipitation climatology has improved as also the ability to reproduce the daily and hourly precipitation extremes at convection permitting scale (*medium confidence*) thanks to coordinated initiative under the CORDEX framework (Euro-CORDEX and Med-CORDEX). Confidence is *high* in the temperature increase with maximum in the north in winter and in the south for summer and is *likely* that precipitation will increase in the north and keep decreasing in the south and in particular in Mediterranean basin where warming exceeding the Northern Hemispheric mean warming are projected by both global and regional model ensembles. Moreover, in the Mediterranean region there is *high confidence* in projection of drought increase and *medium confidence* in increases in the frequency and severity of precipitation deficits and associated trends in soil moisture deficits. River floods will increase with *high confidence* in Central and Western Europe and they will decrease in Eastern and Southern Europe (*medium confidence*). Coastal flooding in low-lying areas are projected to increase with *high confidence* due to the continuum increase of relative sea level rise that will contribute also to increase costal recession (*high confidence*).

Small Islands

Significant warming trends have been observed in the small islands over the latter half of the 20th century. On the other hand, there are few significant trends in precipitation in these regions except for the mid-summer drying trend in the Caribbean, where there is *limited evidence* and *low agreement* on the human influence on this drying trend. Projections indicate warming over the small islands even at 1.5°C global warming (*high confidence*) with massive heatwave events projected in the Caribbean at higher warming levels (*high confidence)* and strong spatial variability in future rainfall changes (*medium confidence*). Projected changes in tropical cyclones and associated rainfall as well as increasing sea level rise will increase the coastal hazards faced by small islands, also through their compounding effects (*medium confidence*). Marine heatwaves will be more intense and prolonged where the largest changes are noted in the equatorial region at 1.5 and 2.0 °C warming levels (*high confidence*).

Monsoons

Global monsoon and precipitation have *likely* increased, mainly in the Northern Hemisphere (*medium confidence*). Northern Hemispheric anthropogenic aerosols have caused a weakening of the regional monsoon circulations in South Asia, East Asia and West Africa during the second half of the 20th century (*very likely*), offsetting a strengthening monsoon precipitation in response to GHG-induced warming (*medium confidence*). Precipitation will *very likely* increase in large parts of monsoon region, in response to GHG-induced warming (*high confidence*). Future changes in South Asian monsoon are *likely* to result in increased precipitation during the summer monsoon but decreases during the winter monsoon (*medium to high confidence*). For the West African monsoon, increased precipitation is projected in central eastern Sahel and decrease in western Sahel. Monsoon precipitation is projected to decrease in North America (*medium confidence*).

Mountains

There is *high confidence* that the lack and the decline of observations over mountain sites pose a serious problem for climate change assessment and *high confidence* on elevation depending warming. There is some evidence that regional climate model can have better performances over complex topography with relatively better confidence in future temperature projection. Mountains are exposed to specific climatic impact drivers drastically influenced by climate change: elevation-dependent warming (*medium confidence*), low-to-mid-altitude snow cover and snow-season decrease, glacier mass reduction, permafrost thawing are projected to continue and amplify (*high confidence*), extreme precipitation and floods in most parts of major mountain ranges (*medium confidence*).

Polar regions

The current climate in polar regions is influenced by interactions between the ice sheet, the ocean, sea ice, and the atmosphere, and their responses to climate drivers – see Chapters 9, 10, 11; SROCC (IPCC, 2019b). Climate change in polar regions, especially Arctic, are among the most pronounced and attributable to anthropogenic factors and have influence on weather pattern and climate of mid-latitudes. Polar regions *very likely* have experienced the highest warming in the last decades that will continue under all emission scenarios (*high confidence*). Precipitation over Arctic and Antarctica *likely* have increased, especially in cold season, but snow cover *very likely* was declining in onset, spatial extend and duration. These tendencies are projected for all warming level scenarios (*high confidence*). Events of rain-on-snow and snow-on-sea ice altered surface mass balance and energy fluxes in polar regions. Depending on future changes in atmospheric temperature and precipitation phases, occurrence of superimposed ice might also become a scenario seen more often than today. {Cross-Chapter Box 10.1}

Urban/megacities

Despite having a negligible impact on global annual mean surface-air warming (*high confidence*), urbanization has exacerbated the effects of global warming in cities through its contribution to the observed warming trend, particularly in annual-mean minimum temperature (*very high confidence*), and increases in mean and extreme precipitation over and downwind of the city, especially in the afternoon and early evening (*medium confidence*). Improvements in urban parameterizations in models have contributed to understanding of urban effects on climate, which can be further enhanced with better climate monitoring networks in cities. How urban heat islands will change under climate change conditions is *very uncertain* but future urbanization is projected to enhance warming (*very high confidence*) and increase extreme precipitation leading to increased flood potential in urban areas (*high confidence).*

Summary of confidence in observed, attributed and projected changes in climatic impacts drivers

Table TS.22 combines the individual continental region tables from the preceding sections into a single table to provide a global overview of the observed, attributed and projected changes in climatic impact drivers demonstrating that in all regions there is clear evidence of changes from all three sources of information for some climatic impact drivers. However, lack of evidence does not imply that changes have not been or will not be experienced, in many cases (especially for attribution) there is a lack of studies and/or data on which to base an assessment of this.

The information in this table is presented as three discrete lines of evidence with their own levels of confidence. There is clearly scope to combine these lines of evidence to provide clearer and potentially stronger evidence of regional climate change for specific climatic impact drivers. This is the ultimate aspiration of the regional assessments in the WG I report and to facilitate this accompanying tables have been constructed which trace the findings in Table TS.22 back to the assessments in the underlying chapters. These tables (currently completed for Africa, Central and South America, Europe and North America for the observed trends and Central and South America and Europe for the attributed changes) are provided in Annex 1 of the Technical Summary and will be used to generate synthesis findings in the Summary for Policymakers. An example of a partially filled table tracing the findings for Africa for a selection of climatic impacts drivers is presented in Table TS.23.

[START TABLE TS.22 HERE]

Table TS.22: Summary of confidence in projected directional changes for climatic impact drivers for the main continental regions described in the preceding sections. The colours represents their aggregate characteristic changes for mid-century RCP8.5 within each AR6 WG I reference region. Dark purple: *high confidence* of increase; light purple: *medium confidence* of increase; white: *low confidence* of increase or decrease; light brown: *medium confidence* of decrease; dark brown: *high confidence* of decrease; grey: CID not broadly relevant. Arrows indicate *medium to high confidence* trends derived from observations and asterisks indicate low, medium and high confidence in attribution of observed changes (which are of the same sign as the projected changes unless stated otherwise).

Climatic Impact Driver	Heat and Cold				Wet and Dry							Wind			Snow and Ice						Coastal and Oceanic					Other		
	Mean temperature	Extreme heat	Cold spell	Frost	Mean precipitation	River flood	Pluvial flood	Landslide	Aridity	Drought	Wildfire	Mean wind speed	Severe wind storm	Sand and dust storm	Snow and land ice	Permafrost	Lake, river and sea ice	Heavy snow and ice storm	Hail	Snow avalanche	Relative sea level	Coastal flood	Coastal erosion	Marine heatwave	Ocean and lake acidity	Air pollution	Atmospheric CO_2	Radiation at surface
Africa																												
North Africa*	↗	↗ *	↘						↗ *	↗											↗		↗	↗	↗		↗	
Sahara	↗	↗	↘																		↗		↗	↗	↗		↗	
West Africa	↗	↗	↘		**		↗ **			↗											↗		↗	↗	↗		↗	
North East Africa	↗ **	↗	↘							o					↘	↘					↗		↗	↗	↗		↗	
Central East Africa	↗ **									o					↘	↘					↗		↗	↗	↗		↗	
Central Africa	↗																				↗		↗	↗	↗		↗	
South West Africa	↗	↗	↘		**				↗	↗ **											↗		↗	↗	↗		↗	
South East Africa	↗	↗	↘		**		**		↗	↗ **											↗		↗	↗	↗		↗	
Asia																												
West Siberia	↗	↗ *	↘ *				↗ *S			*		↘				↘											↗	
East Siberia	↗	↗ *	↘ *				↗					↘				↘											↗	
West Central Asia	↗	↗	↘								↗	↘			↘						↗		↗	↗			↗	
South Asia	↗	↗	↘ ***			*	↗ o*			*		↘			↘						↗		↗	↗				
Southeast Asia	↗	↗ **					**			*											↗		↗	↗			↗	
Russian Far East	↗	↗	↘				↗					↘				↘					↗		↗	↗	↗		↗	
East Asia	↗	↗ ***	↘ ***				↗ *			**		↘									↗		↗	↗			↗	
Tibetan Plateau	↗	↗ **	↘ **				↗ *					↘															↗	
Arabian Peninsula	↗	↗	↘																		↗		↗	↗			↗	
Australasia																												
Northern Australia	↗	↗ ***	↘								*										↗		↗	↗	↗		↗	
Central Australia	↗	↗ ***	↘								*										↗		↗	↗	↗		↗	
Southern Australia	↗	↗ ***	↘		↘		*			**	↗ *				↘						↗		↗	↗	↗		↗	
New Zealand	↗		↘				**			*					↘						↗		↗	↗	↗		↗	
Central and South America																												
Southern Central America	↗	↗ *	↘																		↗		↗	↗	↗		↗	
Northwestern South America	↗	↗	↘ ***				**								↘						↗		↗	↗	↗		↗	
Northern South America	↗	↗	↘				↗ *														↗		↗	↗	↗		↗	
South American Monsoon	↗	↗	↘				*																				↗	
Northeastern South America	↗	↗	↘				↘ **			↗ o											↗		↗	↗	↗		↗	
Southwestern South America	↗	↗	↘	↘			*			↗ *					↘						↗		↗	↗	↗		↗	
Southeastern South America	↗	↗ ***	↘	↘			↗ **														↗		↗	↗	↗		↗	
Southern South America	↗		↘	↘			**								↘						↗		↗	↗	↗		↗	
Europe																												
Mediterranean	↗	↗ ***							↗	↗ **		↘			↘						↗		↗	↗	↗		↗	
Central Europe	↗	↗ ***	↘ ***				↗ *			o		↘	↘		↘	↘					↗		↗	↗	↗		↗	
Eastern Europe	↗	↗ ***										↘													↗		↗	
Northern Europe	↗	↗	↘ ***				↗ ***			*		↘			↘	↘					↗		↗	↗	↗		↗	
North America																												
North Central America	↗	↗ *	↘							o	↗ **	↘		↗							↗	↗	↗	↗	↗		↗	
Western North America	↗ **	↗	↘			*	↗ **			**	↗ *	↘			↘		↘				↗	↗	↗	↗	↗		↗	
Central North America	↗ **	↗ **	↘ ***				↗ **			↗ **	*	↘			↘		↘				↗	↗	↗	↗	↗		↗	
Eastern North America	↗ **	↗ **	↘ ***				↗ **			↘ **		↘			↘ *		↘				↗	↗	↗	↗	↗		↗	
Northeastern Canada	↗	↗ **	**	↘			↗					↘			↘	↘	↘					↗	↗		↗		↗	
Northwest North America	↗	↗ **	↘ **	↘			↗ *			↘	*	↘			↘	↘	↘				↗	↗	↗	↗	↗		↗	
Small Islands																												
Caribbean	↗				**		↘			↗			**								↗		↗	↗	↗		↗	
Pacific	↗																				↗		↗	↗	↗		↗	
Polar Terrestrial Regions																												
Arctic Northwest North America	↗					↗	↗		↘						↘	↘	↘				↗				↗		↗	
Arctic Northeastern Canada	↗	↗				↗	↗		↘			↘			↘	↘	↘				↘				↗		↗	
Greenland	↗	↗				↗	↗		↘						↘	↘	↘								↗		↗	
Arctic North Europe	↗	↗				↗	↗		↘						↘	↘	↘				↗				↗		↗	
Russian Arctic	↗	↗				↗	↗		↘			↘			↘		↘								↗		↗	
West Antarctica	↗														↘										↗		↗	
East Antarctica																									↗		↗	

Notes on attribution evidence (Africa)

WAF: medium confidence that GHG and aerosols caused the drought and the recovery

*SEAF: ** for decrease in extreme rainfall*

Notes on attribution evidence (Asia)

SAS: ch10 attribution on weakening monsoon to aerosols

SEA: low confidence of increase of drought

Notes on attribution evidence (Central and South America)

NWS: medium confidence for decrease of extreme rainfall

*SWS * on increase of drought*

*SSA ** on increase of extreme precipitation*

Key for observational trend evidence

↗	Past upward trend (*medium or high confidence*)
↘	Past downward trend (*medium or high confidence*)

Key for level of confidence in future changes

- High confidence of increase
- Medium confidence of increase
- Low confidence in direction of change
- Medium confidence of decrease
- High confidence of decrease
- Not broadly relevant

Key for attribution evidence

***	High confidence
**	Medium confidence
*	Low confidence
x	Mixed signal
o	No signal

[END TABLE TS.22 HERE]

[START TABLE TS.23 HERE]

Table TS.23: Example of entries for the regional CID assessment traceback table for observed and projected changes for Africa. Entries in blue refer to assessments of observed changes and in black to assessments of projected changes.

	Heat and Cold				Wet and Dry						
Region	Mean temperature	Extreme heat	Cold spell	Frost	Mean precipitation	River flood	Pluvial flood	Landslide	Aridity	Drought	Wildfire	
North Africa*	[CH12.4.1.1][Atlas5.2.2][Atlas5.2.4}	[CH12.4.1.1][CH11Tab11.4][CH12P004]	[CH12.4.1.1][CH11Tab11.4]		[CH12.4.1.2]		[CH12P004]			[CH12.4.1.2][CH12P004]		[
Sahara	[CH12.4.1.1][Atlas5.2.4]	[CH12.4.1.1][CH11Tab11.4][CH12P004]	[CH12.4.1.1][CH11Tab11.4]				[CH12P004]					
West Africa	[CH12.4.1.1][Atlas5.2.2][Atlas5.2.4]	[CH12.4.1.1][CH11Tab11.4][CH12P004]	[CH11Tab11.4]		[CH12.4.1.2]	[CH12.4.1.2]	[CH11P007][CH11Tab11.4][CH12P004]	[CH12.4.1.2]		[CH12.4.1.2][CH11P012][CH12P004]		
North East Africa	[CH12.4.1.1][Atlas5.2][Atlas5.2.4]	[CH12.4.1.1][CH11Tab11.4][CH12P004][CH12.4.1.1]	[CH12.4.1.1]		[CH2AP002][CH12.4.1.2]		[CH12P004]			[CH11Tab11.4][Atkas5.2]		
Central East Africa	[Atlas5.2][Atlas.5.2.4]	[CH12.4.1.1][Atlas.5.2.4][12.4.1.1]			[CH12.4.1.2]		[CH12P004]	[CH12.4.1.2]		[Atlas5.2]		
Central Africa	[Atlas.5.2.4]	[CH12.4.1.1][Atlas.5.2.4][12.4.1.1]			[Atlas5.2.2]			[CH12.4.1.2]		[CH11Tab11.4][CH11P012]		
South West Africa (southern west Africa)	[CH12.4.1.1][Atlas5.2][Atlas.5.2.4]	[CH12.4.1.1][CH11Tab11.4][Atlas5.2.2][Atlas.5.2.4][12.4.1.1]	[CH12.4.1.1][CH11Tab11.4]		[CH2AP002][CH12.4.1.2]		[CH11P007][CH12.4.1.2]		[CH8.4.1]	[CH11P012][CH12.4.1.2][CH11Tab11.4][CH11P014]		[
South East Africa (southern east Africa)	[CH12.4.1.1][Atlas5.2][Atlas.5.2.4]	[CH12.4.1.1][CH11Tab11.4][Atlas5.2.2][Atlas.5.2.4][12.4.1.1]	[CH12.4.1.1][CH11Tab11.4]		[CH2AP002][CH12.4.1.2]		[CH11P007][CH12.4.1.2]		[CH8.4.1]	[CH11P012][CH12.4.1.2][CH11Tab11.4][CH11P014]		[

[END TABLE TS.23 HERE]

Appendices TS

Appendix TS.A TS.4 Traceback Tables

In section TS.4.3 tables are presented summarising the assessment of confidence in observed trends, attribution of trends and observed climate events and projected future changes in a wide range of climatic impact drivers. The information in these tables are presented as three discrete lines of evidence with their own levels of confidence. This appendix provides matching tables which document the source of these assessment in the underlying chapters, either from their executive summaries or sections within the chapters themselves.

The purpose of these tables is to be able to quickly identify the evidence underpinning the assessed confidence in these lines of evidence for each climatic impact driver for each region. This facilitates the process of assessing whether an appropriate combination of these lines of evidence provides clearer and stronger evidence of regional climate change. Summary results from this assessment will be used to generate synthesis findings in the Summary for Policymakers.

These tables have currently been completed for Africa, Central and South America, Europe and North America for the evidence on observed trends and projected changes and partially completed for the other AR6 WG I reference land regions (see 0). Similar tables have been completed for the evidence on attributed changes and events for Central and South America and Europe (see Table TS.A.2). These tables will be fully completed following compilation of the final drafts of the chapters.

[START TABLE TS.A.1 HERE]

Table TS.A.1: This table identifies the location in the underlying chapters of the evidence supporting the assessment of confidence in observed and projected climate changes in the climatic impact drivers identified at the top of each page of the table across the regions identified in the first column of the table. Evidence which is found in a chapter executive summary (ES) statement is identified by its code, e.g. [CH05P010] which denotes the tenth ES statement from Chapter 5. Evidence which is located within the chapters is identified by the chapter section number, e.g. [CH12.4.3.1] or {12.4.3.1} is the section in Chapter 12 in which the evidence is located. Codes written in blue refer to evidence of observed changes and those in black to evidence of projected changes.

	Climatic Impact Driver													
	Heat and Cold				Wet and Dry							Wind		
Africa	Mean temperature	Extreme heat	Cold spell	Frost	Mean precipitation	River flood	Pluvial flood	Landslide	Aridity	Drought	Wildfire	Mean wind speed	Severe wind storm	Sand and dust storm
North Africa*	[CH12.4.1.1] [Atlas5.2.2] [Atlas5.2.4] [CH12.4.1.1] [CH10.6.4.6)	[CH12.4.1.1] [CH11Tab11.4] [CH12P004] [CH12.4.1.1] [CH11Tab11.4]	[CH12.4.1.1] [CH11Tab11.4] [CH12.4.1.1]		[CH12.4.1.2] [Atlas5.2.2] [CH2AP004] [Atlas5.2.4] [CH12.4.1.2]		[CH11Tab11.4] [CH11.4.2] [CH12P004] [CH12.4.1.2] [CH11Tab11.4] [CH11.4.5]		[CH12.4.7.5] [CH12.4.10.3]	[CH11Tab11.4] [CH12.4.1.2] [CH8.3.1.8] [CH12P004] [CH12.4.1.2] [CH11Tab11.4] [CH11.6.5.1] [CH8.4.1.8]	[CH12.4.1.2]	[CH12P004] [CH12.4.1.3]		[CH12.4.1.3] [CH12.4.7.5] [CH12.4.10.3]
Sahara	[CH12.4.1.1] [Atlas5.2.2] [Atlas5.2.4] [CH12.4.1.1]	[CH12.4.1.1] [CH11Tab11.4] [CH12P004] [CH12.4.1.1] [CH11Tab11.4	[CH12.4.1.1] [CH11Tab11.4] [CH12.4.1.1]		[CH8.6.2.2]	[CH12P004]	[CH12P004]		[CH12.4.7.5] [CH12.4.10.3]					[CH12.4.7.5] [CH12.4.10.3] [CH8.6.2.4]
West Africa	[CH12.4.1.1] [Atlas5.2.2] [Atlas5.2.4] [CH12.4.1.1]	[CH12.4.1.1] [CH11Tab11.4] [CH12P004] [CH12.4.1.1] [CH11Tab11.4]	[CH11Tab11.4] [CH12.4.1.1]		[CH12.4.1.2] [Atlas5.2.2] [CH8.3.1.1] [CH8.3.2.4] [CH11Tab11.4] [CH2AP004] [Atlas 5.2.4] [CH12.4.1.2] [CH8.4.1.3] [CH8.4.2.4]	[CH12.4.1.2] [CH12P004]	[CH11P007] [CH11Tab11.4] [Ch114.2] [CH8.3.2.4] [CH12P004] [CH12.4.1.2] [CH11Tab11.4] [CH11.4.5]	[CH12.4.1.2]	[CH12.4.10.3]	[CH12.4.1.2] [CH11P012] [CH11Tab11.4] [CH10.4.1.2.1] [CH12P004] [Atlas5.2.2] [CH12.4.1.2] [CH12.4.10.5] [CH11Tab11.4] [CH11.6.5.1]	[CH12.4.1.2]	[CH12.4.1.3]	[CH12.4.1.3][CH 12.4.1.3]	[CH12.4.1.3]
North East Africa	[CH12.4.1.1] [Atlas5.2] [Atlas5.2.4] [CH12.4.1.1]	[CH12.4.1.1] [CH11Tab11.4] [CH12P004] [CH11Tab11.4] [CH12.4.1.1]	[CH12.4.1.1] [CH12.4.1.1] [CH11Tab11.4]		[CH2AP002] [CH12.4.1.2] [Atlas 5.2.2] [CH8.3.1.1] CH8.3.2.8] [Alas5.2.4] [CH8.4.2.9]	[CH12P004]	[CH12P004] [CH12.4.1.2]			[CH12.4.1.2] [CH11Tab11.4] [Atlas5.2] [CH11Tab11.4] [CH12.4.1.2]				
Central East Africa	[Atlas5.2] [Atlas.5.2.4]	[CH12.4.1.1] [Atlas.5.2.4] [CH12.4.1.1]	[CH12.4.1.1]		[CH12.4.1.2] [CH8.3.1.1] [CH8.4.2.4] [CH8.4.2.9]	[CH12P004]	[CH12P004] [CH11.4.2][	[CH12.4.1.2] [CH12.4.1.2]		[Atlas5.2] [CH8.3.1.8] [CH11.6.2] [CH11.6.5.1] [CH12.4.1.2]				
Central Africa	[Atlas.5.2.4] [CH12.4.1.1]	[CH12.4.1.1] [Atlas.5.2.4] [CH12.4.1.1] [Ch11.3.5]	[CH11Tab11.4] [CH12.4.1.1]		[Atlas5.2.2] [CH8.3.1.1] [CH12.4.1.1]	[CH12P004]	[CH11.4.2] [[CH12P004] [CH11.4.2]	[CH12.4.1.2]		[CH11Tab11.4] [CH11P012] [CH8.3.1.8] [CH11.6.5.1]	[CH12.4.1.2]		[CH12.4.1.3]	
South West Africa	[CH12.4.1.1] [Atlas5.2] [Atlas.5.2.4] [CH12.4.1.1]	[CH12.4.1.1] [CH11Tab11.4] [Atlas5.2.2] [Atlas.5.2.4] [CH12.4.1.1]	[CH12.4.1.1] [CH11Tab11.4] [CH11Tab11.4]		[CH2AP002] [CH12.4.1.2] [CH8.3.1.1] [CH2AP004]		[CH11P007] [CH12.4.1.2] [CH11.4.2] [CH11.4.2]		[CH8.4.1]	[CH11P012] [CH12.4.1.2] [CH11Tab11.4] [CH8.3.1.8] [CH11.6.2] [CH11P014] [CH10.6.2.6] [CH8.4.1.8] [CH11.6.5.1] [CH12.4.1.2]	[CH12.4.1.2]	[CH12P004]	[CH12.4.1.3]	
South East Africa	[CH12.4.1.1] [Atlas5.2] [Atlas.5.2.4] [CH12.4.1.1]	[CH12.4.1.1] [CH11Tab11.4] [Atlas5.2.2] [Atlas.5.2.4] [CH12.4.1.1]	[CH12.4.1.1] [CH11Tab11.4] [CH11Tab11.4] [CH12.4.1.1]		[CH2AP002] [CH12.4.1.2] [CH8.3.1.1] [CH2AP004]		[CH11P007] [CH12.4.1.2] [CH11.4.2]		[CH8.4.1]	[CH11P012] [CH12.4.1.2] [CH11Tab11.4] [CH8.3.1.8] [Ch11.6.2] [CH11P014] [CH10.6.2.6] [CH8.4.1.8] [CH11.6.5.1] [CH12.4.1.2]	[CH12.4.1.2]	[CH12P004]	[CH12.4.1.3]	

Africa	Snow and Ice: Snow and land ice	Snow and Ice: Permafrost	Snow and Ice: Lake, river and sea ice	Snow and Ice: Heavy snow and ice storm	Snow and Ice: Hail	Snow and Ice: Snow avalanche	Coastal and Oceanic: Relative sea level	Coastal and Oceanic: Coastal flood	Coastal and Oceanic: Coastal erosion	Coastal and Oceanic: Marine heatwave	Coastal and Oceanic: Ocean and lake acidity	Other: Air pollution	Other: Atmospheric CO2	Other: Radiation at surface
North Africa*							[CH12.4.1.5][CH 12.4.1.5]		[CH12.4.1.5][CH 12.4.1.5]	[CH12.4.1.5][CH 12.4.1.5]	[CH12.4.1.5][CH 12.4.1.5]		[CH12.4.1.6][CH 12.4.1.6]	[CH12.4.1.6]
Sahara							[CH12.4.1.5] [CH12.4.1.5]		[CH12.4.1.5] [CH12.4.1.5]	[CH12.4.1.5] [CH12.4.1.5]	[CH12.4.1.5] [CH12.4.1.5]		[CH12.4.1.6] [CH12.4.1.6]	[CH12.4.1.6]
West Africa							[CH12.4.1.5] [CH12.4.1.5]		[CH12.4.1.5] [CH12.4.1.5]	[CH12.4.1.5] [CH12.4.1.5]	[CH12.4.1.5] [CH12.4.1.5]		[CH12.4.1.6] [CH12.4.1.6]	[CH12.4.1.6]
North East Africa							[CH12.4.1.5] [CH12.4.1.5]		[CH12.4.1.5] [CH12.4.1.5]	[CH12.4.1.5] [CH12.4.1.5]	[CH12.4.1.5] [CH12.4.1.5]		[CH12.4.1.6] [CH12.4.1.6]	[CH12.4.1.6]
Central East Africa	[CH12.4.1.4]						[CH12.4.1.5] [CH12.4.1.5]		[CH12.4.1.5]	[CH12.4.1.5]	[CH12.4.1.5]		[CH12.4.1.6]	
Central Africa							[CH12.4.1.5] [CH12.4.1.5]		[CH12.4.1.5]	[CH12.4.1.5]	[CH12.4.1.5]		[CH12.4.1.6]	
South West Africa							[CH12.4.1.5] [CH12.4.1.5]		[CH12.4.1.5]	[CH12.4.1.5]	[CH12.4.1.5]		[CH12.4.1.6]	
South East Africa							[CH12.4.1.5] [CH12.4.1.5]		[CH12.4.1.5]	[CH12.4.1.5]	[CH12.4.1.5]		[CH12.4.1.6]	

Climatic Impact Driver

	Climatic Impact Driver													
	Heat and Cold				Wet and Dry							Wind		
Asia	Mean temperature	Extreme heat	Cold spell	Frost	Mean precipitation	River flood	Pluvial flood	Landslide	Aridity	Drought	Wildfire	Mean wind speed	Severe wind storm	Sand and dust storm
West Siberia	{Atlas.5.3.3.2} {Atlas.5.3.3.4}				{Atlas.5.3.3.2} {Atlas.5.3.3.4}	[CH11P010] [CH11P011]								
East Siberia	{Atlas.5.3.3.2} {Atlas.5.3.3.4}				{Atlas.5.3.3.2} {Atlas.5.3.3.4}	[CH11P010] [CH11P011]								
West Central Asia	[CH2AP001] {Atlas.5.3.2.2}				{Atlas.5.3.2.2}									
South Asia														
Southeast Asia					[CH2AP002]									
Russian Far East	{Atlas.5.3.3.2} {Atlas.5.3.3.4}				{Atlas.5.3.3.2} {Atlas.5.3.3.4}	[CH11P010] [CH11P011]								
East Asia									[CH11P012]					
Tibetan Plateau														
Arabian Peninsula	[CH2AP001] {Atlas.5.3.2.2}				{Atlas.5.3.2.2}									

	Climatic Impact Driver													
	Snow and Ice						Coastal and Oceanic					Other		
Asia	Snow and land ice	Permafrost	Lake, river and sea ice	Heavy snow and ice storm	Hail	Snow avalanche	Relative sea level	Coastal flood	Coastal erosion	Marine heatwave	Ocean and lake acidity	Air pollution	Atmospheric CO2	Radiation at surface
West Siberia														
East Siberia														
West Central Asia														
South Asia	[CH2AP006]											[CH06P0002] [CH06P0005]		
Southeast Asia														
Russian Far East														
East Asia												[CH06P0006] [CH06P0005]		
Tibetan Plateau	[CH2AP006]													
Arabian Peninsula														

Australasia	Climatic Impact Driver: Heat and Cold				Wet and Dry							Wind		
	Mean temperature	Extreme heat	Cold spell	Frost	Mean precipitation	River flood	Pluvial flood	Landslide	Aridity	Drought	Wildfire	Mean wind speed	Severe wind storm	Sand and dust storm
Northern Australia	[CH12.4.3.1] [Atlas5.4.2] [Atlas 5.4.4] [CH12.4.3.1]	[CH12.4.3.1] [CH11Tab11.6] [CH11Tab11.6] [CH12.4.3.1]	[CH12.4.3.1] [CH11Tab11.6] [CH11Tab11.6][CH12.4.3.1]	[CH12.4.3.1]	[CH12.4.3.2]	[CH12.4.3.2]	[CH11P007] [CH11Tab11.6] [CH12.4.3.2]				[CH12.4.3.2]	[CH12.4.3.3]	[CH12.4.3.3]	
Central Australia	[CH12.4.3.1] [Atlas5.4.2] [Atlas 5.4.4] [CH12.4.3.1]	[CH12.4.3.1] [CH11Tab11.6] [CH11Tab11.6] [CH12.4.3.1]	[CH12.4.3.1] [CH11Tab11.6] [CH11Tab11.6] [CH12.4.3.1]	[CH12.4.3.1]	[CH12.4.3.2]	[CH12.4.3.2]	[CH12.4.3.2]			[CH11Tab11.6]	[CH12.4.3.2]	[CH12.4.3.3]	[CH12.4.3.3]	
Southern Australia	[CH12.4.3.1] [Atlas5.4.2] [Atlas 5.4.4] [CH12.4.3.1]	[CH12.4.3.1] [CH11Tab11.6] [CH11Tab11.6] [CH12.4.3.1]	[CH12.4.3.1] [CH11Tab11.6] [CH11Tab11.6] [CH12.4.3.1]	[CH12.4.3.1]	[CH2AP002] [CH12.4.3.2] [Atlas5.4.4] [CH12.4.3.2]	[CH11P010][CH 12.4.3.2]	[CH12.4.3.2]		[CH12.4.3.2] [CH11Tab11.6] [CH12.4.3.2]	[CH12.4.3.2] [CH11Tab11.6] [CH12.4.3.2]	[CH12.4.3.2] [CH12.4.3.2]	[CH12.4.3.3]	[CH12.4.3.3]	
New Zealand	[CH12.4.3.1] [Atlas5.4.2] [Atlas 5.4.4] [CH12.4.3.1]	[CH11Tab11.6]	[CH12.4.3.1] [CH11Tab11.6] [CH12.4.3.1]	[CH12.4.3.1]	[Atlas5.4.4][CH 12.4.3.2]		[CH11Tab11.6]			[CH12.4.3.2]		[CH12.4.3.3]	[CH12.4.3.3]	

Australasia	Climatic Impact Driver: Snow and Ice						Coastal and Oceanic					Other		
	Snow and land ice	Permafrost	Lake, river and sea ice	Heavy snow and ice storm	Hail	Snow avalanche	Relative sea level	Coastal flood	Coastal erosion	Marine heatwave	Ocean and lake acidity	Air pollution	Atmospheric CO2	Radiation at surface
Northern Australia							[CH12.4.3.5] [CH12.4.3.5]		[CH12.4.3.5] [CH12.4.3.5]	[CH12.4.3.5] [CH12.4.3.5]	[CH12.4.3.5] [CH12.4.3.5]		[CH12.4.3.6] [CH12.4.3.6]	[CH12.4.3.6]
Central Australia							[CH12.4.3.5] [CH12.4.3.5]		[CH12.4.3.5] [CH12.4.3.5]	[CH12.4.3.5] [CH12.4.3.5]	[CH12.4.3.5] [CH12.4.3.5]		[CH12.4.3.6] [CH12.4.3.6]	[CH12.4.3.6]
Southern Australia	[CH12.4.3.4] [CH12.4.3.3]						[CH12.4.3.5] [CH12.4.3.5]		[CH12.4.3.5] [CH12.4.3.5]	[CH12.4.3.5] [CH12.4.3.5]	[CH12.4.3.5] [CH12.4.3.5]		[CH12.4.3.6] [CH12.4.3.6]	[CH12.4.3.6]
New Zealand	[CH12.4.3.4] [CH12.4.3.3]						[CH12.4.3.5] [CH12.4.3.5]		[CH12.4.3.5] [CH12.4.3.5]	[CH12.4.3.5] [CH12.4.3.5]	[CH12.4.3.5] [CH12.4.3.5]		[CH12.4.3.6] [CH12.4.3.6]	

	Climatic Impact Driver													
	Heat and Cold				Wet and Dry							Wind		
Central and South America	Mean temperature	Extreme heat	Cold spell	Frost	Mean precipitation	River flood	Pluvial flood	Landslide	Aridity	Drought	Wildfire	Mean wind speed	Severe wind storm	Sand and dust storm
Southern Central America	[Atlas 5.5.1.2], [CH12.4.4.1], [Atlas 5.5.1.4], [CH12.4.4.1]	[Atlas5.5.1.4], [CH11Tab11.7], [CH11.3.3], [CH12P007], [CH12.4.4.1], [CH11Tab11.7]	[CH11Tab11.7], [CH12.4.4.1], [CH12.4.4.1]	[CH12.4.4.1], [CH12.4.4.1]	[Atlas5.5.1.2], [Atlas5.5.1.4], [CH12.4.4.1], [CH12.4.4.1]	[CH11Tab11.7], [CH11Tab11.7], [CH12.4.4.2], [CH12.4.4.2]	[CH11Tab11.7], [CH11Tab11.7], [CH12.4.4.2], [CH12.4.4.2]		[CH11Tab11.7], [CH11Tab11.7], [CH12.4.4.2], [CH12.4.4.2], [CH11.6.5]	[CH11Tab11.7], [CH11Tab11.7], [CH12.4.4.2], [CH12.4.4.2]		[CH12.4.4.3]	[CH12.4.4.2]	
Northwestern South America	[CH2AP001], [Atlas 5.5.2.2], [CH12.4.4.1], [Atlas 5.5.2.4], [CH12.4.4.1]	[CH11Tab11.7], [CH12P007], [CH12.4.4.1], [CH12.4.4.1]	[CH11Tab11.7], [CH12.4.4.1], [CH12.4.4.1]	[CH12.4.4.1], [CH12.4.4.1]	[Atlas5.5.2.2], [Atlas5.5.2.4], [CH12.4.4.1], [CH12.4.4.1]	[CH11Tab11.7], [CH11Tab11.7], [CH12.4.4.2], [CH12.4.4.2]	[CH11Tab11.7], [CH11Tab11.7], [CH12.4.4.2], [CH12.4.4.2]	[CH12.4.4.2]	[CH11Tab11.7], [CH11Tab11.7], [CH12.4.4.2], [CH12.4.4.2]	[CH11Tab11.7], [CH11Tab11.7], [CH12.4.4.2], [CH12.4.4.2]				
Northern South America	[Atlas 5.5.2.2], [CH12.4.4.1], [CH12.4.4.1], [Atlas 5.5.2.4]	[CH11.3.3], [CH11Tab11.7], [CH12P007], [CH12.4.4.1], [CH12.4.4.1],	[CH11Tab11.7], [CH12.4.4.1], [CH12.4.4.1]	[CH12.4.4.1], [CH12.4.4.1]	[Atlas5.5.2.2], [Atlas5.5.2.4], [CH12.4.4.1], [CH12.4.4.1],[CH8.3.1.3,p33]	[CH11Tab11.7], [CH11Tab11.7], [CH12.4.4.2], [CH12.4.4.2]	[CH11P007] [CH12.4.4.2] [Atlas5.5.2.2] [CH11Tab11.7]		[CH11Tab11.7], [CH11Tab11.7], [CH12.4.4.2], [CH12.4.4.2]	[CH11Tab11.7], [CH11Tab11.7], [CH12.4.4.2], [CH12.4.4.2]	[CH12.4.4.2]			
South American Monsoon	[Atlas 5.5.2.2], [CH12.4.4.1], [Atlas 5.5.2.4], [CH12.4.4.1]	[Atlas5.5.2], [CH11.3.3], [CH12P007], [CH12.4.4.1], [CH12.4.4.1]	[CH11Tab11.7], [CH12.4.4.1], [CH12.4.4.1]	[CH12.4.4.1], [CH12.4.4.1]	[Atlas5.5.2.2], [Atlas5.5.2.4], [CH12.4.4.1], [CH12.4.4.1], [CH8.2.1],[CH8.4.2.4]	[CH11Tab11.7], [CH11Tab11.7], [CH12.4.4.2], [CH12.4.4.2]	[CH12.4.4.2] [Atlas5.5.2.2]		[CH11Tab11.7], [CH11Tab11.7], [CH12.4.4.2], [CH12.4.4.2]	[CH11Tab11.7], [CH11Tab11.7], [CH12.4.4.2], [CH12.4.4.2]	[CH12.4.4.2]			
Northeastern South America	[Atlas 5.5.2.2], [CH12.4.4.1], [Atlas 5.5.2.4], [CH12.4.4.1]	[CH11.3.3], [CH12P007], [CH12.4.4.1], [CH12.4.4.1]	[CH11Tab11.7], [CH12.4.4.1], [CH12.4.4.1]	[CH12.4.4.1], [CH12.4.4.1]	[Atlas5.5.2.2], [Atlas5.5.2.4], [CH12.4.4.1], [CH12.4.4.1]	[CH11Tab11.7], [CH11Tab11.7], [CH12.4.4.2], [CH12.4.4.2]	[CH11Tab11.7], [CH11Tab11.7], [CH12.4.4.2], [CH12.4.4.2]		[CH11Tab11.7], [CH11Tab11.7], [CH12.4.4.2], [CH12.4.4.2]	[CH11Tab11.7], [CH11Tab11.7], [CH12.4.4.2], [CH12.4.4.2]	[CH12.4.4.2]	[CH12.4.4.2]		
Southwestern South America	[Atlas 5.5.2.2], [CH12.4.4.1], [Atlas 5.5.2.4], [CH12.4.4.1]	[CH11.3.3], [CH12P007], [CH12.4.4.1], [CH12.4.4.1]	[CH11Tab11.7], [CH12.4.4.1], [CH12.4.4.1]	[CH12.4.4.1], [CH12.4.4.1]	[Atlas5.5.2.2], [Atlas5.5.2.4], [CH12.4.4.1], [CH12.4.4.1]	[CH11Tab11.7], [CH11Tab11.7], [CH12.4.4.2], [CH12.4.4.2]	[CH11Tab11.7], [CH11Tab11.7], [CH12.4.4.2], [CH12.4.4.2]	[CH12.4.4.2]	[CH11Tab11.7], [CH11Tab11.7], [CH12.4.4.2], [CH12.4.4.2]	[CH11Tab11.7], [CH11Tab11.7], [CH12.4.4.2], [CH12.4.4.2]				
Southeastern South America	[Atlas 5.5.2.2], [CH12.4.4.1], [Atlas 5.5.2.4], [CH12.4.4.1]	[Atlas5.5.2], [CH11.3.3], [CH12P007], [CH12.4.4.1], [CH12.4.4.1]	[CH11Tab11.7], [CH12.4.4.1], [CH12.4.4.1]	[CH12.4.4.1], [CH12.4.4.1]	[Atlas5.5.2.2], [Atlas5.5.2.4], [CH12.4.4.1], [CH12.4.4.1],[CH8.3.1.3,p33]	[CH11Tab11.7], [CH11Tab11.7], [CH12.4.4.2], [CH12.4.4.2]	[CH11Tab11.7], [CH11Tab11.7], [CH12.4.4.2], [CH12.4.4.2]		[CH11Tab11.7], [CH11Tab11.7], [CH12.4.4.2], [CH12.4.4.2]	[CH11Tab11.7], [CH11Tab11.7], [CH12.4.4.2], [CH12.4.4.2]	[CH12.4.4.2]	[CH12.4.4.2]		
Southern South America	[Atlas 5.5.2.2], [CH12.4.4.1], [Atlas 5.5.2.4], [CH12.4.4.1]	[CH11.3.3], [CH12P007], [CH12.4.4.1]	[CH11Tab11.7], [CH12.4.4.1], [CH12.4.4.1]	[CH12.4.4.1], [CH12.4.4.1]	[Atlas5.5.2.2], [Atlas5.5.2.4], [CH12.4.4.1], [CH12.4.4.1]	[CH11Tab11.7], [CH11Tab11.7], [CH12.4.4.2], [CH12.4.4.2]	[CH11Tab11.7], [CH11Tab11.7], [CH12.4.4.2], [CH12.4.4.2]		[CH11Tab11.7], [CH11Tab11.7], [CH12.4.4.2], [CH12.4.4.2]	[CH11Tab11.7], [CH11Tab11.7], [CH12.4.4.2], [CH12.4.4.2]	[CH12.4.4.2]			

	Climatic Impact Driver													
	Snow and Ice						Coastal and Oceanic					Other		
	Snow and land ice	Permafrost	Lake, river and sea ice	Heavy snow and ice storm	Hail	Snow avalanche	Relative sea level	Coastal flood	Coastal erosion	Marine heatwave	Ocean and lake acidity	Air pollution	Atmospheric CO2	Radiation at surface
Central and South America														
Southern Central America							[CH12.4.4.5], [CH12.4.4.5]	[CH12.4.4.5], [CH12.4.4.5]	[CH12.4.4.5], [CH12.4.4.4]	[CH12.4.4.5], [CH12.4.4.4]	[CH12.4.4.5], [CH12.4.4.5]		[CH12.4.4.6]	
Northwestern South America	[CH12.4.4.4], [CH12.4.4.4]	[CH12.4.4.4], [CH12.4.4.4]	[CH12.4.4.4], [CH12.4.4.4]				[CH12.4.4.5], [CH12.4.4.5]	[CH12.4.4.5], [CH12.4.4.5]	[CH12.4.4.5], [CH12.4.4.5]	[CH12.4.4.5], [CH12.4.4.5]	[CH12.4.4.5], [CH12.4.4.5]		[CH12.4.4.6]	
Northern South America							[CH12.4.4.5], [CH12.4.4.5]	[CH12.4.4.5], [CH12.4.4.5]	[CH12.4.4.5], [CH12.4.4.5]	[CH12.4.4.5], [CH12.4.4.5]	[CH12.4.4.5], [CH12.4.4.5]		[CH12.4.4.6]	
South American Monsoon													[CH12.4.4.6]	
Northeastern South America							[CH12.4.4.5], [CH12.4.4.5]	[CH12.4.4.5], [CH12.4.4.5]	[CH12.4.4.5], [CH12.4.4.5]	[CH12.4.4.5], [CH12.4.4.5]	[CH12.4.4.5], [CH12.4.4.5]		[CH12.4.4.6]	
Southwestern South America	[CH12.4.4.4], [CH12.4.4.4]	[CH12.4.4.4], [CH12.4.4.4]	[CH12.4.4.4], [CH12.4.4.4]				[CH12.4.4.5], [CH12.4.4.5]	[CH12.4.4.5], [CH12.4.4.5]	[CH12.4.4.5], [CH12.4.4.5]	[CH12.4.4.5], [CH12.4.4.5]	[CH12.4.4.5], [CH12.4.4.5]		[CH12.4.4.6]	
Southeastern South America							[CH12.4.4.5], [CH12.4.4.5]	[CH12.4.4.5], [CH12.4.4.5]	[CH12.4.4.5], [CH12.4.4.5]	[CH12.4.4.5], [CH12.4.4.5]	[CH12.4.4.5], [CH12.4.4.5]		[CH12.4.4.6]	
Southern South America	[CH12.4.4.4], [CH12.4.4.4]	[CH12.4.4.4], [CH12.4.4.4]	[CH12.4.4.4], [CH12.4.4.4]				[CH12.4.4.5], [CH12.4.4.5]	[CH12.4.4.5], [CH12.4.4.5]	[CH12.4.4.5], [CH12.4.4.5]	[CH12.4.4.5], [CH12.4.4.5]	[CH12.4.4.5], [CH12.4.4.5]		[CH12.4.4.6]	

Europe	Climatic Impact Driver													
	Heat and Cold				Wet and Dry							Wind		
	Mean temperature	Extreme heat	Cold spell	Frost	Mean precipitation	River flood	Pluvial flood	Landslide	Aridity	Drought	Wildfire	Mean wind speed	Severe wind storm	Sand and dust storm
Mediterranean	[CH12.4.5.1] [Atlas.5.6.4] [CH12.4.5.1] [CH10.6.4.6]	[CH11.3.3] [CH12P008] [Atlas.5.6] [CH11.5.5] [CH12.4.5.1] [CH11.Tab8]	[CH12.4.5.1] [CH12.4.5.1 p5]	[CH12.4.5.1] [CH12.4.5.1 p5]	[CH12.4.5.2] [Atlas.5.6.4] [CH12.4.5.2 p1] [CH10.6.4.6]	[CH11P010] [CH12P008	[CH11P007] [Atlas.5.6] [CH12-12.4.5.2 p2] [CH12.4.5.2 p2]	[CH12.4.5.2 p7]	[CH11P012] [CH12.4.5.2 p8] [CH11.6.5]	[CH11P012] [CH08P005] [CH11.Tab8] [CH11.6.2] [CH12.4.5.2 p8] [CH11.6.5]	[CH12.4.5.2 p8]	[CH12.4.5.3 p1] [CH12.4.5.3 p2]	[CH12.4.5.3] [CH12P008]	
Central Europe	[CH2AP001] [CH12.4.5.1] [Atlas.5.6.4] [CH12.4.5.1]	[CH11.3.3] [CH12P008] [CH11.5.5] [CH12.4.5.1] [CH11.Tab8]	[CH12.4.5.1] [CH12.4.5.1 p5]	[CH12.4.5.1] [CH12.4.5.1 p5]	[CH12.4.5.2 p1]	[CH12P008]	[CH1P007] [Atlas.5.6] [CH12-12.4.5.2 p2]	[CH12.4.5.2 p7]	[CH11P012] [CH12.4.5.2 p8]	[CH12.4.5.3] [CH12.4.5.2 p8]	[CH12.4.5.2 p8]	[CH12.4.5.3 p1] [CH12.4.5.3 p2]	[CH12.4.5.3] [CH12P008]	
Eastern Europe	[CH2AP001] [CH12.4.5.1] [Atlas.5.6.4] [CH12.4.5.1]	[CH11.3.3] [CH12P008] [CH11.5.5] [Atlas.5.6] [CH11.Tab8]	[CH12.4.5.1] [CH11.Tab8] [CH12.4.5.1 p5]	[CH12.4.5.1] [CH12.4.5.1 p5]	[Atlas.5.6.4] [CH12.4.5.2 p1]	[CH12P008	[Atlas.5.6] [CH12-12.4.5.2 p2]	[CH12.4.5.2 p7]	[CH12.4.5.2 p8]	[CH12.4.5.2 p8]	[CH12.4.5.2 p8]	[CH12.4.5.3 p1] [CH12.4.5.3 p2]	[CH12P008]	
Northern Europe	[CH12.4.5.1] [Atlas.5.6.4] [CH12.4.5.1]	[CH11.3.3] [CH12P008] [Atlas.5.6] [CH11.5.5] [CH12.4.5.1] [CH11.Tab8]	[CH12.4.5.1] [CH12.4.5.1 p5]	[CH12.4.5.1] [CH12.4.5.1 p5]	[CH12.4.5.2] [Atlas.5.6.4] [CH12.4.5.2 p1]	[CH12P008]	[CH11P007][Atlas.5.6] [CH11.4.2] [CH12-12.4.5.2 p2]	[CH12.4.5.2 p7]	[CH12.4.5.2 p8]	[CH12.4.5.3] [CH12.4.5.2 p8]	[CH12.4.5.2 p8]	[CH12.4.5.3 p1] [CH12.4.5.3 p2]	[CH12P008]	

	Climatic Impact Driver													
	Snow and Ice						Coastal and Oceanic					Other		
Europe	Snow and land ice	Permafrost	Lake, river and sea ice	Heavy snow and ice storm	Hail	Snow avalanche	Relative sea level	Coastal flood	Coastal erosion	Marine heatwave	Ocean and lake acidity	Air pollution	Atmospheric CO2	Radiation at surface
Mediterranean	[CH09P010] [CH12.4.5.4 p1] [CH09P010]	[CH12.4.5.4 p1]		[CH12.4.5.4 p5]	[CH12.4.5.4 p5]		[CH12.4.5.5] [CH12.4.5.5]	[CH12.4.5.5] [CH12.4.5.5]	[CH12.4.5.5] [CH12.4.5.5]	[CH12.4.5.5] [CH12.4.5.5][CH09P014]	[CH12.4.5.5] [CH12.4.5.5]	[CH12.4.5.6 p1]	[CH12.4.5.5] [CH12P003]	[CH12.4.5.6 p5]
Central Europe	[CH09P010][CH12.4.5.4] [CH12.4.5.4 p1] [CH09P010]	[CH12.4.5.4 p1] [CH09P009]		[CH12.4.5.4 p5]	[CH12.4.5.4 p5]		[CH12.4.5.5] [CH12.4.5.5]	[CH12.4.5.5] [CH12.4.5.5]	[CH12.4.5.5] [CH12.4.5.5]	[CH12.4.5.5] [CH12.4.5.5] [CH09P014]	[CH12.4.5.5] [CH12.4.5.5]	[CH12.4.5.6 p1]	[CH12.4.5.5] [CH12P003]	[CH12.4.5.6 p5]
Eastern Europe	[CH12.4.5.4 p1] [CH09P010]	[CH12.4.5.4 p1] [CH09P009]		[CH12.4.5.4 p5]	[CH12.4.5.4 p5]						[CH12.4.5.5]	[CH12.4.5.6 p1]	[CH12.4.5.5] [CH12P003]	[CH12.4.5.6 p5]
Northern Europe	[CH12.4.5.4] [CH12.4.5.4 p1][CH09P010]	[CH12.4.5.4 p1] [CH09P009]	[CH09P017]	[CH12.4.5.4 p5]	[CH12.4.5.4 p5]		[CH12.4.5.5] [CH12.4.5.5]	[CH12.4.5.5] [CH12.4.5.5]	[CH12.4.5.5] [CH12.4.5.5]	[CH12.4.5.5] [CH12.4.5.5] [CH09P014]	[CH12.4.5.5] [CH12.4.5.5]	[CH12.4.5.6 p1]	[CH12.4.5.6] [CH12P003]	[CH12.4.5.6 p5]

	Climatic Impact Driver													
	Heat and Cold				Wet and Dry							Wind		
North America	Mean temperature	Extreme heat	Cold spell	Frost	Mean precipitation	River flood	Pluvial flood	Landslide	Aridity	Drought	Wildfire	Mean wind speed	Severe wind storm	Sand and dust storm
North Central America	[Atlas.5.7.2] [12.4.6.1], [Atlas.5.7.4]	[12.4.6.1], [12.4.6.1], [11.9]	[12.4.6.1], [12.4.6.1]	[12.4.6.1], [12.4.6.1]	[Atlas.5.7.2] [12.4.6.2], [Atlas.5.7.4]	[12.4.6.2], [11.9]	[CH11P007], [12.4.6.2] [12.4.6.2]	[12.4.6.2]	[12.4.6.2]	[12.4.6.2], [11.9]	[12.4.6.2]	[12.4.6.3]	[12.4.6.3]	[12.4.6.3]
Western North America	[12.4.6.1], [Atlas.5.7.2] [12.4.6.1], [Atlas.5.7.4]	[12.4.6.1], [12.4.6.1], [11.9]	[12.4.6.1], [12.4.6.1]	[12.4.6.1]	[12.4.6.2], [Atlas.5.7.2] [12.4.6.2], [Atlas.5.7.4], [CH2AP004]	[12.4.6.2], [11.9]	[12.4.6.2] [12.4.6.2]	[12.4.6.2]	[12.4.6.2], [CH08P009]	[11.9], [CH11P012] [12.4.6.2], [11.9]	[12.4.6.2], [12.4.6.2]	[12.4.6.3]	[12.4.6.3]	[12.4.6.3], [12.4.6.3]
Central North America	[12.4.6.1], [Atlas.5.7.2] [12.4.6.1], [Atlas.5.7.4]	[12.4.6.1], [12.4.6.1], [11.9]	[12.4.6.1], [12.4.6.1]	[12.4.6.1]	[12.4.6.2], [Atlas.5.7.2] [12.4.6.2], [Atlas.5.7.4], [CH2AP004]	[12.4.6.2], [11.9]	[12.4.6.2] [12.4.6.2]		[12.4.6.2]	[11.9], [12.4.6.2], [11.9]	[12.4.6.2], [12.4.6.2]	[12.4.6.3]	[12.4.6.3]	[12.4.6.3]
Eastern North America	[12.4.6.1], [Atlas.5.7.2] [12.4.6.1], [Atlas.5.7.4]	[12.4.6.1], [12.4.6.1], [11.9]	[12.4.6.1], [12.4.6.1]	[12.4.6.1]	[12.4.6.2], [Atlas.5.7.2] [12.4.6.2], [Atlas.5.7.4], [CH2AP004]	[12.4.6.2], [11.9] [CH11P010]	[12.4.6.2] [12.4.6.2]	[12.4.6.2]	[12.4.6.2]	[11.9], [12.4.6.2], [11.9]	[12.4.6.2], [12.4.6.2]	[12.4.6.3]	[12.4.6.3]	
Northeastern Canada	[12.4.6.1], [Atlas.5.7.2] [12.4.6.1], [Atlas.5.7.4]	[12.4.6.1], [12.4.6.1], [11.9]	[12.4.6.1], [12.4.6.1]	[12.4.6.1], [12.4.6.1]	[12.4.6.2], [Atlas.5.7.2] [12.4.6.2], [Atlas.5.7.4], [CH2AP004]	[12.4.6.2], [11.9]	[12.4.6.2]		[12.4.6.2]	[12.4.6.2], [11.9]	[12.4.6.2], [12.4.6.2]	[12.4.6.3]	[12.4.6.3]	
Northwest North America	[12.4.6.1], [Atlas.5.7.2] [12.4.6.1], [Atlas.5.7.4]	[12.4.6.1], [12.4.6.1], [11.9]	[12.4.6.1], [12.4.6.1]	[12.4.6.1], [12.4.6.1]	[12.4.6.2], [Atlas.5.7.2] [12.4.6.2], [Atlas.5.7.4], [CH2AP004]	[12.4.6.2], [11.9]	[12.4.6.2]	[12.4.6.2]	[12.4.6.2] [CH11P012]	[12.4.6.2], [11.9]	[12.4.6.2], [12.4.6.2]	[12.4.6.3]	[12.4.6.3]	

Climatic Impact Driver

North America	Snow and Ice						Coastal and Oceanic					Other		
	Snow and land ice	Permafrost	Lake, river and sea ice	Heavy snow and ice storm	Hail	Snow avalanche	Relative sea level	Coastal flood	Coastal erosion	Marine heatwave	Ocean and lake acidity	Air pollution	Atmospheric CO2	Radiation at surface
North Central America					[12.4.6.4]		[9.6.1], [12.4.6.5], [12.4.6.5], [9.6.3]	[12.4.6.5], [9.5.6.1], [12.4.6.5], [9.5.6.2]	[12.4.6.5]	[12.4.6.5], [CCBox 9.1], [12.4.6.5], [CCBox 9.1],	[5.3.2.1], [12.4.6.5], [5.3.3.3], [12.4.6.5]	[12.4.6.6]	[12.4.6.6]	[12.4.6.6]
Western North America	[9.5.1], [9.5.3], [12.4.6.4], [Atlas.5.7.2], [9.5.1], [9.5.3], [12.4.6.4], [Atlas.5.7.4]		[12.4.6.4], [12.4.6.4]	[12.4.6.4]	[12.4.6.4]	[12.4.6.4]	[9.6.1], [12.4.6.5], [12.4.6.5], [9.6.3]	[12.4.6.5], [9.5.6.1], [12.4.6.5], [9.5.6.2]	[12.4.6.5]	[12.4.6.5], [CCBox 9.1], [12.4.6.5], [CCBox 9.1],	[5.3.2.1], [12.4.6.5], [5.3.3.3], [12.4.6.5]	[12.4.6.6]	[5.2.1], [12.4.6.6], [5.2.1],	[12.4.6.6]
Central North America	[9.5.1], [9.5.3], [12.4.6.4], [Atlas.5.7.2], [9.5.1], [9.5.3], [12.4.6.4], [Atlas.5.7.4]		[12.4.6.4], [12.4.6.4]	[12.4.6.4]	[12.4.6.4]		[9.6.1], [12.4.6.5], [12.4.6.5], [9.6.3]	[12.4.6.5], [9.5.6.1], [12.4.6.5], [9.5.6.2]	[12.4.6.5]	[12.4.6.5], [CCBox 9.1], [12.4.6.5], [CCBox 9.1],	[5.3.2.1], [12.4.6.5], [5.3.3.3], [12.4.6.5]	[12.4.6.6]	[5.2.1], [12.4.6.6], [5.2.1],	[12.4.6.6]
Eastern North America	[9.5.1], [9.5.3], [12.4.6.4], [Atlas.5.7.2], [9.5.1], [9.5.3], [12.4.6.4], [Atlas.5.7.4]		[12.4.6.4], [12.4.6.4]	[12.4.6.4]	[12.4.6.4]	[12.4.6.4]	[9.6.1], [12.4.6.5], [12.4.6.5], [9.6.3]	[12.4.6.5], [9.5.6.1], [12.4.6.5], [9.5.6.2]	[12.4.6.5]	[12.4.6.5], [CCBox 9.1], [12.4.6.5], [CCBox 9.1],	[5.3.2.1], [12.4.6.5], [5.3.3.3], [12.4.6.5]	[12.4.6.6]	[5.2.1], [12.4.6.6], [5.2.1],	[12.4.6.6]
Northeastern Canada	[9.5.1], [9.5.3], [12.4.6.4], [Atlas.5.7.2], [9.5.1], [9.5.3], [12.4.6.4], [Atlas.5.7.4]	[12.4.6.4], [9.5.2], [12.4.6.4], [9.5.2]	[9.3.1], [12.4.6.4], [9.3.1], [12.4.6.4]	[12.4.6.4]		[12.4.6.4]	[9.6.1], [12.4.6.5], [12.4.6.5], [9.6.3]	[12.4.6.5], [9.5.6.1], [12.4.6.5], [9.5.6.2]	[12.4.6.5]	[CCBox 9.1], [12.4.6.5], [CCBox 9.1],	[5.3.2.1], [12.4.6.5], [5.3.3.3], [12.4.6.5]	[12.4.6.6]	[5.2.1], [12.4.6.6], [5.2.1],	[12.4.6.6]
Northwest North America	[9.5.1], [9.5.3], [12.4.6.4], [Atlas.5.7.2], [9.5.1], [9.5.3], [12.4.6.4], [Atlas.5.7.4]	[12.4.6.4], [9.5.2], [12.4.6.4], [9.5.2]	[9.3.1], [12.4.6.4], [9.3.1], [12.4.6.4]	[12.4.6.4]		[12.4.6.4]	[9.6.1], [12.4.6.5], [12.4.6.5], [9.6.3]	[12.4.6.5], [9.5.6.1], [12.4.6.5], [9.5.6.2]	[12.4.6.5]	[CCBox 9.1], [12.4.6.5], [CCBox 9.1],	[5.3.2.1], [12.4.6.5], [5.3.3.3], [12.4.6.5]	[12.4.6.6]	[5.2.1], [12.4.6.6], [5.2.1],	[12.4.6.6]

Small Islands	Climatic Impact Driver: Heat and Cold				Wet and Dry							Wind		
	Mean temperature	Extreme heat	Cold spell	Frost	Mean precipitation	River flood	Pluvial flood	Landslide	Aridity	Drought	Wildfire	Mean wind speed	Severe wind storm	Sand and dust storm
Caribbean	[CH12.4.7.1], [Atlas.5.8.2], [CH12.4.7.1], [Atlas.5.8.3]	[CH11.9 Tab7], [CH12.4.7.1], [CH11.9 Tab7], [CH12.4.7.1]			[CH12.4.7.2], [Atlas.5.8.2], [CH12.4.7.2], [Atlas.5.8.3]	[CH11 Box5], [12.4.7.2], [CH11 Box5], [12.4.7.2]	[CH11.9 Tab7], [12.4.7.2], [CH11.9 Tab7], [12.4.7.2]	[12.4.7.2], [12.4.7.2]	[CH11 Box5], [12.4.7.2], [CH11 Box5], [12.4.7.2]	[CH11.9 Tab7], [12.4.7.2], [CH11.9 Tab7], [12.4.7.2]	[12.4.7.2], [12.4.7.2]	[12.4.7.3], [12.4.7.3]	[CH11 Box5], [12.4.7.3], [CH11 Box5], [12.4.7.3]	
Pacific	[CH12.4.7.1], [Atlas.5.8.2], [CH12.4.7.1], [Atlas.5.8.3]	[CH11.9 Tab6], [CH12.4.7.1], [CH11.9 Tab6], [CH12.4.7.1]			[CH12.4.7.2], [Atlas.5.8.2], [CH12.4.7.2], [Atlas.5.8.3]	[CH11 Box5], [12.4.7.2], [CH11 Box5], [12.4.7.2]	[CH11.9 Tab6], [12.4.7.2], [CH11.9 Tab6], [12.4.7.2]	[12.4.7.2], [12.4.7.2]	[CH11 Box5], [12.4.7.2], [CH11 Box5], [12.4.7.2]	[CH11.9 Tab6], [12.4.7.2], [CH11.9 Tab6], [12.4.7.2]	[12.4.7.2], [12.4.7.2]	[12.4.7.3], [12.4.7.3]	[CH11 Box5], [12.4.7.3], [CH11 Box5], [12.4.7.3]	

Small Islands	Climatic Impact Driver: Snow and Ice						Coastal and Oceanic					Other		
	Snow and land ice	Permafrost	Lake, river and sea ice	Heavy snow and ice storm	Hail	Snow avalanche	Relative sea level	Coastal flood	Coastal erosion	Marine heatwave	Ocean and lake acidity	Air pollution	Atmospheric CO2	Radiation at surface
Caribbean							[9.6.1.4], [12.4.7.4], [12.4.7.4]	[CH11 Box5], [12.4.7.4], [CH11 Box5], [12.4.7.4]	[12.4.7.4], [12.4.7.4]	[CCBox 9.1], [12.4.7.4], [CCBox 9.1], [12.4.7.4]	[12.4.7.4], [12.4.7.4]	[12.4.7.5], [12.4.7.5]	[12.4.7.5], [12.4.7.5]	[12.4.7.5], [12.4.7.5]
Pacific							[9.6.1.4], [12.4.7.4], [12.4.7.4]	[CH11 Box5], [12.4.7.4], [CH11 Box5], [12.4.7.4]	[12.4.7.4], [12.4.7.4]	[CCBox 9.1], [12.4.7.4], [CCBox 9.1], [12.4.7.4]	[12.4.7.4], [12.4.7.4]	[12.4.7.5], [12.4.7.5]	[12.4.7.5], [12.4.7.5]	[12.4.7.5], [12.4.7.5]

	Climatic Impact Driver													
	Heat and Cold				Wet and Dry							Wind		
Polar Terrestrial Regions	Mean temperature	Extreme heat	Cold spell	Frost	Mean precipitation	River flood	Pluvial flood	Landslide	Aridity	Drought	Wildfire	Mean wind speed	Severe wind storm	Sand and dust storm
Arctic Northwest North America	[12.4.9.2], [Atlas.5.9.2.4], [12.4.9.2], [Atlas.5.9.2.4]	[12.4.9.2], [12.4.9.2]	[12.4.9.2], [12.4.9.2]	[12.4.9.2], [12.4.9.2]	[12.4.9.3], [Atlas.5.9.2.4]	[12.4.9.3], [12.4.9.3]	[12.4.9.3], [12.4.9.3]	[12.4.9.3]	[12.4.9.3], [12.4.9.3]	[12.4.9.3], [12.4.9.3]	[12.4.9.3], [12.4.9.3]	[12.4.9.4], [12.4.9.4]	[12.4.9.4]	
Arctic Northeastern Canada	[12.4.9.2], [Atlas.5.9.2.4], [12.4.9.2], [Atlas.5.9.2.4]	[12.4.9.2], [12.4.9.2]	[12.4.9.2], [12.4.9.2]	[12.4.9.2], [12.4.9.2]	[12.4.9.3], [Atlas.5.9.2.4]	[12.4.9.3], [12.4.9.3]	[12.4.9.3], [12.4.9.3]	[12.4.9.3]	[12.4.9.3], [12.4.9.3]	[12.4.9.3], [12.4.9.3]	[12.4.9.3], [12.4.9.3]	[12.4.9.4], [12.4.9.4]	[12.4.9.4]	
Greenland	[12.4.9.2], [Atlas.5.9.2.4], [12.4.9.2], [Atlas.5.9.2.4]	[12.4.9.2], [12.4.9.2]	[12.4.9.2], [12.4.9.2]	[12.4.9.2], [12.4.9.2]	[12.4.9.3], [Atlas.5.9.2.4]		[12.4.9.3], [12.4.9.3]	[12.4.9.3]	[12.4.9.3], [12.4.9.3]	[12.4.9.3], [12.4.9.3]		[12.4.9.4]	[12.4.9.4]	
Arctic North Europe	[12.4.9.2], [Atlas.5.9.2.4], [12.4.9.2], [Atlas.5.9.2.4]	[12.4.9.2], [12.4.9.2]	[12.4.9.2], [12.4.9.2]	[12.4.9.2], [12.4.9.2]	[12.4.9.3], [Atlas.5.9.2.4]	[12.4.9.3], [12.4.9.3]	[12.4.9.3], [12.4.9.3]	[12.4.9.3]	[12.4.9.3], [12.4.9.3]	[12.4.9.3], [12.4.9.3]	[12.4.9.3], [12.4.9.3]	[12.4.9.4], [12.4.9.4]	[12.4.9.4]	
Russian Arctic	[12.4.9.2], [Atlas.5.9.2.4], [12.4.9.2], [Atlas.5.9.2.4]	[12.4.9.2], [12.4.9.2], [11.9]	[12.4.9.2], [12.4.9.2]	[12.4.9.2], [12.4.9.2]	[12.4.9.3], [Atlas.5.9.2.4]	[12.4.9.3], [CH11P010] [12.4.9.3] [CH11P011]	[12.4.9.3], [12.4.9.3]	[12.4.9.3]	[12.4.9.3], [12.4.9.3]	[12.4.9.3], [12.4.9.3]	[12.4.9.3], [12.4.9.3]	[12.4.9.4], [12.4.9.4]	[12.4.9.4]	
West Antarctica	[12.4.9.2], [Atlas.5.9.1.4], [CH2AP001], [12.4.9.2], [Atlas.5.9.1.4]	[12.4.9.2]	[12.4.9.2]	[12.4.9.2]	[12.4.9.3]-l, [Atlas.5.9.1.4]-m			[12.4.9.2]				[12.4.9.4], [12.4.9.4]	[12.4.9.4]	
East Antarctica	[12.4.9.2], [Atlas.5.9.1.4], [12.4.9.2], [Atlas.5.9.1.4]	[12.4.9.2]	[12.4.9.2]	[12.4.9.2]	[12.4.9.3], [Atlas.5.9.1.4]							[12.4.9.4], [12.4.9.4]	[12.4.9.4]	

	Climatic Impact Driver													
	Snow and Ice						Coastal and Oceanic					Other		
	Snow and land ice	Permafrost	Lake, river and sea ice	Heavy snow and ice storm	Hail	Snow avalanche	Relative sea level	Coastal flood	Coastal erosion	Marine heatwave	Ocean and lake acidity	Air pollution	Atmospheric CO2	Radiation at surface
Polar Terrestrial Regions														
Arctic Northwest North America	[9.5.1], [9.5.3], [12.4.9.5], [Atlas.5.9.2.4], [9.5.1], [9.5.3], [12.4.9.5], [Atlas.5.9.2.4]	[12.4.9.5], [9.5.2], [12.4.9.5], [9.5.2]	[9.3.1], [12.4.9.5], [9.3.1], [12.4.9.5]	[12.4.9.5]		[12.4.9.5]	[9.6.1], [12.4.9.6], [12.4.9.6], [9.6.3]	[12.4.9.6], [9.5.6.2]	[12.4.9.6]	[12.4.9.6], [CCBox 9.1], [12.4.9.6], [CCBox 9.1],	[5.3.2.1], [12.4.9.6], [5.3.3.3], [12.4.9.6]	[12.4.9.7]	[5.2.1], [12.4.9.7], [5.2.1],	[12.4.9.7]
Arctic Northeastern Canada	[9.5.1], [9.5.3], [12.4.9.5], [Atlas.5.9.2.4], [9.5.1], [9.5.3], [12.4.9.5], [Atlas.5.9.2.4]	[12.4.9.5], [9.5.2], [12.4.9.5], [9.5.2]	[9.3.1], [12.4.9.5], [9.3.1], [12.4.9.5]	[12.4.9.5]		[12.4.9.5]	[9.6.1], [12.4.9.6], [12.4.9.6], [9.6.3]	[12.4.9.6], [9.5.6.2]	[12.4.9.6]	[12.4.9.6], [CCBox 9.1], [12.4.9.6], [CCBox 9.1],	[5.3.2.1], [5.3.3.3], [12.4.9.6]	[12.4.9.7]	[5.2.1], [12.4.9.7], [5.2.1],	[12.4.9.7]
Greenland	[9.4.1.1], [12.4.9.5], [9.4.1.2], [12.4.9.5]	[12.4.9.5], [9.5.2], [12.4.9.5], [9.5.2]	[9.3.1], [12.4.9.5], [9.3.1], [12.4.9.5]	[12.4.9.5]		[12.4.9.5]	[9.6.1], [12.4.9.6], [12.4.9.6], [9.6.3]	[12.4.9.6], [9.5.6.2]	[12.4.9.6]	[12.4.9.6], [CCBox 9.1], [12.4.9.6], [CCBox 9.1],	[5.3.2.1], [5.3.3.3], [12.4.9.6]	[12.4.9.7]	[5.2.1], [12.4.9.7], [5.2.1],	[12.4.9.7]
Arctic North Europe	[9.5.1], [9.5.3], [12.4.9.5], [Atlas.5.9.2.4], [9.5.1], [9.5.3], [12.4.9.5], [Atlas.5.9.2.4]	[12.4.9.5], [9.5.2], [12.4.9.5], [9.5.2]	[9.3.1], [12.4.9.5], [9.3.1], [12.4.9.5]	[12.4.9.5]		[12.4.9.5]	[9.6.1], [12.4.9.6], [12.4.9.6], [9.6.3]	[12.4.9.6], [9.5.6.2]	[12.4.9.6]	[12.4.9.6], [CCBox 9.1], [12.4.9.6], [CCBox 9.1],	[5.3.2.1], [5.3.3.3], [12.4.9.6]	[12.4.9.7]	[5.2.1], [12.4.9.7], [5.2.1],	[12.4.9.7]
Russian Arctic	[9.5.1], [9.5.3], [12.4.9.5], [Atlas.5.9.2.4], [9.5.1], [9.5.3], [12.4.9.5], [Atlas.5.9.2.4]	[12.4.9.5], [9.5.2], [12.4.9.5], [9.5.2]	[9.3.1], [12.4.9.5], [9.3.1], [12.4.9.5]	[12.4.9.5]		[12.4.9.5]	[9.6.1], [12.4.9.6], [12.4.9.6], [9.6.3]	[12.4.9.6], [9.5.6.2]	[12.4.9.6]	[12.4.9.6], [CCBox 9.1], [12.4.9.6], [CCBox 9.1],	[5.3.2.1], [12.4.9.6], [5.3.3.3], [12.4.9.6]	[12.4.9.7]	[5.2.1], [12.4.9.7], [5.2.1],	[12.4.9.7]
West Antarctica	[9.4.2.1], [9.5.1], [9.5.3], [12.4.9.5], [Atlas.5.91.4], [9.4.2.2], [9.5.1], [9.5.3], [12.4.9.5], [Atlas.5.9.1.4]	[12.4.9.5], [9.5.2], [12.4.9.5], [9.5.2]	[9.3.2], [12.4.9.5], [9.3.2], [12.4.9.5]	[12.4.9.5]		[12.4.9.5]	[9.6.1], [12.4.9.6], [12.4.9.6], [9.6.3]	[12.4.9.6], [9.5.6.2]	[12.4.9.6]	[12.4.9.6], [CCBox 9.1], [12.4.9.6], [CCBox 9.1],	[5.3.2.1], [12.4.9.6], [5.3.3.3], [12.4.9.6]		[5.2.1], [12.4.9.7], [5.2.1],	[12.4.9.7]
East Antarctica	[9.4.2.1], [9.5.1], [9.5.3], [12.4.9.5], [Atlas.5.91.4], [9.4.2.2], [9.5.1], [9.5.3], [12.4.9.5], [Atlas.5.9.1.4]	[12.4.9.5], [9.5.2], [12.4.9.5], [9.5.2]	[9.3.2], [12.4.9.5], [9.3.2], [12.4.9.5]	[12.4.9.5]			[9.6.1], [12.4.9.6], [12.4.9.6], [9.6.3]			[12.4.9.6], [CCBox 9.1], [12.4.9.6], [CCBox 9.1],	[5.3.2.1], [5.3.3.3], [12.4.9.6]		[5.2.1], [12.4.9.7], [5.2.1],	[12.4.9.7]

[END TABLE TS.A.1 HERE]

[START TABLE TS.A.2 HERE]

Table TS.A.2: This table identifies the location in the underlying chapters of the evidence supporting the assessment of confidence in observed climate changes and climate events which have been attributed to anthropogenic causes. As for 0, the climatic impact drivers are identified at the top of each page of the table and the regions identified in the first column of the table and the codes identify the sections or tables in the underlying chapters which provide the evidence. This table has been completed for regions in two continents, Europe and Central and South America and also identifies where there is no evidence of attribution.

	Climatic Impact Driver													
	Heat and Cold				Wet and Dry							Wind		
	Mean temperature	Extreme heat	Cold spell	Frost	Mean precipitation	River flood	Pluvial flood	Landslide	Aridity	Drought	Wildfire	Mean wind speed	Severe wind storm	Sand and dust storm
Central and South America														
Southern Central America	[CH03{3.3.1.D &A}]	[CH11Tab11.1]	[CH11Tab11.1] low confidence cold spells in South America		[CH3{3.3.2.1P01 1}]		no evidence					[CH11Tab11.1} low confidence in all basins		
Northwestern South America	[CH03{3.3.1.D &A}]	[CH11Tab11.1]	[CH11TabApp]		[CH3{3.3.2.1P01 1}]		[CH11Tab11.7]					[CH11Tab11.1} low confidence in all basins		
Northern South America	[CH03{3.3.1.D &A}]	[CH11Tab11.1]	[CH11Tab11.1] low confidence cold spells in South America		[CH3{3.3.2.1P01 1}]		[CH11Tab11.7]					[CH11Tab11.1} low confidence in all basins		
South American Monsoon	[CH03{3.3.1.D &A}]	[CH11Tab11.1]	[CH11Tab11.1] low confidence cold spells in South America		[CH3{3.3.2.1P01 1}]		[CH11Tab11.7]					[CH11Tab11.1} low confidence in all basins		
Northeastern South America	[CH03{3.3.1.D &A}]	[CH11Tab11.1]	[CH11Tab11.1] low confidence cold spells in South America		[CH3{3.3.2.1P01 1}]		[CH11Tab11.7]					[CH11Tab11.1} low confidence in all basins		
Southwestern South America	[CH03{3.3.1.D &A}]	[CH11Tab11.1]	[CH11Tab11.1] low confidence cold spells in South America				[CH11Tab11.7]		[CH11Tab11.7], low confidemce	[CH11Tab11.7], [CH11TabApp] low confidence		[CH11Tab11.1} low confidence in all basins		
Southeastern South America	[CH03{3.3.1.D &A}]	[CH11Tab11.7]	[CH11Tab11.1] low confidence cold spells in South America		[CH3{3.3.2.1P01 0}]		[ch11Tab11.7], [CH10.4.10.2.4]					[CH11Tab11.1} low confidence in all basins		
Southern South America	[CH03{3.3.1.D &A}]	[CH11Tab11.7] low confidence	[CH11Tab11.1] low confidence cold spells in South America				[CH11Tab11.7] low confidence					[CH11Tab11.1} low confidence in all basins		

	Climatic Impact Driver													
	Snow and Ice						Coastal and Oceanic					Other		
	Snow and land ice	Permafrost	Lake, river and sea ice	Heavy snow and ice storm	Hail	Snow avalanche	Relative sea level	Coastal flood	Coastal erosion	Marine heatwave	Ocean and lake acidity	Air pollution	Atmospheric CO2	Radiation at surface
Central and South America														
Southern Central America							[CH09P013]	no evidence	no evidence	[CH09box9.1]	no evidence	no evidence	use global statement? Not sure that is attributed to burning of ff in WG1?	no evidence
Northwestern South America							[CH09P013]	no evidence	no evidence	[CH09box9.1]	no evidence	no evidence		no evidence
Northern South America							[CH09P013]	no evidence	no evidence	[CH09box9.1]	no evidence	no evidence		no evidence
South American Monsoon							[CH09P013]	no evidence	no evidence	[CH09box9.1]	no evidence	no evidence		no evidence
Northeastern South America							[CH09P013]	no evidence	no evidence	[CH09box9.1]	no evidence	no evidence		no evidence
Southwestern South America							[CH09P013]	no evidence	no evidence	[CH09box9.1]	no evidence	no evidence		no evidence
Southeastern South America							[CH09P013]	no evidence	no evidence	[CH09box9.1]	no evidence	no evidence		no evidence
Southern South America							[CH09P013]	no evidence	no evidence	[CH09box9.1]	no evidence	no evidence		no evidence

	Climatic Impact Driver													
	Heat and Cold				Wet and Dry							Wind		
Europe	Mean temperature	Extreme heat	Cold spell	Frost	Mean precipitation	River flood	Pluvial flood	Landslide	Aridity	Drought	Wildfire	Mean wind speed	Severe wind storm	Sand and dust storm
Mediterranean	[CH03{3.3.1.1D &A}]	[CH11Tab11.8]	[CH11Tab11.8]	no evidence	no evidence	low confidence [CH11P010]	[CH11Tab11.8] (mediumconfidence observed trend not attributable)	no evidence	[CH08P005]	[Atlas5.6previousfindingsfromIPCC][CH11Tab11.8]	no evidence	no evidence	no evidence	not relevant
Central Europe	[CH03{3.3.1.1D &A}]	[CH11Tab11.8]	[CH11Tab11.8]	no evidence	no evidence	low confidence [CH11P010]	low confidence [CH11Tab11.8]	no evidence	no evidence	[Atlas5.6previousfindingsfromIPCC][CH11Tab11.8]	no evidence	no evidence	no evidence	not relevant
Eastern Europe	[CH03{3.3.1.1D &A}]	[CH11Tab11.8]	[CH11Tab11.8]	no evidence	no evidence	low confidence [CH11P010]	no evidence	no evidence	no evidence	no evidence	no evidence	no evidence	no evidence	not relevant
Northern Europe	[CH03{3.3.1.1D &A}]	[CH11Tab11.8]	[CH11Tab11.8]	no evidence	no evidence	low confidence [CH11P010]	[CH11Tab11.8] (not in summer, but HC in winter)	no evidence	[CH11Tab11.8]	no evidence	no evidence	no evidence	no evidence	not relevant

	Climatic Impact Driver													
	Snow and Ice						Coastal and Oceanic					Other		
Europe	Snow and land ice	Permafrost	Lake, river and sea ice	Heavy snow and ice storm	Hail	Snow avalanche	Relative sea level	Coastal flood	Coastal erosion	Marine heatwave	Ocean and lake acidity	Air pollution	Atmospheric CO2	Radiation at surface
Mediterranean	no evidence	no evidence	no evidence	no evidence	no evidence	no evidence	[CH09P013]	no evidence	no evidence	[CH09box9.1]	no evidence	no evidence		[Atlas5.6P03]
Central Europe	no evidence	no evidence	no evidence	no evidence	no evidence	no evidence	[CH09P013]	no evidence	no evidence	[CH09box9.1]	no evidence	no evidence		[Atlas5.6P03]
Eastern Europe	no evidence	no evidence	no evidence	no evidence	no evidence	no evidence	[CH09P013]	no evidence	no evidence	[CH09box9.1]	no evidence	no evidence		[Atlas5.6P03]
Northern Europe	[CH03P013]	no evidence	no evidence	no evidence	no evidence	no evidence	[CH09P013]	no evidence	no evidence	[CH09box9.1]	no evidence	no evidence		[Atlas5.6P03]

[END TABLE TS.A.2 HERE]

[START TABLE TS.A.3 HERE]

Table TS.A.3: Footnotes to the evidence on projected changes in climatic impact drivers represented by the colours in Table TS.13 in the summary section of TS4.3. (Only climatic impact drivers with at least one footnote are represented in this table.)

	Climatic Impact Driver														
	Wet and Dry							Wind		Snow and Ice		Coastal and Oceanic			Other
	Mean precipitation	River flood	Pluvial flood	Landslide	Aridity	Drought	Wildfire	Mean wind speed	Severe wind storm	Snow and land ice	Snow avalanche	Relative sea level	Coastal flood	Coastal erosion	Air pollution
Africa															
North Africa*														4	
Sahara														4	
West Africa	1				3	3								4	
North East Africa	2				2	2								4	
Central East Africa	2				2	2								4	
Central Africa														4	
South West Africa														4	
South East Africa														4	
Asia															
West Siberia															
East Siberia															
West Central Asia														4	
South Asia									5					4	
Southeast Asia									5					4	
Russian Far East														4	
East Asia									5					4	
Tibetan Plateau															
Arabian Peninsula									5					4	
Australasia															
Northern Australia									8					4	
Central Australia		#							8					4	
Southern Australia									8	9	9			4	
New Zealand	6			7					8	9	9			4	
Central and South America															
Southern Central America														4	
Northwestern South America	10													4	
Northern South America														4	
South American Monsoon															
Northeastern South America														4	
Southwestern South America		11	11											4	
Southeastern South America		11	11											4	
Southern South America														4	

	Climatic Impact Driver														
	Wet and Dry							Wind		Snow and Ice		Coastal and Oceanic			Other
	Mean precipitation	River flood	Pluvial flood	Landslide	Aridity	Drought	Wildfire	Mean wind speed	Severe wind storm	Snow and land ice	Snow avalanche	Relative sea level	Coastal flood	Coastal erosion	Air pollution
Europe															
Mediterranean								13						4	14
Central Europe						15								4	14
Eastern Europe															14
Northern Europe		12											16	4	14
North America															
Mexico					23	23								4	
Western North America	18			20	19,22,23	19,22,23	21			17	17		20	4	
Central North America					22,23	22,23								4	
Eastern North America	20				22,23	22,23				17	17			4	
Northeastern Canada	20				20,22,23	20,22,23	21			17,6	17	19	19	4,21	
Northwest North America	20				20,22,23	20,22,23				17	17			4	
Small Islands															
Caribbean														4	
Pacific	24		24		24	24			25					4	
Polar Terrestrial Regions															
Arctic Northwest North America					22,23	23	21,22		22	17				4	
Arctic Northeastern Canada					22,23	23	21,22		28	17				4	
Greenland					22,23	23			28	17		27			
Arctic North Europe					22,23	23	21,22		28	17		26		4	
Russian Arctic					22,23	23	21,22		22	17				4	
West Antarctica										17					
East Antarctica															

1. High confidence in drying in western portions of West Africa and wettening in eastern portions of West Africa
2. Drying trend when averaged over each region for most indices
3. High confidence in drought in western parts of West Africa
4. Along sandy coasts and in the absence of sufficient sediment supply from terrestrial or offshore sources

* North Africa is not an official region of IPCC AR6, but assessment here is based upon the African portions of the Mediterranean Region

5. Cyclones decrease in number but increase in intensity
6. Mean preciptation increases(decreases) in south and west(north and east)
7. Low confidence of increase
8. Direction of change is inconsistent between CMIP5 and CMIP6 98P wind projections

(except over Tasmania and south island of NZ where there is low confidence of a small increase, no CMIP6 model agreement)

9. Only relevant at high altitudes

no literature, only based on Fig 12.10

10. With strong wettening in coastal areas
11. Except Southern Cone of South America
12. Excluding southern UK
13. Only in Western Mediterranean
14. High confidence of hazard increase for ozone air pollution , and low confidence in hazard decrease for aerosol pollution
15. Low confidence based on precipitation indices and high confidence based on soil moisture indices (Chapter 11)
16. Low confidence, low agreement for for Baltic Sea and in the Iberia and British Isles
17. Snow and wet avalanches may increase at some high elevation locations even as decreases are seen in lower elevations
18. Increasing in northern regions and decreasing toward south
19. Decreasing in northern regions and increasing toward south
20. Higher confidence in northern regions and lower toward south
21. Higher confidence in southern regions and lower toward north
22. Higher confidence in increase for some climatic impact driver indices during summertime
23. Higher confidence in decreases to soil moisture aridity and drought than streamflow or meteorological aridity and drought
24. In parts of western and equatorial Pacific but with spatial variations
25. Over central Pacific but decrease in other parts of the Pacific
26. Except for Baltic coasts where relative sea levels fall
27. Decreasing in west and increasing in east
28. Higher confidence in increase for some climatic impact driver indices during wintertime

[END TABLE TS.A.3 HERE]

Appendix TS.B Acronyms and Abbreviations for the AR6 WGI Technical Summary

[START TABLE TS.B.1 HERE]

Table TS.B.1: List of acronyms and abbreviations for the AR6 WGI Technical Summary

Acronym	Full Name
AIS	Antarctic Ice Sheet
AMOC	Atlantic Meridional Overturning Circulation
AMV	Atlantic Multidecadal Variability
AOD	Aerosol Optical Depth
AR	Assessment Report
AZM	Atlantic meridional and zonal modes (sometimes referred to as AMM, as well in the literature)
BC	Black Carbon
BVOC	Biogenic Volatile Organic Compound
CDR	Carbon Dioxide Removal
CE	Common Era
CEDS	Community Emissions Data Systems
CFC	Chlorofluorocarbon
CID	Climatic Impact Driver
CMIP	Coupled Model Intercomparison Project
CO	Carbon Monoxide
CO_2	Carbon Dioxide
CORDEX	Coordinated Regional Climate Downscaling Experiment
CRU	Climatic Research Unit (University of East Anglia)
DCPP	Decadal Climate Prediction Project
DI	Dimensions of Integration
DMS	Dimethyl Sulphide
EAIS	East Antarctic Ice Sheet
ECP	Extended Concentration Pathway
ECS	Equilibrium Climate Sensitivity
EECO	Early Eocene Climatic Optimum
EgC	Trillion tonnes of Carbon
ENSO	El Niño and Southern Oscillation
ERF	Effective Radiative Forcing
ERFaci	ERF due to aerosol-cloud interactions
ERFari	ERF due to aerosol-radiation interactions
ES	Executive Summary
ESL	Extreme Sea Level
ESM	Earth System Model

FAQ	Frequently Asked Questions
GCM	Global Climate Model
GHG	Greenhouse Gas
GLOF	Glacial Lake Outburst Flood
GMA	Global Monsoon Area
GMSL	Global Mean Sea Level
GMSLR	Global Mean Sea Level Rise
GMST	Global Mean Surface Temperature
GPCC	Global Precipitation Climatology Centre
GPCP	Global Precipitation Climatology Project
GrIS	Greenland Ice Sheet
GSAT	Global Surface Air Temperature
GtC	Giga tonnes (10^9 grams) of carbon
GTP	Global Temperature change Potential
GWPs	Global Warming Potentials
HCFC	Hydrochlorofluorocarbon
HFC	Hydrofluorocarbon
IAM	Integrated Assessment Modelling
ICE	Initial Condition Ensemble
IOB	Indian Ocean Basin and Dipole Modes (sometimes referred to as IOD as well)
IPBES	Intergovernmental Science-Policy Platform on Biodiversity and Ecosystem Services
IPCC	Intergovernmental Panel on Climate Change
IRF	Instantaneous Radiative Forcing
IRFari	Instantaneous Radiative Forcing due to aerosol-radiation interactions
ITCZ	Inter Tropical Convergence Zone
LDT	Last Deglacial Transition
LGM	Last Glacial Maximum
LIA	Little Ice Age
LIG	Last interglacial
LLCF	Long-lived climate forcers
LSAT	Land Surface Air Temperature
MH	Mid-Holocene
MHW	Marine Heatwaves
MICI	Marine Ice Cliff Instability
MISI	Marine Ice Sheet Instability
MJO	Madden-Julian Oscillation
MME	Multi-Model Ensembles
MPWP	Mid-Pliocene Warm Period
MWP	Medieval Warm Period

N_2O	Nitrous Oxide
NAM	Northern Annular Mode
NAO	North Atlantic Oscillation
NDC	Nationally Determined Contribution
NO_2	Nitrogen Dioxide
NO_x	Nitrogen Oxides
NTCF	Near-Term Climate Forcing
OH	Hydroxyl free radical
OHC	Ocean Heat Content
OS	Overshoot
pCO2	Partial pressure of carbon dioxide
PDF	Probability Distribution Function
PDV	Pacific Decadal Variability
PETM	Paleocene-Eocene Thermal Maximum
PgC	Petagram of carbon, 10^{15} grams of Carbon
PM	Particulate Matter
RCMIP	Reduced Complexity Model Intercomparison Project
RCM	Regional Climate Model
RCPs	Representative Concentration Pathway
RFC	Reasons For Concern
RX1day	Maximum 1-day precipitation
SACZ	South Atlantic Convergence Zone
SAM	Southern Annular Mode
SD	Standard Deviation
SDG	Sustainable Development Goals
SH	Southern Hemisphere
SLCF	Short-Lived Climate Forcers
SM	Supplementary Material
SO2	Sulphur Dioxide
SPM	Summary for Policymakers
SR1.5	Special Report on Global Warming of 1.5°C
SRCCL	Special Report on Climate Change and Land, full name “Special Report on climate change, desertification, land degradation, sustainable land management, food security, and greenhouse gas fluxes in terrestrial ecosystems”
SRES	Special Report on Emissions Scenarios
SRM	Solar Radiation Modification
SROCC	Special Report on the Ocean and Cryosphere in a Changing Climate
SSP	Shared Socio-Economic Pathway
SST	Sea Surface Temperature

SWE	Snow Water Equivalent
TCR	Transient Climate Response
TCRE	Transient Climate Response to Emissions
TC	Tropical Cyclones
Tg	Teragram (10^{12} grams)
TP	Tibetan Plateau
TS	Technical Summary
TXx	Maximum daily-maximum temperature
UN	United Nations
UNFCCC	United Nations Framework Convention on Climate Change
VOC	Volatile Organic Compound
WAIS	Western Antarctic Ice Sheet
WBGT	Wet Bulb Global Temperature
WG	Working Group
WHO	World Health Organization
WL	Warming Level
WMGHG	Well-Mixed Greenhouse Gas
ZEC	Zero Emissions Commitment
ZJ	Zettajoules

[END TABLE TS.B.1 HERE]

Figures

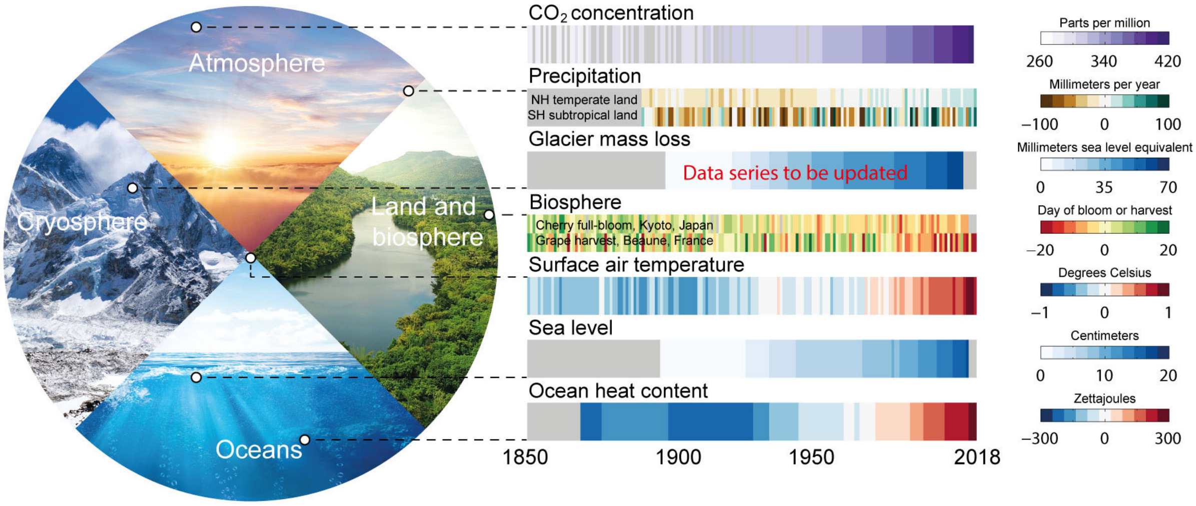

Figure TS.1: Changes are observed throughout the climate system. Left: The main domains of the climate system: Atmosphere, land and biosphere, cryosphere and oceans. Right: The evolution of a range of indicators of ongoing changes, since 1850 or the start of the observational record, covering all four climate system domains. Each stripe indicates the global, annual mean anomaly for a single year (except for precipitation which shows a latitude band mean, and the biosphere which shows local observations), relative to a multi-year baseline (except for CO2 concentration, which is absolute, and glacier mass loss, which shows integrated values). Grey indicates missing data. Datasets and baselines used are: CO2: Antarctic ice cores (Lüthi et al., 2008; Bereiter et al., 2015) and direct air measurements (Tans and Keeling, 2019) (see Figure 1.3 for details). Precipitation: Global Precipitation Climatology Centre (GPCC) V8 (updated from Becker et al., 2013), baseline 1961-1990 using land areas only. Latitude bands are 33°N-66°N and 15°S-30°S. Glacier mass loss: TO BE UPDATED. Biosphere: Cherry blooming dates from Aono and Saito, 2010, grape harvest dates from Labbe et al., 2019. Surface air temperature: HadCRUT5.0 (Morice et al., submitted), baseline 1961-1990. Sea level: (Dangendorf et al., 2019), baseline 1900-1929. Ocean heat content: (Zanna et al., 2019), baseline 1961-1990. {Figure 1.2}

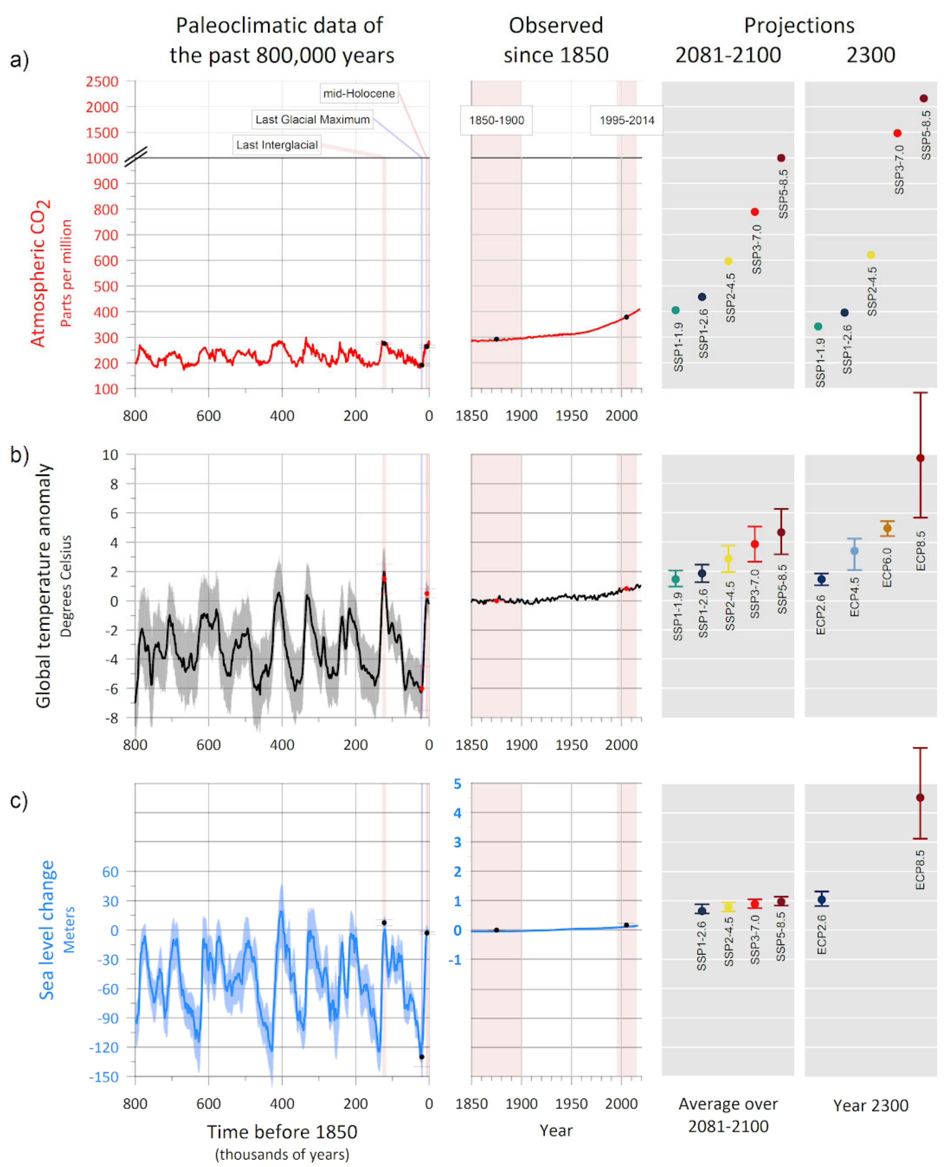

Figure TS.2: Long-term context of anthropogenic climate change based on selected palaeoclimatic reconstructions over the past 800,000 years, observed changes and future projections using CMIP6 SSPs (2081-2100) and CMIP5 RCP-extensions (2300) for three key indicators: atmospheric CO_2 concentrations, global mean surface temperature (GMST), and global mean sea level (GMSL). Details available from Figure 1.3. Dots/whiskers on the right-hand side panels of the figure (grey background) indicate the projected median and ranges derived from SSP-based (2081-2100; Chapters 4 and 9) and RCP-extension simulations (2300; IPCC SROCC, 2019). Best estimates (dots) and uncertainties (whiskers) as assessed by Chapter 2 (Figure 2.33 and Annex II) for each of the three indicators and selected palaeo-reference periods used in this report (Cross-Chapter Box 2.1) are included in the “paleoclimate” (left) and “observed” (middle) panels. The scenarios used here are introduced in Section TS1.3. [PLACEHOLDER: year 2300 RCP extensions (ECP) based projections to be updated to SSP-based projections from Ch4/9 for the FGD if available]

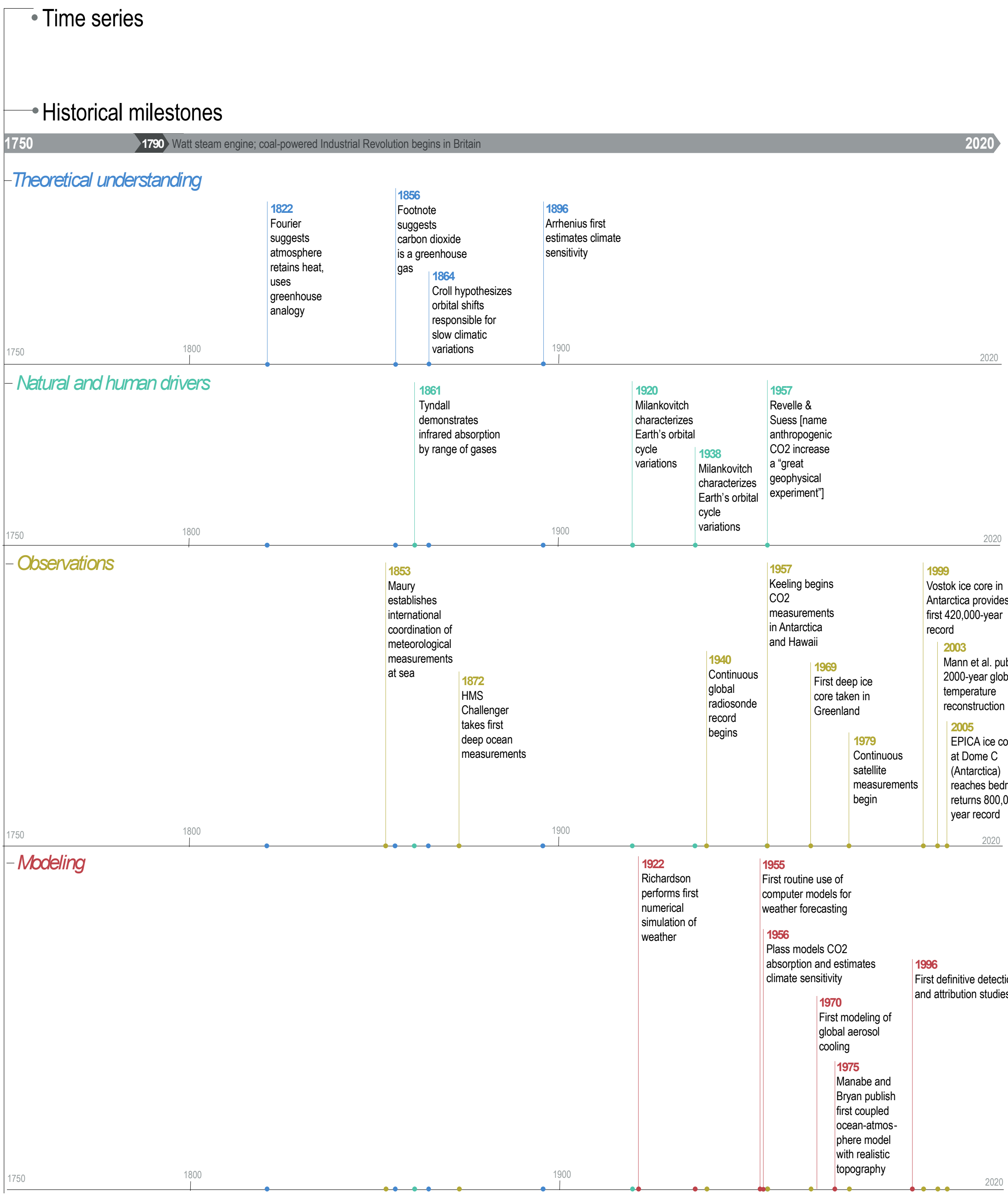

Figure TS.3: Timeline of key events and climate knowledge developments. {1.3}

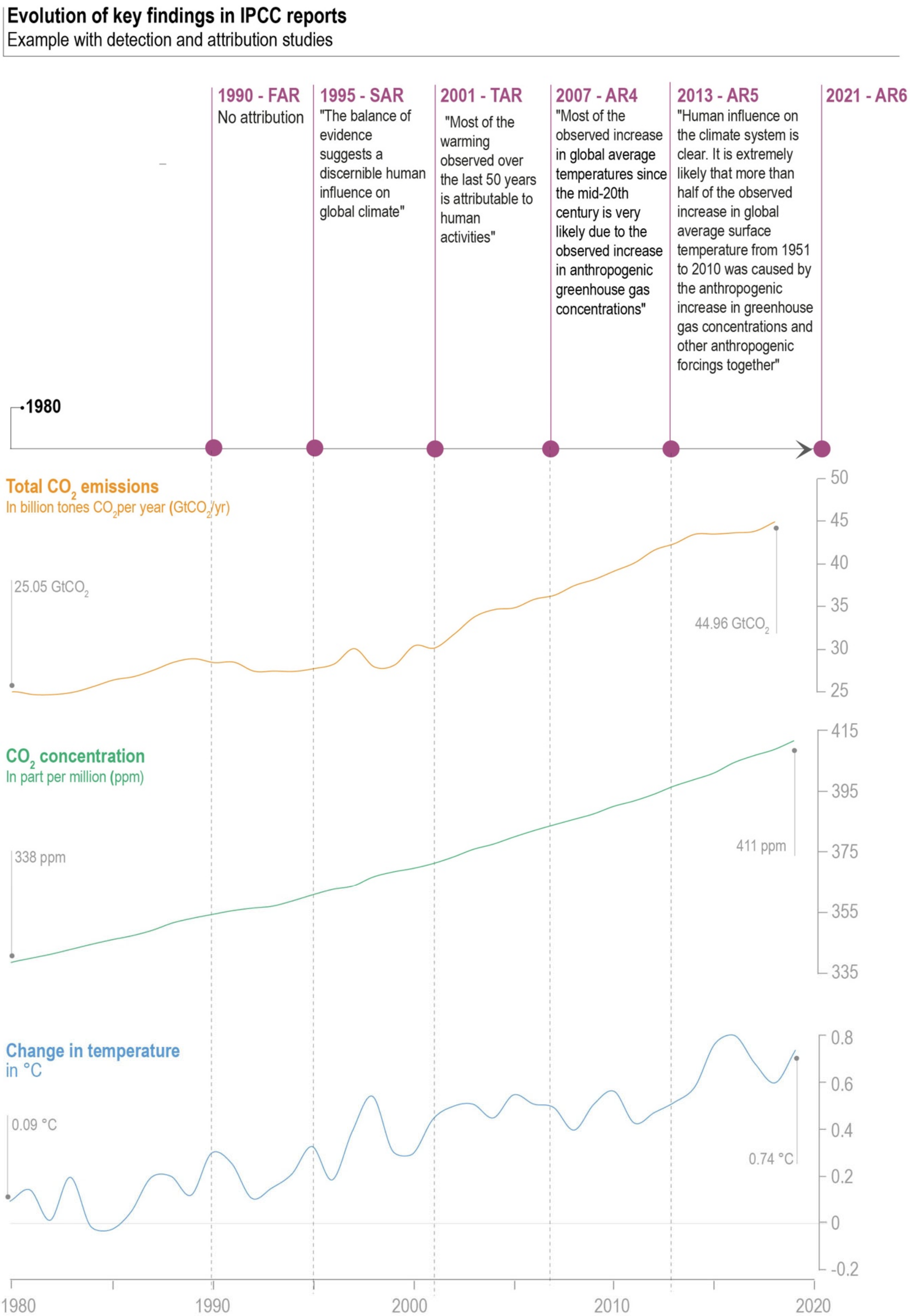

Figure TS.4: Synthesis of evolution of key attribution findings throughput IPCC Assessment Reports, from the First Assessment Report (FAR) through AR6. Based on Table 1.A.1 from Chapter 1.

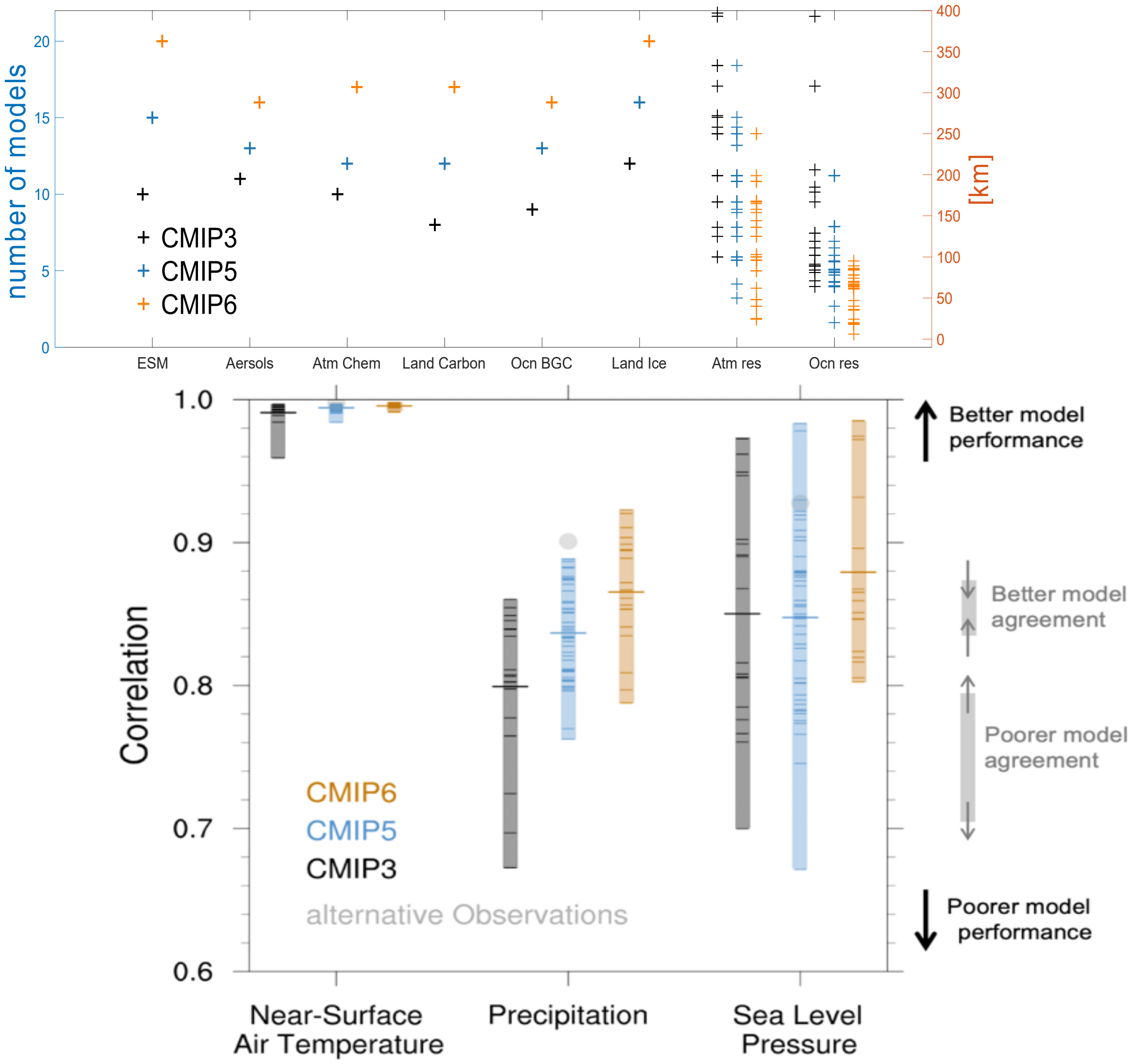

Figure TS.5: (a) Evolution of inclusion of processes and resolution from CMIP3 to CMIP6 [placeholder, based on Fig1.17, to be updated]. (b) Centred pattern correlations between models and observations for the annual mean climatology over the period 1980–1999. Results are shown for individual CMIP3 (black), CMIP5 (blue) and CMIP6 (brown) models as short lines, along with the corresponding ensemble range (shading). The correlations are shown between the models and the reference observational data set listed in Table 3.5. In addition, the correlation between the reference and alternate observational data sets are shown (solid grey circles). To ensure a fair comparison across a range of model resolutions, the pattern correlations are computed after regridding all datasets to a resolution of 2.5° in longitude and 2.5° in latitude. Only one realization is used from each model from the CMIP3, CMIP5 and CMIP6 historical simulations.

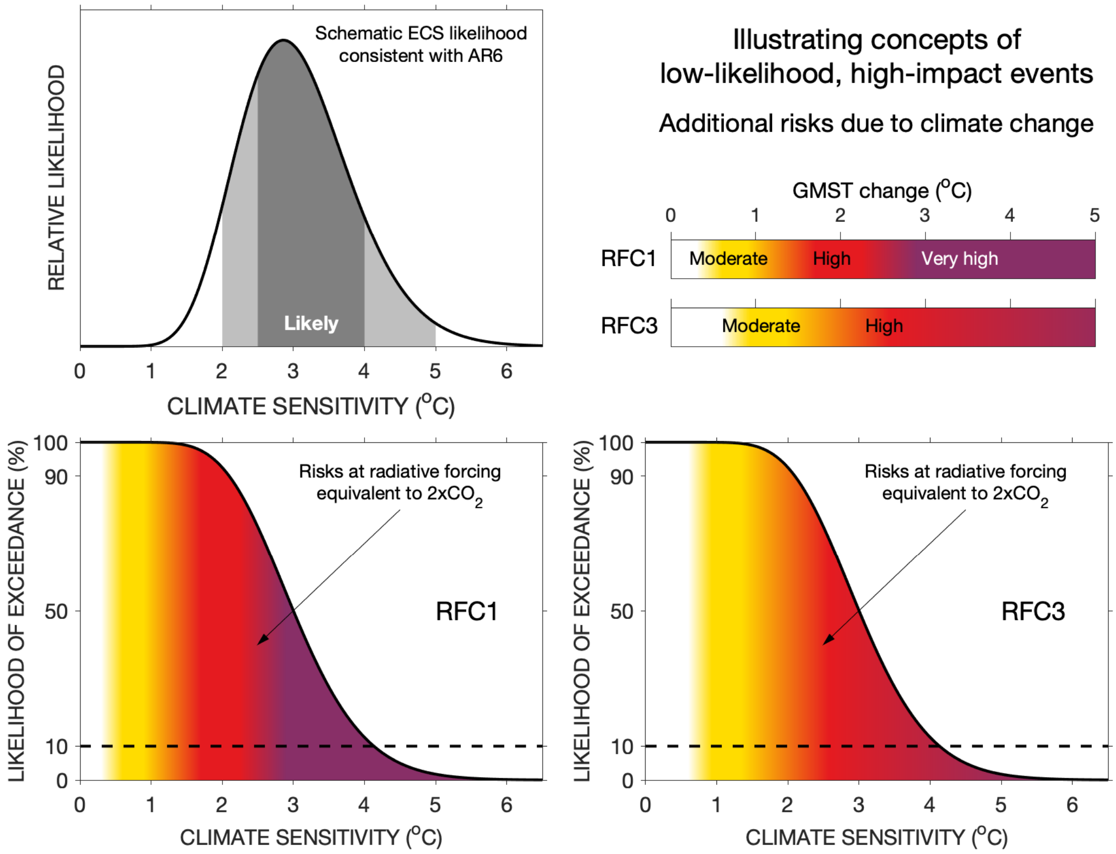

Figure TS.6: Illustrating concepts of low-likelihood, high impact events. (top) Schematic likelihood distribution (pdf) consistent with the IPCC AR6 assessments that "Equilibrium climate sensitivity (ECS) is *likely* in the range 2.5°C to 4.0°C and *very likely* in the range 2.0°C to 5.0C" (see Figure 1.12 for details). The assessed '*likely*' and '*very likely*' ranges are highlighted. (bottom) The likelihood that ECS is larger than the indicated value (1-cdf). The colours indicate the additional risk due to climate change using the Reasons For Concern, specifically RFC1 (bottom left, the risks to unique and threatened systems) and RFC3 (bottom right, the risks due to the distribution of impacts) as assessed in IPCC AR5, assuming that GMST has stabilised after an increase in radiative forcing equivalent to a doubling of CO_2. The dashed black line highlights the 10% likelihood.

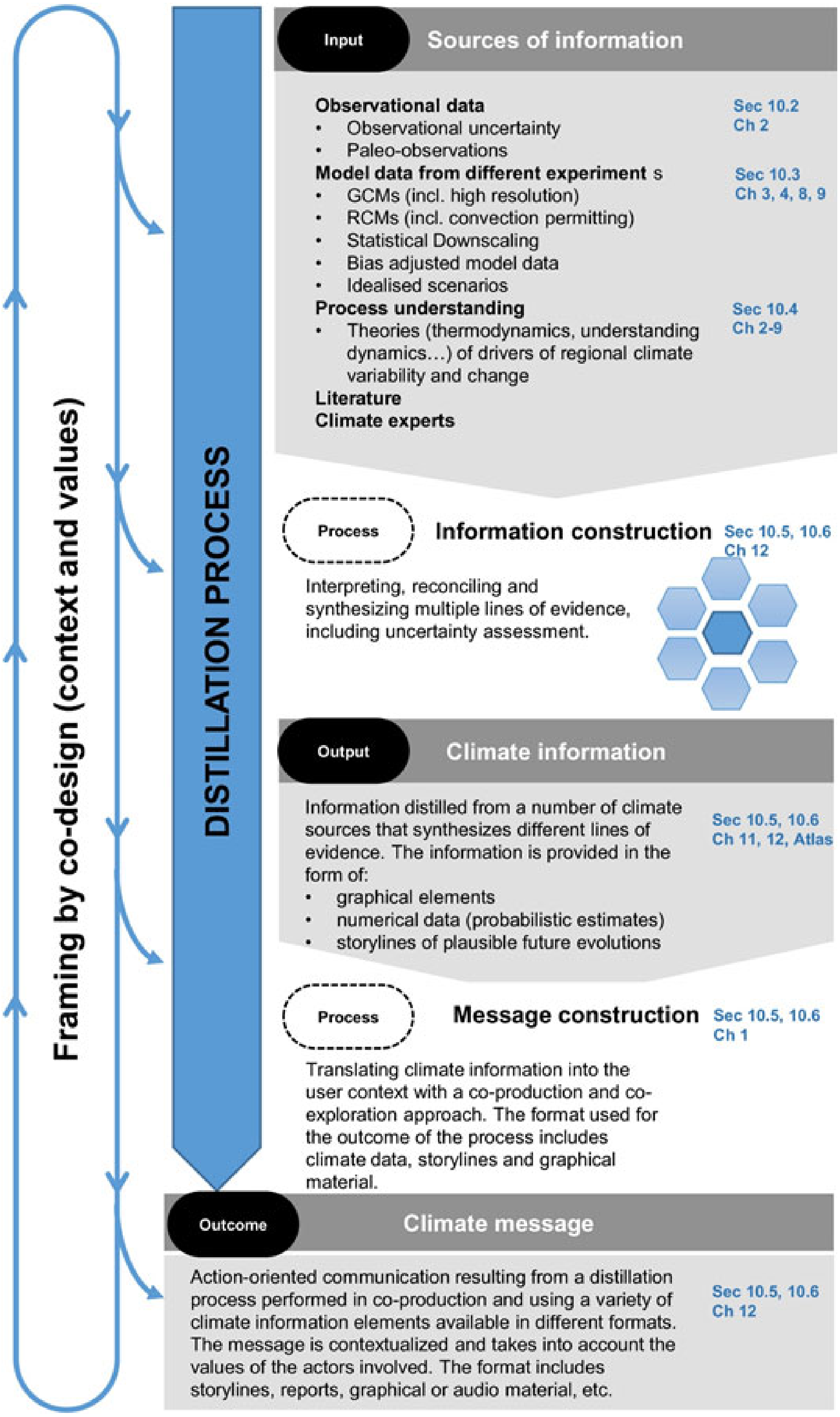

Figure TS.7: Simplified view of the construction of a regional climate message including sources, context, values and storylines, with the processes that lead to the distillation of the message. The chapters and sections where the elements entering the message construction are assessed are indicated. {Figure 10.1}

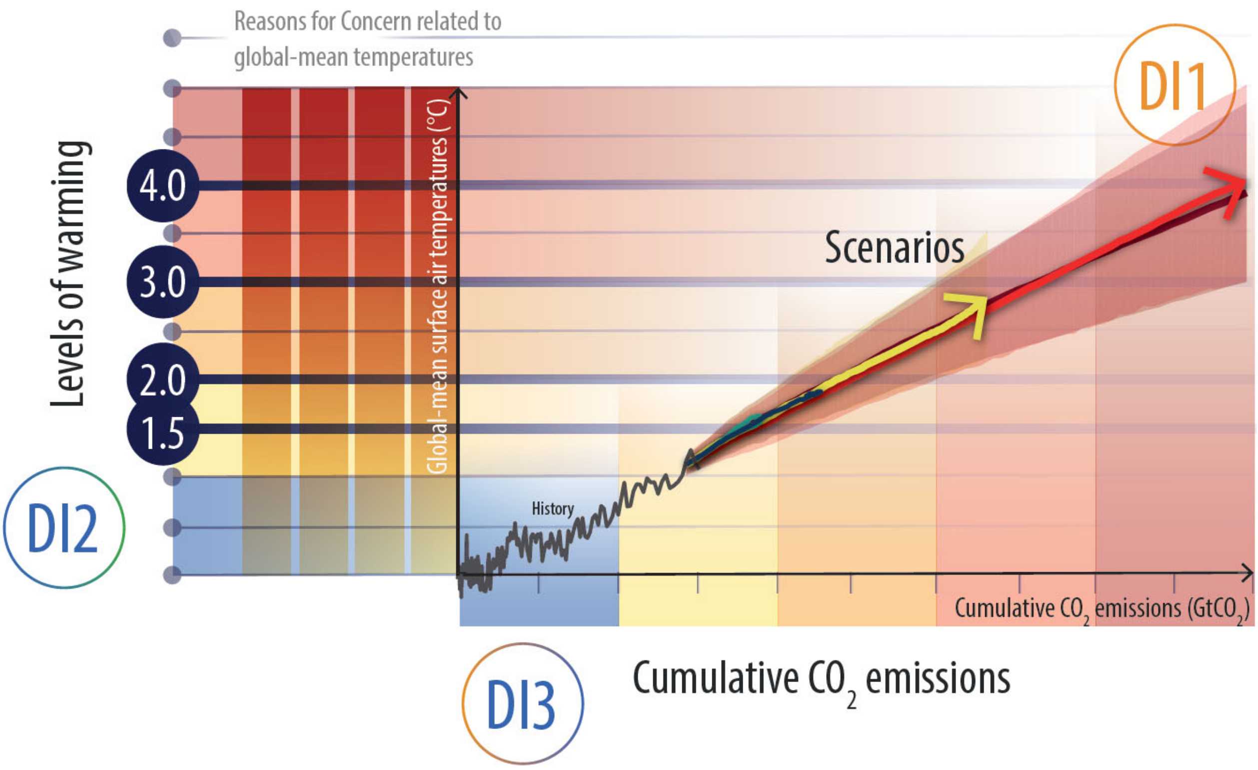

Figure TS.8: The Dimensions of Integration (DI) across Chapters and Working Groups in the IPCC AR6 assessment report. This report adopts three explicit dimensions of integration to integrate knowledge across chapters and Working Groups. The first dimension (DI 1) are scenarios, the second dimension (DI 2) are global-mean temperature levels relative to pre-industrial levels and the third dimension (DI 3) are cumulative CO_2 emissions. {Figure 1.28}

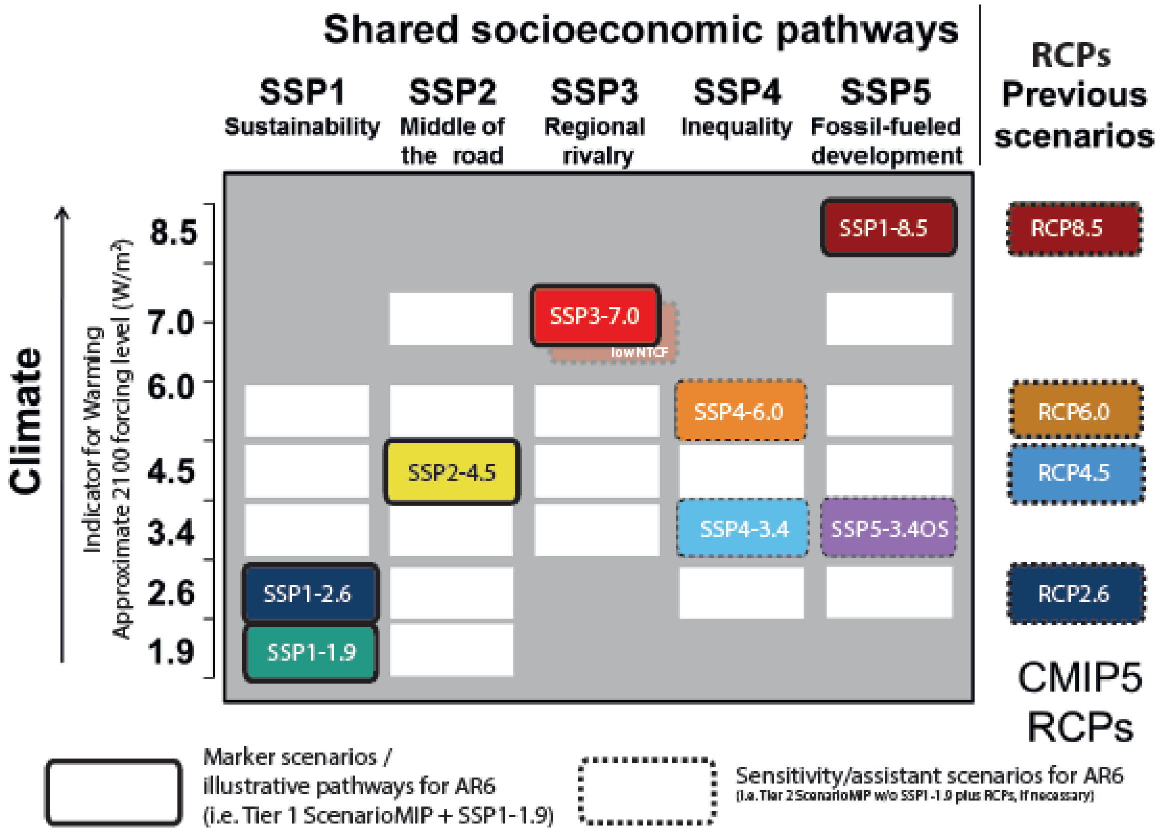

Figure TS.9: SSP-RCP scenario matrix, with the SSP socioeconomic narratives shown as columns and the indicative radiative forcing levels by 2100 shown as rows. RCPs are shown for comparison.{1.6.1; Figure 1.24}

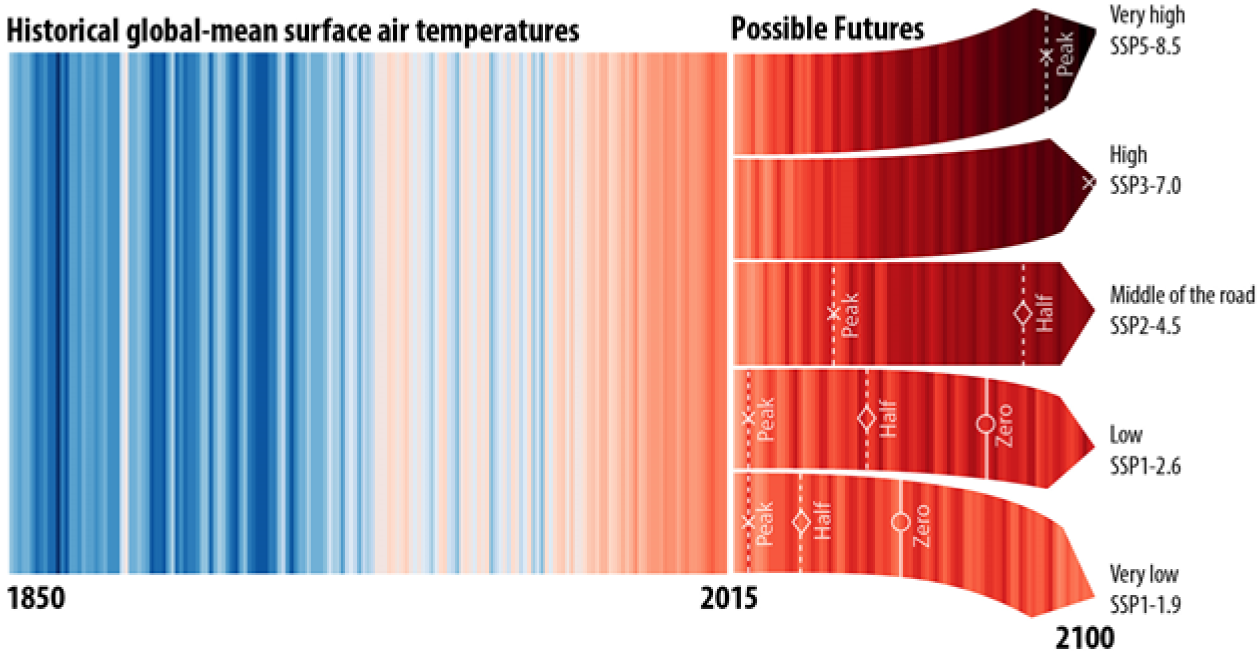

Figure TS.10: SSP-Stripes: Historical global-mean surface air temperatures illustrated as warming stripes from blue (cold) to red (warm) until 2015 and climate model projections for possible futures under five scenarios from "very low" SSP1-1.9 to "very high" SSP5-8.5 . The underlying future climate projection data is taken from MIROC6 - an Earth System Model (ESM) with a relatively low climate sensitivity. The majority of CMIP6 ESMs show higher future projections. The points in time when total CO_2 emissions peak, reach halved levels of the peak and reach net-zero emissions are indicated by crosses, diamonds and open circles, respectively. {1.6.1.3; Figure 1.22}

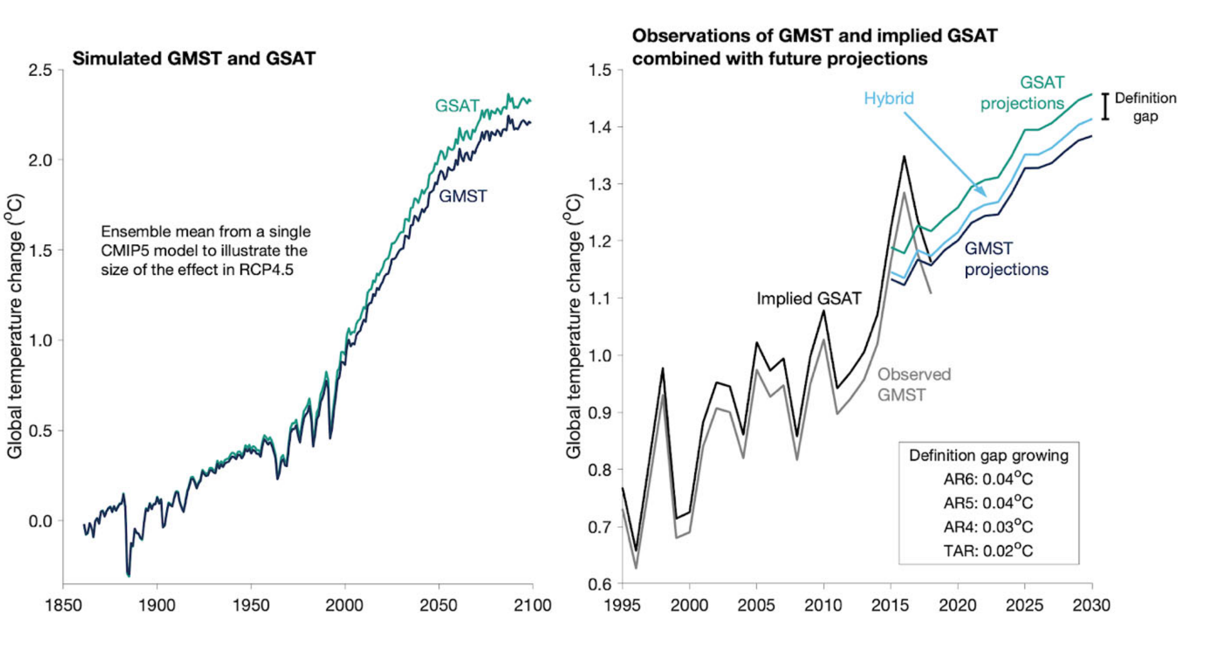

Box TS.1, Figure 1: Left panel: example of the growing impact with time of the use of surface air temperatures everywhere (GSAT) versus surface air temperatures over land and sea surface temperatures over the ocean (GMST) from an ensemble using historical and RCP4.5 forcings out to 2100. Right panel: quantification of the growing impact of the hybrid choice to merge historical GMST and projected GSAT (the definition gap). Observed GMST and implied GSAT using the adjustment of 4% herein are shown up until 2018. Thereafter model-based projections are shown for GMST and GSA.

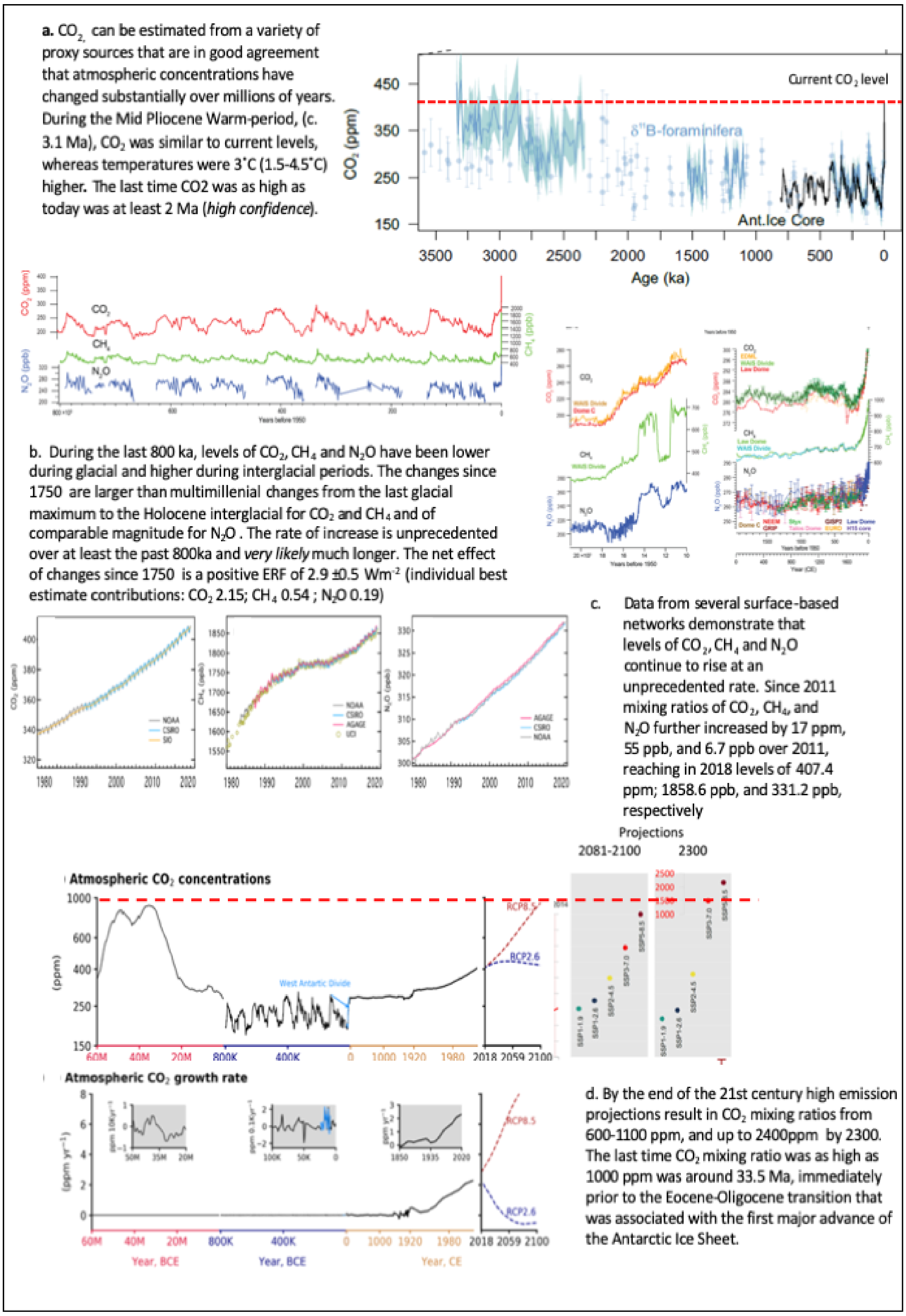

Figure TS.11: Changes in well-mixed Greenhouse gas (WMGHG) concentrations. a) changes in CO2 from proxy sources over the past 3.5Ma. b) changes in all three WMGHGs from ice core records over the past 800ka with inset changes since the Last Glacial Maximum and over the Common Era respectively. c) Directly observed changes since the mid-20th century. d) Changes in CO2 over much longer periods and under various SSP scenarios considered in this report including the rate of change which is highly unusual. *[Purpose: Main driver of climate system changes over the industrial period, changes exceptional in long-term context. - Includes GHG growth rates: shows that although the paleo perturbations were as large or larger than the anthropogenic one, that the rates were at least an order of magnitude lower.]*

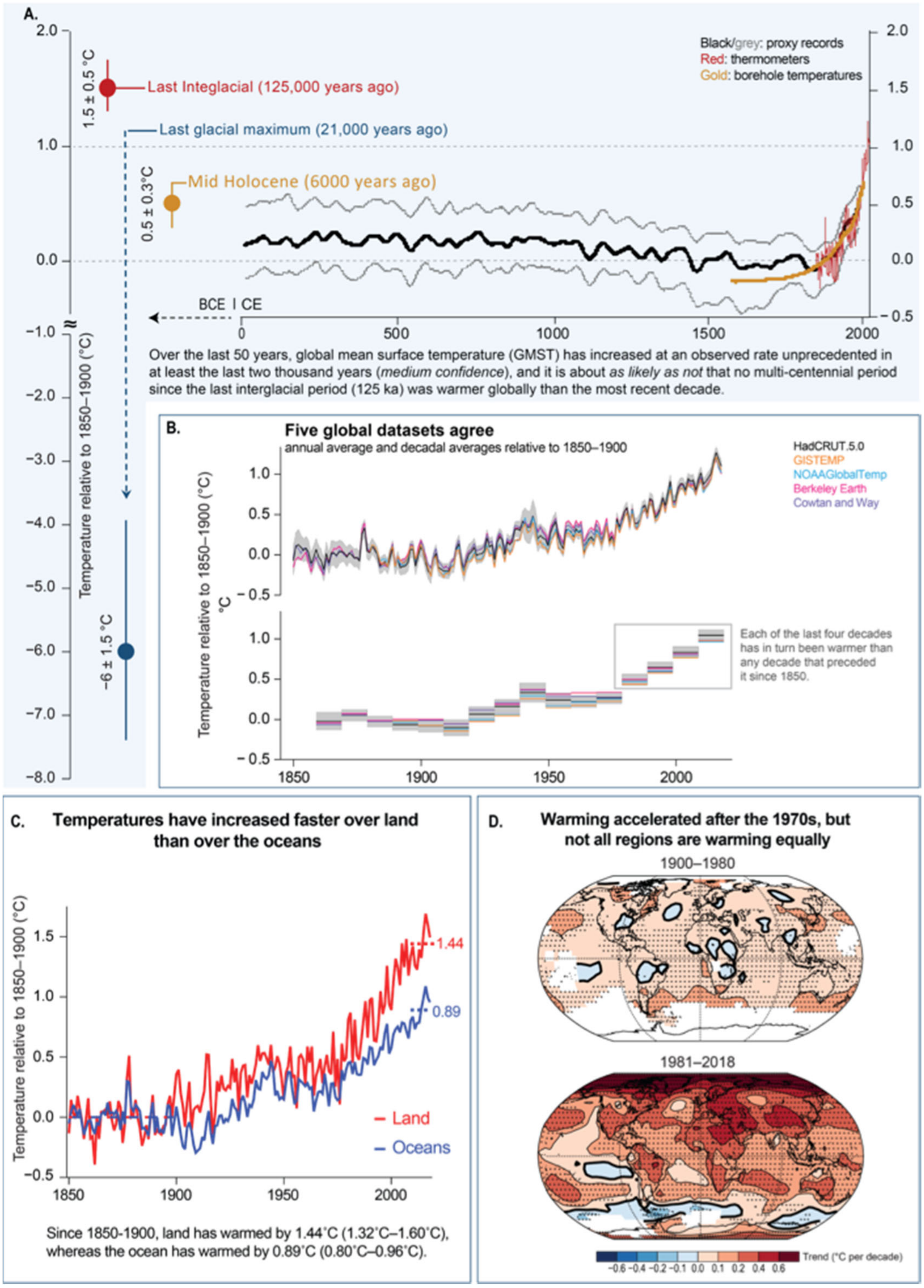

Figure TS.12: Earth's surface temperature history with key findings annotated within each panel. (a) Global mean surface temperature over the Common Era (time series) and during three paleo reference periods. Median multi-method reconstruction (black line), with 2.5th and 97.5th percentiles of the ensemble members (grey bands), smoothed with a 31-year low-pass filter. Mean global ground surface temperature reconstruction from borehole temperature profiles (gold line). Mean temperature of three instrumental-based datasets as shown in panel (b) (red line). Large circles are best estimates (bars are ± 2SD) for mid-Holocene, last glacial maximum, and last interglacial period based on the assessment in section 2.3.1.1.1. All temperatures relative to the 1850-1900 reference period. (b) Annually (top panel) and decadally (bottom panel) resolved averages for the 5 GMST datasets assessed in Section 2.3.1.1.3 from 1850 to 2018. The grey shading in each panel shows the uncertainty associated with the

HadCRUTv5 estimate. (c) Multi-product mean annual timeseries for the products assessed in Section 2.3.1.1.3 for SST over the oceans (blue trace) and LSAT over the land (red trace) and indicating the warming in the most recent 10 years compared to the 1850-1900 reference period. (d) Spatially resolved trends (°C per decade) for HadCRUTv5 over 1900-1980 and then 1981-2018. Trends have been calculated where data is present in both the first and last decade and for at least 70% of all years within the period using OLS. Significance is assessed with AR(1) correction and denoted by stippling. *[Purpose: The key multi-panel GSAT figure, showing 2000-yr and 170-yr time series, paleo estimates, geographical patterns of recent changes (Arctic & continental amplification).]*

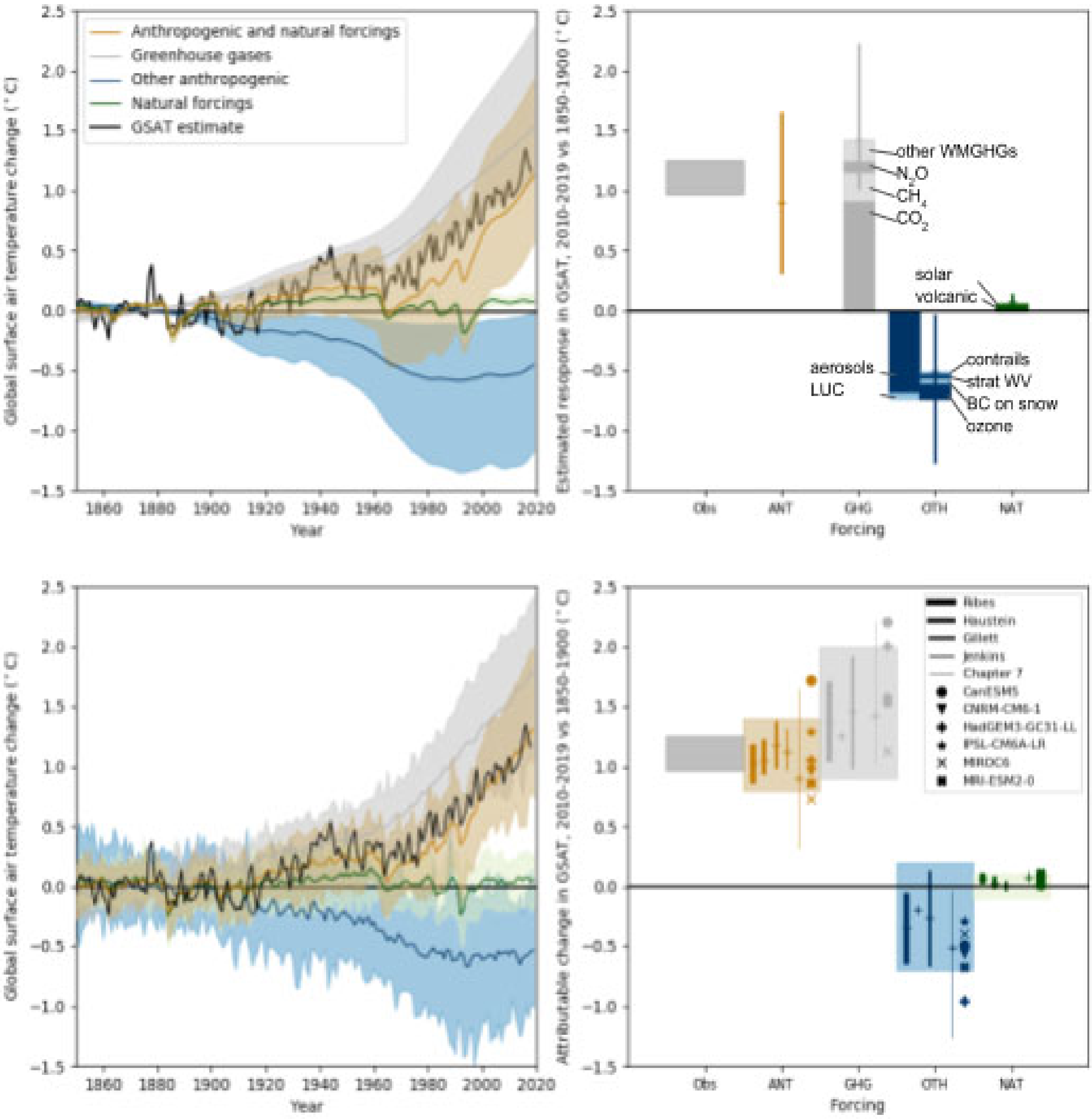

Figure TS.13: Attribution of GSAT evolution (left) and 2010-2019 change relative to 1850-1900 (right) based on assessed ERFs and an emulator (top), and CMIP6 models simulations and attribution studies (bottom). GSAT response to individual forcings simulated by an emulator (Cross-Chapter Box 7.1) with assessed climate system parameters and ERF time series (top left), and temperature change between 1850-1900 and 2010-2019 (top right). Stacked bars show the median temperature response to each individual forcing, and uncertainty ranges show the responses to anthropogenic (ANT), well-mixed greenhouse gas (GHG), other anthropogenic (OTH) and natural (NAT) forcings. Observed GMST and simulated GMST in response to greenhouse gases, other anthropogenic forcings, natural forcings and combined forcings (lower left, modified from FAQ 3.3, Figure 1), and assessed GSAT changes to 2010-2019 relative to 1850-1900, attributable to anthropogenic forcings, well-mixed GHGs, other anthropogenic forcings and natural forcings (lower right, Figure 3.7). Bars labelled 'Chapter 7' correspond to the uncertainty ranges shown in the top right, and are one line of evidence used to derive the assessed attributable GSAT changes shown. Observed GSAT changes are taken from Cross-Chapter Box 2.3. *[Purpose: Summary of natural and anthropogenic global climate forcings since 1750, and assessed GSAT responses - Clearly shows human influence on global climate system.]*

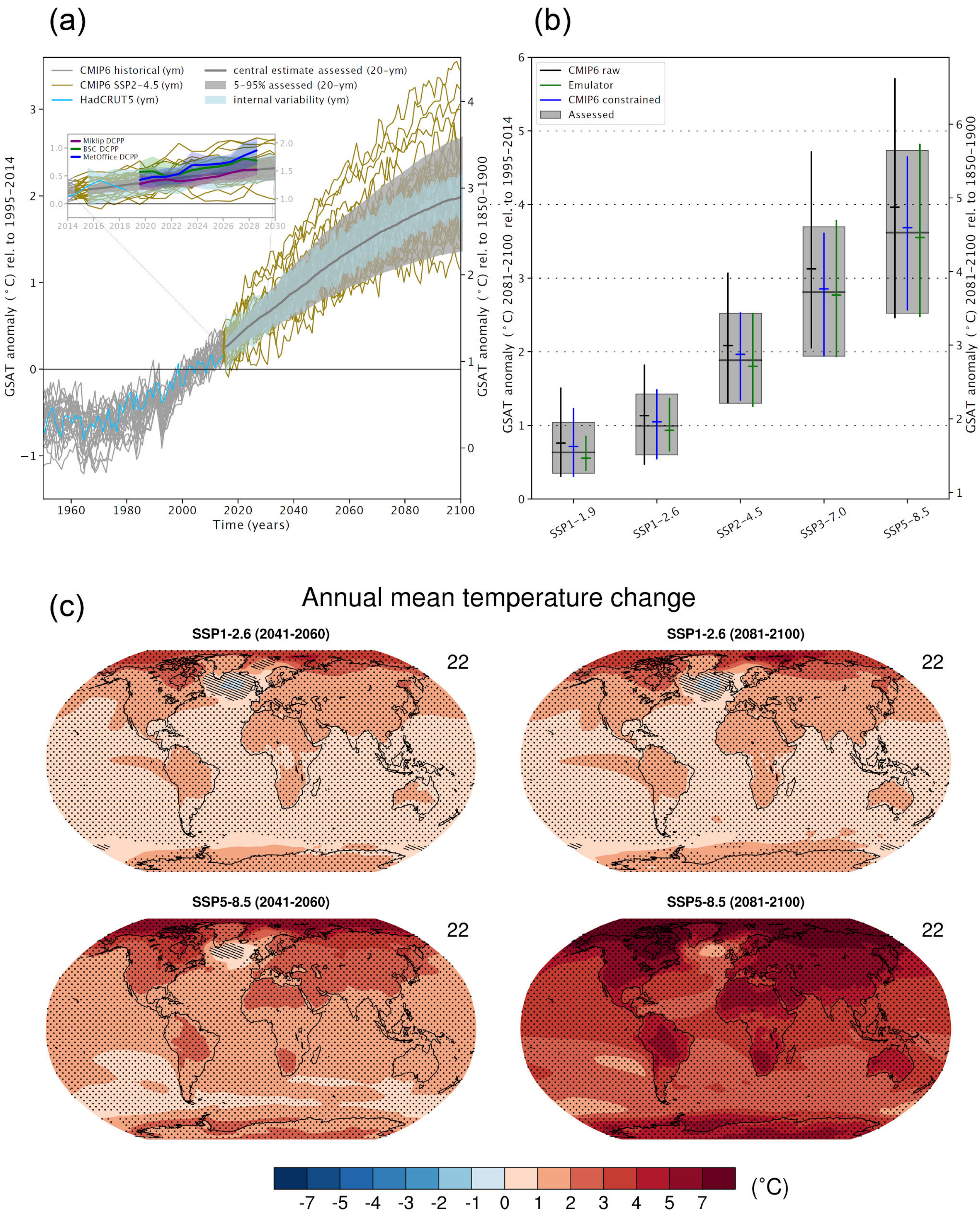

Figure TS.14: Lines of evidence for assessed GSAT. (a) CMIP6 annual-mean GSAT simulations and various contributions to uncertainty in the projections ensemble. The figure shows anomalies relative to the period 1995–2014 (left y-axis), converted to anomalies relative to 1850–1900 (right y-axis); the difference between the y-axes is 0.91°C. Shown are historical simulations with 29 CMIP6 models (grey) and projections simulations following scenario SSP2-4.5 (dark yellow). The cyan curve shows the observations (HadCRUT5, (Morice et al., 2020)). The black curve and dark shading show, respectively, the central estimate and *very likely* range of assessed 20-year averaged future GSAT change. Light blue shading shows the contribution of internal variability to annual-mean GSAT change; the shading is based on the 50-member ensemble CanESM5 such that the deviations from the CanESM5 ensemble mean have been added to the central estimate of assessed GSAT change. The inset shows a cut-out from the main plot and additionally for the period 2019–2028 in purple, green, and blue the initialised prediction ensembles from three models contributing to DCPP (Boer et al., 2016); solid curves show the ensemble means and shading the range of each prediction system. (b) Raw CMIP6, historically constrained CMIP6, emulator, and assessed GSAT changes for the long-term period, 2081–2100, relative to the average over 1995–2014 (left y-axis) and 1850–1900 (right y-axis); the y-axes differ by 0.91°C. The emulator ranges are defined through choices for climate feedback parameter and ocean heat uptake coefficient such that the best estimate, lower bound of the *very likely* range, and upper bound of the *very likely* range of the emulator ECS and TCR take the corresponding values of AR6-assessed ECS and TCR. The assessed ranges (horizontal black lines and grey boxes) are constructed by taking the average of the constrained CMIP6 estimates (blue bars) and the emulator estimates (green bars). (c) Multi-model mean change in annual-mean near-surface air temperature (°C) in 2041–2060 and 2081–2100 in (top) SSP1-2.6 and (bottom) SSP5-8.5 relative to 1995–2014. Stippling indicates regions where the multi-model mean change exceeds two standard deviations of pre-industrial internal variability and where at least 90% of the models agree on the sign of change, as a measure of robustness. Hatching indicates regions where the multi-model mean signal is less than one standard deviation of internal variability.{1.3, 2.3, 4.3, Box 4.1, 7.5} *[Purpose: This figure shows time series, period differences, and maps of GSAT following multiple lines of evidence. The multiple lines of evidence are raw CMIP6 projections, historically constrained CMIP6 projections, initialized predictions, and emulator results (Cross-Chapter Box 7.1). This figure combines Box 4.1 Fig. 1, Fig. 4.9, and Fig. 4.21.]*

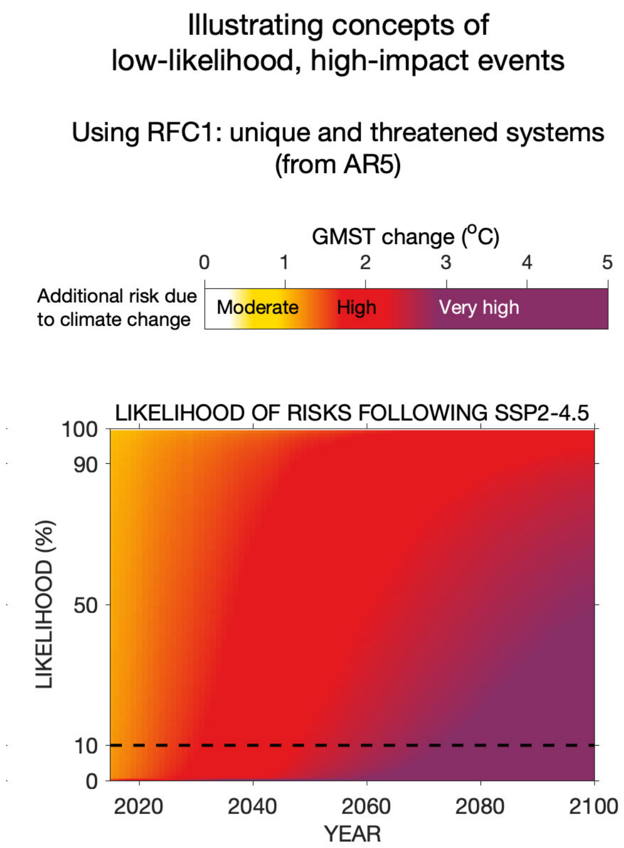

Box TS.2, Figure 1: Illustrating concepts of low-likelihood, high impact events. The colours indicate the additional risk due to climate change using the Reasons For Concern (see IPCC AR5 WGII SPM), specifically RFC1 describing the risks to unique and threatened systems. The likelihood of additional risks assuming radiative forcing follows the assessed GSAT change under the SSP2-4.5 scenario. *[Purpose: To illustrate the concepts of low-likelihood, high-impact events.]*

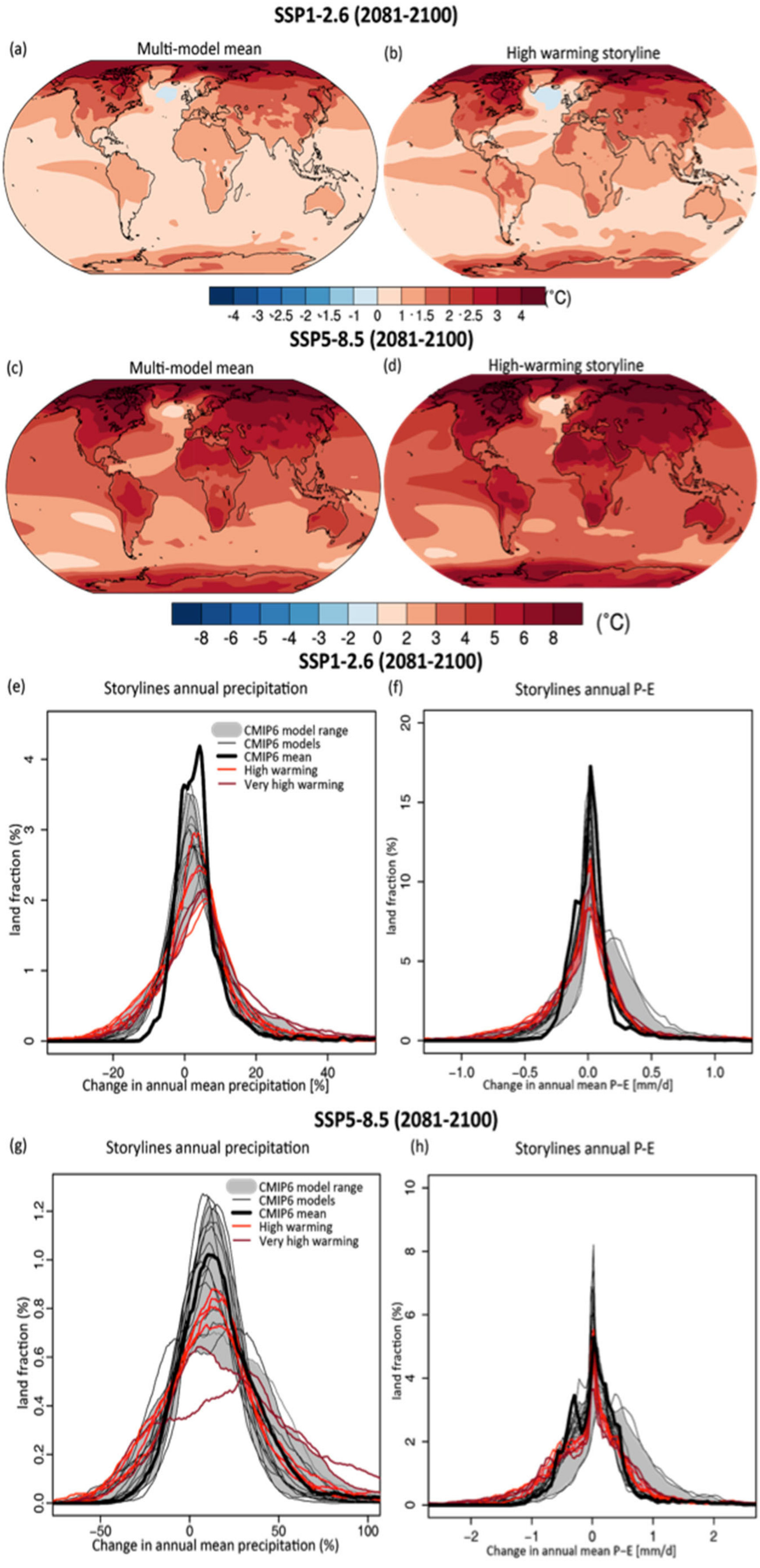

Box TS.2, Figure 2: (a,c) CMIP6 multi-model mean and (b,d) low-probability high-warming storyline for annual mean temperature change in 2081–2100 relative to 1995–2014 in (a,b) SSP1-2.6 and (c,d) SSP5-8.5.

The low-probability high-warming for 2081–2100 corresponds to multi-model average across the five models with GSAT warming nearest to the upper bound of the assessed *very likely* range. (e,f) Area fraction of changes in (e,g) annual mean precipitation and (f,h) precipitation minus evapotranspiration (P-E) in 2081–2100 relative to 1995–2014 in (e,f) SSP1-2.6 and (g,h) SSP5-8.5 for individual model simulations (thin black lines) and high-warming storylines with GSAT warming near the upper bound (thin red lines) and exceeding the upper bound (thin brown lines). The grey range illustrates the 5–95% range across CMIP6 models and the thick black line the area fraction of the multi-model mean pattern. *[Purpose: To illustrate high warming storylines compared to the CMIP6 multi-model-mean.]*

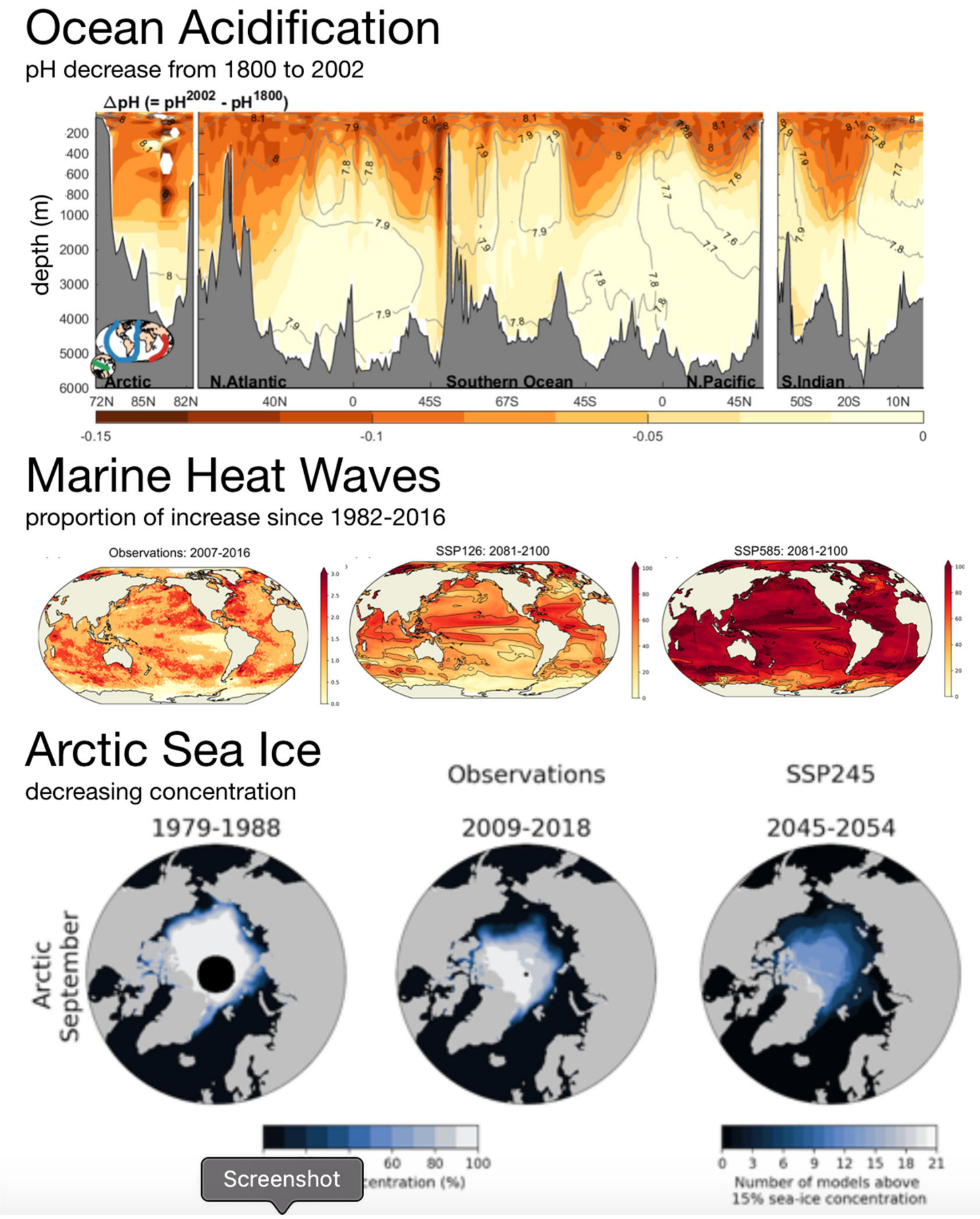

Figure TS.15: Key recognizable indicators of oceanic climate change. *[Purpose: Immediately meaningful indicators of ocean changes from a global perspective: observed trends and projections of marine heat waves, Arctic sea ice, pH. Could include O2 change as well (From Fig 5.21; Cross-Chapter Box 9.1, Fig 1; 9.15). Placeholder for more simplified statistics.]*

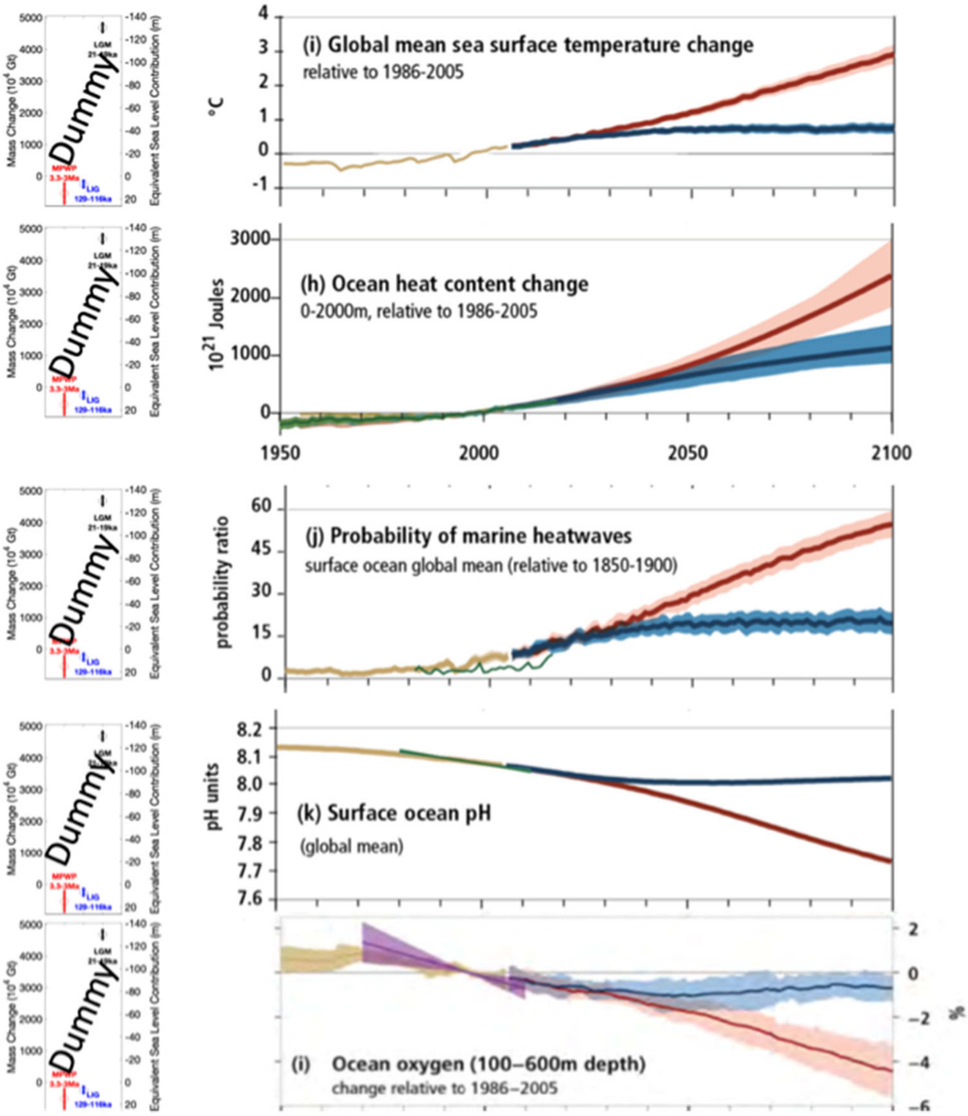

Figure TS.16: [Preliminary – From SROCC Figure 1.5 to be expanded in the FGD to include ocean heat content (2 y-axis to include pot'l temperature change), SST, and pH in same format as sea level (paleo, obs, historical, projections] *[PURPOSE: Ocean summary figure (excl. sea level, which appears in Box TS.3). Observed, simulated present, projected changes of globally relevant non-sea-level ocean variables.]*

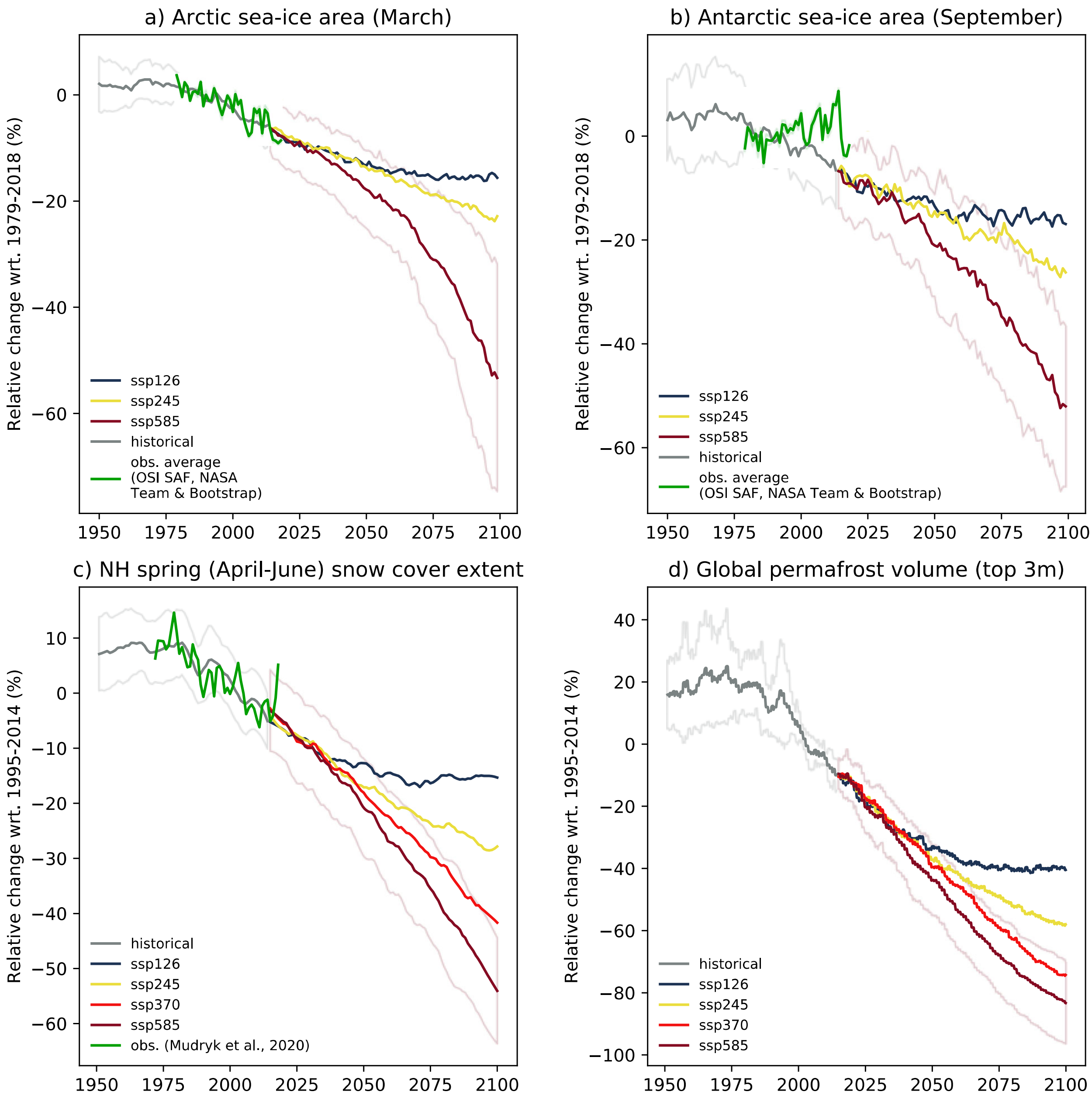

Figure TS.17: Observed, simulated and projected relative changes of cryospheric components of the climate system. a) March (late winter, close to annual maximum) Arctic sea ice anomaly (reference period: 1979-2018); b) September (late winter, close to annual maximum) Antarctic sea ice anomaly (reference period: 1979-2018); c) Northern hemisphere spring (April to June average) seasonal snow extent (reference period: 1995-2014); d) global volume of permafrost in the top 3 m below the surface (reference period: 1995-2014). Observations shown where available. *[Purpose: Shows that observed losses occur across all major cryosphere components (except Antarctic sea ice), and that models reproduce this loss where it occurs. Shows that projected cryospheric loss is consistent across cryosphere elements & highly scenario-dependent. Complement for glaciers and ice sheets in sea level box. Antarctica (not shown here, but in sea level box) is the only cryospheric component that isn't highly scenario-dependent on a 100-yr time scale (at least in current models)].*

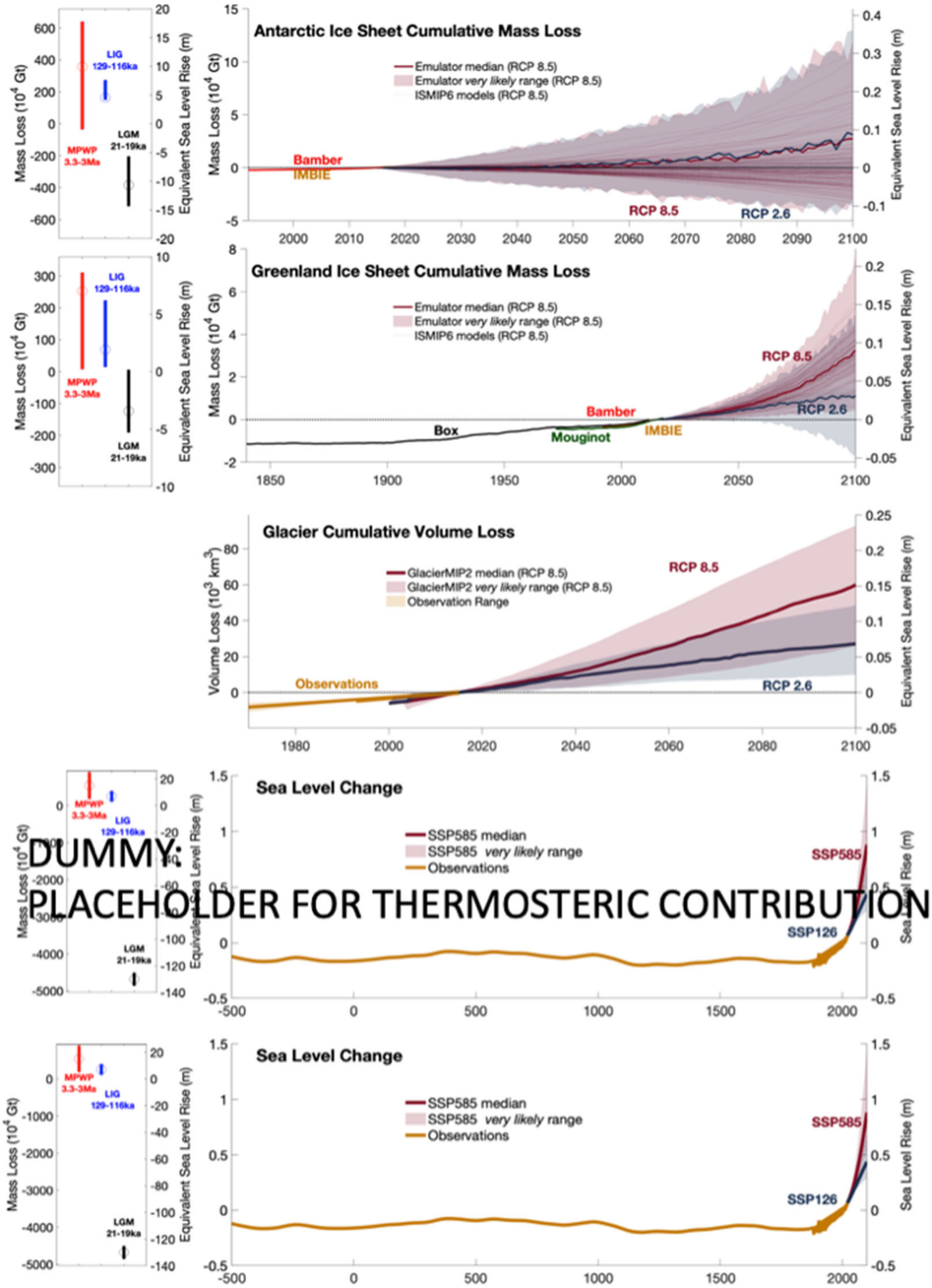

Box TS.3, Figure 1: The idea is to combine Figure 2.27 (observations / paleo) with Figure 9.30 (projections), along with Fig 9.19 (GrIS), Fig 9.20 (AIS), Fig 9.22 (glaciers), and Fig. CCB92.1 (Thermosteric). Possibly include a panel inset with information on attribution? This shows thermosteric, glaciers, AIS, GrIS and total sea level for historical where possible (including paleo ranges) and projections (to 2300 when available). Not clear if all panels should have aligned x axis years & y-axis scale for SL. *[Purpose: To summarise the different components of GMSL change, both in terms of historical observations and future projections. One of the issues is avoiding redundancy with sections 2.3 and 2.4. An alternative, simplified approach might focus on the total GMSL time series and tabulate the different contributions for past observed periods and for future projections by scenario]*

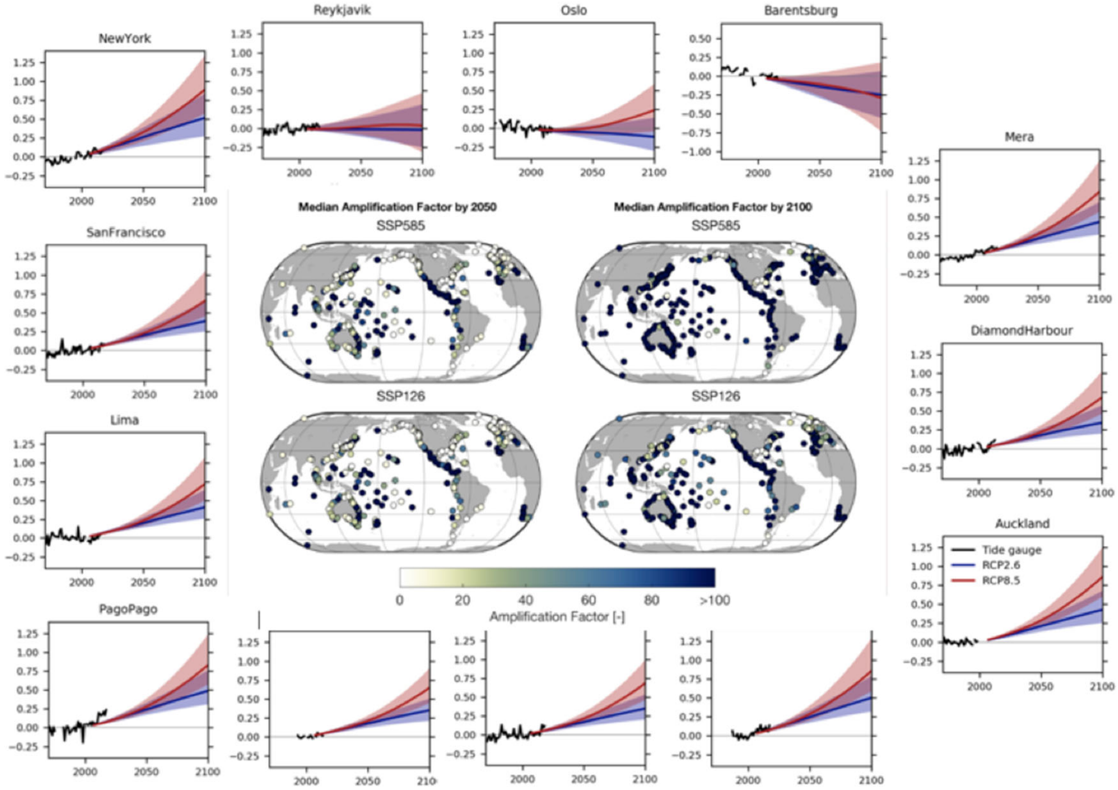

Box TS.3, Figure 2: [Placeholder] Example local sea-level projections compared to local tide gauge observations to illustrate the range of future behaviours and observed interannual variability. Combined with flooding frequency elements of Figure 9.34 to make the link to projected changes in coastal sea-level extremes [link to TS4]. *[Purpose: To illustrate the large geographic variations in regional sea-level change/projections (we cannot rely on GMSL for this information) and the differing regional variability as shown by tide gauge records. Then to make the link to changes in local sea-level extremes, which are dominated by the time-mean sea-level change (rather than changes in drivers of extremes).]*

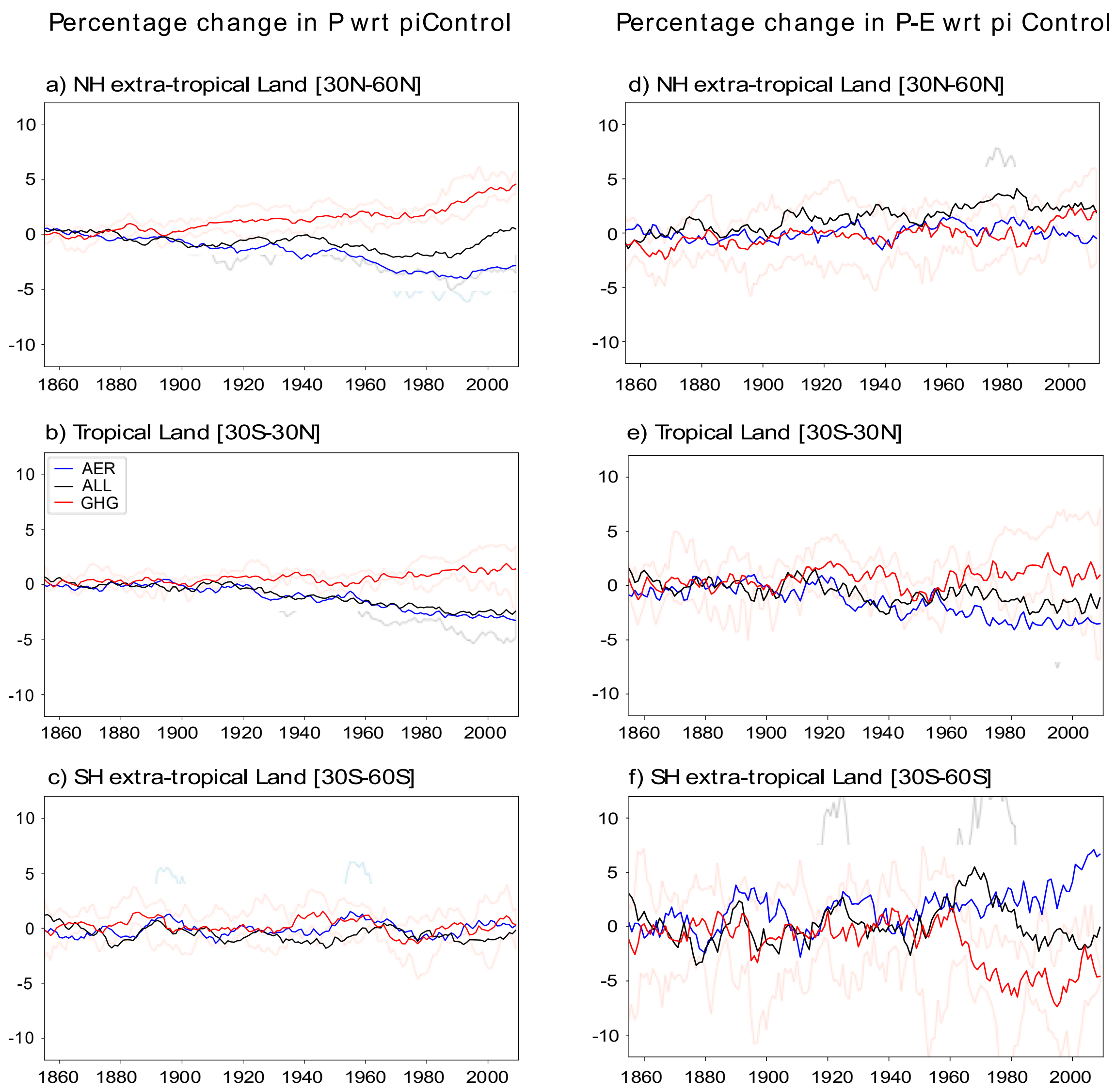

Figure TS.18: Time series of past relative changes (1850-2014) of precipitation (P, left column) and precipitation minus evaporation (P-E, right column) over land areas for all historical forcings (black), aerosol forcing only (blue), and GHG forcing only (red). Top row: NH extratropics (30N-60N); middle row: Tropics (30S-30N); bottom row: SH extratropics (30S-60S). *[Purpose: Illustrate key message that anthropogenic aerosol forcing has obscured the effects of GHG forcing on the precipitation (P) and net flux of water from the atmosphere to the Earth's surface (precipitation minus evaporation i.e., P-E) over the land regions of the tropics and the Northern Hemispheric extratropics since the early 20th century, with more prominent changes during the last 6-7 decades. Signatures of human induced changes in P and P-E are not clearly detectable over the land regions of the Southern Hemispheric extra-tropics which are dominated by large internal variability.]*

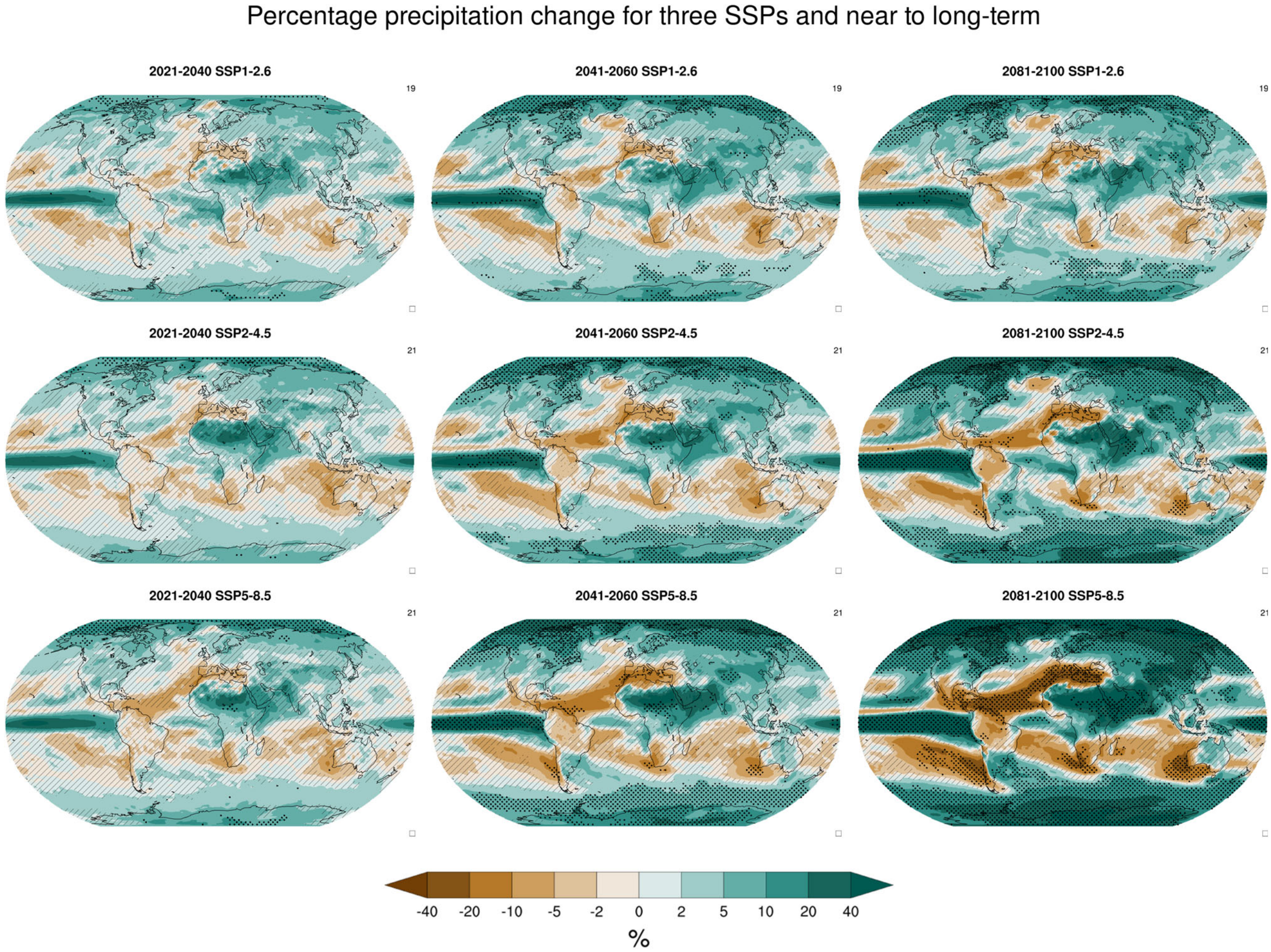

Figure TS.19: CMIP6 multi-model mean projected changes (%) in near-term (left column), mid-term (middle column) and long-term (right column) annual mean precipitation under three SSP scenarios: SSP1-2.6 (top row), SSP2-4.5 (middle row) and SSP5-8.5 (bottom row) relative to 1995–2014. Stippling indicates regions where the multi-model mean change exceeds two standard deviations of pre-industrial internal variability and where at least 90% of the models agree on the sign of change, as a measure of robustness. Hatching indicates regions where the multi-model mean signal is less than one standard deviation of internal variability. Top-right panel numbers indicate the number of CMIP6 models used for estimating the ensemble mean. *[Purpose: Emphasize the robustness of the geographical pattern of projected precipitation changes, and highlight the time and scenario dependence of their magnitude.]*

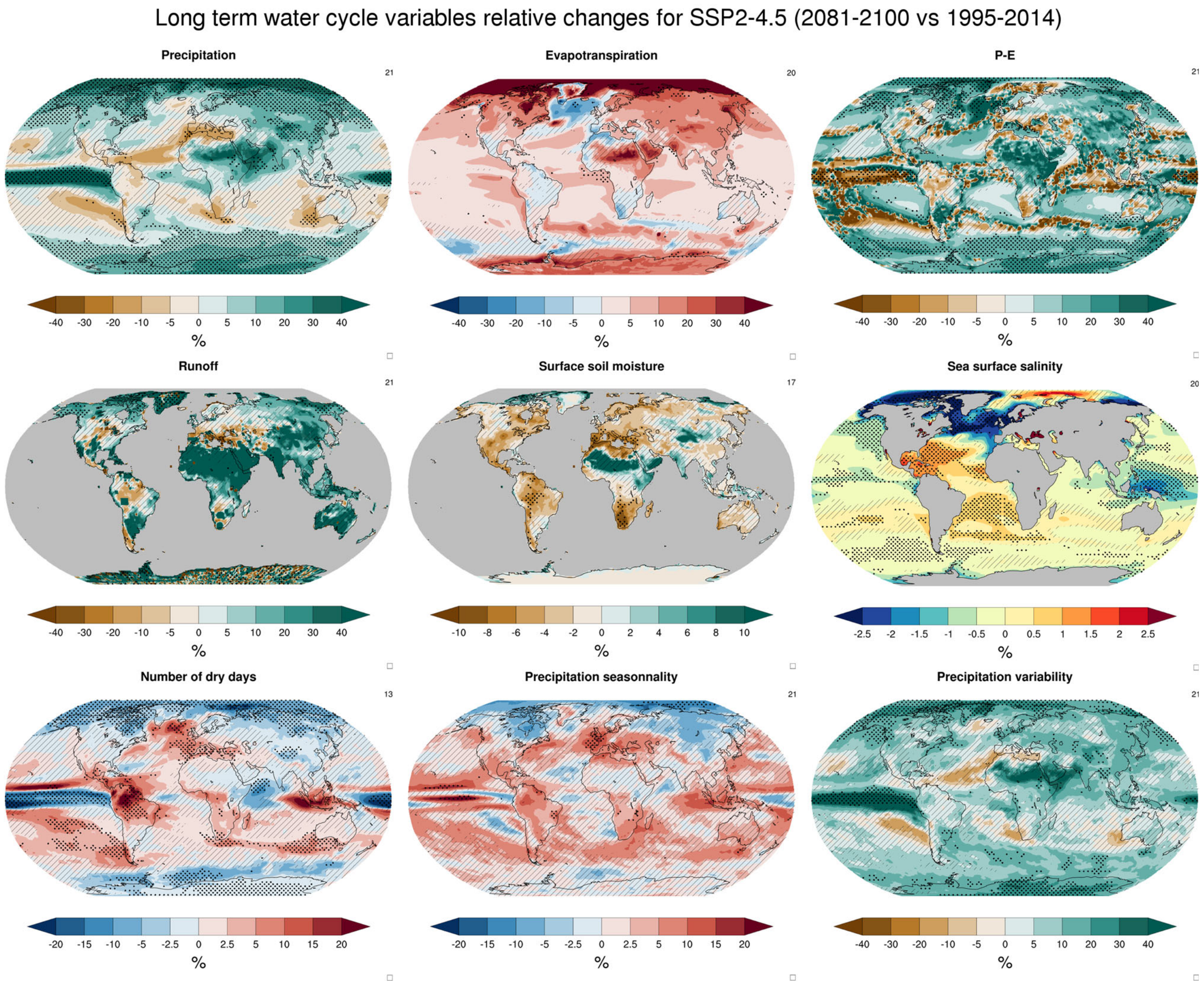

Figure TS.20: Summary of long-term (2081-2100) projected annual mean water cycle changes (%) relative to present-day (1995-2014) in the SSP2-4.5 emission scenario for: precipitation (P), surface evapotranspiration (E), Precipitation minus - Evapotranspiration (P-E), total runoff, surface soil moisture, sea surface salinity, number of dry days, precipitation seasonality index (red shading highlights areas with increased rainfall seasonality), precipitation interannual variability (as estimated by the relative change in the standard deviation of annual precipitation). Top-right panel numbers indicate the number of CMIP6 models used for estimating the ensemble mean. *[Purpose: Synthetic overview of changes in multiple components/features of the global water cycle, with the following important key messages: 1) long-term changes in runoff, soil moisture and sea surface salinity result from changes in both P and E, 2) they are generally less robust than changes in P or E, 3) changes in P seasonality and variability (intraseasonal and interannual) can be more pronounced or robust than changes in annual mean P at the regional scale.]*

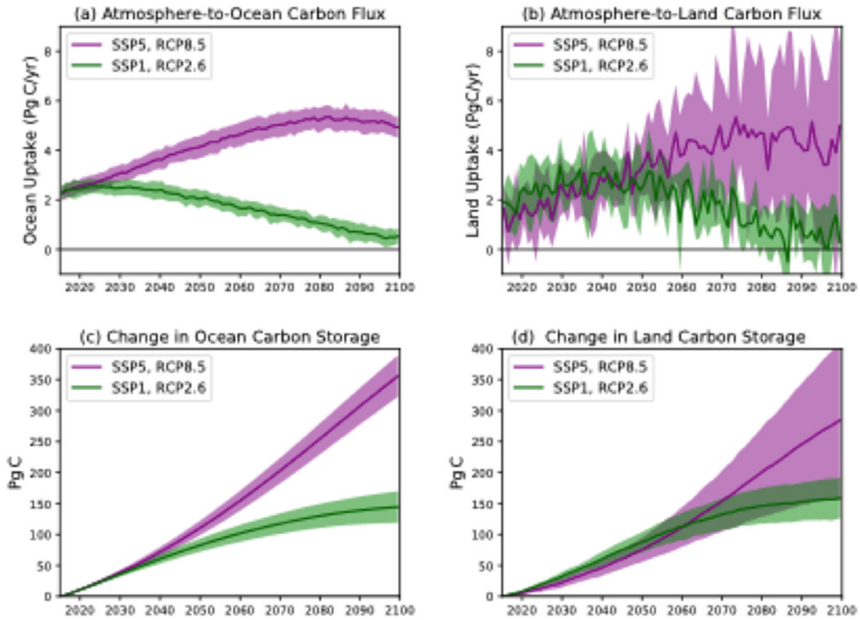

Figure TS.21: Projections of: (a) atmosphere-to-ocean carbon flux; (b) atmosphere-to-land carbon flux; (c) change in ocean carbon storage; (d) change in land carbon storage; from the CMIP6 ensemble of ocean and land for SSP 2.6 (green) and 8.5 (purple). Shaded regions indicate the ensemble spread. *[Purpose: To show projections of future changes in carbon uptake and storage for ocean and land in CMIP6 ensemble.]*

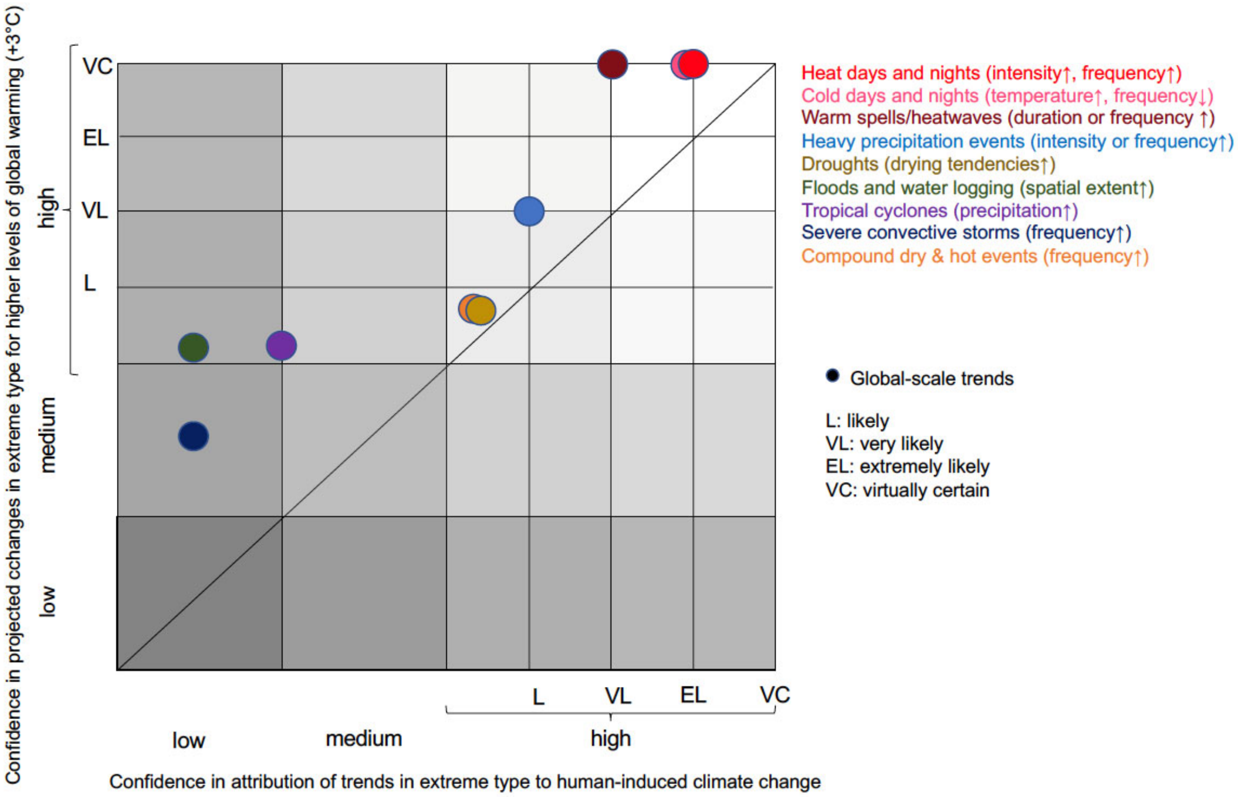

Figure TS.22: Summary figure on confidence in global-scale projected trends in extreme types at +3°C vs confidence in attribution of global-scale observed trends in extremes types. [*Purpose : Show that confidence in projected changes in extremes is linked (and typically somewhat higher) than confidence in attribution of observed trends in extremes.]*

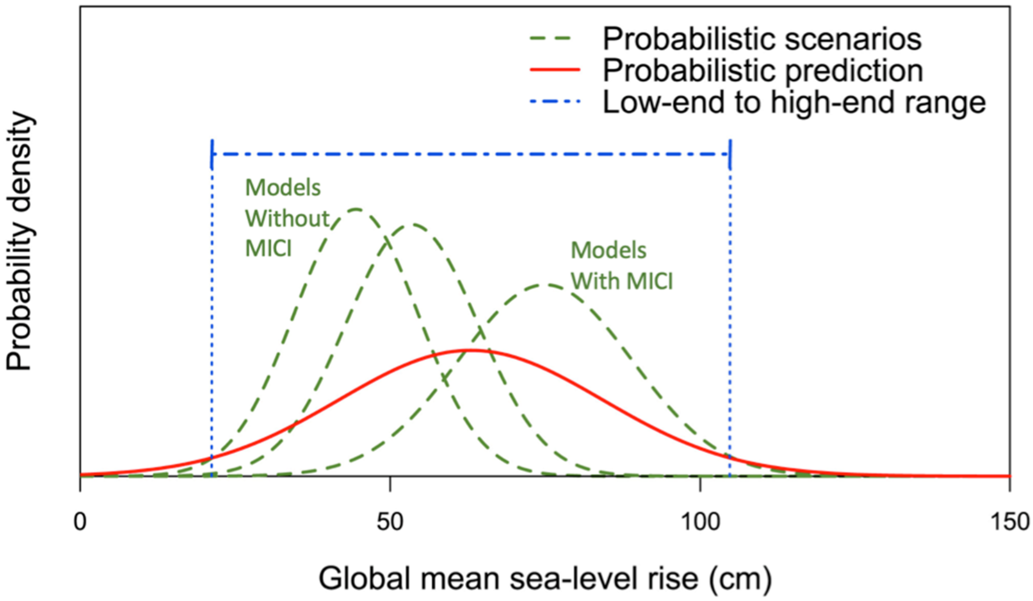

Figure from: Jochen Hinkel, John A. Church, Jonathan M. Gregory, Erwin Lambert, Gon΄eri Le Cozannet, Jason Lowe, Kathleen L. McInnes, Robert J. Nicholls, Thomas D. van der Pol, and Roderik van de Wal, Meeting user needs for sea level rise information: A decision analysis perspective, Earth's Future 7 (2019), no. 3, 320–337.

Box TS.4, Figure 1: The idea is to show probability distributions together with a decision tree--probability without tipping vs. probability after tipping. Inspirational Chapter figures--1.12, 9.19, 9.27, 9.32. This figure is from the cited paper listed, and it shows some of the key aspects of compiling sea level models with different physics/tunings/sensitivity. Modified to suggest the conditional probability distribution of MICI vs. no MICI (an example, but could also be AMOC collapse, methane clathrates, etc.). This figure could be made quantitative for Marine Ice Cliff Instability using Fig. 9.27 data from literature ranges. *[Purpose: The idea is to show probability distributions together with a decision tree-probability without tipping vs. probability after tipping. Inspirational Chapter figures--1.12, 9.19, 9.27, 9.32. Suggestions for additional figure ideas to illustrate/combine other elements of Irreversibility, Abrupt Change and Tipping Points are].*

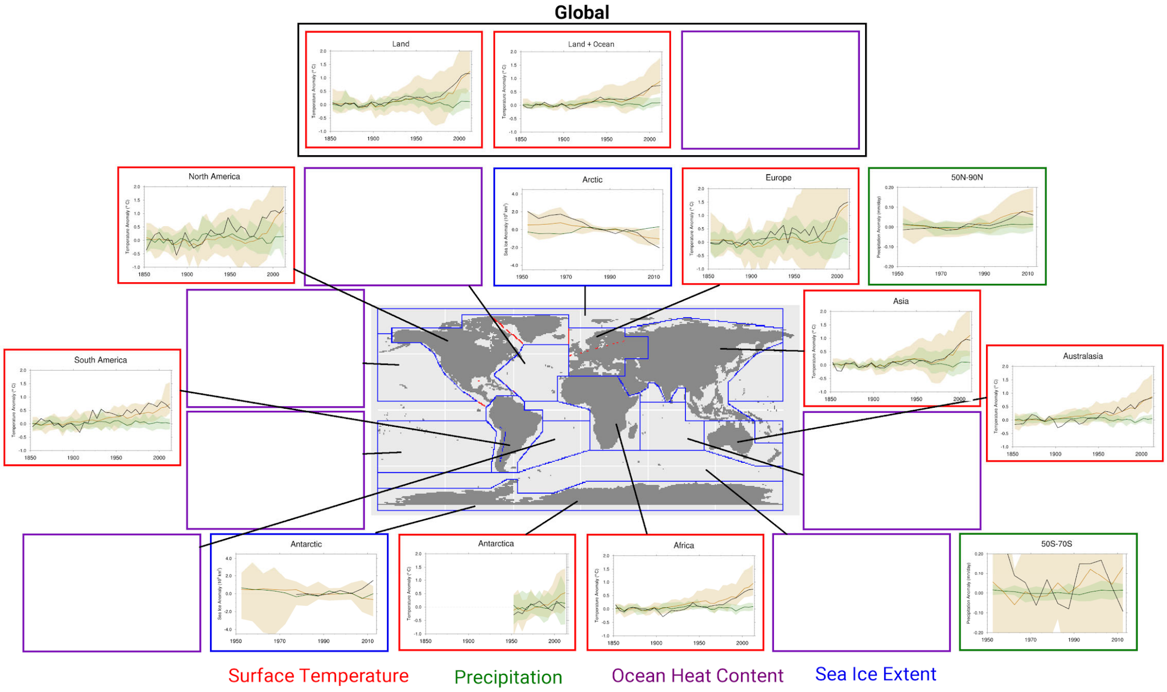

Figure TS.23: Summary figure showing simulated and observed changes in key large-scale indicators of climate change across the climate system, for continental, ocean basin and larger scales. Black lines show observations, red lines and shading show the multi-model mean and 5-95th percentile ranges for CMIP6 historical simulations including anthropogenic and natural forcing, and green lines and shading show corresponding ensemble means and 5-95th percentile ranges for CMIP6 natural-only simulations. (Updated from Figure 3.7) *[Purpose: To compare the observed and simulated changes over the historical period for a range of variables are regions, with and without anthropogenic forcings, for attribution. Suggestions for alternative ways to present this information are welcome.]*

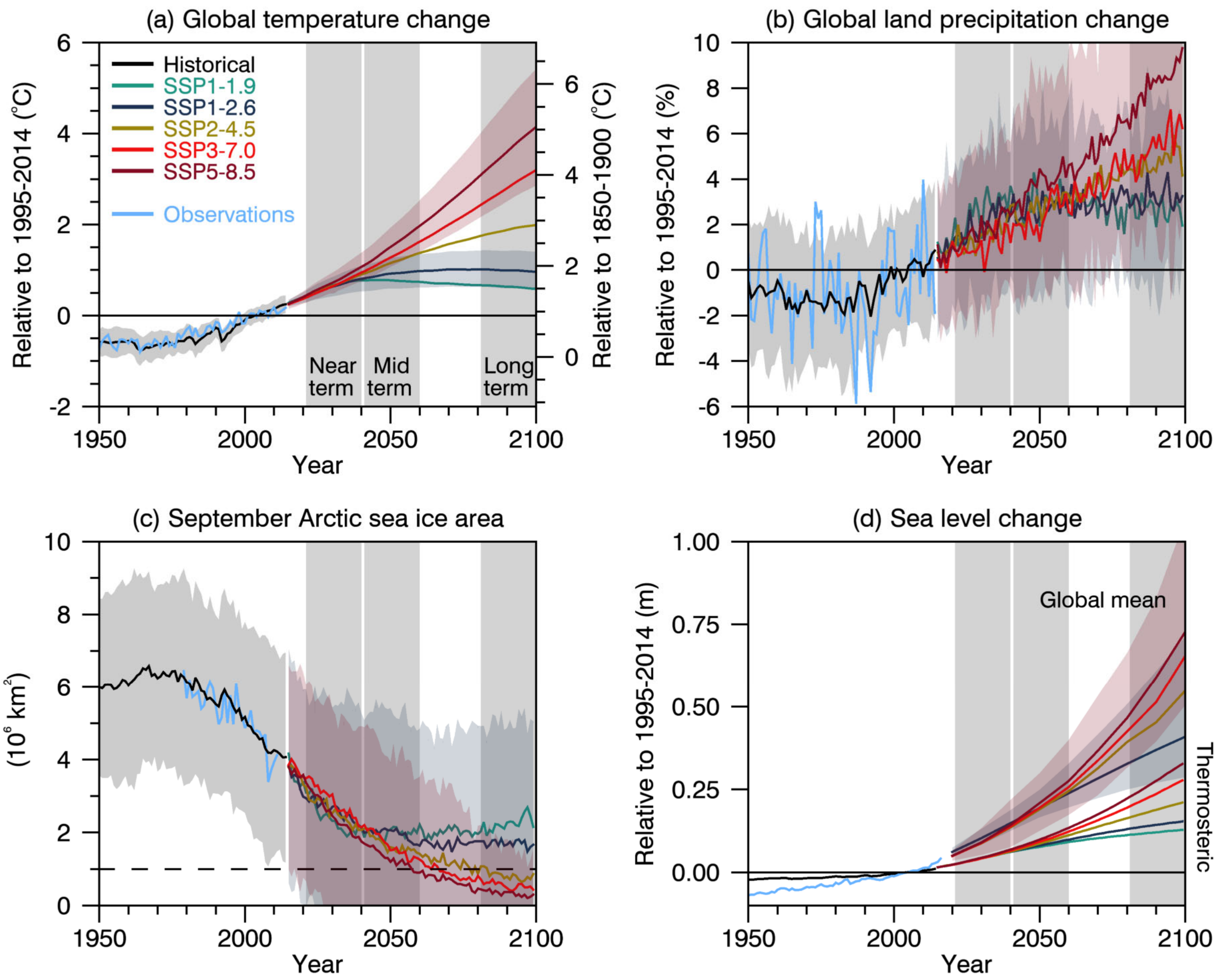

Cross-Section Box 1, Figure 1: Selected indicators of global climate change from CMIP6 historical and scenario simulations. (a) Global surface air temperature changes relative to the 1995–2014 average (left axis) and relative to the 1850–1900 average (right axis); the axes differ by 0.87°C. (b) Global land precipitation changes relative to the 1995–2014 average. (c) September Arctic sea-ice area. (d) Global sea level change relative to the 1995–2014 average. Curves with shading are global mean sea level (GMSL) and curves without shading are the contributions due to thermal expansion. (a), (b) and (d) are annual averages, (c) are September averages. In (a), the assessed time series of 20-year averages are shown from 2015 onwards, combining multiple lines of evidence. In (b) and (c), the curves show averages over the r1 simulations contributed to the CMIP6 exercise, the shadings around the SSP1-2.6 and SSP5-8.5 curves show 5 to 95% ranges (i.e., mean ± standard deviation times 1.645), and the numbers near the top show the number of model simulations. In (d), the contribution from ocean thermal expansion (thermosteric) is based on the r1 simulations in CMIP6; the contributions from land-ice melt have been computed using an emulator as in Chapter 9. [Note: In (a), the offset between the left and the right y-axes use the GMST instead of GSAT change, from 1850–1900 to 1995–2014. The axes thus assume an offset of 0.87°C, rather than 0.91°C, between these two time periods. The figure will be updated with the proper GSAT offset in the FGD.] {Figure 4.1}

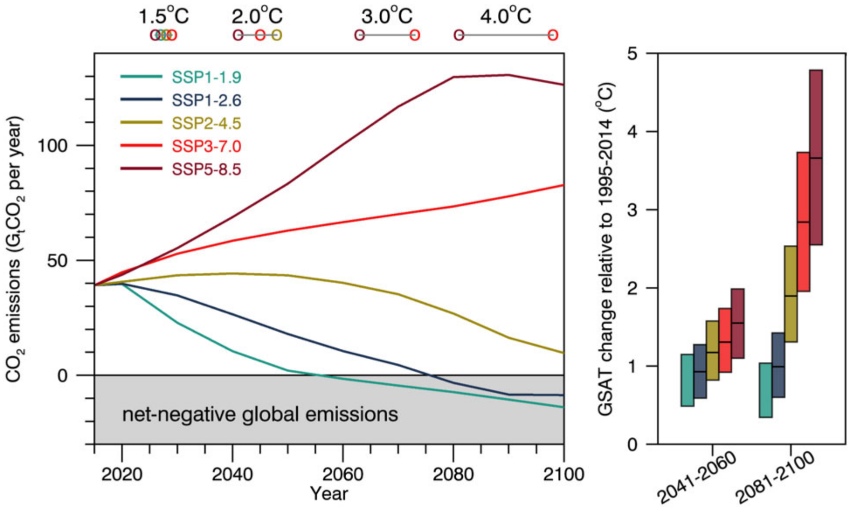

Cross-Section Box 1, Figure 2: Combining ranges of projected temperature change and the time when particular warming levels are reached: time series of SSP-based annual CO2 emissions from fossil fuel combustion and land use change for the core set of five illustrative SSP scenarios used in this report. SSP-based temperature projections for two time periods in the 21st century (vertical bars to the right of the panel). Time when particular warming levels are reached in the SSPs (along the top axis, with circles under each warming level indicating best estimates for the individual scenarios. 5-95% uncertainty ranges will be added in final version). [*Purpose: This figure combines key dimensions of integration (scenarios and warming levels) used across the WGI report and presents them along a time-axis in a single figure. The figure illustrates the relationship between scenario, projected warming, and time of reaching a particular temperature level.*]

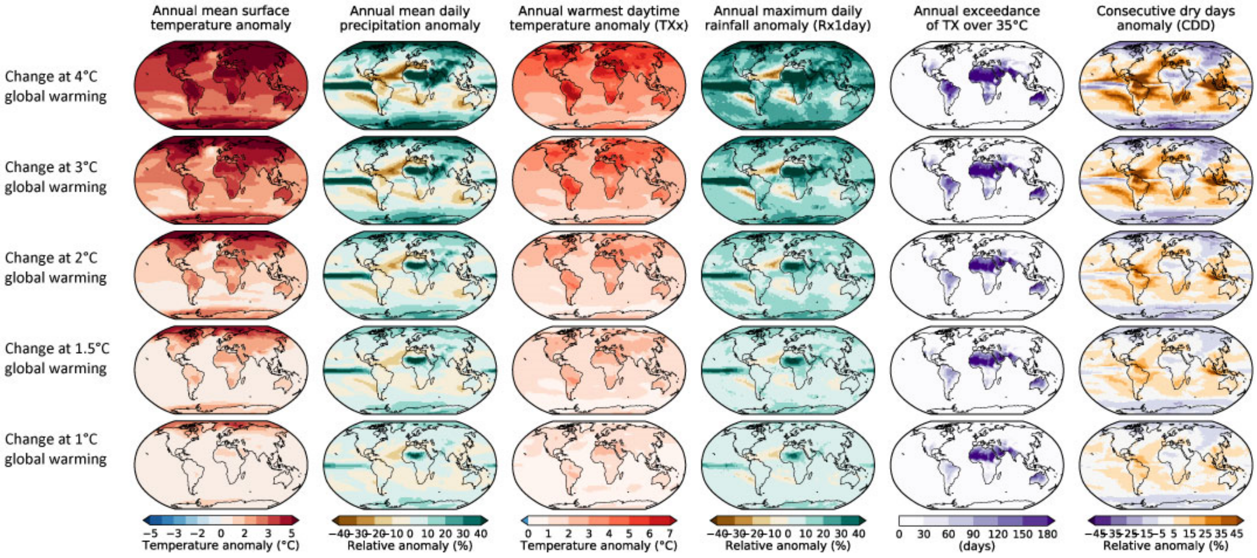

Cross-Section Box 2, Figure 1: Large scale changes as function of the level of global mean surface warming relative to 1850-1900. Left to right: Surface temperature (GSAT), precipitation, annual daily maximum temperature (TXx), annual daily maximum 1-day precipitation (Rx1day), number of days per year with maximum temperature exceeding 35 °C, and consecutive dry days. Warming levels (bottom to top) are 1°C (close to present day conditions), 1.5°C, 2°C, 3°C and 4°C. Results are based on the full CMIP6 ensemble, one member per model, and combining simulations of SSP1-1.9, SSP1-2.6, SSP2-4.5, SSP3-7.0, and SSP5-8.5. *[Purpose: Show the regional distribution of changes across a range of indicators, as function of warming level. The figure is essentially a "lookup-table" of changes at a given location and level of warming.]*

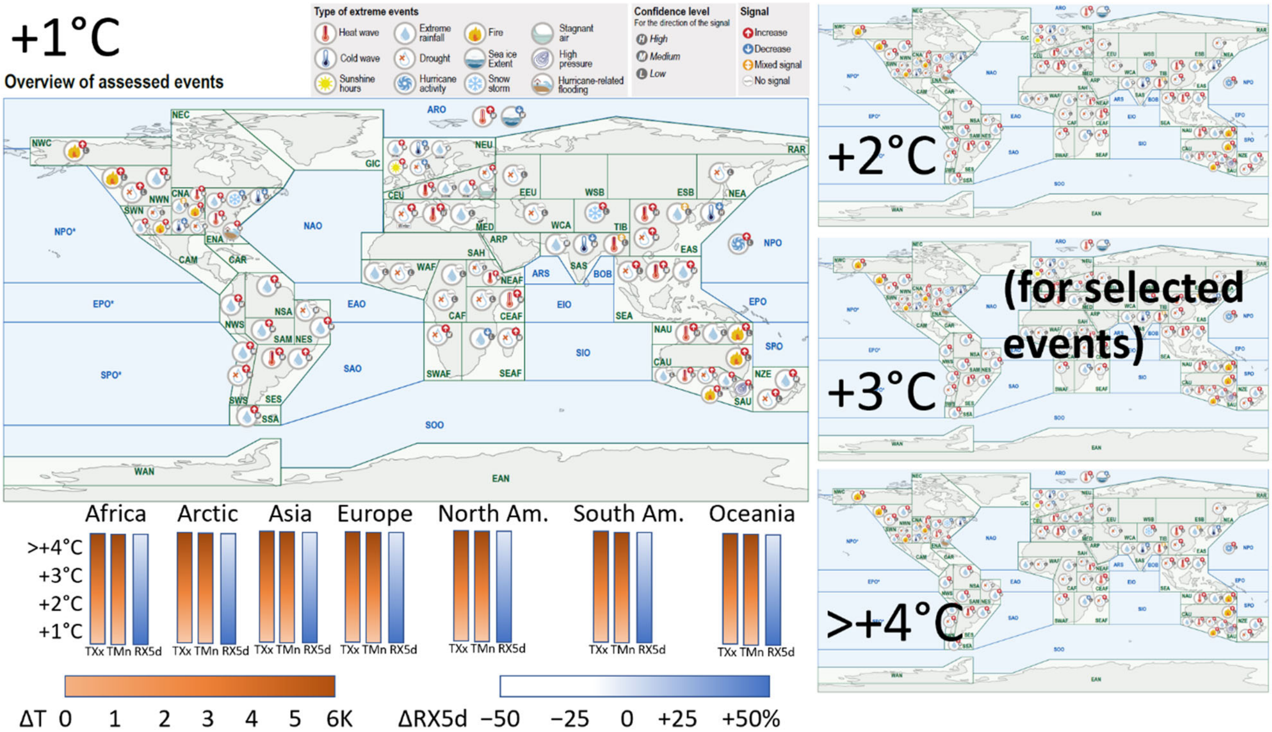

Cross-Section Box 2, Figure 2: Overview of changes attributed to anthropogenic influences under present warming, and their expected evolution to higher levels of global mean surface warming. Bars show the evolution of regional annual mean values based on the maps in Cross-Section Box 2 Figure 1. [*Purpose: Show what attributable changes are expected at different levels of global warming, starting with existing assessments of attributed changes at current warming. Also, provide continuous bar charts of changes in support of the Reasons For Concern assessed in WG2.]*

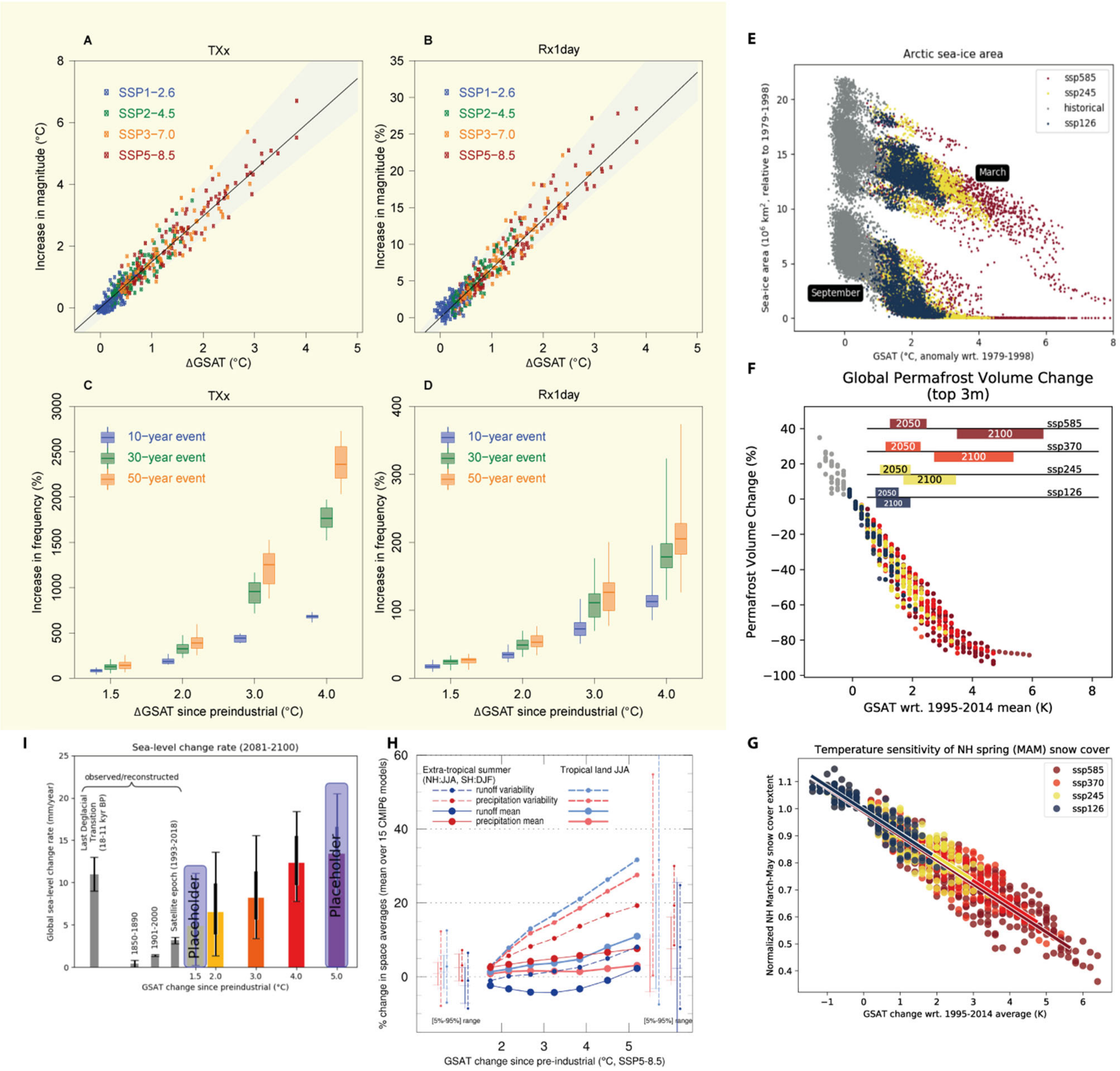

Cross-Section Box 2, Figure 3: Several fundamental indicators change near-linearly with GSAT, indicating a near pathway independence of changes for fast-reacting indicators, reducing the dependence of projections of future changes on scenario details. Yellow box: How the rate (A, B) and frequency (C, D) of warm (A, C) and wet (B, D) extremes change with WL. Rates scale nearly linearly, while frequency increases more strongly, and with larger percentage increases for less frequent events, for each step in global surface warming. Clockwise from top right: E: Arctic sea ice extent in March and September. March ice scales linearly, while September ice reaches zero in most scenarios between warming of 2 °C and 3 °C. F: Global permafrost volume scales linearly until around 3 °C, then shows signs of accelerated melt in CMIP6 models. G: Spring snow cover in the Northern Hemisphere scales linearly with WL. H: Precipitation and runoff, mean and variability. I: Rate of sea level rise, at present and future levels of surface warming, compared to observed or reconstructed rates since the Last Glacial Maximum. [SOD comment: Panels will be harmonized for the FGD. In particular, the reference periods will all be 1850-1900; in the present draft they vary between panels. The evolution of large scale changes with global warming level (WL). The purpose of this figure is to show how a range of indicators scale with warming level; some linearly, some not.]

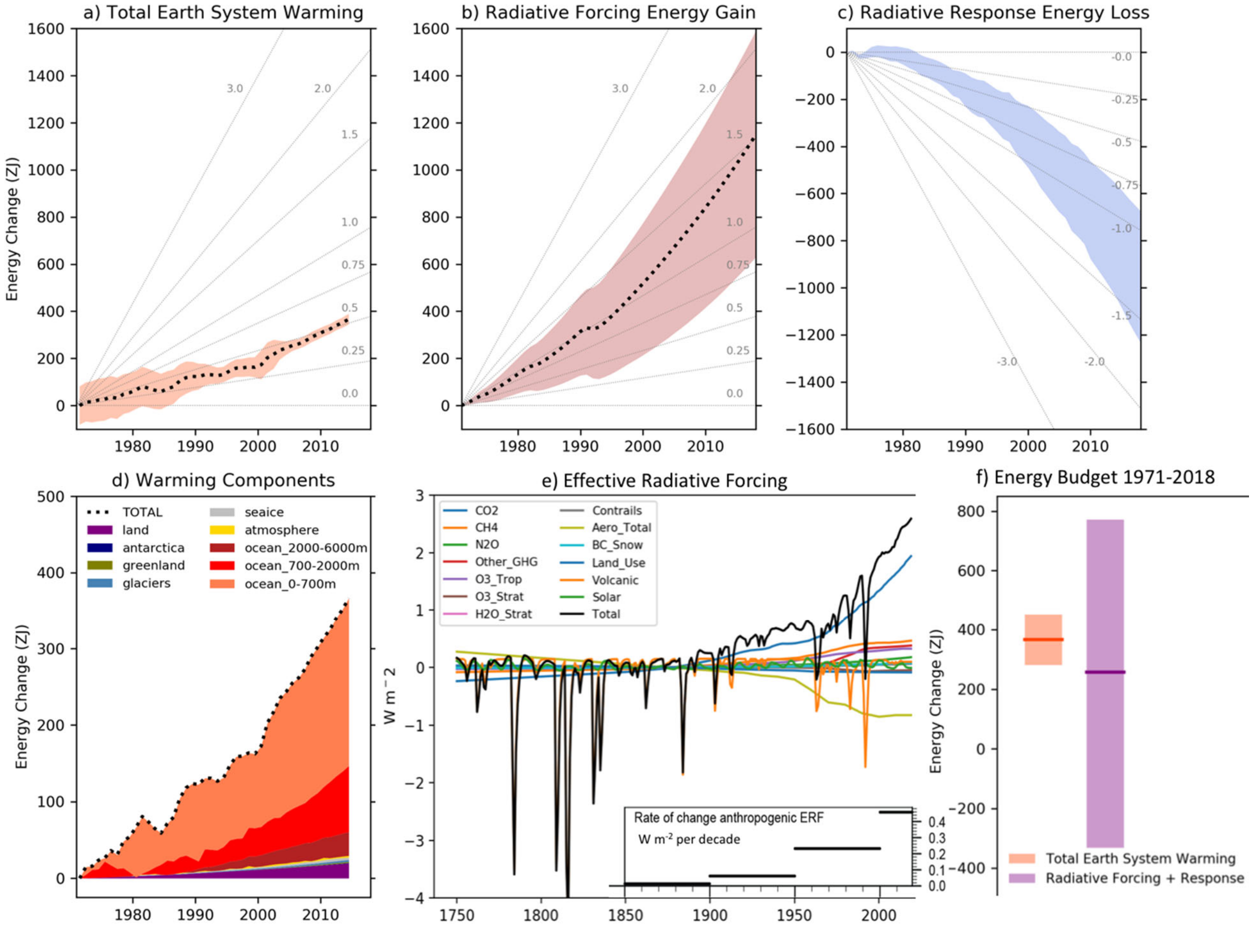

Figure TS.24: Estimates of the net cumulative energy change (ZJ = 10^{21} Joules) for the period 1971-2018 associated with: (a) Total Earth System Warming; (b) Effective Radiative Forcing; (c) Earth System Radiative Response. Shaded regions indicate the 5th to 95th percentile uncertainty range. The grey lines indicate equivalent heating rates in W m^{-2}, expressed relative to Earth's surface area. Panel (d) shows the breakdown of components, as indicated in the legend, for Total Earth System Warming. Forcing and Response timeseries are computed using a baseline period of 1850-1900. Panel (e) shows changes in ERF. The global annual mean temporal evolution since 1750 is shown as the central assessment value. ERF of changes to the atmospheric composition are shown for the gases carbon dioxide (CO_2), methane (CH_4), nitrous oxide (N_2O), synthetic greenhouse gases, and tropospheric ozone (O_3). Aerosol changes include the sum of the ERF due to aerosol – radiation and aerosol – cloud interactions. Other anthropogenic forcings include stratospheric ozone, stratospheric water vapour, land use / land cover changes, black carbon deposition on snow, and contrails. The two other key ERFs shown are for variability in TSI and in volcanic forcing. The sum of the best estimates for all forcings is shown as the total forcing. The inset in the lower right shows the rate of change (linear trend) in total anthropogenic ERF (total without TSI and volcanic ERF) for the periods 1850–1900, 1900–1950, 1950–2000 and 2000–2019. Panel (f) shows the Earth Energy Budget assessed for the period 1971-2018, i.e. the consistency between Total Earth System Warming and the implied heat storage from Effective Radiative Forcing plus Earth System Radiative Response. Shading represents the 5% to 95% uncertainty range. Forcing and Response timeseries are computed using a baseline period of 1850-1900. [placeholder: Total Earth System Warming components to be updated to 2018 for final draft. Reported values for sum of components in main text are based on extrapolation of 2006-2015 rate to 2018. The aerosol ERF estimate is based on AR5 and will be updated for the final draft.]

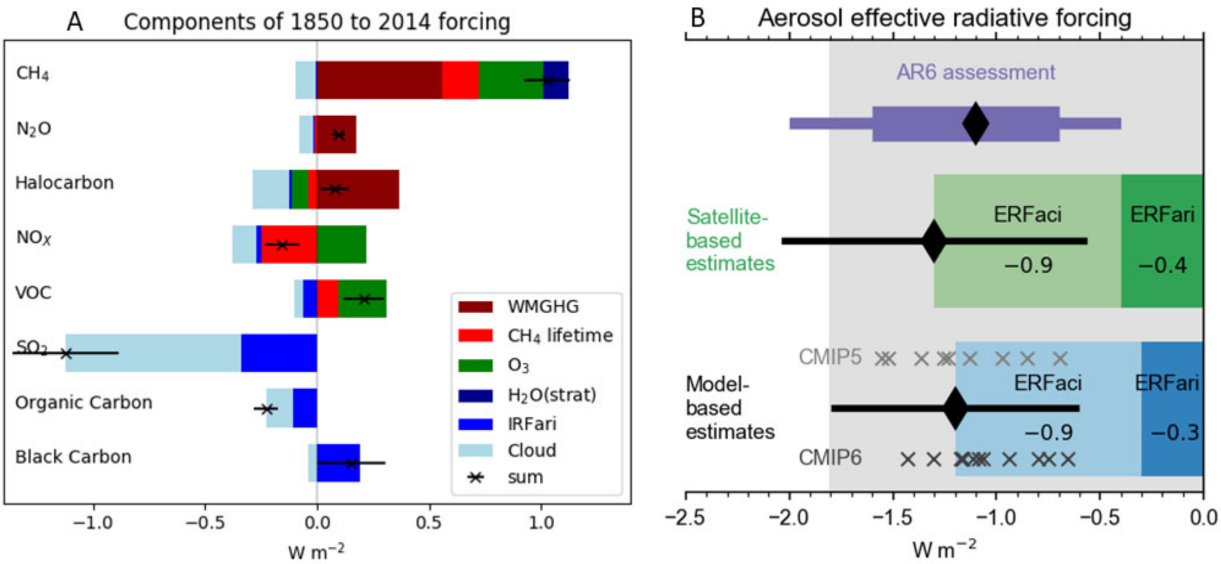

Figure TS.25: A) Components of radiative forcing from 1850 to 2014 by emitted species based on CMIP6 models. “VOC” includes CO as well as other non-methane hydrocarbons. WMGHGs are from analytical formulae, H_2O (stratosphere) is unchanged since AR5. Other components are multi-model means and are based on model simulations where one species at a time is increased from 1850 levels to 2014. Error bars are 5-95% and account for uncertainty in radiative efficiencies and multi-model error in the means. IRFari and cloud effects are calculated from separate radiation calls for clear-sky and aerosol free conditions. “Cloud” includes cloud adjustments (semi-direct effect) and ERFaci. The aerosols (SO2, organic carbon, black carbon) components are scaled to sum to −0.25 W m−2 for IRFari and −0.95 W m−2 for “cloud”. (B) Net aerosol ERFari+aci from different lines of evidence. Green bars show the assessment based on satellite observations. Blue bars show the assessment based on climate models, with individual models from CMIP5 and CMIP6 depicted. Both the satellite- and model-based assessments are for 1750-2014. Individual assessed best-estimate contributions from ERFari and ERFaci are shown with darker and paler shading respectively. Overlaid black diamond and black lines show the best estimate and very likely range of satellite- and model-derived ERFari+aci Grey shading shows the very likely range consistent with energy budget constraints. Purple bars show the assessed very likely range (thin), likely range (thick), and best estimate (black diamond) from all lines of evidence in this assessment for 1750-2018. *[Purpose: The intent of this figure is to show advances since AR5 in the understanding of (A) emissions-based ERF for SLCFs (SOD Figure 7.10) and (B) Aerosol ERFari+aci from different lines of evidence (satellite-based, model based and overall assessment of aerosol ERF; SOD Figure 7.8)]*

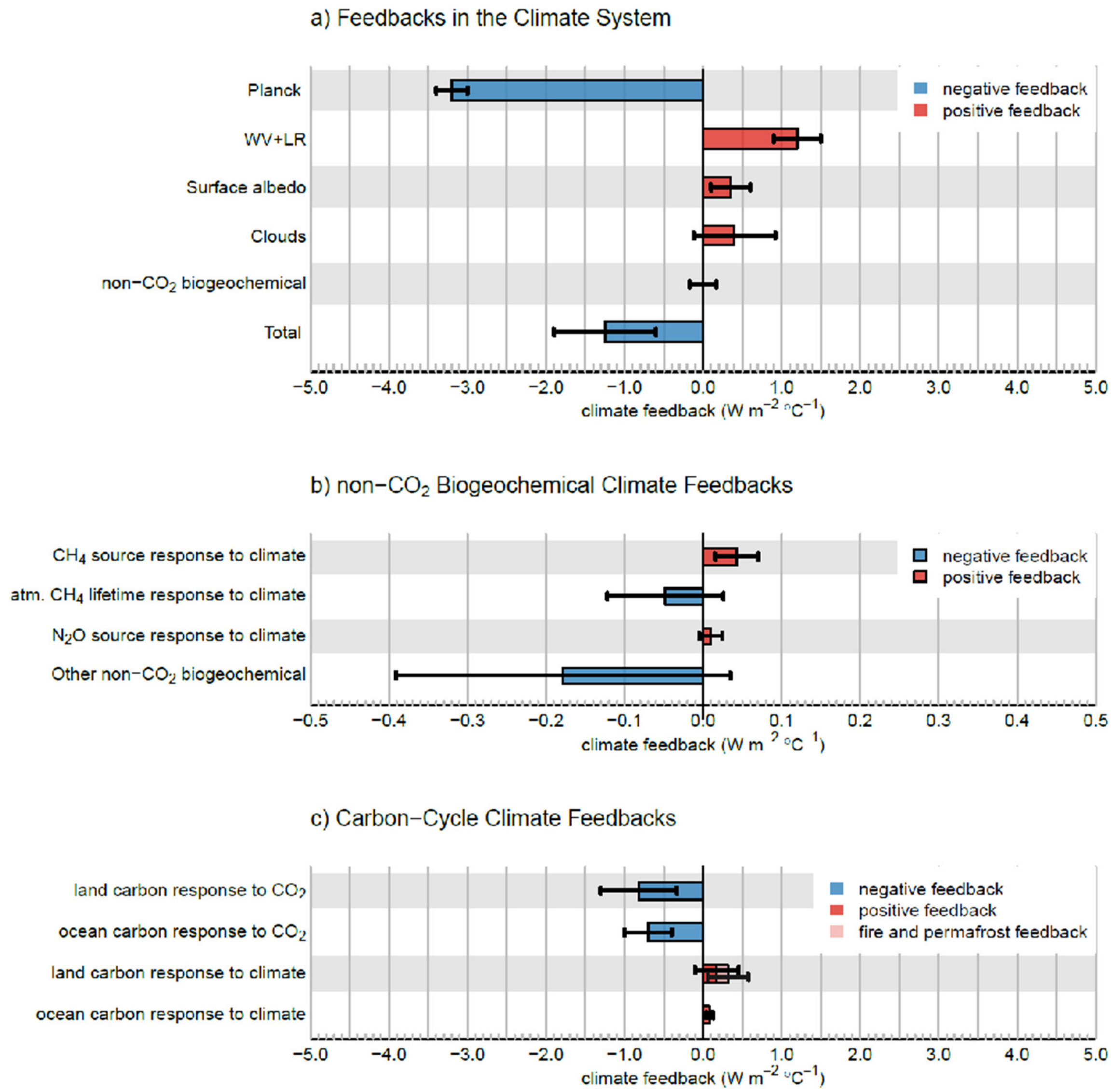

Figure TS.26: An overview of physical and biogeochemical feedbacks in the climate system. a) Synthesis of physical and non-CO_2 biogeochemical feedbacks that are included in the definition of ECS assessed in this Technical Summary. These feedbacks have been assessed using multiple lines of evidence including observations, models and theory. "WV+LR" stands for water vapour and lapse rate feedback. The net feedback is the sum of the Planck response and water vapour, lapse rate, surface albedo, cloud, and non-CO_2 biogeochemical feedbacks. Positive feedbacks (red bars) amplify and negative feedbacks (blue bars) diminish the initial climate response to radiative forcing. Bars denote the mean feedback values and uncertainties represent *very likely* ranges assuming variance between individual components are independent; b) Estimated values of individual non-CO_2 biogeochemical feedbacks. The atmospheric methane lifetime and other non-CO_2 biogeochemical feedbacks have been calculated using global Earth System Model simulations from AerChemMIP, while the CH_4 and N_2O source response to climate have been assessed for the RCP8.5 scenario in year 2100, using simplified radiative forcing equations. There is insufficient evidence to support a central estimate of the total non-CO_2 biogeochemical feedback so it is assessed to have zero-mean value in panel (a). Note the different x-axis scale for panel (b). c) carbon-cycle feedbacks as assessed by models participating in the C4MIP of CMIP6. An independent estimate of the additional positive carbon-cycle climate feedbacks from fire and permafrost thaw, which is not considered in most C4MIP models is added . Note that these feedbacks act through modifying the atmospheric concentration of CO_2 and thus are not included in the definition of ECS, which assumes a doubling of CO_2. *[Purpose: The intent of this figure is to show the physical and biogeochemical feedbacks on global temperature (new, based on Ch 5, 7).]*

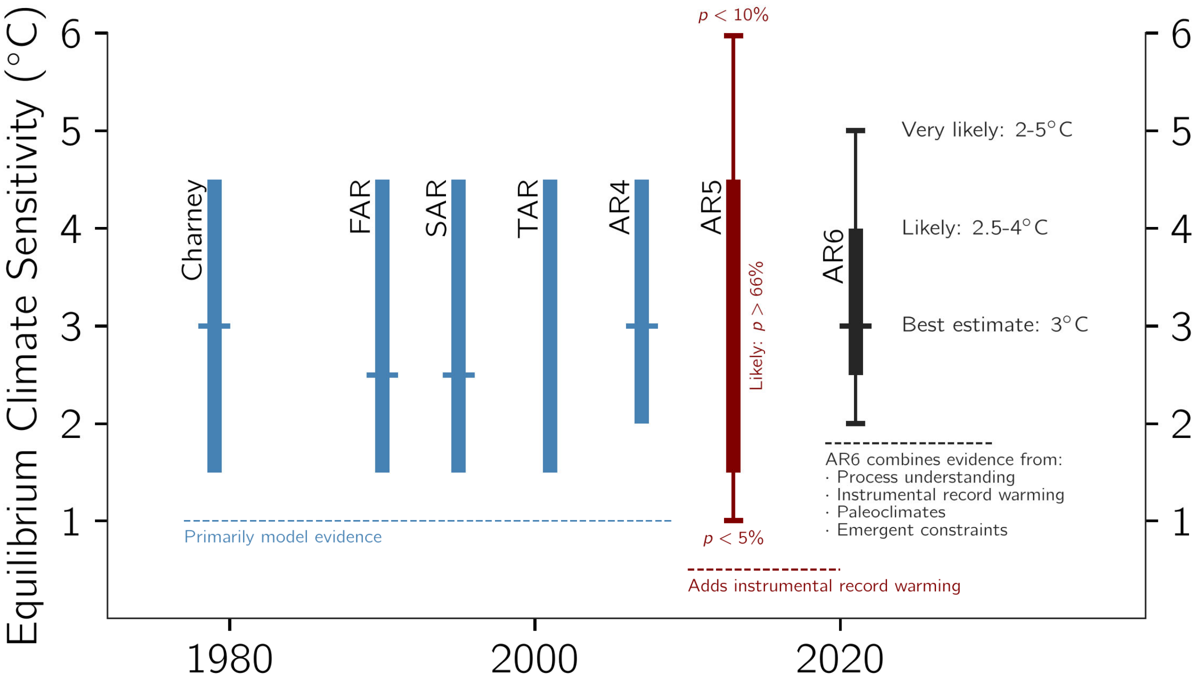

Figure TS.27: Evolution of the uncertainty range is ECS as assessed by the Charney report and a succession of IPCC Assessment Reports. Reports are coloured according to the lines of evidence considered in the assessment, those lines of evidence being listed in the same colour below each group. Best estimates are marked by horizontal bars, *likely* ranges by thick vertical bars, and *very likely* ranges by whiskers. {Updates: add ranges for the four lines of evidence used in AR6, and add ECS in individual CMIP5/6 models}. [*Purpose***:** *This figure shows how the uncertainty range in ECS derived from different lines of evidence as assessed by the Charney report and successive IPCC Assessment Reports. This figure will be a replacement for SOD Fig 7.23.]*

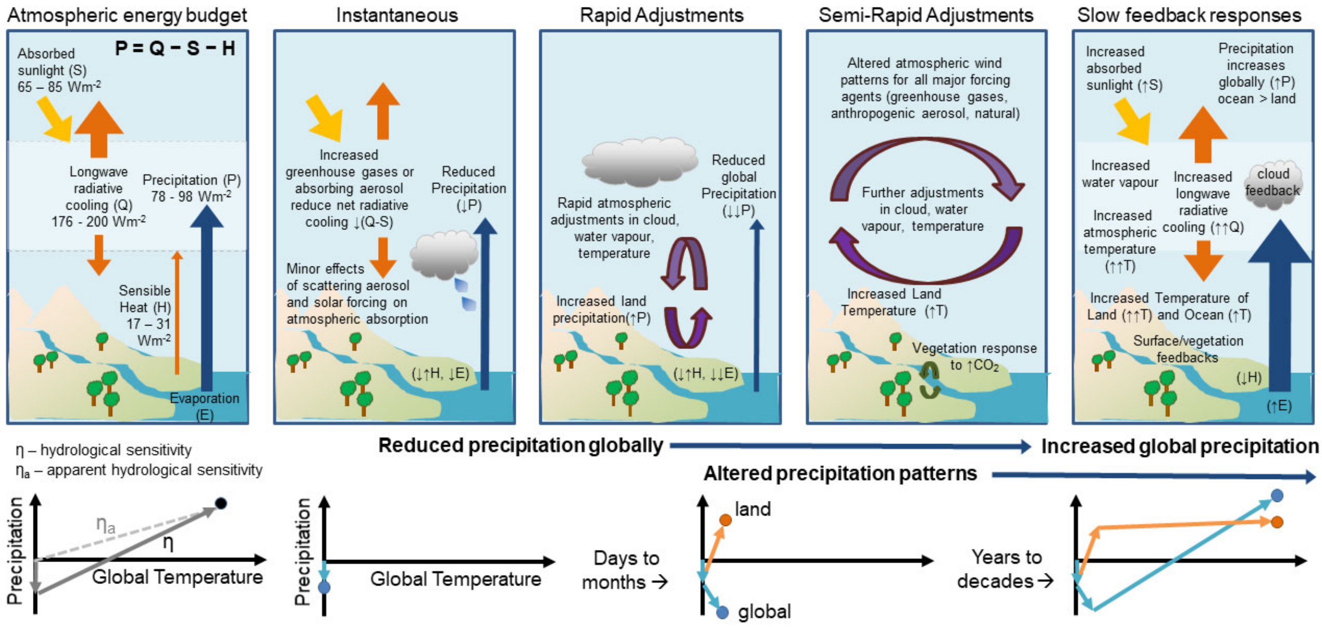

Figure TS.28: Schematic representation of rapid and slow responses of the atmospheric energy balance and global precipitation to radiative forcing. (Figure 8.3)

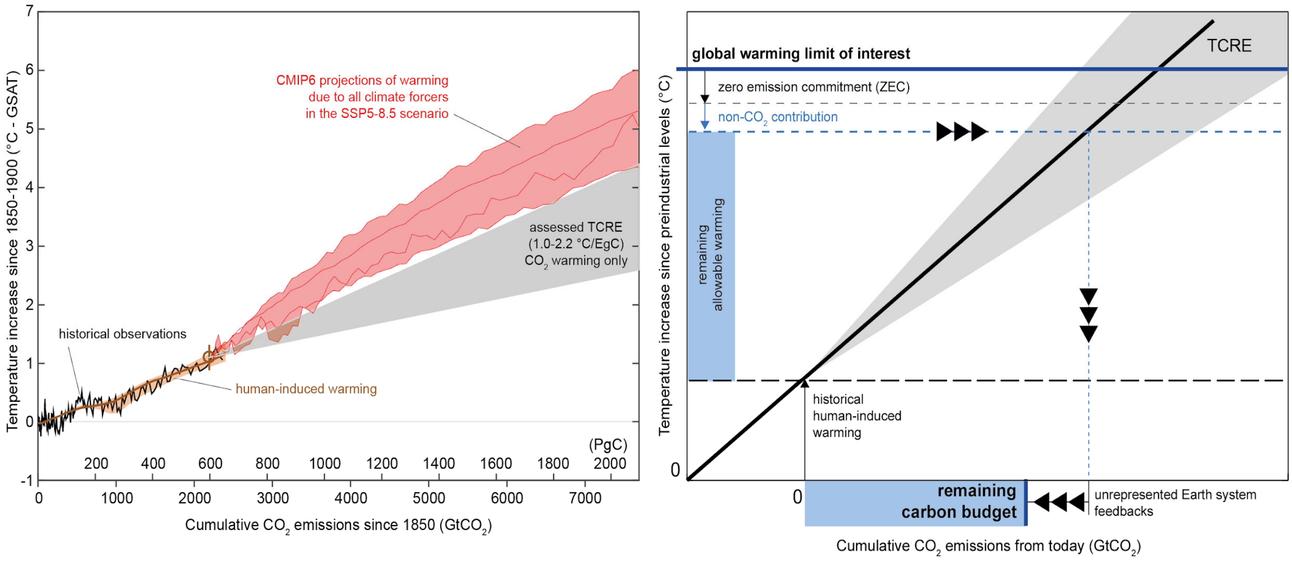

Figure TS.29: Illustration of relationship between cumulative emissions of CO_2 and global mean surface air temperature increase (left) and conceptual schematic of the assessment of the remaining carbon budget from its constituting components (right). Historical data in the left-hand panel (thin black line data) shows historical CO_2 emissions together with the assessed global surface air temperature increase from 1850-1900. Orange-brown range with its central line show the human-induced share of historical warming. The circle and vertical line show the assessed range of historical human-induced warming for the 2010–2019 period relative to 1850-1900. The grey cone shows the assessed range for the transient climate response to cumulative emissions of carbon dioxide (TCRE) assessed to fall *likely* in the 1.0–2.2 °C/EgC range, starting from 2015. The red range and thin red lines within it represent CMIP6 simulations of the SSP5-8.5 scenario, starting from 2015. {Updates: to include an additional cone showing future GSAT change versus cumulative emissions for assessed GSAT ranges following the SSP5-8.5 scenario.}. [*Purpose: The proportionality between cumulative CO2 emissions and global surface air temperature in observations and models (left) as well as the assessed range of TCRE and the right-hand panel shows how information is combined to derive remaining carbon budgets consistent with limiting warming to a specific level. Update to AR5 SPM.10, SOD Figure 5.31.]*

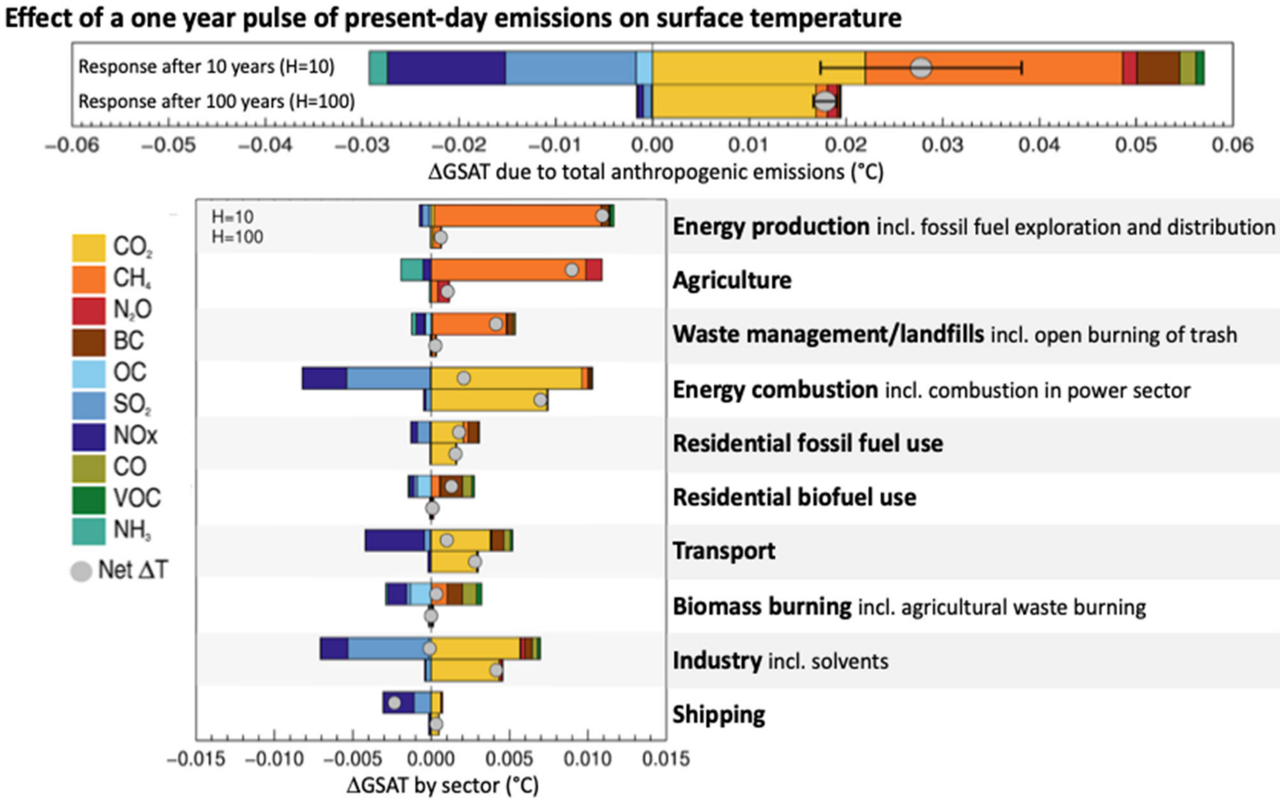

Figure TS.30: Global Surface Air Temperature (GSAT) effect for 10 and 100 years after one-year pulse of present-day emissions (year 2014 in Community Emissions Data Systems (CEDS) emissions (Hoesly et al. 2018)) of short-lived climate forcers (SLCFs) and CO_2 for: a) global total emissions, and b) emissions from 10 major economic sectors sorted by total net effect on the 10-year timescale. The temperature response is broken down by individual species. Error bars in the top panel show uncertainty (±1 standard deviation) in net temperature impact due to uncertainty in radiative forcing of the individual species (calculated using a Monte Carlo approach and best estimate uncertainties from the literature - see Lund et al. (2020) for details). The CO_2 emissions from biomass burning and biofuel use in residential sector (RES) are not considered. HFCs are not yet part of the chart. Sectoral split is based on Hosely et al. 2018, Höglund-Isaksson et al. (2020) and Klimont et al. (2017).{Ideas from Joeri: I would like to highlight that reductions in CO2 emissions result in an almost instantaneous change in the rate of warming. I think the figure probably needs a more direct visualisation of the "thought experiment" of simply looking at current emissions for one year, and then basically switching all emissions off and wait for 10 and 100 years, respectively. The bars can maybe also be distributed on a global map for the regional contributions and linked to icons that represent the various sectors for the sectorial emissions.} *[Purpose**:** This figure shows the sectoral contribution to present-day climate change by specific climate forcers including CO2 as well as SLCFs. (Updated SOD 6.16).]*

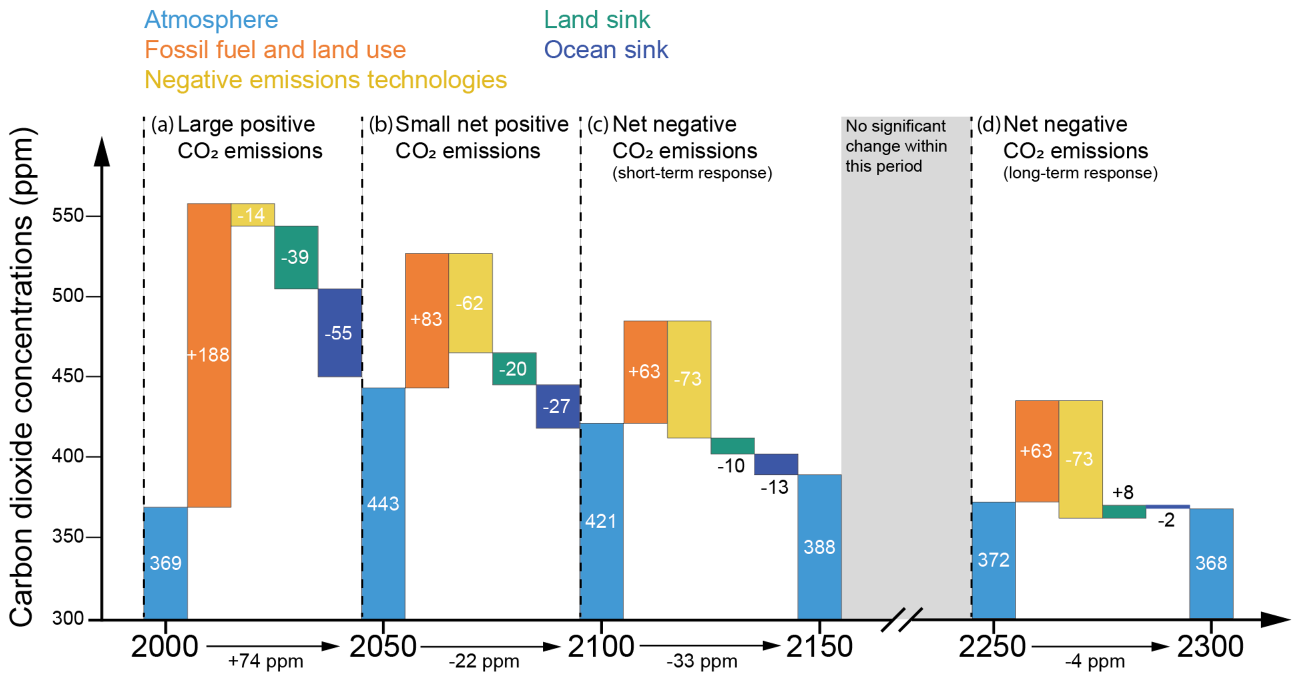

Figure TS.31: Carbon flux components during different stages of ESM simulations driven by RCP2.6. (a) Large positive CO_2 emissions, (b) Small net positive CO_2 emissions, (c) Net negative CO_2 emissions (short-term response), (d) Net negative CO_2 emissions (long-term response). Fossil fuel and land use emissions as well as emissions from negative emission technologies are from the RCP2.6 scenario. Due to small differences between the compatible CO_2 emissions diagnosed from the ESMs and the emissions in RCP2.6, emissions and land and ocean carbon fluxes over each 50-year period do not balance precisely. [*Purpose: This figure shows how atmospheric CO2 evolves under negative emissions and its dependence on the negative emissions technologies. It also shows the evolution of the ocean and land sinks (Figure 5.33).]*

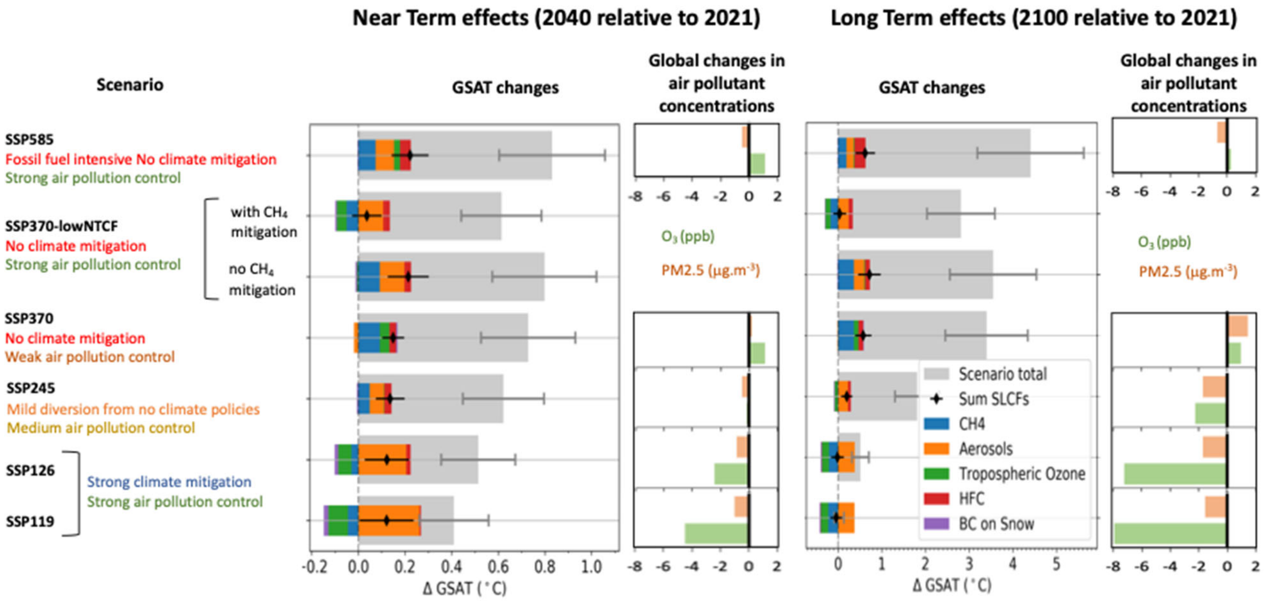

Figure TS.32: Effect of 5 groups of short-lived climate forcers (SLCFs) (net aerosols, tropospheric ozone, Hydrofluorocarbons (HFCs), methane and black carbon (BC) on snow) and total forcing across the main Shared Socio-Economic Pathway (SSP) scenarios on future Global Surface Air Temperature (GSAT) for 2040 and 2100 relative to year 2021. The GSAT changes are based on calculations of historic and future of Effective Radiative Forcing (ERF) evolution from three simple climate models/emulators participating in the Reduced Complexity Model Intercomparison Project (RCMIP). The temperature response to the ERFs are calculated with one common impulse response function for the climate response, equal to the Instantaneous Radiative Forcing (IRF) used for metric calculations in Chapter 7. The IRF has an equilibrium climate sensitivity of 3.3°C (feedback parameter of 0.885 C $(Wm^{-2})^{-1}$). The uncertainties are the intra-model standard deviation. The scenario total (grey bar) includes all anthropogenic forcings (LLCFs, SLCFs and Land Use Changes). The global changes in air pollutant concentrations (ozone and $PM_{2.5}$) are based on multimodel simulations (AerChemMIP) and represent change in annual mean surface continental concentrations for the near and long-term relative to 2021. *[Purpose: The intent of this figure is to show the climate and air quality (surface ozone and PM2.5) response to SLCFs in the SSP scenarios (new figure based on Figures 6.17, 6.18, and 6.19) for near and long-term.]*

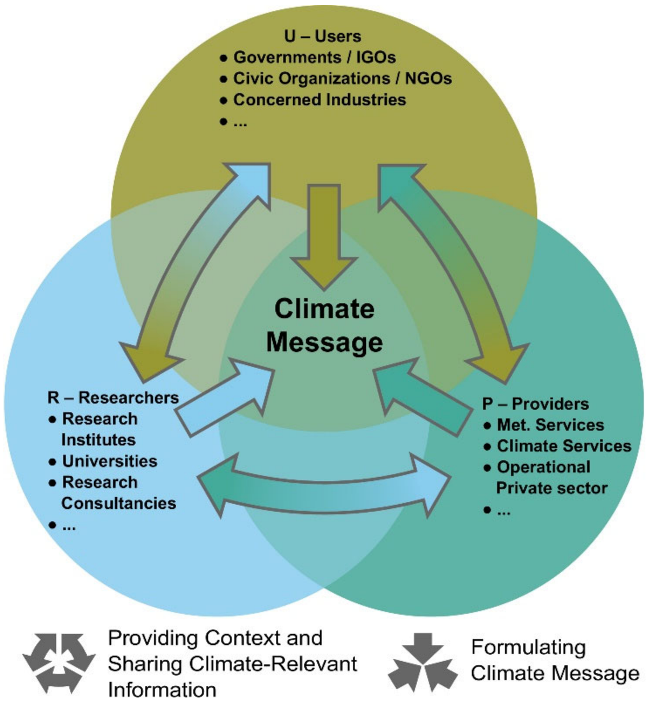

Figure TS.33: Effective messaging requires shared development of the actionable information that engages all parties involved and the values that guide their engagement. Participants in the development of climate messages come from varying perspectives, based in part on their professions and communities. Each of the three broad categories shown in the Venn diagram (U, P, R) is not a homogenous group, and often has a diversity of perspectives, values and interests among its members. The subheadings in each category are illustrative and not all-inclusive. The arrows connecting those categories represent the distillation process of providing context and sharing climate relevant information. The arrows that point toward the centre represent the distillation of climate messages that involves all three categories.

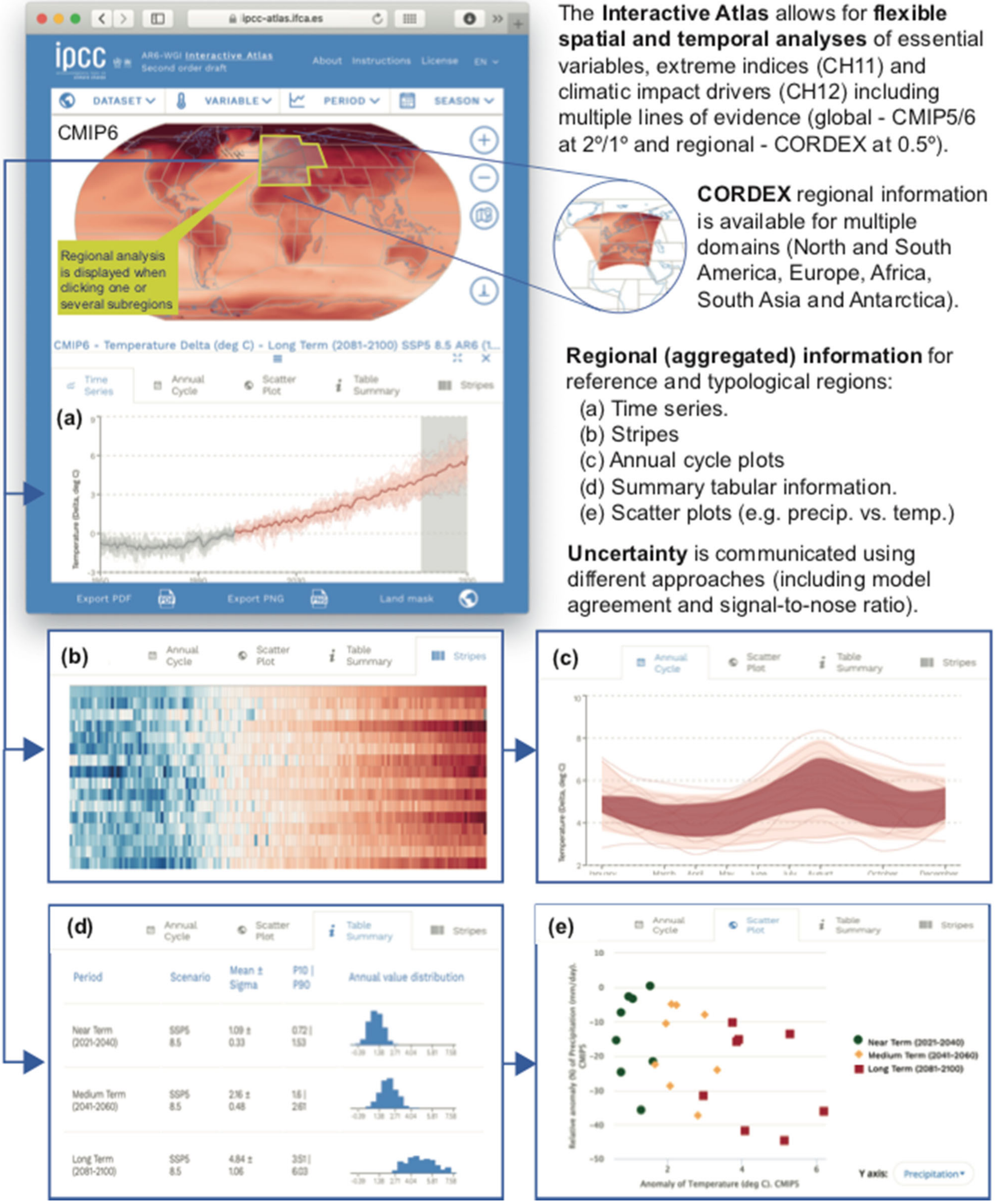

Box TS.5, Figure 1: Screen shots from the Interactive Atlas showing the main interface and WGI Reference regions (top map) and various formats for displaying summary information over the reference regions (bottom four graphics panels). Other details of model ensembles, resolutions and the summary statistics available are displayed in the text of the figure.

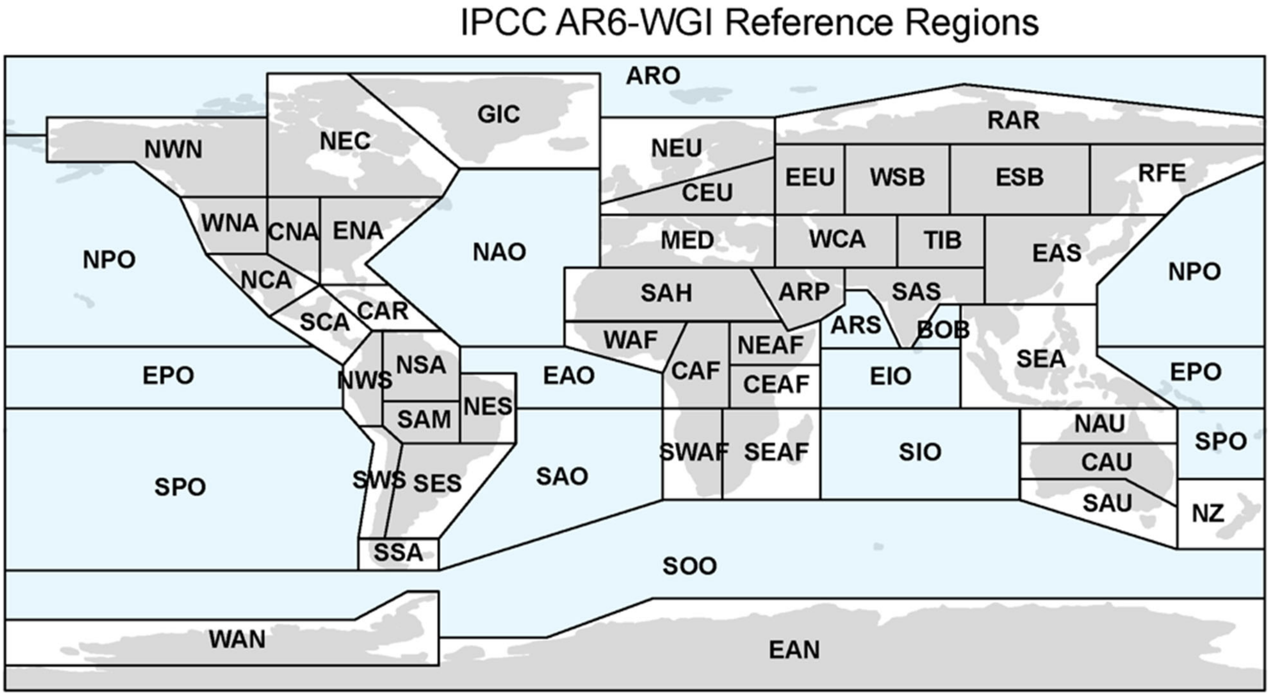

1	GIC	Greenland/Iceland
2	NEC	N.E.Canada
3	CNA	C.North-America
4	ENA	E.North-America
5	NWN	N.W.North-America
6	WNA	W.North-America
7	NCA	N.Central-America
8	SCA	S.Central-America
9	CAR	Caribbean
10	NWS	N.W.South-America
11	SAM	South-American-Monsoon
12	SSA	S.South-America
13	SWS	S.W.South-America
14	SES	S.E.South-America
15	NSA	N.South-America
16	NES	N.E.South-America
17	NEU	N.Europe
18	CEU	C.Europe
19	EEU	E.Europe
20	MED	Mediterranean

21	WAF	West-Africa
22	SAH	Sahara
23	NEAF	North-East-Africa
24	CEAF	Central-East-Africa
25	SWAF	South-West-Africa
26	SEAF	South-Eeast-Africa
27	CAF	Central-Africa
28	RAR	Russian-Arctic
29	RFE	Russian-Far-East
30	ESB	E.Siberia
31	WSB	W.Siberia
32	WCA	W.C.Asia
33	TIB	Tibetan-Plateau
34	EAS	E.Asia
35	ARP	Arabian-Peninsula
36	SAS	S.Asia
37	SEA	S.E.Asia

38	NAU	N.Australia
39	CAU	C.Australia
40	SAU	S.Australia
41	NZ	New-Zealand
42	EAN	E.Antarctica
43	WAN	W.Antarctica
44	ARO	Arctic-Ocean
45	NPO	N.Pacific-Ocean
46	EPO	Equatorial.Pacific-Ocean
47	SPO	S.Pacific-Ocean
48	NAO	N.Atlantic-Ocean
49	EAO	Equatorial.Atlantic-Ocean
50	SAO	S.Atlantic-Ocean
51	ARS	Arabian-Sea
52	BOB	Bengal-Gulf
53	EIO	Equatorial.Indic-Ocean
54	SIO	S.Indic-Ocean
55	SOO	Southern-Ocean

Box TS.5, Figure 2: AR6 WG I reference regions used for the regional analysis of atmospheric variables and land surface variables in the several WG I chapters including the Atlas and the Interactive Atlas. The definition of the regions and companion notebooks and scripts are available at the ATLAS GitHub (TS4).

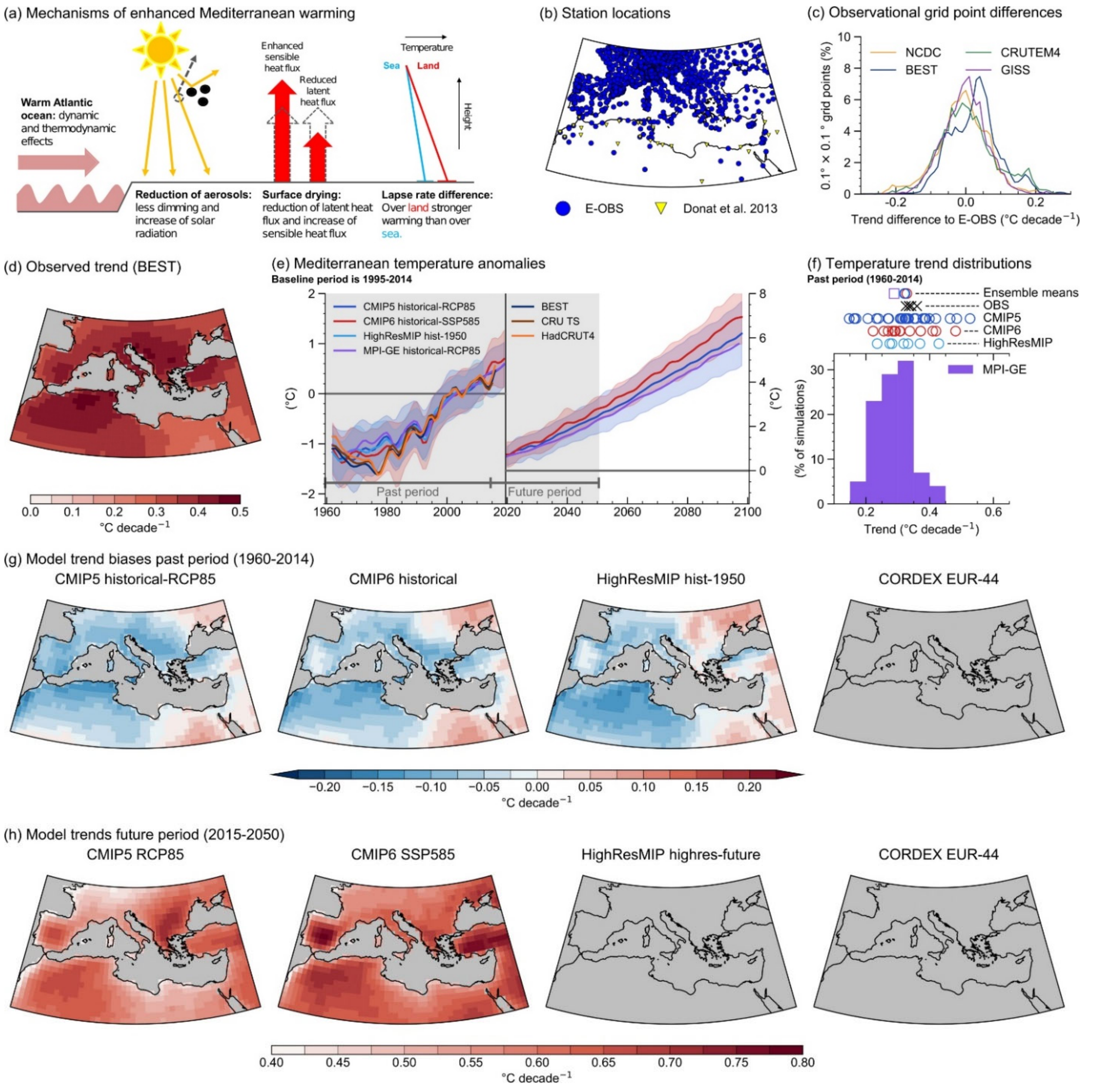

Box TS.5, Figure 3: Example of constructing regional climate message from multiple lines of evidence for the case of Mediterranean summer warming. (a) Mechanisms and feedbacks involved in enhanced Mediterranean summer warming. (b) Locations of observing stations in E-OBS v19e (Cornes et al., 2018) and Donat et al. (2014). (c) Differences in temperature observational data sets with respect to E-OBS for the land points between the Mediterranean Sea and 46°N and west of 30°E. (d) Observed summer (June to August) surface air temperature trends (°C per decade) over the 1960–2014 period from BEST (Rohde et al., 2013) dataset. (e) Time series of area averaged (25°N–50°N, 10°W–40°E) land point summer temperature anomalies (°C, baseline 1995–2014). Black, brown, orange and violet lines show low-pass filtered temperature of BEST, CRU TS v4.02 (Harris et al., 2014), HadCRUT4 (Morice et al., 2012) and the MPI-GE (Maher et al., 2019), respectively. Dark blue, red and light blue lines and shadings show low-pass filtered ensemble means and standard deviations of CMIP5 (30 members), CMIP6 (15 members) and HighResMIP (7 members), respectively. The filter is the same as the one used in Figure 10.11. (f) Distribution of 1960–2014 summer temperature trends (°C per decade) for observations (black crosses), the MPI-GE (violet histogram) and for ensemble means and single runs of CMIP5 (dark blue circles), CMIP6 (red circles) and HighResMIP (light blue circles). (g) Bias in ensemble mean 1960–2014 trends (°C per decade) of CMIP5, CMIP6, HighResMIP and CORDEX in reference to BEST. (h) Projections of ensemble mean 2014–2050 trends (°C per decade) of CMIP5, CMIP6, HighResMIP and CORDEX. All trends are estimated using ordinary least-squares.

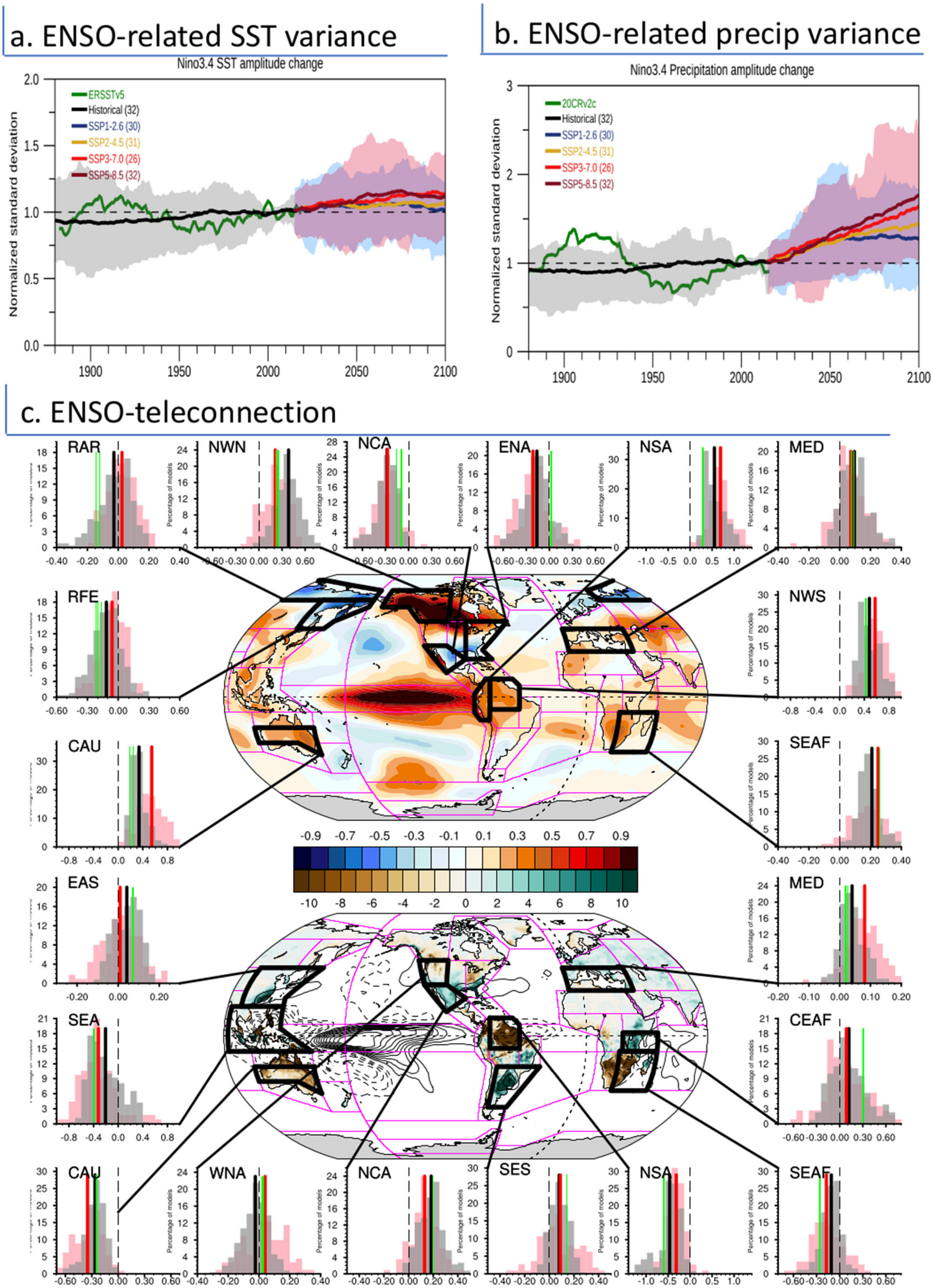

Figure TS.34: **a.** Observed, modelled and projected evolution of annual ENSO SST variability over the Nino 3.4 region from 1880 to 2100. Thick lines stand for multi-model ensemble mean for historical and four

SSP runs and shading is the 5-95% range across CMIP6 models for historical simulation (grey), SSP1-2.6 (mid blue) and SSP5-8.5 (pink), respectively. The amplitude of ENSO variability is defined as the standard deviation of the Nino 3.4 SST index over backward 30-year running windows. Values are normalized with respect to the 1995-2014 period. The number of available models is listed in parentheses. The observed change (green line) based on ERSST version 5 is also shown from 1881-2014. **b.** Same as **a.** except for rainfall over the Nino 3.4 region. The green line indicates the rainfall variability change based on 20C ERA reanalysis from 1881-2014. **c.** Observed, simulated and projected ENSO teleconnections for 2m-temperature and precipitation during December--February. Teleconnections are identified by linear regression with the Niño 3.4 SST index based on ERSSTv5 during the period 1958-2014. Maps show observed patterns for temperature from the Berkeley Earth dataset over land and from ERSSTv5 over ocean (top) and for precipitation from GPCC over land and GPCP over ocean (contour, period: 1979-2014). Distributions of regression coefficients for regional means drawn from 261 historical simulations from 30 CMIP6 models in gray and for 113 SSP5-8.5 projections in light pink are provided for a subset of pre-defined AR6 regions in Atlas for temperature (top) and precipitation (bottom). Multi-model multi-member ensemble means are indicated by thick vertical coloured lines (black for historical and red for SSP5-8.5). Green vertical lines stand for observational estimates based on Berkeley Earth and GISTEMP datasets for temperature and from GPCC and GPCP datasets for precipitation.

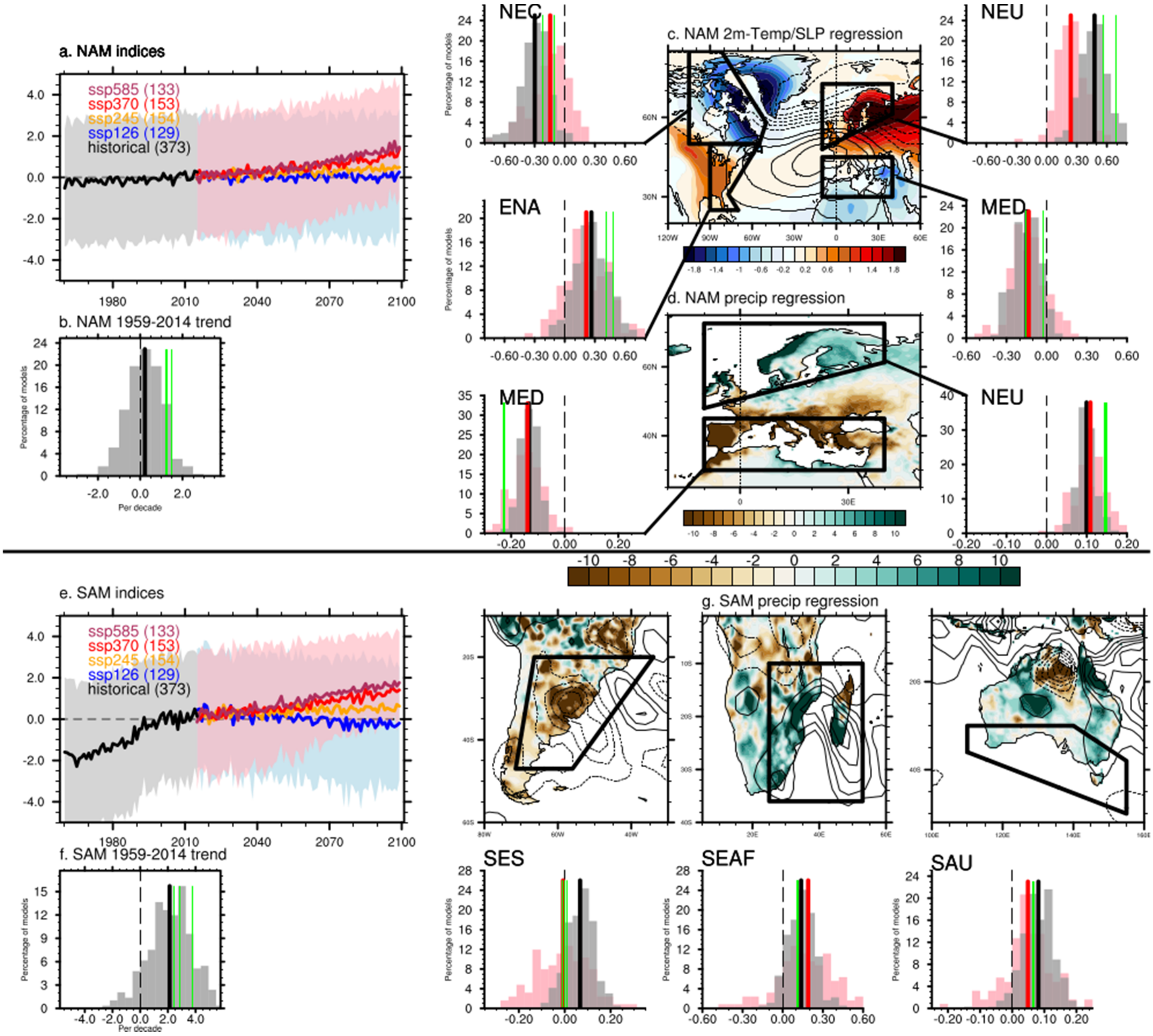

Figure TS.35: Evolution of observed, simulated and projected NAM and SAM indices and associated teleconnection for boreal winter/austral summer (Dec.-Feb. average). **a.** Observed, modelled and projected evolution of the NAM index defined as the latitudinal difference of the zonally averaged mean sea level pressure between 35ºN and 65ºN (Jianping and Wang, 2003) from 1958 to 2100, with respect to 1995-2014 used as a reference period. Thick lines stand for multi-model ensemble mean for historical and four SSP runs and shading is the 5-95% range across CMIP6 models for historical simulation (grey), SSP1-2.6 (mid blue) and SSP5-8.5 (pink), respectively. The number of available models/members is listed in parentheses [and observational estimates are given in green-to be added in final draft]. **b.** Histogram of the 1958-2014 trends built from all historical members (grey). The black vertical line indicates the multi-model multi-member ensemble mean; green lines stand for observational estimates. [placeholder: because the effect of O3 recovery is important, flattening trend when computing over 2000-2014 should be shown. A PDF of the 2000-2014 trend will be added in the final version] **c.** Observed, simulated and projected NAM teleconnections for 2m-temperature and precipitation during December-January-February. Teleconnections are identified by linear regression with the NAM index. Maps show observed patterns for temperature from the Berkeley Earth dataset over land and from ERSSTv5 over ocean (top) and for precipitation from GPCC. Distributions of regression coefficients for regional means drawn over 1995-2014 from 373 historical simulations from [XX] CMIP6 models in grey and for 133 SSP5-8.5 projections over 2081-2100 in light pink are provided for a subset of pre-defined AR6 regions in Atlas for temperature (top) and precipitation (bottom). Multi-model multi-member ensemble means are indicated by thick vertical coloured lines (black for historical and red for SSP5-8.5). Green vertical lines stand for observational estimates based on Berkeley Earth and GISTEMP datasets for temperature and from GPCC and GPCP datasets for precipitation. Efg. Same for SAM based on latitudinal difference of the zonally averaged mean sea level pressure (between 40ºS and 65ºS as defined in Gong and Wang (1999). Only teleconnections for precipitation are assessed over Southern Hemisphere continents for SAM.

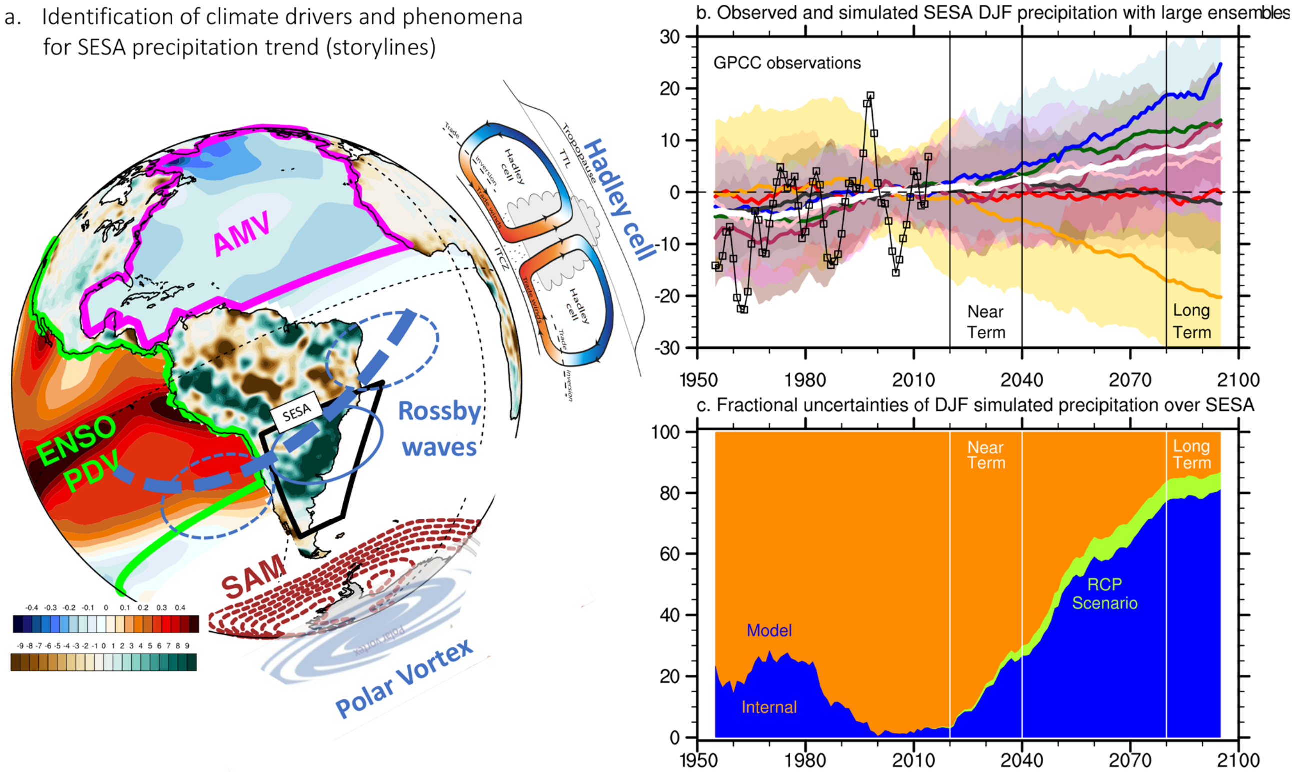

Figure TS.36: a. Identification of the climate drivers and their influences on climate phenomena contributed through teleconnection to Southeastern South America summer (Dec.-Feb.) precipitation trends observed over 1950-2014. Drivers include modes of variability such as AMV, ENSO, PDV and SAM [placeholder: as well as external forcing (GHGs and ozone depletion) – currently not shown and to be added schematically]. Observed anomalous SST patterns of the oceanic modes are shown (red-blue colour bar in °C) as well as mean sea level pressure anomalies for SAM (brown contour every 0.5 hPa) as displayed in Technical Annex VI. Observed precipitation linear trend from GPCC is shown on continents (green-brown colour bar in mm/month/decade) and the SESA AR6 WG I reference region is outlined with the thick black contour. Climate phenomena leading to local impact on SESA (moisture convergence, changes in ascending motion and storm-track location) are schematically presented and include the Hadley Cell, the Southern Hemisphere polar vortex as well as the forced Rossby waves related to large-scale SST anomalies. b. Timeseries of decadal precipitation anomalies for DJF SESA simulated from 7 large ensembles of historical + RCP8.5 simulations over 1950-2100. Shading corresponds to the 5^{th}-95^{th} range of climate outcomes given from each large ensemble for precipitation (in mm/month) and thick coloured lines stand for their respective ensemble mean. The thick timeseries in white corresponds to the multi-model multi-member ensemble mean with model contribution being weighted according to their ensemble size. GPCC observation is shown in light black line with squares over 1950-2014 and the 1995-2014 baseline period has been retained for calculation of anomalies in all datasets. c. Fractional contribution of individual sources of uncertainties (internal in orange, model in blue and scenario in green) to total uncertainty for SESA DJF precipitation following Hawkins and Sutton (2009). All computations are done with respect to 1995-2014 taken as the reference period and the scenario uncertainty is estimated from CMIP5 using the same set of models as for the large ensembles that have run different RCP scenarios following Lehner et al. (2020). Near-term and long-term temporal windows defined in AR6 are highlighted in b. and c.

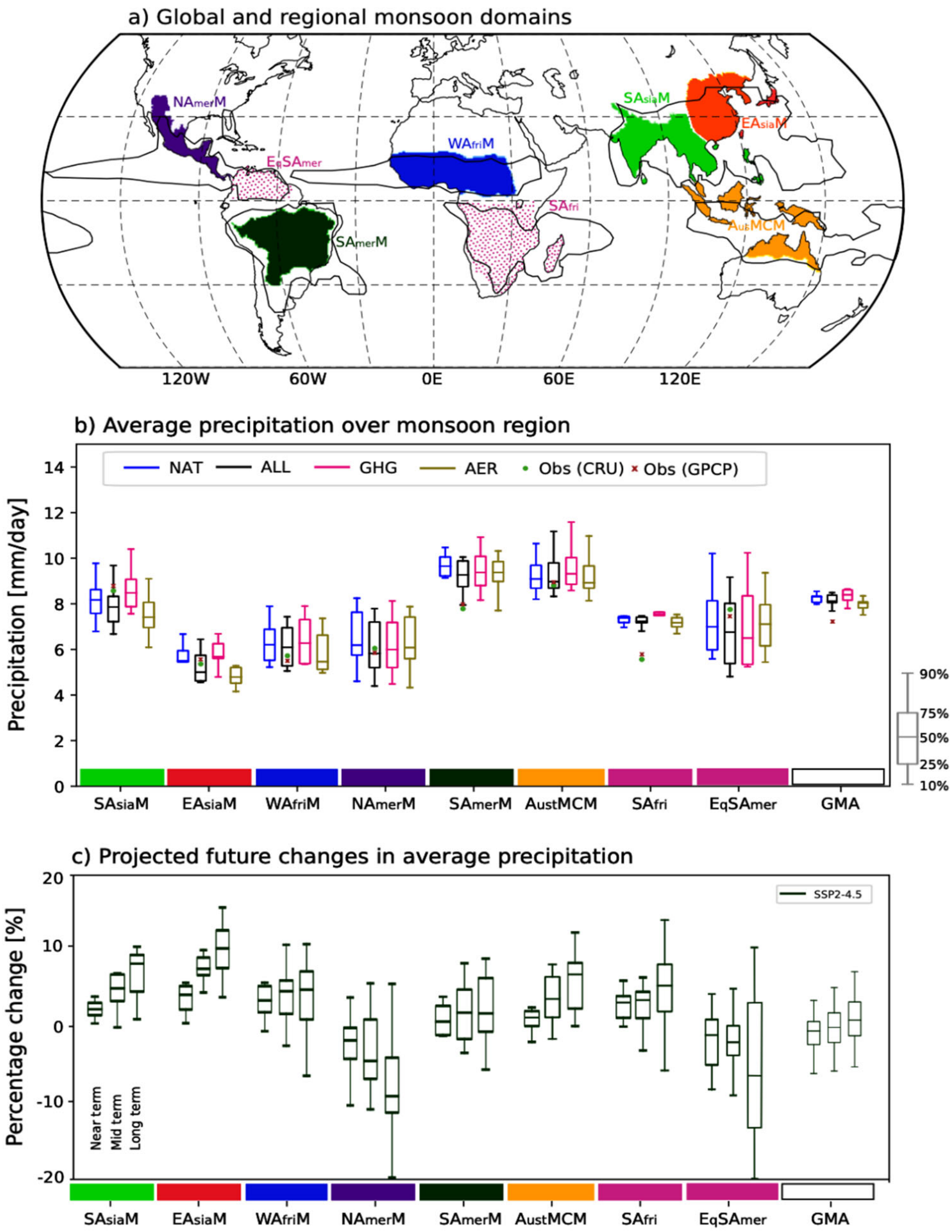

Box TS.6, Figure 1: (a) Global monsoon domain and regional land monsoon domains: Global monsoon domain (contour) is defined by the local summer-minus-winter precipitation rate exceeds 2 mm day^{-1}, and the local summer precipitation exceeds 55% of the annual total. The regional monsoon domains are defined based on published literature and also accounting for the fact that the climatological summer monsoon rainy season varies across the individual monsoon regions *viz.,* South and Southeast Asia ***(SAsiaM**, Jun-Jul-Aug-Sep)*, East Asia ***(EAsiaM**, Jun-Jul-Aug)*, West Africa ***(WAfriM**, Jun-Jul-Aug-Sep),* North America ***(NAmerM**, Jul-Aug-Sep)*, South America ***(SAmerM**, Dec-Jan-Feb)*, Australia and Maritime Continent Monsoon ***(AusMCM**, Dec-Jan-Feb)*. Also shown are regions in equatorial South America ***(EqSAmer)*** and South Africa ***(SAfri)***, which receive seasonal rainfall although the qualification of monsoon is subject to discussion. (b) Regional mean monsoon precipitation based on seven CMIP6 models from all anthropogenic radiative forcings (ALL) GHG only radiative forcings (GHG) aerosol only radiative forcings (AER) and natural only experiment. Mean value of observation is from CRU and GPCP data. Precipitation averaged over global monsoon area (GMA) is also shown. (c) Percentage change in projected seasonal mean precipitation over regional monsoon and global monsoon domain in the near-term (2021-2040), mid-term (2041-2060), and long-term (2081-2100) under SSP 2-4.5 based on seven CMIP6 models.

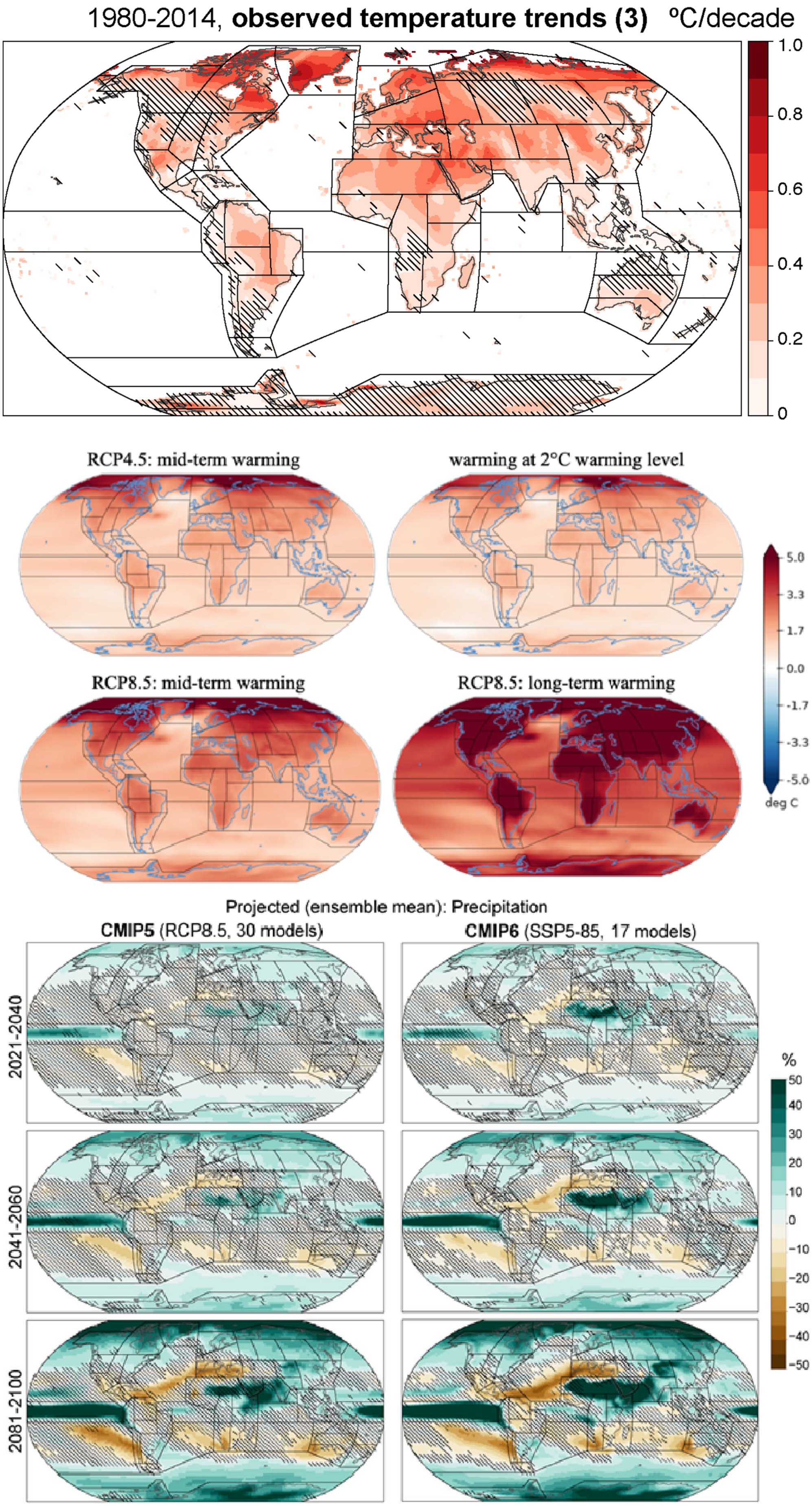
1980-2014, **observed temperature trends (3)** °C/decade
1.0
0.8
0.6
0.4
0.2
0
RCP4.5: mid-term warming
warming at 2°C warming level
RCP8.5: mid-term warming
RCP8.5: long-term warming
5.0
3.3
1.7
0.0
-1.7
-3.3
-5.0
deg C
Projected (ensemble mean): Precipitation
CMIP5 (RCP8.5, 30 models)
CMIP6 (SSP5-85, 17 models)
2021-2040
2041-2060
2081-2100
%
50
40
30
20
10
0
-10
-20
-30
-40
-50

Figure TS.37: Demonstrating the spatial variation in annual mean observed and projected climate change for different future time periods, warming levels and emissions scenarios.
Top map: Consensus on the observed temperature trends from the three observational datasets (CRU TS, BERKELEY and EWEMBI). Hatching indicates regions where no or only one dataset provides a significant trend. Linear trends are calculated for the common 1980–2014 period and expressed in °C per decade (temperature) with respect to the climatological mean over this period.
Middle four maps: Global temperature changes projected for mid-century (left-hand column) under RCP4.5 (top) and RCP8.5 (bottom) compared to, in the right column, a global mean warming level of 2°C (top) and at the end of the century under RCP8.5 emissions (bottom) from an ensemble of nine CMIP5 GCMs. Note that the future period warmings are calculated against a baseline period of 1986–2005 whereas the global mean warming level is defined with respect to a 'pre-industrial' baseline of 1861–1890. Thus, the other three RCP-based maps would show greater warmings with respect to this earlier baseline. Bottom six maps: Future projected changes of annual mean precipitation in the CMIP5 (left-hand column) and CMIP6 (right-hand column) ensembles. Projected changes are calculated as the climatology differences for near-term (2021-2040), medium-term (2041-20160| and long-term (2081-2100) periods for the emissions scenario RCP8.5 (SSP5-8.5 for CMIP6) with respect to the historical period (1986-2005); values are expressed relative differences (%). Hatching indicates lack of model agreement (less than 80% of agreement) and the black lines mark out the WG I reference regions defined in Box TS.1, Figure 2:. Similar analysis for other indices and scenarios (including warming levels) are available at the Interactive Atlas (http://ipcc-atlas.ifca.es).

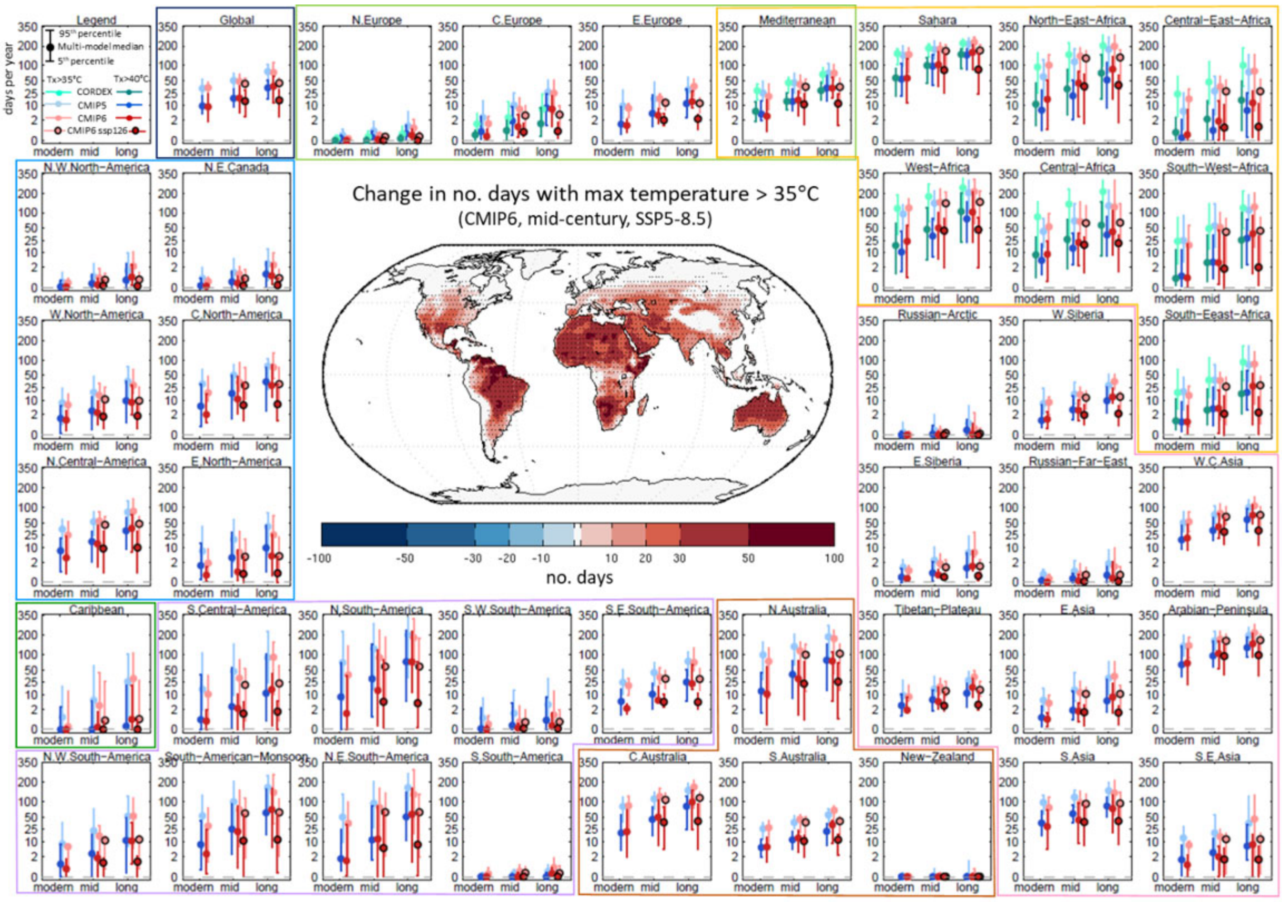

Figure TS.38: Projected change in the mean number of days per year with maximum temperature exceeding 35°C and 40°C. The map shows the median change in the number of days for 35°C between the mid-century (2041-2060) and historical (1995-2014) periods for the CMIP6 ensemble and Scenario SSP5-8.5. The ensemble includes 10 CMIP6 models [*Placeholder: number will change over time*]. Stippling indicates areas where more than 2/3 of models agree on the sign of change. Plots in the "satellite boxes" show the median (dots) and the 5-95% range of model ensemble values across each model ensemble and for each time period (historical [modern], mid-century [mid] and end of century [long]) for the regional mean of the index over land areas for the AR6 regions (defined in Chapter 1 and grouped here by continent). Two exceedance thresholds are considered: 35°C (light colours) and 40°C (dark colors). Both extreme scenarios are shown for CMIP6 only (red; SSP1-2.6 [circled dots] and SSP5-8.5 [open dots]) while for CMIP5 only one scenario is shown (blue; RCP8.5). Available CORDEX results are also shown for RCP8.5 (green) [*Placeholder: here only for Europe and Africa, will be extended*]; [*Placeholder: no bias adjustment is applied here, but it will be used in the FGD*]. {Figure 12.4}

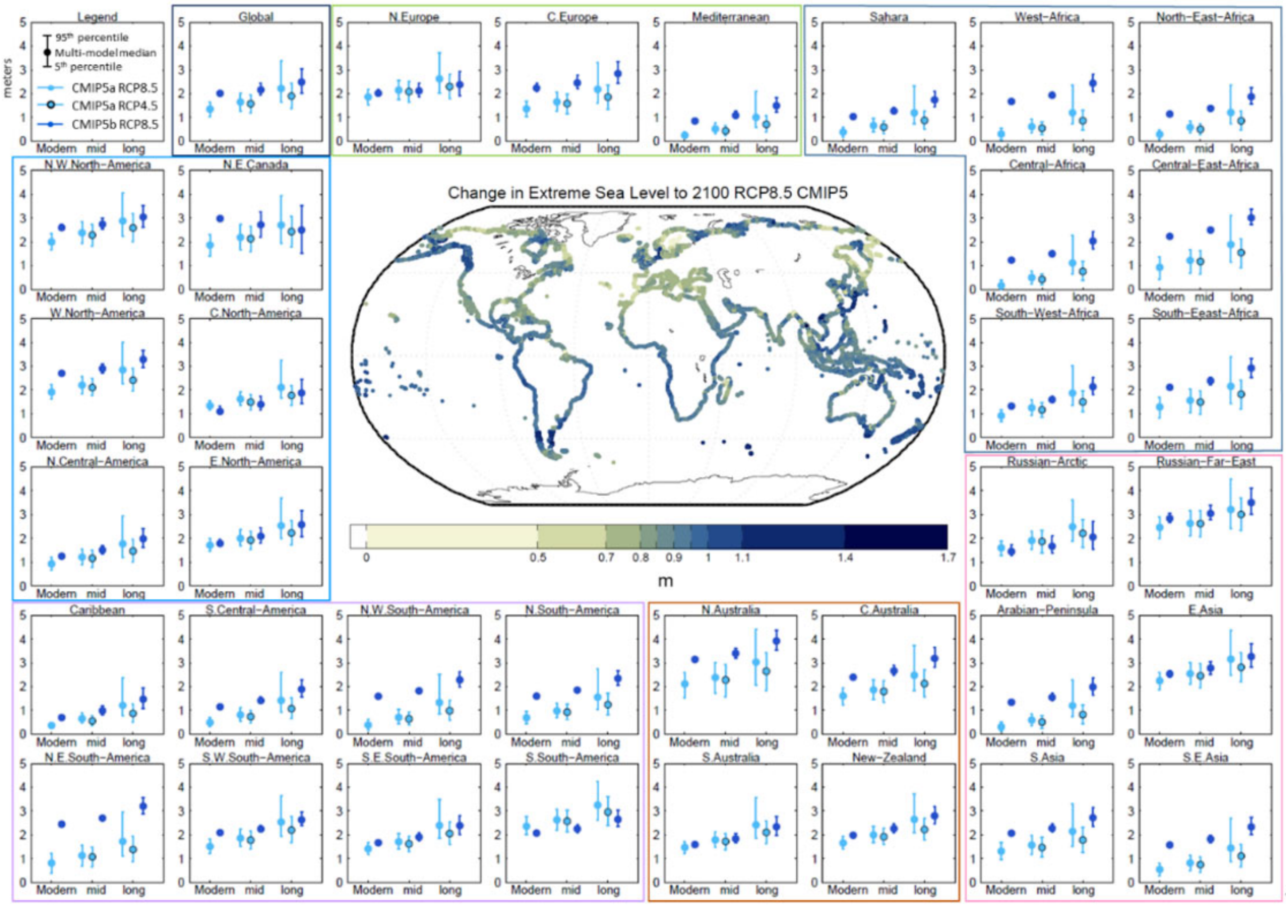

Figure TS.39: Projections of extreme sea level (1:100 yr return period total water level). Central map: change in extreme sea level (ESL) for the year 2100 relative to 1980-2014 from Vousdoukas et al. (2018)'s CMIP5 based dataset. Satellite plots: regional mean ESL values for the modern period (1979/1980 - 2014), mid-term (2050) and long term (2100) for the Vousdoukas et al. (2018) (light blue), and the (Kirezci et al., submitted) (dark blue) CMIP5 based datasets, for the AR6 regions. Data represent RCP8.5, except circled dots which represent RCP4.5. Dots represent the median estimate (regionally averaged), and bars the 5-95th percentiles representing the uncertainty associated with the projections for the AR6 sub-regions (defined in Chapter 1 and grouped here by continent). [*Placeholder: A CMIP6 estimate will also be added, and the central map and RCP4.5 or 2.6 will come from this instead.*] Units m. {Figure 12.7}

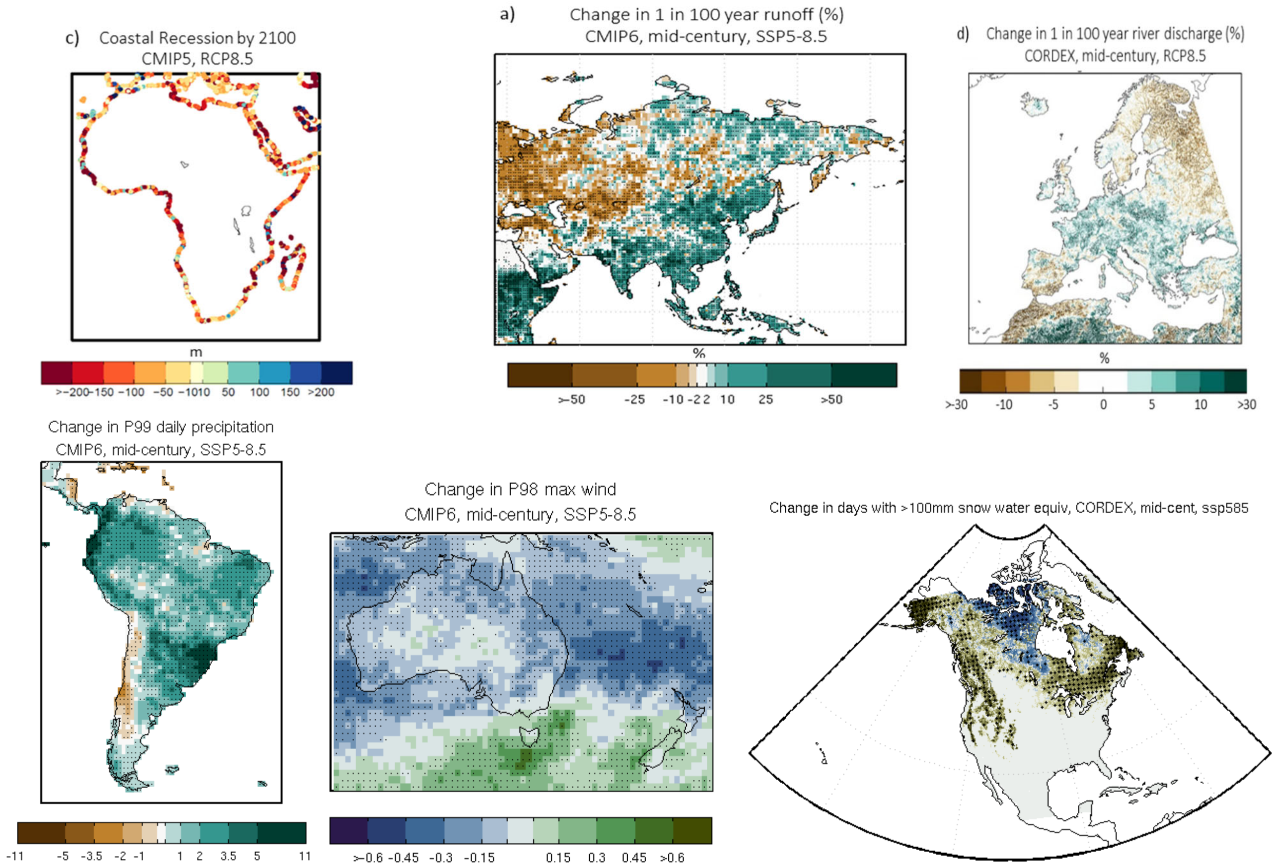

Figure TS.40: Projected changes in selected climate impact driver indices for selected regions. (a) coastal recession for sandy coasts by the year 2100 relative to 2010 (meters; negative values indicate recession) from the CMIP5 based data set presented by (Vousdoukas et al., 2020); (b) change of extreme runoff in Asia.; (c) change in 1/100jr river discharge in Europe (from CORDEX); (d) 99th percentile of daily precipitation (mm day^{-1}); (e) 98th percentile of daily maximum wind (m s^{-1}) ; (f) number of days with snow water equivalent (SWE) over 100 mm between (from CORDEX). {Figure 12.8, Figure 12.9, Figure 12.10, Figure 12.11, Figure 12.12, Figure 12.13}